Delft University of Technology

A Multi-Objective Optimization Framework for the Design of Offshore Wind Farms

Fragoso Rodrigues, Silvio

Important note
To cite this publication, please use the final published version (if applicable).
Please check the document version above.

A Multi-Objective Optimization Framework for the Design of Offshore Wind Farms

Proefschrift

ter verkrijging van de graad van doctor
aan de Technische Universiteit Delft,
op gezag van de Rector Magnificus prof. Ir. K.C.A.M. Luyben;
voorzitter van het College voor Promoties,
in het openbaar te verdedigen op
vrijdag 10 juni 2016 om 12:00 uur

door

Sílvio Miguel Fragoso RODRIGUES

Engenheiro Electrotécnico e de Computadores, Instituto Superior Técnico da Universidade
Técnica de Lisboa
geboren te Lissabon, Portugal

Dit proefschrift is goedgekeurd door de

promotor:	prof.dr.eng. J.A. Ferreira
copromotor:	prof.dr.ir. P. Bauer
copromotor:	dr. P. A. N. Bosman

Samenstelling promotiecommissie bestaat uit:

Rector magnificus,	voorzitter
promotor:	prof.dr.eng. J.A. Ferreira
copromotor:	prof.dr.ir. P. Bauer
copromotor:	dr. P. A. N. Bosman

onafhankelijke leden:

prof.dr.eng. T. Thiringer	Chalmers Tekniska Högskola
dr.ir. D. Thierens	Universiteit Utrecht
prof.dr. G.J.W. van Bussel	Technische Universiteit Delft
prof.dr. J.J. Smit	Technische Universiteit Delft

Life is fair, sometimes.

Pavol Bauer

Contents

Summary

Designing a state-of-the-art offshore wind farm is a highly complex problem since it involves a large amount of variables and constraints. The manual and sequential design approach used so far is no longer sufficient to guarantee optimized systems because interactions between the different components are disregarded.

All the commercial wind farm design tools were specifically built for onshore environments, hence none of them considers all the relevant design aspects of the problem. On the other hand, the academic studies in the field designed for offshore do not capture all the important design aspects. Moreover, existing optimization approaches do not include multi-objective optimization, meaning that the designer does not gain any knowledge from the problem trade-offs.

The main objective of this thesis was the development of a framework to *integrate*, *automate* and *optimize* the design of offshore wind farms. To this end, the recent trends of the offshore wind farm components were investigated to ensure that the framework captured all the relevant design aspects. Moreover, innovative models which comprised the complete electrical infrastructure needed to connect the farms to the power grid were developed. Finally, a state-of-the-art multi-objective optimization algorithm was tailored to the design process of offshore wind farms.

The framework was applied to the Dutch Borssele offshore area. Different layouts demonstrated to be the best alternative when distinct economic indicators, e.g. levelized cost of energy and net present value, were applied. Furthermore, choosing different economic parameters, e.g. price of energy and interest rate, also influenced the outcome of the optimization even while using the same economic indicator.

The results demonstrate that it is important to give wind farm developers the complete picture of attainable trade-offs for the problem at hand before any design decisions are made. Only in this way, the developers will be able to select the wind farm layout that best meets their desires.

Samenvatting

Een state-of-the-art offshore windpark ontwerpen is een zeer complex probleem door het grote aantal variabelen en randvoorwaarden dat hierbij komt kijken. De tot nu toe gebruikte handmatige en stapsgewijze ontwerpmethode is niet langer voldoende om een optimaal systeem te garanderen, omdat de wisselwerkingen tussen de verschillende onderdelen verwaarloosd worden.

Alle commerciële ontwerpmiddelen voor windparken zijn specifiek gemaakt for onshore-omgevingen, waardoor geen van allen rekening houden met de relevante ontwerpaspecten van het probleem. Aan de andere kant omvatten academische studies binnen het vakgebied en gericht op offshore toepassingen niet alle belangrijke ontwerpoverwegingen. Daar komt bij dat bestaande methodes geen gebruik maken van multi-objective optimalisatie, waardoor de ontwerper geen inzicht krijgt in de afwegingen van het ontwerp.

Het hoofddoel van dit proefschrift is het ontwikkelen van een framework voor de *integratie*, *automatisering* en *optimalisatie* van het ontwerp van offshore windparken. Hiervoor zijn de recente trends op het gebied componenten voor offshore windenergie onderzocht, om te zorgen dat het framework alle relevante ontwerpaspecten omvat. Verder zijn innovatieve modellen ontwikkeld die de complete elektrische infrastructuur beschrijven die nodig is voor het aansluiten van windparken op het elektriciteitsnetwerk. Tenslotte wordt een state-of-the-art multi-objective optimalisatie-algoritme speciaal aangepast voor het ontwerpproces van offshore windparken.

Het framework is toegepast op het Nederlandse windgebied Borssele. Bij het toepassen van verschillende economische indicatoren, zoals onder andere levelized production cost en netto contante waarde, bleken verschillende lay-outs de beste keuze zijn. Verder blijken verscheidene economische parameters, zoals de energieprijs en rente, de optimalisatie-uitkomst ook te beinvloeden, zelfs bij gebruik van dezelfde economische indicator.

De resultaten laten zien dat het belangrijk is om windparkontwerpers een totaalbeeld van haalbare afwegingen te geven voor een gegeven probleem, voordat enige keuzes gemaakt worden. Alleen op deze manier kunnen de ontwerpers het ontwerp kiezen dat het beste met hun wensen overeen komt.

Introduction

Currently there are serious concerns regarding the environment and the footprint made by human activities. Thus, fuel oil, coal and nuclear power plants are now being decommissioned at a faster pace than installed in the European Union (EU) [1]. In 2007 the EU targeted to generate 20% of its energy consumption through renewable sources, to improve 20% of its energy efficiency by 2020 and to reduce emissions by 80–95% by 2050 when compared to 1990 levels [2].

Specifically, wind energy is anticipated to help Europe meet these challenging targets. Wind energy is a renewable energy source which provides one of the lowest costs of energy [3]. In 2012, the total power capacity installed in the EU was 931.9 GW, with wind power having an 11.4% share. The annual wind power installations have increased in the last years, from 3.2 GW in 2000 to 11.9 GW in 2012, corresponding to an annual growth of approximately 11.6% [1]. By 2020, the installed capacity is expected to increase by 120 GW. A large share is foreseen to be offshore, where steadier and higher mean wind speeds are found [4, 5].

According to the European Commission, offshore wind will substantially contribute to the energy policy objectives of the EU. Hence, the offshore wind installed capacity is predicted to grow considerably in the coming years. This growth, when compared to the installed capacity at the end of 2007, is believed to be approximately 30 to 40 times higher by 2020, and 100 times in 2030 [6]. Specifically, the EU and the European Wind Energy Association (EWEA) expect that 40 GW of offshore wind will be installed in Europe by 2020 and 150 GW by 2030 [7]. These predictions need a yearly increase rate of 29.6% and 19.1% to be satisfied, respectively. Figure 1.1 shows that these may represent plausible scenarios since the required growths fall between the average (36.1%) and minimum (8.3%) registered European industry growth rates [8].

The initial offshore steps were simple, to minimize risk and to serve mostly as proof of concept [9–11]. Hence, the projects had few turbines, occupied small areas and were placed in shallow waters located up to 10 km from shore (see Figures 1.2a, 1.3b, 1.3c and 1.3e). The capital expenditure (CAPEX) was low (€ 15 million on average) and highly dependent on the turbine number [9–11].
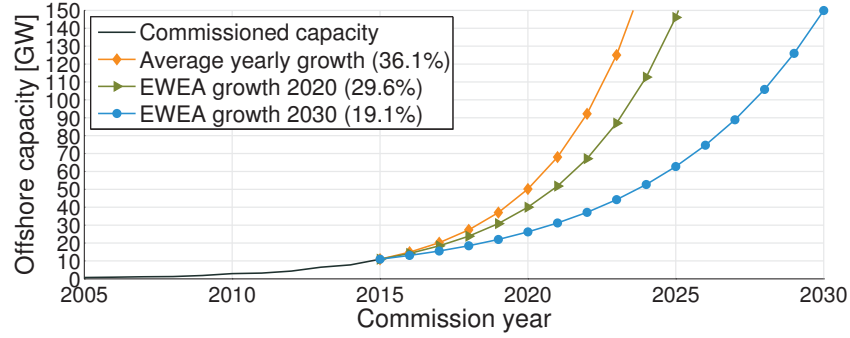
Figure 1.1: Expected offshore wind installed capacity for different growth values.

(a) Danish Vindeby project [9].

(b) British Gwynt y Môr project [12].
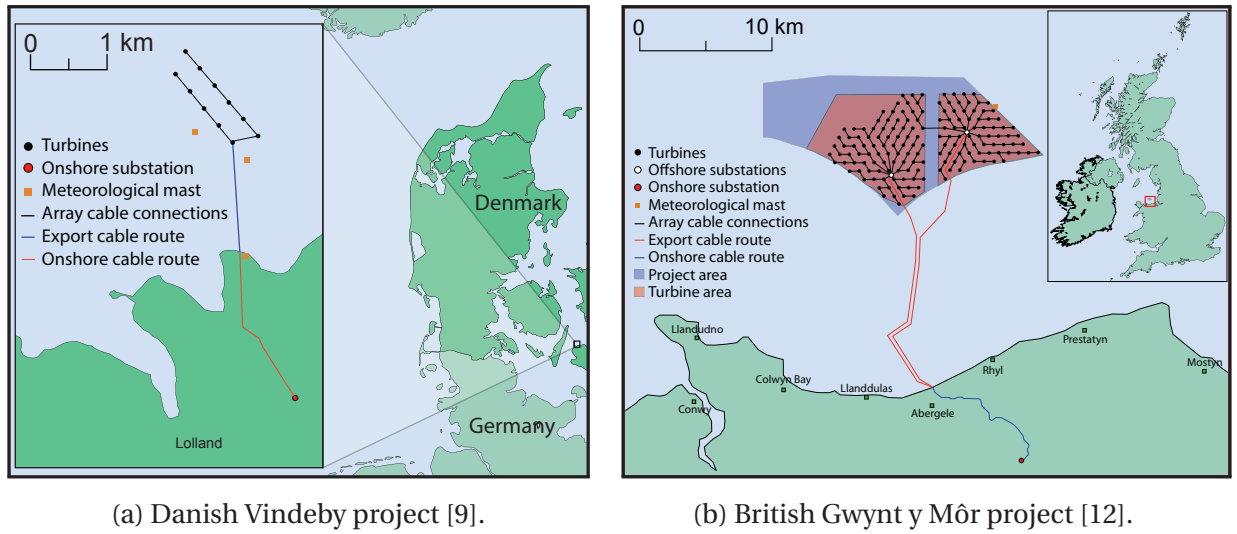
Figure 1.2: Differences in topology and design complexity between two OWFs.

Since 1991, when Denmark erected Vindeby, the world's first offshore wind farm (OWF), the installed capacity of the offshore wind industry has grown on average 52% each year and, therefore, much has changed [9–11]. Since 2002, commercial projects are larger, with an average installed capacity of 154 MW (see Figure 1.3a). Moreover, the distances to shore also increased (Figure 1.3d), hence state-of-the-art projects also use offshore transformer substations and converter stations, if high-voltage dc (HVdc) transmission systems are used. They are also more capital intensive (costing on average € 487 million) due mainly to the larger seabed areas, higher distances to shore, deeper waters and higher number of turbines, which led to more complex designs (see Figure 1.3f) [9–11]. Figure 1.2 shows the difference in complexity between Vindeby and one of the most recent projects, the British wind farm, Gwynt y Môr.
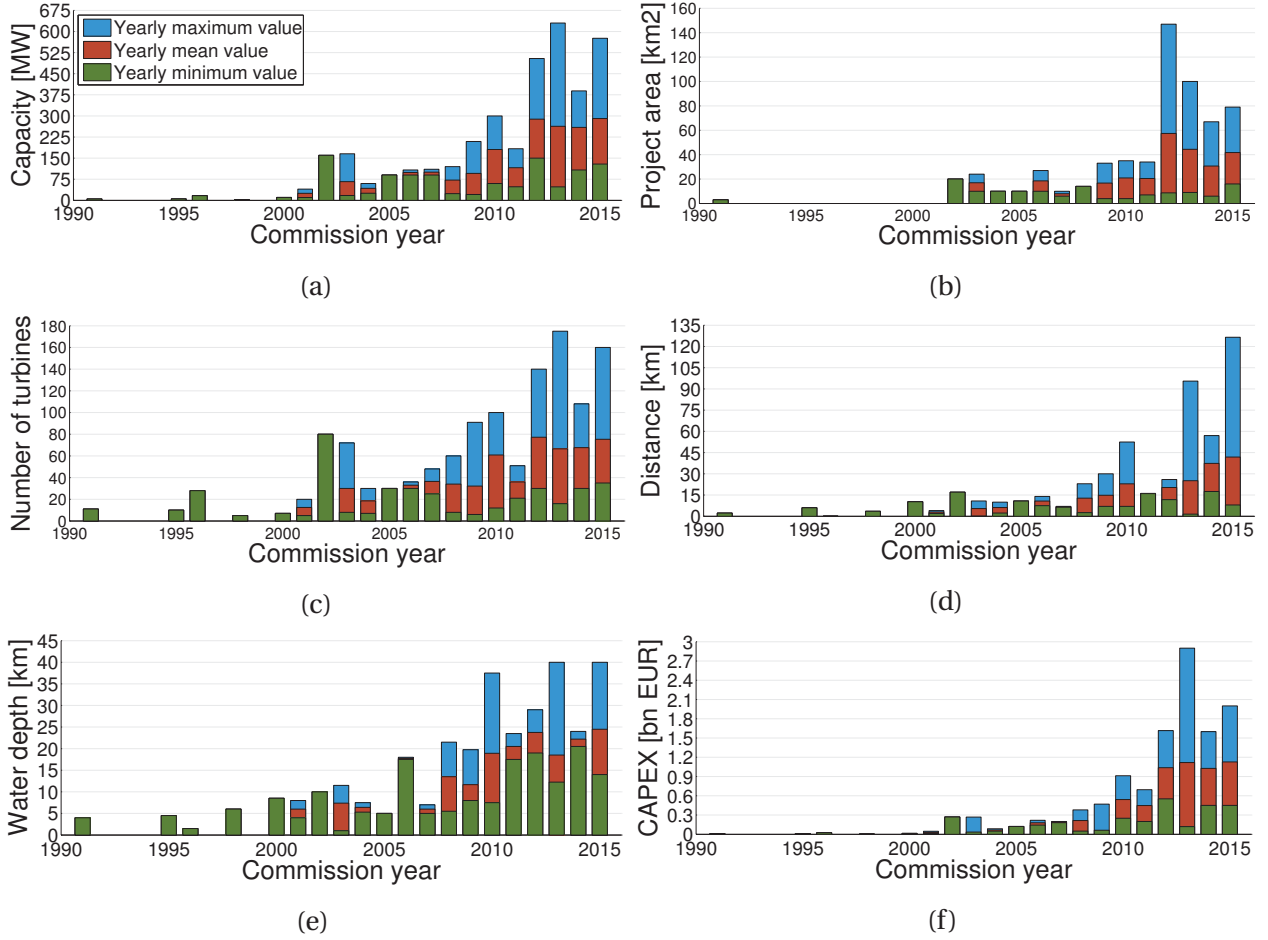
Figure 1.3: Yearly statistics of key characteristics of commissioned and under construction European OWFs composed of five or more turbines [9–11, 13, 14]. The OWFs composed of a single row of turbines were considered to have null area.

1.1 Motivation

Designing a large OWF is a very complex task. In the design phase, an enormous amount of time is spent on manually creating wind farm designs and cable routing. Moreover, the components and technologies that lead to an optimized and feasible system have to be assessed. Approximately 4% of the investment costs are allocated to the development phase [15].

Additionally, current wind farm design processes have another important drawback: due to the complexity of designing a wind farm, the standard practice is to follow a sequential optimization approach (or "decoupled strategy") as shown in Figure 1.4 [16, 17]. Such a strategy does not guarantee system optimality (as interactions between the different system components are disregarded) and, moreover, early project decisions may become constraints in later stages [18]. A reduction of up to 10% in the cost of energy is possible through better integrated design methods [18].

Figure 1.4: Current sequential approach for wind farm layout design [16].
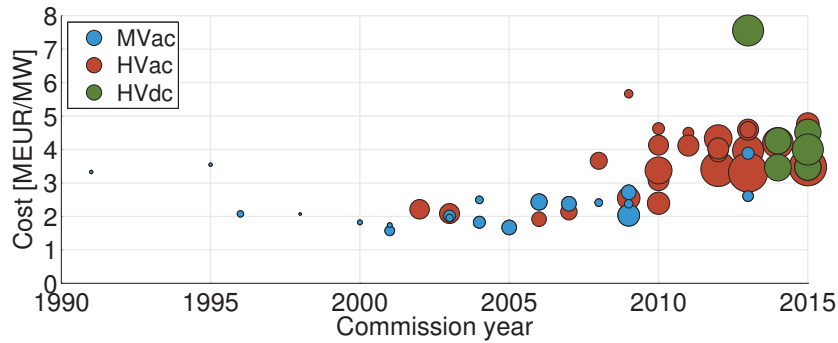
Figure 1.5: Cost per MW installed of the European OWFs composed of five or more turbines [9, 10]. Monetary values updated considering a Eurozone inflation of 1.85% [19].

Among others, these drawbacks led to OWFs with high costs. In fact, electricity generated offshore is currently approximately 50% more expensive when compared to onshore wind [18]. Figure 1.5 clearly demonstrates that the cost per mega-watt (MW) installed of OWFs has increased since the initial projects and has not reduced in recent years.

Currently, the offshore wind industry is aiming at reducing its energy cost to breach the 100 €/MWh barrier as soon as 2020 [20–25]. Several recent technical reports have pointed out different key opportunities that may help reduce the cost of energy generated offshore [21–26]:

- Introduction of turbines with higher rated powers and reliability;

- Greater activity at the front-end engineering and design (FEED) phase;

- More use of geotechnical and geophysical surveying;

- Greater competition in key supply markets, e.g. turbines, foundations and installation;

- Exploitation of economies of scale and greater standardization;

- Optimization of current installation methods;

- Development of products specifically designed for offshore wind environments;

- Deeper and commercial floating water support structures;

- Lower capital costs through de-risking construction and operation & maintenance;

- Increased collaboration and knowledge sharing among the different parties.

This thesis will focus on a greater activity in the FEED phase of the project (see Figure 1.6). The FEED phase of an OWF is performed during the design phase, after the initial feasibility studies have been done and permission has been granted, and before final investment decisions are made [21]. FEED studies allow wind farm developers to make a pre-selection of economically viable design concepts and respective key components [22]. In this phase, several layout concepts are designed. Although the final wind farm layout will be based on these designs, it may still differ considerably [27]. Feedback from industry is that the FEED phase, if carried out properly, avoids significant changes during later project stages, which may lead to cost reductions [23].

The drive for more activity during the project FEED phase has come from [22]:

- Recent OWFs make use of larger seabed areas, which have, in most cases, variable water depth and seabed conditions increasing the design complexity. Moreover, the transmission system and export corridor constraints also increased due to the higher distances to the point of connection to the onshore electrical grid. This leads to more complex and constrained wind farm designs;

- Higher number of wind turbines leads to more complex collection systems. To achieve wind farms with higher efficiency it is crucial to optimize the wind farm layout and the collection system routing simultaneously;

- Past projects have shown that unexpected costs which occurred during the installation phases could have been avoided if a deeper characterization of seabed and other conditions would have been performed during earlier phases of the project;

- Currently there are more technological options available within the offshore wind industry. A higher number of distinct components, e.g. turbines, cables, transformers, support structures are available in the market. It is important to assess the overall system integration to guarantee that optimized systems are obtained.

Feedback from industry is that a more thorough wind farm design and optimization at the development stage may lead to cost reduction in later stages of the project. Moreover, a combination of an enhanced use of FEED in combination with geotechnical and geophysical surveying will lead to lower costs and avoid expensive installation delays. In fact, the levelized cost of energy (LCOE)

Figure 1.6: Lifecycle of an OWF and location of the FEED phase which this thesis focuses on [28].

is anticipated to reduce cost by approximately 2% due to greater analysis and optimization during the FEED phase [21, 26].

The designs of the first OWFs were rather simple due to the relatively benign and uniform seabed conditions. Hence, the final collection system layout was mainly defined through a basic trade-off between capital costs and turbine separation [22]. Greater distances between turbines led to lower shadowing effects and, hence, to an overall higher energy production. However, they also meant higher CAPEX and operational expenditure (OPEX) and lower energy production per unit of seabed.

Recent OWFs, due to their number of turbines and heterogeneous seabed area, require the analysis of more sophisticated trade-offs and interactions between the design parameters. Among others, wake effects, collection and export cables costs and energy losses, components costs, installation and OPEX costs are conflicting design components that need to be addressed to obtain an optimized wind farm design [21]. For example, reduced support structure and installation costs may be achieved through the avoidance of the most challenging seabed areas. Increased energy production through reduction of wake losses and electrical array losses is also a possibility.

There are several commercial wind farm design tools which were specifically built for onshore environments. They consider irrelevant design aspects for offshore areas such as visual impact (mostly irrelevant for far offshore), shadow flickering, noise levels [29] and complex terrain elevations [30, 31]. Although it is possible to use them to design OWFs, none considers some of the important offshore aspects such as collection and transmission systems design, number and location of offshore substations and transmission technology. Furthermore, no commercial tool uses a multi-objective algorithm to optimize the trade-offs between the chosen goals.

On the other hand, several academic studies were specifically tailored to design OWFs. The main goal of the Offshore Wind Farm Layout Optimization (OWFLO) project was the development of an optimization software to provide insights into the trade-offs between cost and energy [32]. However, no information regarding the existing trade-offs may be obtained since the LCOE was the optimization goal. Furthermore, the design of the wind farm collection system, which is a key design aspect, was not considered.

The trade-offs inherent to OWFs design problems were identified in [33]. However, these trade-offs were captured by optimizing directly the LCOE, and therefore, the wind farm designers are, once again, only presented with one final layout. Furthermore, the water depth and the wind speed were considered as functions of the distance to shore, which is a rough estimation.

The main goal of the project Topology Optimization of Wind Farms (TopFarm) was to design an optimization tool for wind farm developers [34]. Although TopFarm has a comprehensive number of modules, it lacks key aspects. For example, the collection system routing was determined by solving the auxiliary road problem, i.e. interconnecting all turbines and assuming that the cables could transport all the power connected to them. Furthermore, the TopFarm tool does not consider offshore substations or export cables, which are key factors for OWF developers.

Although more than 150 research articles on the wind farm layout optimization problem (WFLOP) may be found in literature, few studies have investigated the inherent trade-offs of designing an OWF [35]. Comprehensive studies that explicitly consider multiple goals during the optimization process are even more rare [36]. Furthermore, none of them captured all the key aspects pertaining to the development of OWFs.

1.2 Approach

The proposed design approach is to take into consideration the trade-offs that arise while designing an OWF. For example, Figure 1.7 shows an example of a trade-off between the energy produced and the investment cost of OWFs. Although the energy production is maximized by placing more turbines in the wind farm area, this also makes the investment cost rise. Hence, these design goals are conflicting, meaning there is not a single solution for the problem, but a set of solutions which represent the trade-off. In the multi-objective space, a layout is optimal if there is no other layout that is better in all objectives.

In this way, the optimization phase will not only provide the wind farm developers with one final wind farm layout, but instead it will provide several wind farm layouts which are optimized and represent the trade-off between the design goals. No *a priori* economic knowledge, such as the interest rate or energy selling price, is required, i.e. it is not necessary to combine different optimization goals in a weighted combination, as for example the LCOE in which the energy production, CAPEX and OPEX are combined through economic parameters. In this way, wind farm designers may have a clear picture of the design possibilities at hand and will be able to choose one wind farm layout and its components that they prefer. Furthermore, the use of an optimization framework will also lead to lower wind farm development costs due to a reduction of the required manual work to analyze and iterate over different wind farm designs.
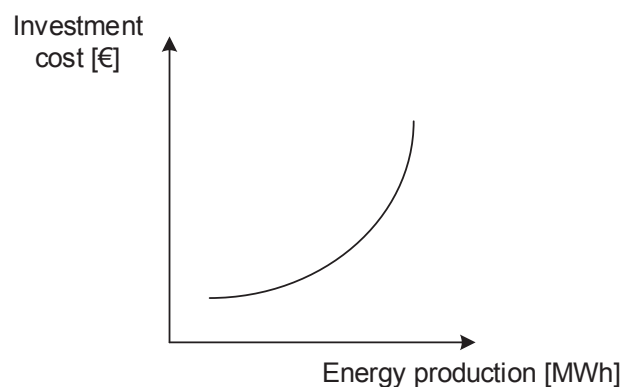
Figure 1.7: Trade-off between two conflicting goals: energy production and investment cost.

1.3   Objectives & Research Questions

The main research objective of this thesis is to investigate how to create a framework to *integrate*, *automate* and *optimize* the design of OWF layouts and their electrical infrastructures. Furthermore, innovative models which comprise the wind farm energy production and the complete electrical infrastructure are needed to connect the wind farms to the onshore electrical grid. Additionally, a state-of-the-art multi-objective optimization algorithm specially tailored to the design process of OWFs is to be obtained.

The main research question of this thesis is formulated as follows:

How to create a multi-objective optimization framework for the design of offshore wind farm layouts and their electrical infrastructure?

To answer the question above the following key questions are considered:

1. *What are the trends of the main characteristics of offshore wind farms?*

2. *What are the industrial trends of offshore wind farm components?*

3. *Why is (multi-objective) optimization needed?*

4. *Which is the best multi-objective optimization algorithm for the design of offshore wind farm layouts and their electrical infrastructure?*

5. *Which modeling techniques are required?*

6. *Which are the important variables and objectives in the optimization process?*

1.4   Contributions

The main contributions of this thesis are:

1. Investigation of the recent trends of the OWF components and design techniques;

2. Development of innovative loss models which comprised the complete electrical infrastructure needed to connect OWFs to the onshore power grid;

3. Tailoring of a state-of-the-art multi-objective optimization algorithm to the design of OWFs.

1.5   Thesis Layout

The thesis layout, shown graphically in Figure 1.8, is as follows:

2. Trends of Offshore Wind Projects answers the first key question by giving an overview of the commissioned and under construction European OWFs and the trends of their key characteristics - commissioning country, installed capacity, number of turbines, water depth, project area, distance to shore, transmission technology and investment cost. The present and future statuses of the main European offshore wind players are introduced. A similar analysis is also performed for the most important countries outside Europe.

3. Multi-Objective Optimization of Wind Farm Layouts addresses key questions number 3 and 4. The characteristics that a multi-objective optimization algorithm should have to optimize the layout of OWFs are identified. The trade-off between problem dimensionality/complexity and design freedom of different turbine-placement grid resolutions and the influence of problem size on performance are investigated. Furthermore, several constraint-handling techniques are investigated to assess which one presents the best performance.

4. Steady-state loss models for Optimization Purposes covers the fifth key question. The aim is the development of models to calculate the power losses of offshore cables, transformers and converters. The models were required to capture the main steady-state loss sources while being computationally light for the optimization process. Furthermore, all the models consider the dependence between power losses and the temperature of operation. The output of the proposed models is then compared with existing models in the literature.

5. Multi-Objective Optimization Framework for Offshore Wind Farms deals with key questions number 2, 3 and 6. A survey of existing optimization approaches is given. Thereafter, the main gaps and drawbacks of these approaches are presented. A thorough explanation of why optimization is needed and the advantages of multi-objective optimization are presented. A multi-objective optimization framework for OWFs is then formulated. The design variables, constraints and optimization objectives that play an important role in the optimization process are identified. Alongside, the industrial trends of the components of an OWF are presented. Afterwards, a case study is formulated to demonstrate the capabilities of the proposed optimization framework.

6. Wake Losses Optimization of Offshore Wind Farms with Movable Floating Wind Turbines presents a novel layout optimization framework for wind farms composed of movable floating turbines. The industrial trends presented in Chapter 5 identified that floating wind turbines will play an important role to harvest energy deep offshore. The proposed framework uses an evolutionary optimization strategy in a nested configuration which simultaneously optimizes the anchoring locations and the wind turbine position within the mooring lines for each individual wind direction.

7. Conclusions summarizes the results obtained for each key question and gives the final conclusions. Recommendations for future research and to OWF developers are also presented.
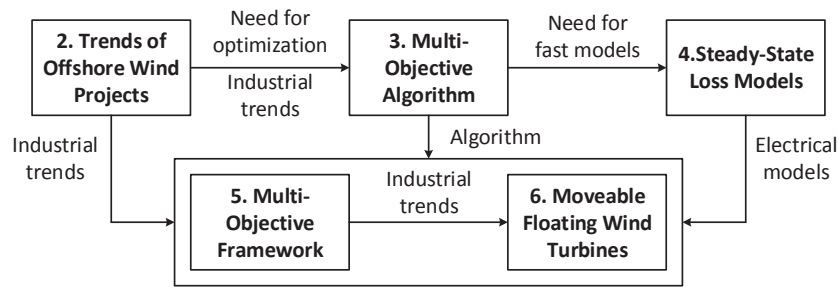
Figure 1.8: Thesis layout and interdependencies between chapters.

References

[1] EWEA, "Wind in power: 2012 european statistics," Tech. Rep., 2013.

[2] Council of the European Union. (2009) Last accessed 3rd August 2015. [Online]. Available: www.consilium.europa.eu/uedocs/cms_data/docs/pressdata/en/ec/110889.pdf

[3] Office of Energy Efficiency & Renewable Energy. [Last accessed 8th August 2015]. [Online]. Available: www.energy.gov/eere/wind/advantages-and-challenges-wind-energy

[4] R. Green, and N. Vasilakos, "The economics of offshore wind," *Energy Policy*, vol. 39, no. 2, 2011.

[5] EWEA, "The european offshore wind industry - key trends and statistics 2013," Tech. Rep., 2014.

[6] European Commission. [Last accessed 1st March 2015]. [Online]. Available: www.eur-lex.europa.eu/LexUriServ/LexUriServ.do?uri=CELEX:52008DC0768:EN:HTML

[7] EWEA, "Deep water - the next step for offshore wind energy," Tech. Rep., 2013.

[8] E. Ochieng *et al.*, "Future for offshore wind energy in the United Kingdom: The way forward," *Renew. and Sustainable Energy Reviews*, vol. 39, no. 0, pp. 655–66, 2014.

[9] LORC. [Last accessed 1st March 2015]. [Online]. Available: www.lorc.dk/offshore-wind-farms-map/list

[10] 4C Offshore. [Last accessed 23rd March 2015]. [Online]. Available: www.4coffshore.com/windfarms

[11] The Wind Power. (2014) [Last accessed 1st March 2015]. [Online]. Available: www.thewindpower.net/windfarms_offshore_en.php

[12] RWE. [Last accessed 31st March 2015]. [Online]. Available: www.rwe.com/web/cms/en/1252456/rwe-innogy/sites/wind-offshore/under-construction/gwynt-y-mr/tech-and-spec/

[13] Renewables Map. [Last accessed 1st March 2015]. [Online]. Available: www.renewables-map.co.uk/windfarm.asp

[14] M. Bilgili, A. Yasar, and E. Simsek, "Offshore wind power development in europe and its comparison with onshore counterpart," *Renew. and Sustainable Energy Reviews*, vol. 15, no. 2, pp. 905–15, 2011.

[15] BVG Associates, "Value breakdown for the offshore wind sector," Tech. Rep., 2010.

[16] Wind Energy, "Wind Energy - The Facts Part I Technology," Brussels, Belgium, Tech. Rep., 2009.

[17] S. Lumbreras, and A. Ramos, "Offshore wind farm electrical design: a review," *Wind Energy*, vol. 16, no. 3, pp. 459–473, 2013.

[18] DNV GL, "Project FORCE - Offshore Wind Cost Reduction through Integrated Design," Hovik, Norway, Tech. Rep., 2014.

[19] Trading Economics. [Last accessed 8th August 2015]. [Online]. Available: www.tradingeconomics.com/euro-area/inflation-cpi

[20] B. Christensen, "The Road to Below 10 ct EUR/kWh - Siemens response to the challenge," in *EWEA Offshore*, Copenhagen, Denmark, March 2015.

[21] BVG Associates, "Future renewable energy costs: offshore wind - how technology innovation is anticipated to reduce the cost of energy from european offshore wind farms," KIC InnoEnergy, Eindhoven, The Netherlands, Tech. Rep., 2014.

[22] The Crown Estate, "Offshore Wind Cost Reduction - Pathways Study," London, United Kingdom, Tech. Rep., 2012.

[23] Offshore Wind Cost Reduction Task Force, "Offshore wind cost reduction task force report," Tech. Rep., June 2012.

[24] Offshore Renewable Energy Catapult, "Cost reduction monitoring framework," Glasgow, Scotland, Tech. Rep., Feb. 2015.

[25] Offshore Wind Programme Board, "Sharing good practice in the supply chain to facilitate cost reduction," Tech. Rep. Rev 03.

[26] BVG Associates, "Offshore wind technology pathways for scotland," Tech. Rep., 2012.

[27] RWE, "Galloper wind farm project environmental statement - chapter 5 project details," Tech. Rep., 2011.

[28] Scottish Enterprise, "Offshore wind fact overview of a wind farm project," Glasgow, Scotland, Tech. Rep., March 2010.

[29] S. Sorkhabi *et al.*, "Constrained multi-objective wind farm layout optimization - introducing a novel constraint handling approach based on constraint programming," in *Proceedings of International Design Engineering Technical Conference*, Boston, USA, August 2015.

[30] N. A. Kallioras *et al.*, "Optimum layout design of onshore wind farms considering stochastic loading," *Advances in Engineering Software*, vol. 88, pp. 8–20, 2015.

[31] M. Song *et al.*, "Optimization of wind turbine micro-siting for reducing the sensitivity of power generation to wind direction," *Renewable Energy*, vol. 85, pp. 57–65, 2016.

[32] C. N. Elkinton, J. F. Manwell, and J. G. McGowan, "Offshore wind farm layout optimization (OWFLO) project: an introduction," in *In Proceedings of the European Offshore Wind Conference & Exhibition*, Copenhagen, Denmark, Oct. 2005.

[33] M. A. Lackner, and C. N. Elkinton, "An analytical framework for offshore wind farm layout optimization," *Wind Engineering*, vol. 31, pp. 17–31, Jan. 2007.

[34] P.-E. Rethore *et al.*, "Topfarm: Multi-fidelity optimization of offshore wind farm," in *ISOPE conference*, Hawaii, USA, 2011.

[35] J. F. Herbert-Acero *et al.*, "A review of methodological approaches for the design and optimization of wind farms," *Energies*, vol. 7, no. 11, pp. 6930–7016, 2014.

[36] S. Khan, and S. Rehman, "Computational intelligence techniques for placement of wind turbines: A brief plan of research in saudi arabian perspective," in *Energy Conference and Exhibition (EnergyCon), 2010 IEEE International*, Dec 2010, pp. 519–523.

Trends of Offshore Wind Projects

The aim of this paper is to present the current status of the offshore wind industry and to identify trends in Offshore Wind Farms (OWFs). This was accomplished via a thorough analysis of the key characteristics - commissioning country, installed capacity, number of turbines, water depth, project area, distance to shore, transmission technology and investment cost – of the commissioned and under construction European OWFs. Furthermore, the current status of the several countries outside of Europe was also investigated. The analysis revealed that the European offshore wind power grew on average 36.1% yearly since 2001. Currently, there are 7748 MW installed and 3198 MW under construction distributed among 76 OWFs situated in European waters. These projects are spread among ten countries, with the highest share of offshore projects belonging to the northern European countries. The UK has 46% of the total installed European offshore wind capacity with 26 projects, Germany ranks second with 16, while Denmark is third with 13 projects. The analysis also showed that, although the installed capacity of the OWFs is growing, the projects' area is not increasing at the same pace due to the release of turbines with higher rated capacities which allow projects to increase their power nameplate without proportionally increasing the number of turbines. The average distance to shore and the water depth are both increasing throughout the years. Although the average investment cost per project is rising with the higher distances to shore and water depths, the multi-GW plans of the northern European and Asian countries indicate that the industry will continue to grow. The European Union targets of having 40 GW of offshore wind capacity deployed by 2020 in Europe and 150 GW by 2030 may represent plausible scenarios since the required growth is below the current European average.

2.1 Introduction

The global energy consumption is growing and it is expected to increase by 36% until 2035 [1]. In 2010, 81.1% of all the world primary energy use was obtained through fossil fuels: oil, coal and natural gas [2]. The use of fossil fuels has energy source has several disadvantages: they are non-renewable at human time-scale, they increase the greenhouse effect through the release of CO_2 and they are not evenly spread throughout the world. Hence, countries with either small or no fossil resources should minimize their dependency. The solution is to either decrease the energy consumption or to alter the energy source to cleaner and renewable energy sources.

In 2007 the European Union (EU) targeted to generate 20% of its energy consumption through renewable sources and to improve 20% of its energy efficiency by 2020 compared to 1990 levels. Hence, it is predicted that 34% of electricity will need to be generated from renewable sources [3,4]. By 2050, the EU has committed to reduce emissions by 80–95% when compared to 1990 levels [5].

Renewable energy sources are anticipated to help Europe meeting these targets. Specifically, the EU and the European Wind Energy Association (EWEA) expect that 40 GW of offshore wind will be installed in Europe by 2020 and 150 GW by 2030 [6]. In fact, the northern European countries have been investing in Offshore Wind Farms (OWFs) for more than two decades due to higher and steadier mean wind speeds and lower visual impact [7,8]. Figure 2.1 shows that higher mean wind speeds are found offshore. The Irish and North seas have the most promising offshore wind resource of northern Europe, whereas the Aegean Sea and two areas located south of France and Spain are the most suitable for offshore wind deployment in southern Europe.

Although the general opinion is that there is plenty of free offshore space to install wind farms, there is more to the problem than meets the eye. Figure 2.2 shows the Belgian Exclusive Economic Zone (EEZ), in the North Sea, which with an area of 3453 km^2 (nine times smaller than the Belgian land area) is the 9th smallest and one of the most exploited EEZs in the world [10, 11]. The EEZ is the sea zone which stretches from the baselines from which the breadth of the territorial sea is measured to 200 nautical miles (approximately 370 km) towards the sea. Within the EEZ the state has sovereign rights for exploring, conserving and managing the natural resources of the waters and seabed. Furthermore, it has also exclusive right to construct, authorize and regulate the construction, operation and use of artificial islands and structures for economic exploitation and exploration of the zone, such as the production of energy from the water, currents and wind [12]. In 2005, the legal allocated offshore area represented 264% of the Belgian EEZ with a small fraction of 0.6% being appointed to offshore wind development [13]. The area of an OWF has to comply with several constraints which are both nature and human-based. The following criteria are important for the choice of a location (not in order of importance) [11]:

- Military operation or exercise zones;
- Piloting zones;
- Environmental protected areas;

- Lanes and harbor entrances;
- Oil & gas lease or concession areas;
- Minimum suitable available space;
- Minimum distance to the high voltage grid;
- Suitable wind resource;
- Distance to nearest port with sufficient capacity;
- Environmental impact;
- Seabed characteristics;
- Vessel traffic routes, separation and precautionary zones;
- Fishing areas;
- Extraction, dredging and dumping sites;
- Water depth;
- Pipelines (oil & gas) and cables (power & telecom) rights of way;
- Existing OWFs and wave park areas;
- Shipwrecks, UneXploded Ordnance (UXO) and other obstructions;
- No anchoring areas;
- Suitable export corridor area.
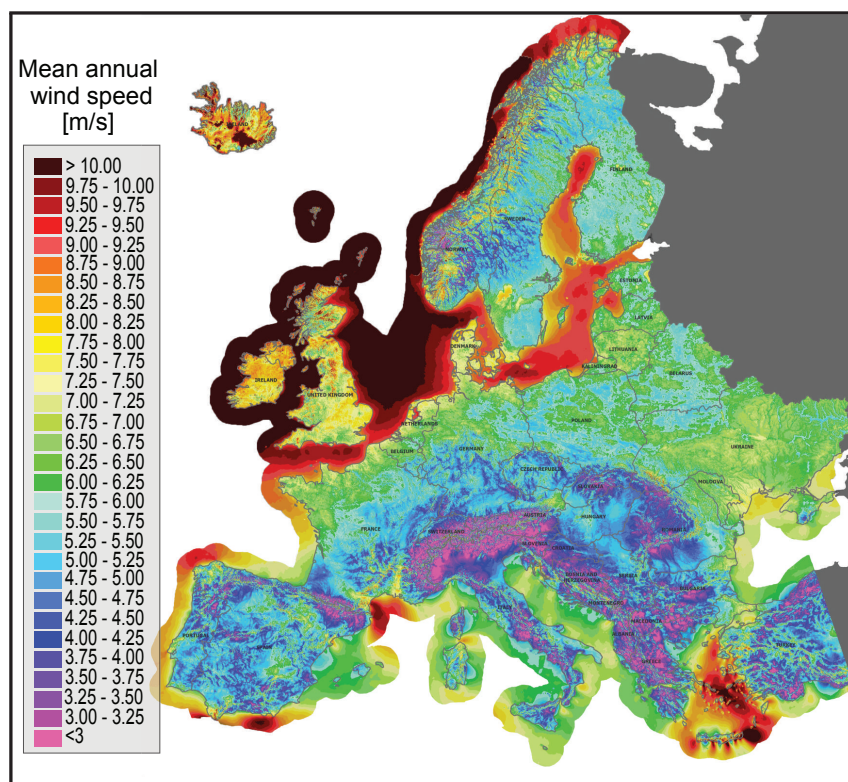
Figure 2.1: Annual European mean wind speeds at a 80 m height. Reproduced from [9].
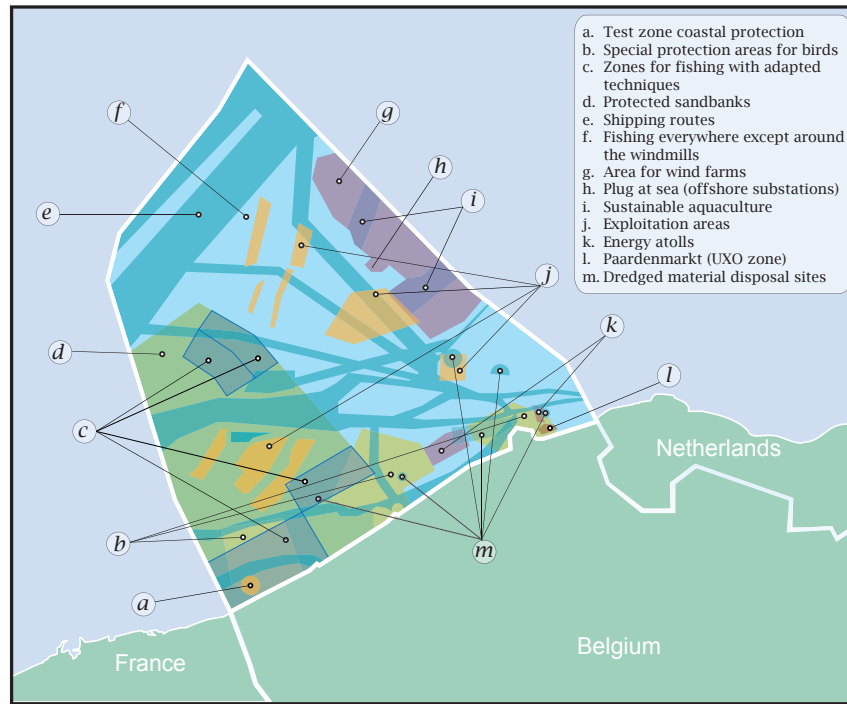
Figure 2.2: Reserved areas of the Belgian EEZ [14].

The northern European seas have good wind resource, as previously noted, and a seabed with relatively low water depths. These characteristics have allowed the northern European countries to make the initial offshore move and to be leaders of the offshore wind industry nowadays. The initial offshore steps, as with any technology, were simple in order to minimize risk and to serve mostly as proof of concept [15–17]. Hence, the projects had few turbines (twelve on average) and were placed in shallow waters located up to 10 km from shore. The Capital Expenditure (CAPEX) was low (€ 15 million on average) and highly dependent on the number of turbines [15–17].

Since 1991, when Denmark erected Vindeby, the world's first OWF, the installed capacity of the offshore wind industry has grown on average 52% each year and, therefore, much has changed [15–17]. Since 2002, commercial projects are larger, with an average installed capacity of 154 MW. They are also more capital intensive (costing on average € 487 million) due mainly to the larger seabed areas, distance to shore, water depth and number of turbines, which lead to more complex designs [15–17]. Moreover, state-of-the-art projects also use offshore transformer substations and converter stations, if high-voltage dc (HVdc) transmission systems are used.

Different literature works have presented reviews of the offshore wind industry status [7, 18–23]. Moreover, several papers have addressed the topic in more specific areas. For example, the current status and the development of the Chinese offshore wind industry were presented in [24–28]. North America current position and plans were described in [18], whereas the British industry was described in [19]. Other works have focused on the economics of offshore wind [7, 29–31].

However, the existing surveys do not present updated information since new plans are made and existing ones are either canceled or altered at a fast pace in the offshore energy industry. In fact, several review works have presented planned OWFs which have not been built [18–20] and currently contain outdated information, e.g. maximum water depth [18]. The annual EWEA reports present the current data regarding the number of offshore projects and their main characteristics [8, 32, 33]. However, no further description nor analysis of the data is given. Furthermore, none of the existing works has presented the history of the offshore wind industry from its origins until future developments, while describing the current state of the main players.

The aim of this paper is to identify the trends of the key characteristics of OWFs, namely: commissioning country, installed capacity, number of turbines, water depth, project area, distance to shore, energy production, transmission technology and investment cost. Furthermore, we also present the recently approved tendering phases of the northern European countries, the current status of Brazil, China, Japan and USA, as well as the future plans of the offshore wind industry. The remainder of the work is organized as follows: firstly a historical background which covers the initial OWFs is provided. After, it is described the current status, growth and trends of the key characteristics of the commissioned and under construction European OWFs. Afterwards, the industry's short and long term plans are presented, followed by a summary in which the main findings of the work are highlighted.

2.2   Initial near-shore steps

The first offshore wind milestone was achieved more than two decades ago, back in 1990, with the installation of one wind turbine near Norgersund, in southern Sweden. The wind turbine (nowadays decommissioned), named Wind World W2500/220, had a 25-m rotor and was installed approximately 300 m from the coast in a 7-m water depth, using a steel tripod foundation [34].

One year later, Denmark built Vindeby, the world's first near-shore wind farm, in the Great Belt (see Figure 2.3). It consists of eleven turbines with a total installed capacity of 4.95 MW and it is located 2 km from shore and in waters 4-m deep. Vindeby was an important achievement for the offshore wind industry since it was the first project with multiple turbines.

Until 2001, eight more wind farms were built, all located in northern Europe (for details on these projects see Table 2.1). Denmark and the Netherlands erected the four initial projects, while in 1998, Sweden built Bockstigen, its first project located off the coast. Afterwards, in 2000, the Swedish established a new world record in the Utgrunden 1 project, by commissioning turbines located circa 10 km away from the coast. Also in 2000, the first development in the British offshore wind power, the Blyth project, was commissioned under the British government now discontinued Non-Fossil Fuel Obligation renewable energy support scheme [35].

In 1999, the British government published guidelines to build "development" farms with the objective of allowing wind farm developers to gain technical and environmental experience. The
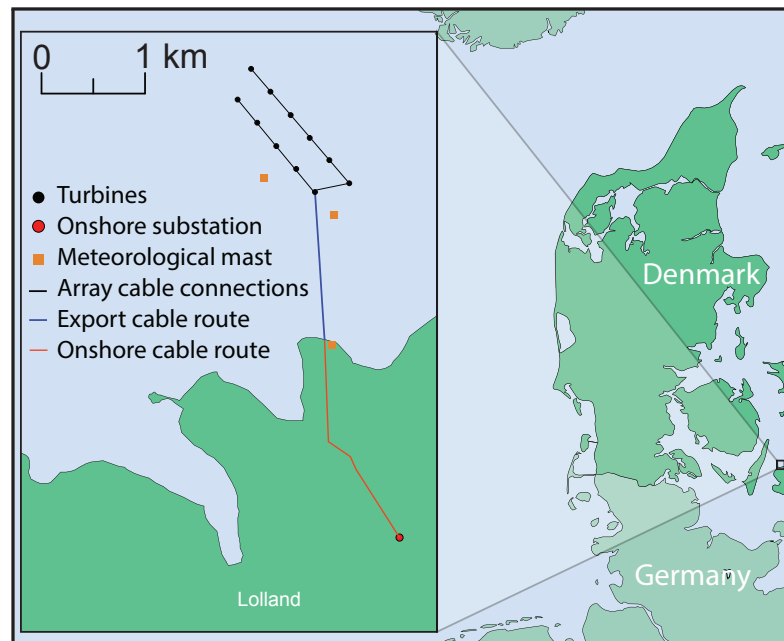
Figure 2.3: Location and layout of the Danish Vindeby project.

projects' locations, chosen by the potential developers, were limited to areas smaller than 10 km^2 and with a maximum of 30 turbines. In 2001, seventeen applications were granted permission to erect wind farms in the so-called Round 1 [36].

The 40 MW Middelgrunden wind farm, which had the highest installed capacity amongst the initial projects, was built in the Danish river the Sound in 2001. The project is composed of 20 turbines and cost circa € 47 million. Half of the project is owned by a cooperative of ten thousand private investors, whereas the other half belongs to the local utility Copenhagen Energy [37].

The low installed capacities – averaging 11 MW – combined with the short distances to shore led to wind project designs in which no transformer substations were employed; the energy was transported to shore using the collection system's Medium-Voltage ac (MVac) voltage. Nonetheless, industrial progress can be observed since ten years later, the Middelgrunden's voltage level had tripled in comparison with the 10 kV system used in Vindeby.

In the initial projects, the CAPEX was highly correlated with the number of turbines due to their simple design (the cabling systems of the Vindeby project are shown in Figure 2.3). Table 2.1 shows that for the first five projects, the CAPEX and number of turbines had a one-to-one ratio with each turbine requiring an investment of € 1 million. Projects commissioned in 2000 and 2001 required € 2 million of investment per turbine, which can be explained by the deeper waters and higher rated voltages of the collection systems.

Although the initial turbines were installed in near-shore projects placed in shallow waters, they were necessary to provide valuable lessons quickly learned by the industry. In fact, the initial profitability and risk assessment was completed; it was time to go deeper and bigger.

Table 2.1: Project details of the initial near-shore wind farms [15–17, 21, 38].

Project	Vindeby	Lely	Tuno Knob	Irene Vorrink	Bockstigen	Blyth	Utgrunden 1	Middelgrunden	Yttre Stengrund*
Year	1991	1994	1995	1996	1998	2000	2000	2001	2001
Country	Denmark	Netherlands	Denmark	Netherlands	Sweden	UK	Sweden	Denmark	Sweden
Location	Great Belt	Lake IJssel	Kattegat	Lake IJssel	Baltic Sea	North Sea	Baltic Sea	The Sound	Baltic Sea
Capacity [MW]	4.95	2	5	16.8	2.75	4	10.5	40	10
# of turbines	11	4	10	28	5	2	7	20	5
CAPEX [M€]	10	4.5	11.7	23.5	4	4.6	14	46.9	13
Water depth [m]	4	3.5	4.5	1.5	6	8.5	8.5	4	8
Distance [km]	2.3	0.8	6	0.03	3.5	1.6	10.3	2	4
Voltage [kV]	10	10	12	10	10	11	21	30	20

* - Decommissioned [39].

2.3   Current European status

Due to the success of the initial projects and the large growth potential, several northern European countries started to invest heavily in the offshore industry. In fact, since 2001, the offshore installed capacity has increased on average 36.1% per year [15–17]. Figure 2.4 shows that the 1 GW mark of the European installed capacity was reached in 2007, 17 years after the first offshore installation. More surprisingly, the 3 GW mark was almost reached only three years after, in 2010. From 2010 to 2015, the average yearly installation was around 1.6 GW, with the northern European countries contributing the most [15, 16].

Figure 2.5 gives a time-lapse of the locations of the commissioned and under construction offshore projects in the northern European waters for three different years. Up to 2006, 22 offshore projects were commissioned, with Denmark having the largest share with eight projects, while the UK took the second place with five OWFs. From 2006 to 2010, the number of wind farms more than doubled and the installed capacity increased by 222% from 910 MW to 2933 MW [15–17]. During this period of time, Denmark had increased its number of projects to twelve, with a total capacity of 861 MW, representing approximately 29% of the total capacity. Meanwhile, the UK had started to expand its offshore wind industry, having grown circa 241% in that same four-year period. In fact, with the completion of the Lynn and Inner Dowsing project in 2008, the UK dethroned Denmark and became, since then, the offshore wind power world leader [40]. At the end of 2010, the UK had twelve commissioned projects with a total capacity of 1341 MW, representing approximately 46% of the European installed capacity.

The British rapid growth of its installed capacity came from two tendering rounds. The initial Round 1, composed of twelve projects with a total capacity of 1.2 GW, started with the North Hoyle OWF, completed in December 2003, and ended with Teesside commissioned ten years later. A competitive biding process for Round 2 sites was launched in 2003. Differently from the initial approach, the new areas were tendered to prospective developers on a competitive bid basis and were located further offshore (between 8–13 km) to reduce visual and environmental
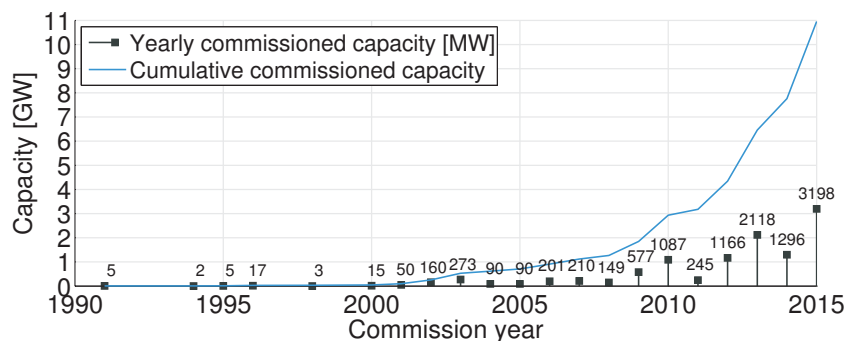
Figure 2.4: Yearly and cumulative offshore commissioned capacity for commissioned and under construction European projects [15–17, 21, 38].

impact [41, 42]. Projects with a combined capacity of 7.2 GW were awarded in Round 2. The first Round 2 project was Gunfleet Sands II, completed in April 2010. On that same year, the UK extended the initial rounds with an additional 2 GW of offshore wind capacity [43].

Currently, there are 7748 MW installed offshore and 3198 MW under construction (totalizing 10.95 GW), representing a 273% growth of the commissioned capacity when compare to 2010

(a) 2006: 22 OWFs, 910 MW   (b) 2010: 43 OWFs, 2933 MW   (c) 2015: 76 OWFs, 10946 MW
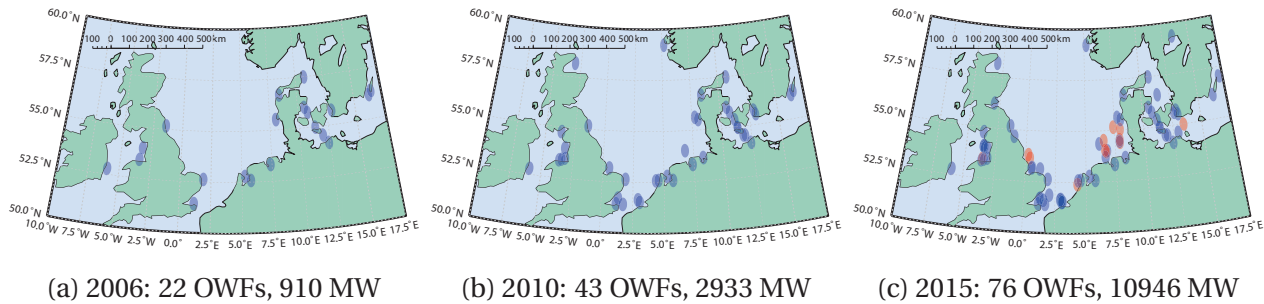
Figure 2.5: Time-lapse of commissioned (blue circles) and under construction (red circles) OWFs in the north of Europe [15–17, 21, 38].

(a) Number of OWFs per country. Others: Sweden 5, Finland 2, Ireland 1, Norway 1, Portugal 1.

(b) Installed capacity (MW) per country. Others: Finland 32.3 MW, Ireland 25.2 MW, Norway 2.3 MW, Portugal 2 MW, Sweden 201.4 MW.

(c) Number of turbines installed per country. Others: Finland 11, Ireland 7, Norway 1, Portugal 1, Sweden 86.

(d) Number of OWFs per sea basin. Others: Atlantic Ocean 1, Ems River 1, Lake Vanern 1, Limfjorden 1.

Figure 2.6: Market shares for commissioned and under construction European OWFs [15–17, 21].

values [15–17]. The 76 European OWFs are distributed among ten countries, with the highest share of offshore projects belonging to the northern European countries (see Figure 2.6a). The UK has the lion share with 46% of the total installed offshore wind capacity (see Figure 2.6b) with 26 offshore projects (commissioned and under construction) which provide more than 3% of all British electricity [44]. Germany ranks second with 16 OWFs (3476 MW), while Denmark is in third place with 13 projects, representing 12% of the existing capacity (Figure 2.6a). These three countries constitute 88% of all the offshore installed capacity in Europe.

Once all the OWFs currently under construction are finalized, a total of 3217 turbines will be supplying energy to European grids. Figure 2.6c shows the turbine distribution among the different countries. The UK takes the lead with a 44% turbine share, followed by Germany with 26%. The average turbine size in the UK is 3.48 MW, while the later entrance in the offshore industry has allowed Germany to have the highest average turbine size (4.14 MW) [15, 16]. Most European projects are located in the northern part, with the North Sea having the biggest share with 42 OWFs (Figure 2.6d), followed by the Baltic Sea with 19 projects and the Irish Sea with 11 OWFs, whereas Portugal is the only country to have an offshore turbine in the south of Europe [45].

Table 2.2 provides key project details for several OWFs built in the second wave of projects in the European offshore wind scene. Denmark commissioned the Horns Rev 1 and Nysted 1 projects which were the first far and large offshore farms with capacities exceeding 100 MW, in 2002 and 2003, respectively. Currently, the UK has the OWFs with the highest installed capacities: London Array 1 and Gwynt y Môr. The former was commissioned in 2013 and consists of 175 wind turbines (Siemens SWT-3.6-120), totalizing 630 MW, making it the project with both the highest installed capacity and number of turbines [15]. Compared to Vindeby, the London Array 1 project has an installed capacity 127 times higher and 164 more turbines. Its CAPEX was 200 times greater and it was placed in waters three times deeper (13 m).

The Gwynt y Môr project, with a capacity nameplate of 576 MW, expected to be commissioned in 2015, is the second largest OWF (its layout is shown in Figure 2.7). It is a complex project not only due to physical – challenging seabed conditions – and human-made constraints – a pre-existing pipeline crosses the project area making it separated in two zones – but also due to the high number of turbines and distance to shore. In 2014, the UK approved the East Anglia 1 OWF [46]. Once completed, the OWF will be composed of circa 240 turbines, totalizing 1200 MW, which is approximately double the capacity of the London Array 1. Recently, the Creyke Beck project, which is composed of two 1.2 GW OWFs, was approved to be built in the Dogger Bank area [47].

Table 2.2: Project details of several European OWFs [15–17, 21, 38].

Project	Horns Rev 1	Nysted 1	Lillgrund	Prinses Amalia	Horns Rev 2	Belwind 1	London Array 1	Riffgat	Gwynt y Môr
Year	2002	2003	2008	2008	2009	2010	2013	2014	2015
Country	Denmark	Denmark	Sweden	Netherlands	Denmark	Belgium	UK	Germany	UK
Location	North Sea	Baltic Sea	The Sound	North Sea	North Sea	North Sea	North Sea	North Sea	Irish Sea
Capacity [MW]	160	166	110	120	209	165	630	108	576
# of turbines	80	72	48	60	91	55	175	30	160
CAPEX [M€]	270	269	200	380	470	614	2000	450	2000
Water depth [m]	10	8	7	22	13	29	13	21	20
Distance [km]	17	11	7	23	30	46	19.5	23	16
Voltage [kV]	150	132	130	150	150	150	150	150	132
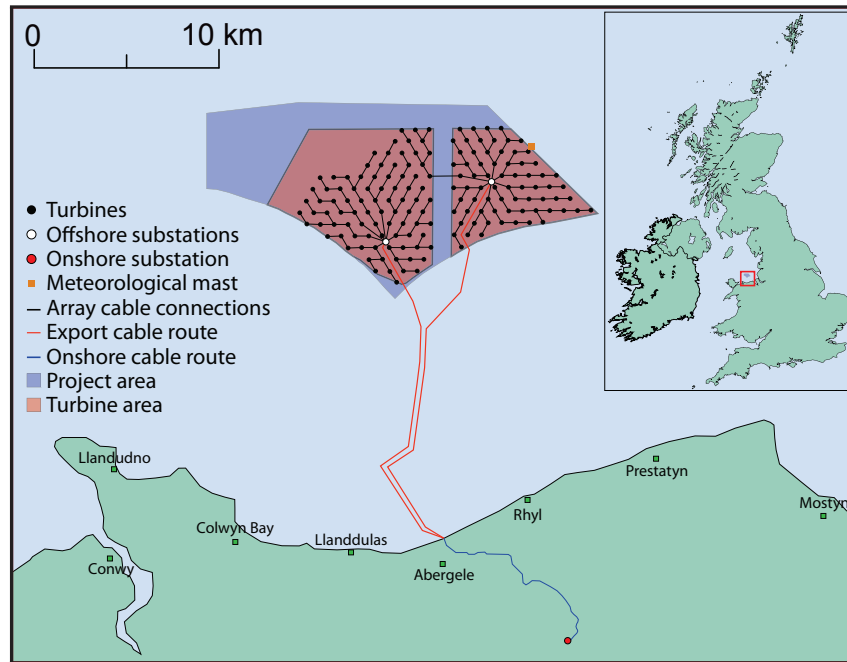
Figure 2.7: Location and layout of the British Gwynt y Môr OWF [48].

2.3.1 Trends

In this section the trends of the main key characteristics of the European OWFs are analyzed.

2.3.2 Installed Capacity

The average size of OWFs has increased since the initial projects. Figure 2.8a shows the projects with the highest and lowest installed capacities and the average project size for each year. Between 2011 and 2012, the average project size more than double from 116 MW to 289 MW [15–17]. In 2015, the average installed capacity of an OWF was circa 59 times higher than the Vindeby project. Although the trend towards larger projects is expected to continue in the coming years [8], Figure 2.8a shows that the average European project size stabilized around 275 MW between 2012-2015 since wind farm developers are planning farms with more modest capacities, although larger projects will be commissioned in the near future [16].

2.3.3 Area and number of turbines

The area used by the projects is not proportional to the installed capacity, since the average capacity for 2015 will be similar to the one in 2012 (Figure 2.8a), whereas the project average area will decrease 27% during the same period (see Figure 2.8b). The developments achieved by the turbine industry can explain this phenomenon. The turbine rated capacities have been raising throughout the years, allowing the OWFs to enlarge their power nameplate without proportionally increasing the number of turbines. This trend can be seen in Figure 2.8c which shows the projects

with the highest and lowest number of turbines per project as well as the average number of turbines per project for each year.

2.3.4 Distance to shore

Another aspect which is also rapidly growing over the years is the average distance to shore (see Figure 2.8d). The first projects registered low distances to shore (<10 km), while over the years, the average distance to shore of the projects has been rapidly increasing. The average distance to shore of projects commissioned in 2013 was around 25 km, value which increased to 42 km in 2015 [15, 16]. Currently, the OWF located the furthest away from shore is the German Global Tech 1 which is being built 127 km away from shore, a distance circa 56 times higher than the modest 2.25 km of the Vindeby project [49].
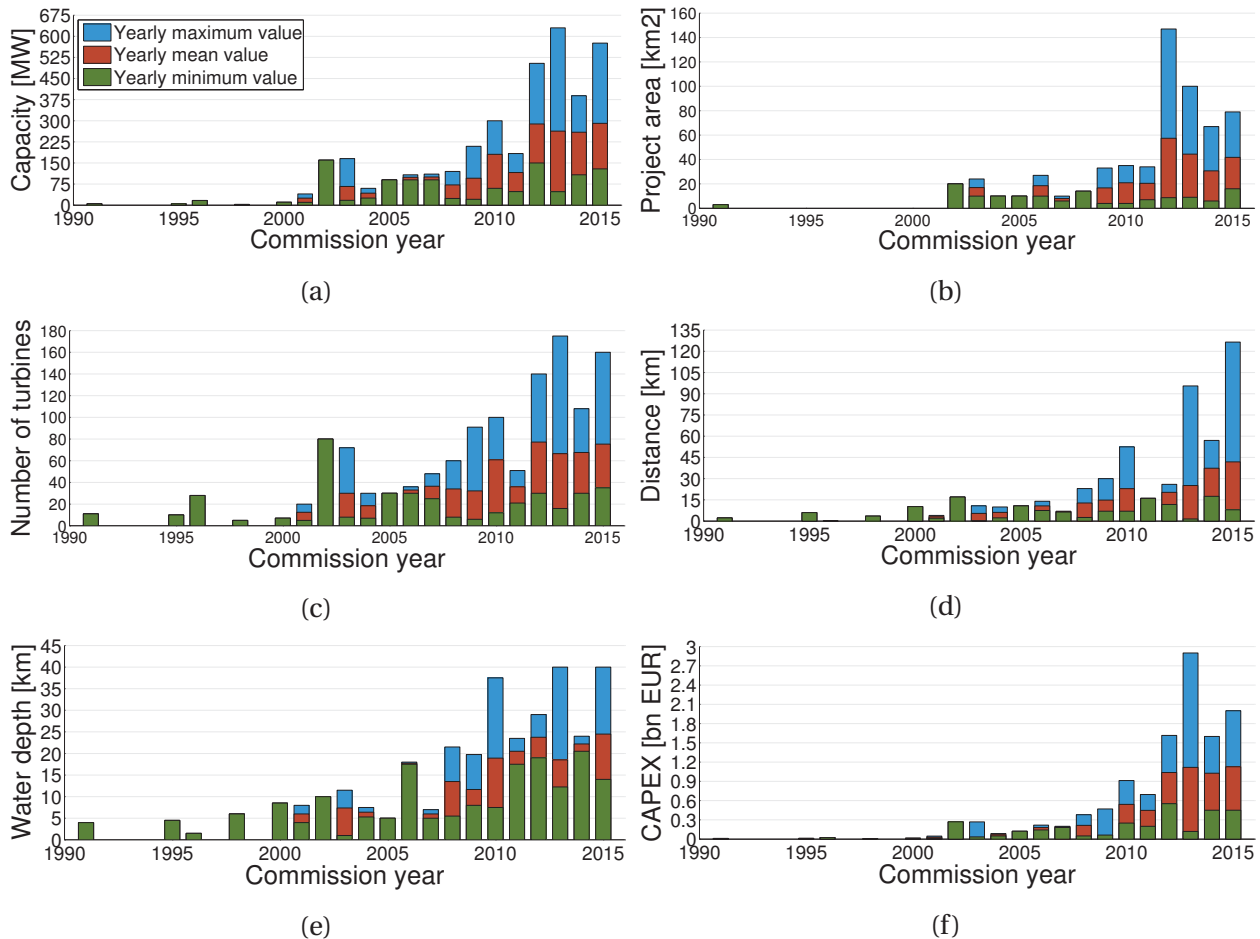
Figure 2.8: Yearly statistics of key characteristics of commissioned and under construction European OWFs composed of five or more turbines [15–17, 21, 38]. The OWFs composed of a single turbine row were considered to have null area.

2.3.5 Water depth

Greater distances to shore usually result in deeper waters. Figure 2.8e shows that the average water depth has increased throughout the years and it is expected to continue [8]. The projects commissioned in 2015 have an average water depth of circa 25 m. In 2010, the deepest waters, using grounded turbines, were conquered with 45 m-high jacket foundations, in the Alpha Ventus wind farm [15]. The next generation of OWFs is expected to be constructed further away from shore at deeper water sites [33].

Costs

Despite the technological advances made in the offshore wind industry, the average project CAPEX is rising, as shown in Figure 2.8f. The higher distances to shore and the deeper water levels may explain the higher capital need of the recent offshore developments since these lead to cost increase of foundations, grid connection and installation [50]. Furthermore, the costs of recent large OWFs increased due to the higher associated risks perceive by the investors [51]. Up to 2014, the most expensive project was the Bard Offshore 1 wind farm with a CAPEX around € 2900 million. It has an installed capacity of 400 MW and is situated at a mean distance of circa 95 km from the coast.

Offshore environments also lead to higher Operational and Maintenance (O&M) costs. These costs can represent up to 30% of the total CAPEX of the project [31]. The main reasons behind these figures are the reduced site access, due to wave and wind conditions, expensive transportation and repair personnel.

2.3.6 Energy production

Similarly to the installed capacity, also the capacity factor of OWFs is increasing. The capacity factor represents the part of the year needed by the wind farm to reach its annual energy production if producing permanently at full power. Table 2.3 shows the capacity factor of several OWFs since construction (the capacity factor of projects with an asterisk is only relative to 2011 [22]). Although the average capacity factor of the Danish projects is 41%, the older projects register low capacity factors. The short distances to shore and low installed capacities – hence low number of turbines – may help explaining the dissatisfactory capacity factors achieved by these projects. Exception is made for the Roland I project, which despite its very short distance to shore, presents a capacity factor of 44.3%. This capacity factor is comparable to the ones anticipated to be achieved in future far and large OWFs installed in the North Sea. Furthermore, four of the turbines of the Roland I project – the Bonus 2.3 MW/82 (now Siemens Wind Power) turbines – are the world's most productive turbines, having surpassed the 100 GWh mark in 2014 [52].

Table 2.3 shows that recent OWFs have higher capacity factors. The Anholt 1 project has achieved a remarkable energy yield level, obtaining a capacity factor of approximately 50%. The first German OWF, alpha ventus, had an average annual yield of 253 GWh between 2011 and 2013, representing

a capacity factor of 48% [53]. Also in 2011, both Horn Rev projects achieved a capacity factor close to 50% [22]. A combination of factors explain the higher capacity factors achieved by recent OWFs:

- They are situated further away from the shore. Higher distances to shore are correlated with higher mean wind speeds (see Figure 2.1);

- They are composed of recent wind turbines which are more reliable and robust. In the past, gearboxes and generators were the main responsible of turbine downtime [22];

- Installation of more turbines helps smoothing the effect of individual turbine availability;

- More knowhow of offshore wind industry. The lack of experience in the harsh offshore environment and the inauspicious weather conditions have led to relative low wind farm availability in the past [22].

Table 2.3: Capacity factor of several European OWFs [15, 16, 22, 52].

Project	Commission year	Capacity factor [%]	Capacity [MW]	Distance to shore [km]
Vindeby	1991	23.2	4.95	2.3
Tuno Knob	1995	30.2	5	6
Middelgrunden	2001	25.5	40	2
Horns Rev I	2002	41.9	160	17
Frederikshavn	2003	30.7	7.6	3.2
Nysted I	2003	37.2	165.6	10.8
Ronland I	2003	44.3	17.2	0.1
Samso	2003	39.4	23	3.5
North Hoyle	2004	34.1	60	7.5
Scroby Sands	2004	29.3	60	2.3
Kentish Flats	2005	30.8	90	10.75
Barrow	2006	34.2	90	7.5
Egmond aan Zee	2006	33.5	108	14
Beatrice*	2007	34.8	10	23
Burbo Bank 1	2007	30.1	90	6.4
Lillgrund	2007	35.1	110.4	7
Horns Rev II	2009	49.2	209.3	30
Hywind*	2009	50.1	2.3	10
Rhyl Flats	2009	33.5	90	8
Sprogo	2009	35.6	21	10.6
Alpha ventus	2010	48.1	60	52.5
Gunfleet Sands	2010	33.8	172.8	7
Robin Rigg	2010	37.4	180	12
Rodsand	2010	44.1	207	8.8
Thanet	2010	31.1	300	11.4
Avedore Holme	2011	38.3	10.8	0.1
Baltic 1	2011	47.2	48.3	16
Walney 1	2011	35.8	183.6	16.2
Anholt 1	2013	50.1	399.6	17.5

2.3.7 Transmission technology

Initial OWFs exported their energy production via MVac transmission systems due to their low installed capacities and close proximity to shore. In fact, MVac has been used as transmission technology only for distances shorter than 15 km and installed capacities up to 100 MW. The industry has used HVac technology for longer distances and higher capacities, since transporting energy with MVac, under these circumstances, was no longer profitable (see Figure 2.9b). Furthermore, these projects required CAPEX values lower than € 300 million, as shown in Figure 2.9c.

In 2002, the Danish Horns Rev 1 became the first project to use high-voltage ac (HVac) transmission technology with a rated voltage of 150 kV. Moreover, the Horns Rev 1 project was revolutionary for its time since it was the first to make use of an offshore transformer station. The need for an offshore transformer came not only from the high installed capacity (160 MW) but also from the average distance of 17 km to shore (see Table 2.2).

Transmissions systems with HVac technology were used at three projects with the highest installed capacities, namely London Array 1, Gwynt y Môr and Greater Gabbard. Despite their high installed capacities (>500 MW) they were erected at distances from shore below 26 km. Belwind 1 and Alpha Ventus are the OWFs which were built the furthest away from the coast and that make use of HVac technology [15, 16]. The former has an installed capacity of 165 MW and a distance to shore of 46 km, while the latter has a 60 MW capacity nameplate and it is situated at 52.5 km from land. Both OWFs were commissioned in the North Sea in 2010.

(a)   (b)

(c)   (d)
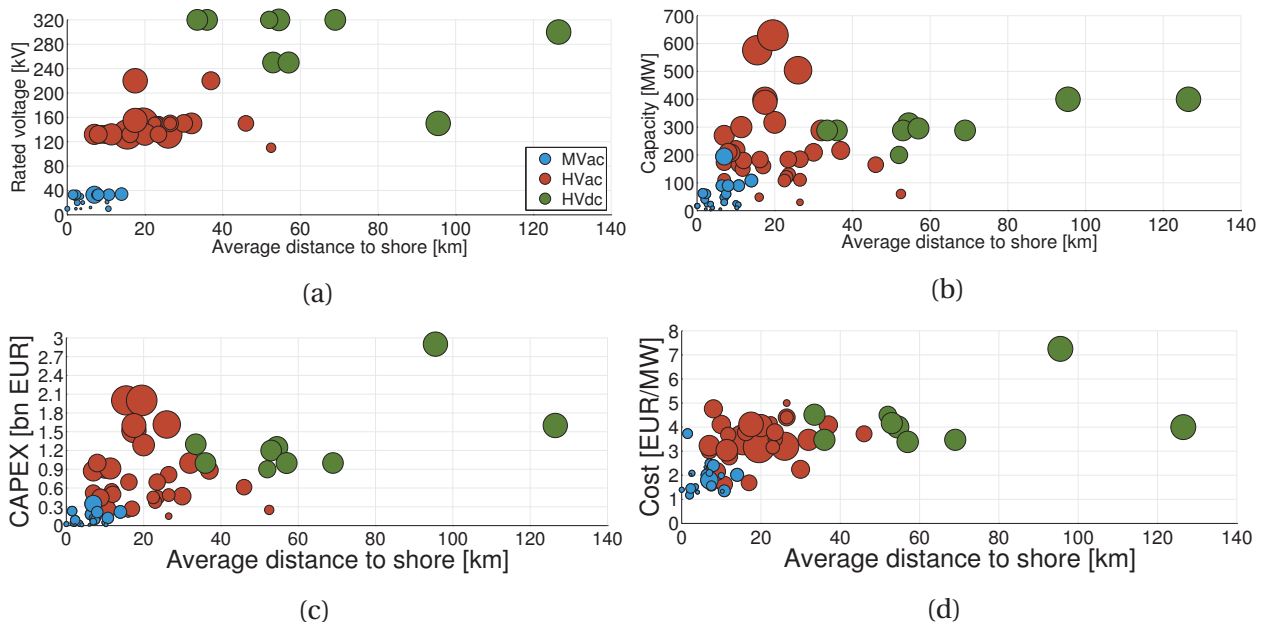
Figure 2.9: Influence of the distance to shore on project's cost, power capacity, transmission voltage level and technology for commissioned and under construction European OWFs composed of five or more turbines [15–17, 21, 38]. Bubble area represents the power capacity of the OWFs.

Thus far, the industry has HVdc as the technology of choice when distances higher than 50 km and installed capacities above 100 MW are considered (Figure 2.9b). Germany is the only country currently building OWFs connected to shore through HVdc technology. Figure 2.10 shows in detail the locations of these German projects, while Table 2.4 provides several project details.

Figure 2.11 shows the installed capacity percentage distribution of the three difference transmission technologies. The HVac technology is used to transport the energy generated offshore of 65% of the installed capacity (≈ 7 GW). HVdc transmissions systems will soon interconnect 3 GW (25%) to shore, whereas the pioneer MVac technology used in the first OWFs, currently has the lowest share, interconnecting circa 1 GW (10% of the installed capacity).

Transmission voltages

Although, the most common voltage levels used with HVac are 132 kV and 150 kV, as shown in Figure 2.9a, the industry is progressing; the first OWFs to employ 220 kV transmission systems were the Anholt farm, commissioned in 2013, and NorthWind, commissioned in 2014 [16]. The Netherlands has approved the Gemini OWF, which is expected to be commissioned in 2017 [54].
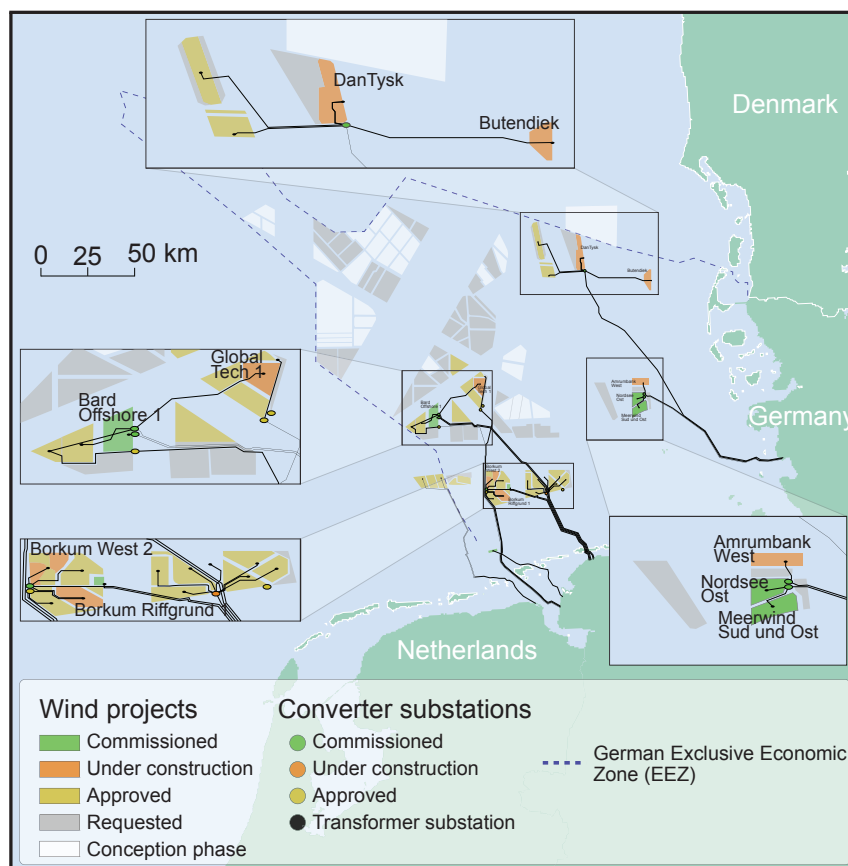
Figure 2.10: German commissioned and under construction projects in the North Sea with HVdc transmission technology [15, 16].

Table 2.4: Project details of commissioned and under construction OWFs with HVdc transmission systems [15, 16].

Project	Bard Offshore 1	Meerwind Sud und Ost	Nordsee Ost	Global Tech 1	Borkum West 2	DanTysk	Butendiek	Borkum Riffgrund 1	Amrumbank West
Year	2013	2014	2014	2015**	2015**	2015**	2015	2015**	2015**
Cost [M€]	2900	1200	1000	1600	1600	1000	1300	1250	1000
Capacity [MW]	400	288	295.2	400	400	288	288	312	288
# of turbines	80	80	48	80	80	80	80	78	80
Water depth [m]	40	24	24	40	31	26	19	26	23
Distance [km]	96	53	57	127	52	69	34	55	36
Voltage [kV]	±150	±250		±300	±320	±320		±320	±320
Substation	BorWin 1	HelWin 1		BorWin 2	DolWin 1	SylWin 1		DolWin 3	HelWin 2
Provider	ABB	Siemens		Siemens	ABB	Siemens		Alstom	Siemens
Converter	CTL	MMC		MMC	CTL	MMC		N/A*	N/A*

N/A - Data not available; ** - Planned (currently under construction).
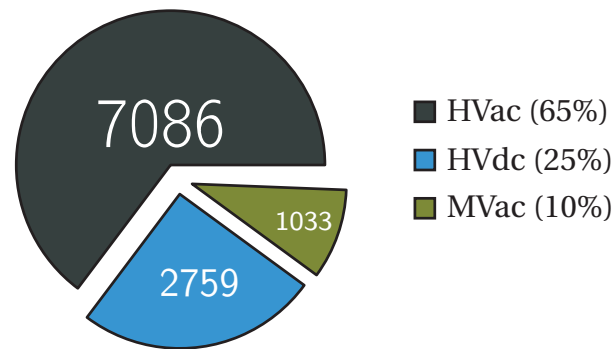
Figure 2.11: Aggregated installed capacity (in MW) per transmission system technology of commissioned and under construction European OWFs, composed of five or more turbine [15–17].

The project will have a total capacity of 600 MW, it will be erected at 85 km from shore and its energy production will be transported to shore via a 220 kV HVac transmission system.

Similarly to the HVac technology, also the HVdc voltage levels have been increasing. The Bard Offshore 1 project, commissioned in 2013, became the first OWF with a HVdc transmission system. It has a ± 150 kV rated voltage and makes use of cascaded two-level converter (CTL) technology from ABB. Currently, five OWFs are being erected, which will utilize modular multi-level converters (MMC) with a ± 320 kV rated voltage (see Table 2.4).

Hitherto, there is no relationship between the rated voltages of the HVdc transmission systems and the installed capacities nor with the projects CAPEX (Figure 2.9). For example, the Global Tech 1 offshore farm, currently under construction, will have an installed capacity of 400 MW and it will be the project located furthest away from shore with an average distance of 127 km (see Table 2.4). It will make use of a ± 320 kV transmission system and it is expected to cost € 1.6 billion. On the other hand, the Bard Offshore 1 has the same installed capacity, it uses a ± 150 kV rated voltage, it was erected 96 km from the coast and cost € 2.9 billion. Analyzing Table 2.4, one might infer that the rated voltage levels are increasing throughout the years and the industry is using the highest rated voltage levels commercially available. For example, the converter that will be hosted in 2019 at the BorWin Delta substation is expected to have a ± 600 kV rated voltage [16].

Investment costs

The projects with MVac transmission systems have the lowest cost per MW installed: 1.9 €/MW (see Figure 2.9d). HVac technology with a cost of 3.4 €/MW places second, whereas projects interconnected via HVdc demand higher investment costs, requiring 4.4 € per MW installed (Figure 2.9c). Among others, the converter and the extra offshore platform required to house it may explain the additional overhead cost. Nonetheless, when the distances and project capacities are high enough, the usage of HVdc transmission systems is still justifiable since, despite the higher CAPEX values, they are still the best option in the long run due to the lower transmission losses [55–57].

2.4   Around the corner

The status quo is expected to be maintained, with the UK and Germany continuing to be the top world players of the offshore wind industry [17]. A study conducted by the financial analysts Ernst&Young placed the UK at the top of the global investors list in offshore wind energy, while Germany, which previously held the first position, is now in second place [58]. Nonetheless, other countries, namely Belgium, the Netherlands and Denmark, have several projects to be tendered in the coming years. Next, it is given the current plans of the northern European countries for the coming years.

2.4.1   Belgium

In 2004, the Belgian federal government determined an area of approximately 260 km^2 on its EEZ for the installation of water, current or wind energy projects. The area, meanwhile reduced to 240 km^2 in 2011, consists of eight project zones (see Figure 2.12) and approximately 2.25 GW may be installed [59]. Currently, Belgium has 712 MW installed in eight different OWFs which are clustered in three main projects:

- C-Power - composed of three projects constructed in different phases (Thornton Bank 1-3);

- Belwind - the main existing project has 165 MW and was built in 2010. In 2013, a 6 MW wind turbine (Alstom's Haliade 150-6MW) was installed as a demonstration project [60];

- Northwind - finished in 2014, with 216 MW, making it the largest Belgian OWF.

The Belgian government has made plans to develop an offshore grid to interconnect the OWFs to the onshore electricity network. In parallel, the Belgian Electricity Act was amended to abolish the previous support for the submarine cable financing in which the Belgian transmission system operator, Elia, had to pay 33% of the submarine cable cost [59]. Elia intends to build two offshore substations (as shown in Figure 2.12) to which the OWFs will be connect to. Elia is also planning to strengthen the electricity grid with a new 380 kV HV line between Zomergem and a new substation in Zeebrugge (see Figure 2.12). This grid reinforcement is vital to allow the energy generated offshore to be exported to the rest of the country.

In 2014, the Belgian federal government approved the conditions for construction and operation of one or more energy atolls [59]. An energy atoll is an artificial island for hydro-electric energy storage, which will stock the excess electricity production of the OWFs by pumping water to a reservoir in the center of the island (see Figure 2.13). Whenever needed, the atoll will inject electricity into the Belgian grid, reducing the inherent wind intermittency problem. Although pumped storage is a proven technology, the Belgian atoll will be the first application to the offshore wind industry. The 2.4 km wide energy atoll will be constructed 3 km from the coast, financed by private industry and requiring five years to be built [14].
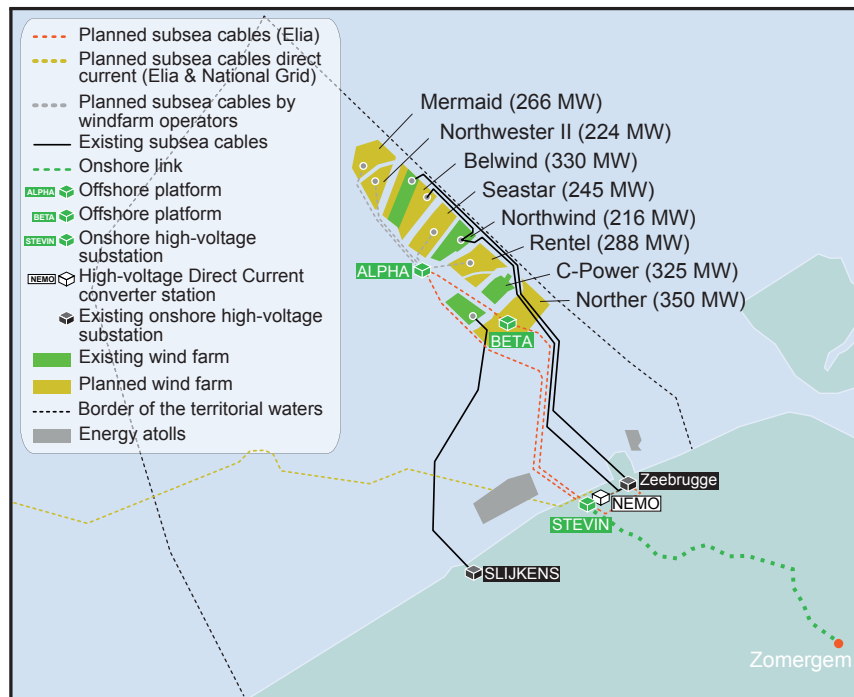
Figure 2.12: Current and planned Belgian offshore projects: OWFs and energy atolls [14, 59].

Figure 2.13: Belgian energy atoll. Illustration by kind permission of DEME.

2.4.2   Denmark

Denmark is expanding its offshore wind installed capacity with 1.35 GW by 2022 [61]. To do so, the Danish Energy Agency is performing transparent and competitive tendering phases. Energinet.dk, which is a non-profit enterprize owned by the Danish Climate and Energy Ministry, will provide the necessary infrastructures for offshore grid connection, Environmental Impact Assessments (EIAs), conduct geotechnical and geophysical surveys and acquire metocean data. Hence, before the tendering phases, the results of the preliminary investigations will be publicly available to provide the possible candidates with important information to assess the profitability of the areas. The objective is to minimize risks and increase competition among tenderers [62]. Energinet.dk will be the responsible for the offshore substations, cabling systems and necessary onshore network reinforcements (these costs will be paid by the electricity consumers directly), whereas the wind farm developers will be in charge of the internal grid of the project [62]. The 1.35 GW are distributed between three main projects: Horns Rev 3 with 400 MW, Kriegers Flak with 600 MW and 350 MW split by several near-shore wind farms. Figure 2.14 shows the location of the projects as well as areas reserved for future plans.

The near-shore tender was recently reduced from its original 450 MW to 350 MW (each wind farm has a 200 MW maximum cap). There are six different areas, located 4 km from the coast, which have been appointed for near-shore wind farms. The wind farms have to be fully commissioned before 2020 and the developers will be responsible for interconnecting the project to the coast. The costs from the coast to the network connection point will be covered by the electricity consumers [62].

These wind farms will be visible from the shore, and hence local support becomes a key part for the projects to be successful. The Danish population has always been supportive of the offshore wind industry: half of Middelgrunden OWF is owned by a cooperative composed of ten thousand private investors (see Section 2.2). In order to maintain local support, the wind farm developers have to offer 20% (not mandatory to be achieved) of the project to private and business sectors. If a 30% share is obtained there will be an extra monetary compensation for the project developer [62].

In addition to the near-shore projects, 50 MW are reserved for turbine prototypes [61]. These turbines are not limited to the six near-shore areas and may be installed in any suitable place. The test projects may be composed of up to eight turbines and have to aim at the reduction of the costs of offshore wind turbines.

The Horns Rev 3 wind farm will have an installed capacity of 400 MW and it be located north of the OWFs Horns Rev 1 and 2. The project, expected to be completed before 2020, has a mean wind speed of 9.8 m/s, water depths varying between 10-20 m and a total area of 200 km^2 [62]. The company Vattenfall Vindkraft A/S won the tender with an electricity price of 103.1 € /MWh [63]. This makes Horns Rev 3 the cheapest OWF in Europe at the moment and it will use a HVac transmission system with a rated voltage of 220 kV.

The Kriegers Flak project will have an installed capacity of 600 MW and it will be located at Kriegers Flak in the Baltic Sea. The area for preliminary investigations has approximately 250 km^2, mean wind speed of 9.5 m/s and the sea depth ranges between 15-30 m [62]. The project may be divided into two sub-areas (200 and 400 MW) due to reservation of the middle part of the area for extraction of raw materials. Data regarding the OWF area has been recently published [64].

The deadline for the commission of the project has been postponed by two years to the end of 2021. The delay was due to the alterations of the grid connection. Initially, it was planned a combined grid connection between Kriegers Flak to Germany and Denmark. However, due to very high price rises of the main HVdc components the plan was canceled, with the grid connection now being based on proven HVac technology [65]. Three companies will provide the cables for the transmission system, namely ABB, LS Cable and System and Nexans. The € 100 million contract for the transmission system represents approximately a fourth of total construction project and its installation will begin in autumn of 2016 [66].

2.4.3   Germany

Although Germany is currently one of the biggest market players of the offshore wind industry, it had to slowdown its offshore wind campaign [67]. In fact, TenneT, the transmission system operator responsible for the interconnection of the German OWFs in the North Sea, froze new agreements for grid connection of German OWFs between 2011-2013. Several reasons may explain this slowdown [68]:

- Uncertainty due to alterations to the regulatory frameworks;
- Technical challenges regarding grid reinforcements;
- Construction of the HVdc transmission systems to interconnect the OWFs to the mainland electricity network.

In 2014, the German target of achieving 10 GW of offshore wind installed capacity by 2020 was amended in the Renewable Energy Act and now a maximum of 6.5 GW is expected until 2020 [68]. Furthermore, the financial benefit rate for new OWFs was altered to 194 € /MWh for eight years, being reduced to 35 € /MWh afterwards [69].

Germany is currently building four different large OWF clusters: BorWin, DolWin, HelWin and SylWin. Each cluster is planned to have several converter platforms which will transport the energy to shore via HVdc. A total installed capacity of circa 10.5 GW, distributed across 13 offshore converter stations, will be commissioned between 2013–2025. Figure 2.15 displays the project clusters along with some key characteristics [15, 16]. According to governmental plans, Germany should have an installed capacity of 15 GW by 2030 [70].
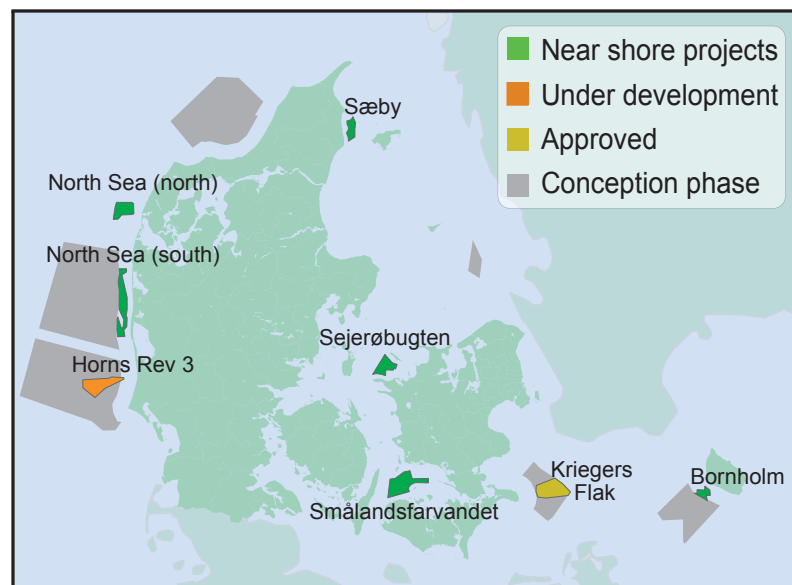
Figure 2.14: Approved, under development and future areas for development of Danish OWFs [62].

Cluster name	Number of converter stations	Aggregated power (GW)	Commissioning years
a. BorWin	5	3.9	2013-2023
b. DolWin	4	3.5	2014-2025
c. HelWin	2	1.27	2014-2015
d. SylWin	2	1.76	2015-2024
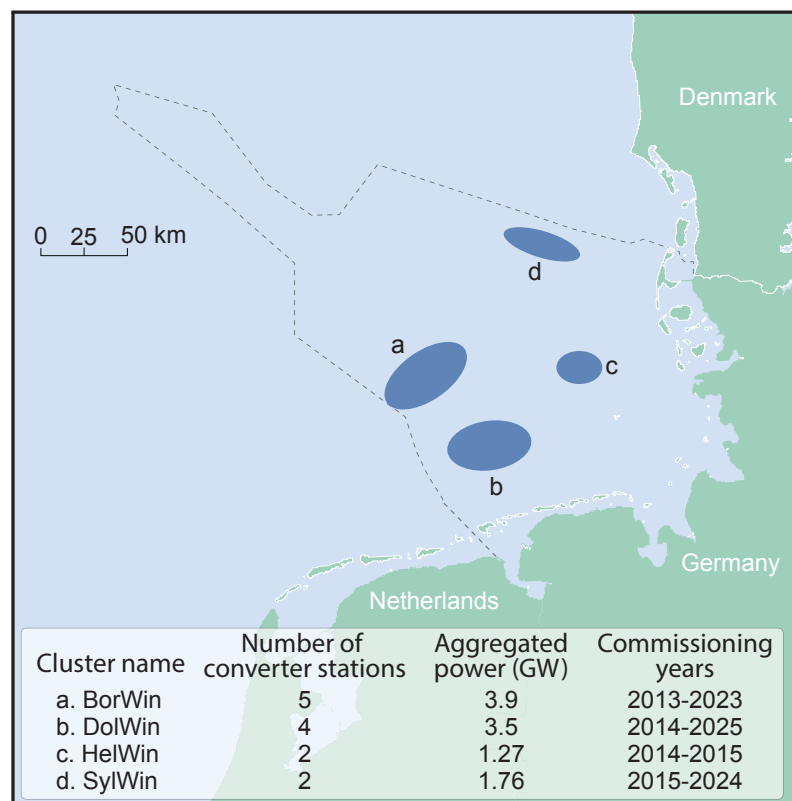
Figure 2.15: German offshore wind clusters in the North Sea [15, 16].

2.4.4 Netherlands

In 2013, the Netherlands defined an Energy Agreement which set as target to increase its renewable energy production by 14% until 2020 [71]. To achieve this target the government has allocated up to € 18 billion to subsidize the offshore wind industry. The Energy Agreement identified the need for an additional offshore capacity of 3.5 GW by 2023. For this purpose, 700 MW licences and respective subsidies will be tendered annually between 2015–2019 [59]. Differently from the initial plan, existing project grants will be canceled and hence, the holders of the current licences will have to participate in the new application procedure. Furthermore, similarly to the Danish approach, governmental agencies will be responsible for the initial site studies and surveys [72].

Several areas, shown in Figure 2.16, have been identified for the development of OWFs. The areas Borssele, IJmuiden Ver, Hollandse kust and Ten Noorden van de Waddeneilanden cover approximately 2900 km^2 (representing 5% of the Dutch EZZ [73]) and have a potential offshore wind capacity of 17.4 GW (assuming an average of 6 MW/km^2) [74]. The new National Waterplan 2016-2021 will allow Hollandse Kust Noord and Zuid Holland to include an additional area inside the territorial waters between the 10 and 12 mile zones as shown in Figure 2.16. This is anticipated to help reducing the development costs of the projects due to the shorter distance to shore [74].

The first tender will be for the Borssele area (see Figure 2.16), which has been divided into four sub-areas. Borssele I and II were tendered in autumn of 2015, whereas Borssele III and IV will be tendered in 2016 [75]. In 2017-2018 the area Hollandse kust Zuid-Holland will be tendered, followed by the Hollandse kust Noord-Holland in 2019.

TenneT, designated operator of the future offshore grid in 2014, will build five 700 MW standard-ized platforms [59]. Each platform will connect two OWFs to the onshore electricity grid via 220 kV cables. This approach is anticipated to cut costs when compared to the usual method in which an OWF is individually connected to shore [59].

2.4.5 United Kingdom

The UK is anticipated to maintain its position as the main European offshore wind driving force, with a third round for site allocations which was launched in June 2008 [19]. The Round 3 programme, the largest commitment to developing offshore renewable energy in the world, will result in several projects being developed until 2020 [76].

In the previous offshore wind tendering rounds, individual project sites had been awarded to developers. However, a zone approach was adopted in Round 3, meaning that wind farm developers were given the exclusive rights for the development of OWFs over larger seabed areas [76]. This allows the developers to explore the potential for offshore wind across their zone and develop individual projects in a more planned and coordinated way.

A total of nine zones were selected after a careful feasibility study to guarantee that all the necessary conditions for OWF development were satisfied, e.g. good wind resources, relatively
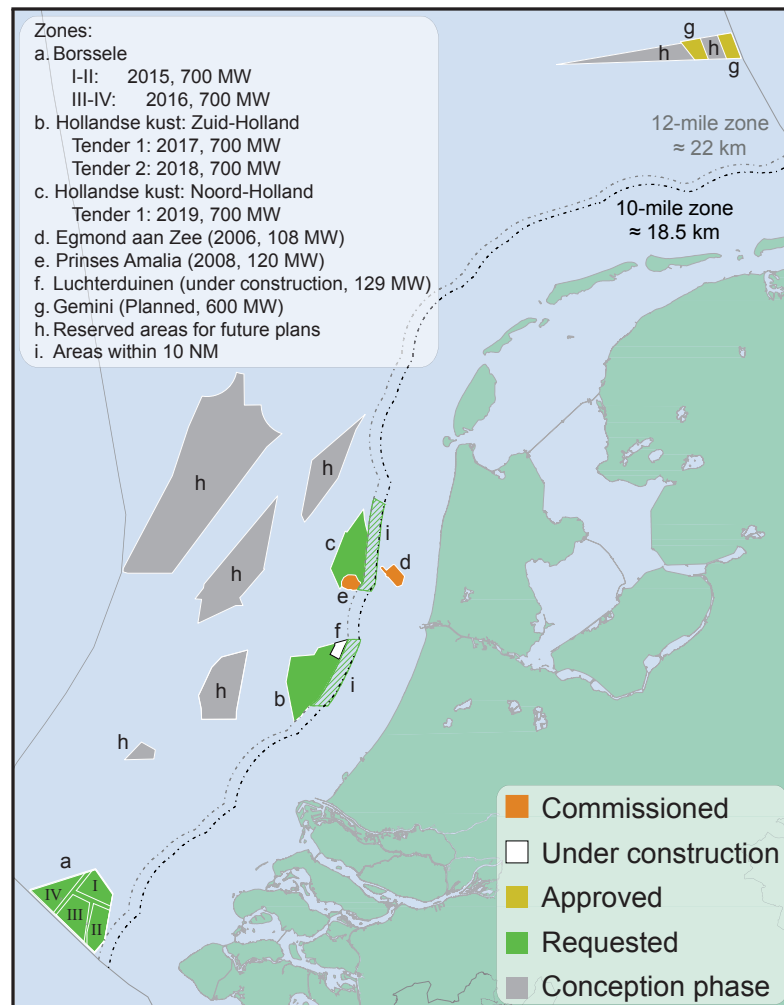
Figure 2.16: Dutch commissioned, under construction, planned and future OWF locations [73,74].

shallow water depths (≤60 m) and favorable ground conditions [76]. Most of the zones have potential for the construction of multiple wind farm sites. The bidding closed in March 2009 with over 40 applications and multiple tenders for each zone. In January 2010, the successful bidders were announced, awarding rights for the development of 32 GW, circa four times higher than Rounds 1 and 2 combined [76].

Since the awarding auction was announced there have been some alterations to the initial plans. The RWE Innology company, the successful bidder of the Bristol Channel Zone, canceled its plan for the area due to economical inviability; the Atlantic Array wind farm, which attracted environmentalists criticism regarding the impact on marine wildlife, would have had an installed capacity of 1.2 GW [77]. Another modification was made by the consortium with the rights to explore the Dogger Bank zone, the largest of Round 3. The initial 9 GW plans were scale down by 20% to a 7.2 GW installed capacity, as the developers preferred to focus on projects with higher probability to succeed [78]. These two alterations led to a final Round 3 programme with 28.9 GW spread across the nine development zones around the UK, as illustrated in Figure 2.17.
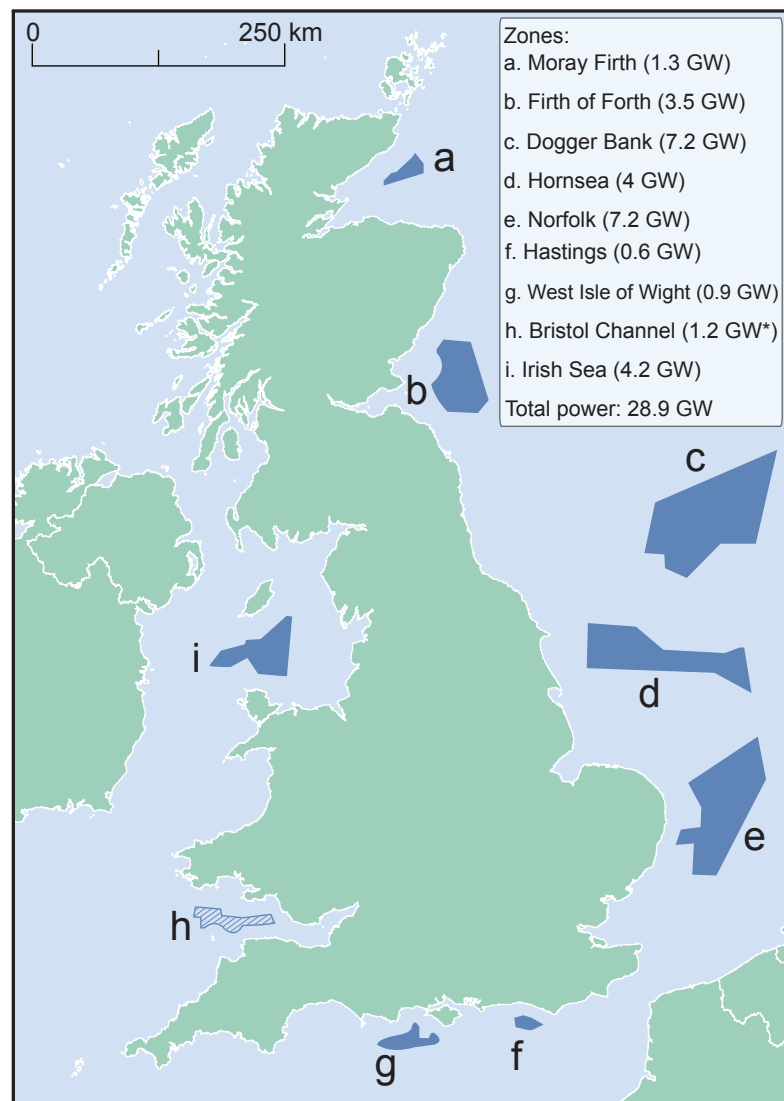
Figure 2.17: Consented areas for the Round 3 phase of the British OWF development (* the Bristol Channel Zone was canceled) [76].

Despite the fast pace with which northern European countries are deploying new turbines offshore, the wind industry is currently behind expectations [3]. The objective of surpassing the 9 GW mark by the end 2013 was not achieved since only circa 6.5 GW were commissioned at that date. Furthermore, hesitating political support for offshore wind industry – especially in key markets such as the British and German ones – led to a decrease of new projects being accepted and delays of planned projects, which will most likely result in an installation plateau until 2015–2016 [79, 80].

2.5 Further ahead

In 2009, the EU and the EWEA indicated that 40 GW of offshore wind capacity would be deployed by 2020 and 150 GW by 2030, from more than 100 OWFs only in the North Sea [81–83]. These predictions need a yearly increase rate of 29.6% and 19.1% to be satisfied, respectively. Figure 2.18 shows that these may represent plausible scenarios since the required growths fall between the average (36.1%) and minimum (8.3%) registered European industry growth rates [84].

In the far future it is expected that countries which currently have very low or no market shares of the offshore wind industry will emerge as key players. Figure 2.19 shows the total offshore wind power capacity of the main world players in the far future (commissioned, under construction, accepted and planned) [17]. The UK, Germany and the Netherlands are anticipated to be the European countries with the highest shares, whereas Brazil, China, Japan and USA are expected to excel outside Europe. Next, it is given an overview of the current status and future plans of these non-European main players.
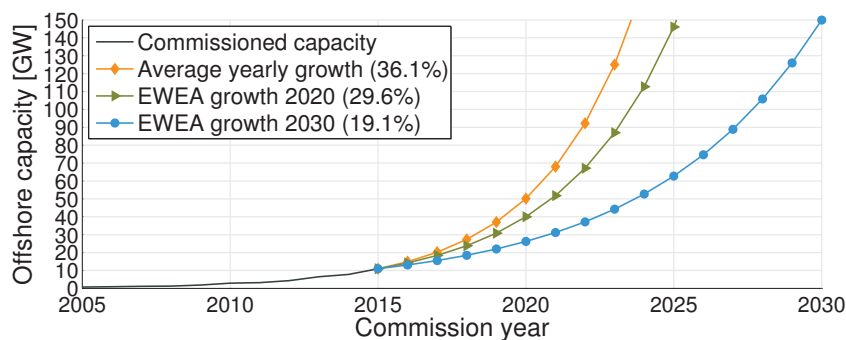
Figure 2.18: Expected offshore wind installed capacity for different growth values.
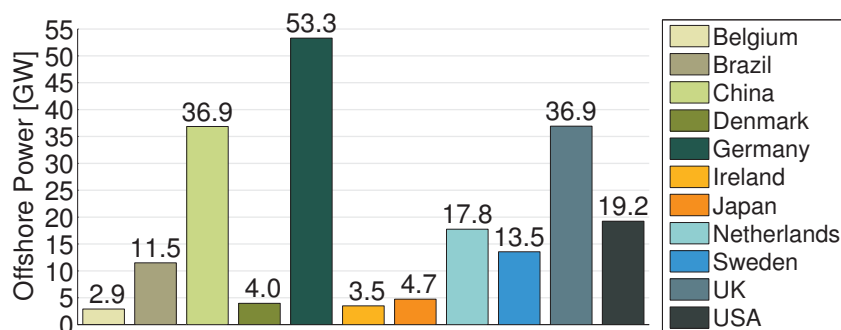
Figure 2.19: Aggregated offshore wind capacity for the main world players (commissioned, under construction, accepted and planned) [17].

2.5.1 Outside Europe

Brazil

According to Brazil's electricity agency, out of the country's 135 GW of total installed capacity only 4.2% comes from its 258 wind farms [85]. Although 350 GW are estimated as the total onshore wind potential, only a small portion can be exploited in practice. Currently, Brazil is still investing in its incipient onshore wind industry: 3 GW are currently under construction and more 6.7 GW have been approved to start construction [85]. Nevertheless, Brazil could still complement its wind energy market by going offshore, as recently mentioned by its new energy minister [86].

One of the biggest technical difficulties to start the offshore wind market in Brazil is measuring or estimating the country's potential. This is mainly due to the lack of offshore wind speed measuring equipment and the extensive 7200 km coastline. Nevertheless, using measurements and data from NASA satellites, together with data provided by Petrobras, the DHN lab and INPE's PIRATA program, it has been estimated that the Southeastern and Southern Brazilian regions (circa 40% of the coastline) have 215 GW of offshore wind power potential in areas up to 100-m water depths [87]. Recently, the total Brazilian offshore potential for water depths up to 100 m was estimated at 606 GW thanks to the higher wind speeds in the Northern and Northeastern regions. It is worth noting that the first 10 km from the coast have an impressive 57 GW potential [88].

Figure 2.20 shows the first Brazilian OWF, Asa Branca, which is being planned by the local company Eolica Offshore since 2002 [89]. The wind farm site, located 5 km offshore, has 270 km^2, an average annual wind speed of circa 9.5 m/s and water depths ranging from 5 to 25 m. The project is expected to have a 12 MW pilot ready by 2016 and a first demonstrator, with a capacity of 258 MW, in 2018 [90]. Eolica Offshore expects to build another 22 offshore wind clusters of 500 MW each to reach a total installed power of 11.2 GW in the next 20 years [90]. Nonetheless, the project is lagging the original plan in which at least 200 turbines should have been installed by now [90].

A second conceptual OWF project is being promoted in Brazil's Northeastern region by Ende Srl [91]. The Italian company is currently assessing the viability of a 288 MW project off the cost of Caucaia, in Fortaleza, and is to start a new feasibility study for another OWF next to the Pecem port [91].

China

China is the second world's largest economy and its recent economic growth has came with an increase of energy consumption. China's energy demand has been mostly met mostly by coal (70%) and oil (19%) power plants, although hydro starts to have a meaningful share [92]. In 2006, the Chinese government set ambitious targets for its renewable energy through the Renewable Energy Law (REL), which requires that 15% of the primary energy comes from renewables sources by 2020 [93]. Nowadays, China has the highest onshore wind installed capacity (96.37 GW) and has plans to install an additional 21.5 GW during 2015, to help meeting the "12th Five-Year national development plan" [94].
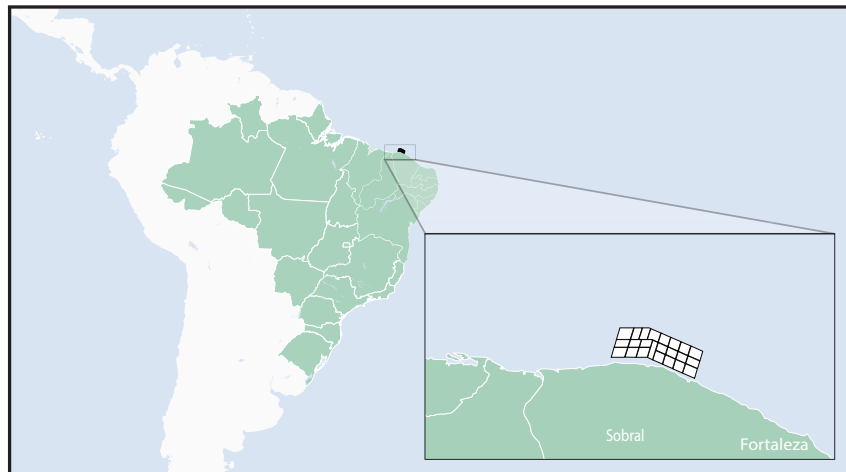
Figure 2.20: Planed location for the Brazilian OWF, Asa Branca [90].

The fast growth of the onshore wind industry has led to turbines which were either not connected to the grid or that could not inject their energy production to the network due to congestion problems [92]. Furthermore, high transmission costs and energy losses have been registered since the main onshore wind resources are located in the northern and western regions of China, whereas the main electricity demand is located along the east coastline [92]. The installation of offshore turbines becomes interesting since the most attractive offshore wind resources are located along the southeast coast and nearby islands [28].

China has the 19th world's largest EEZ and a coastline with more than 18000 km [95]. The development potential is approximately 200 GW at 5-25 m water depth, whereas approximately 500 GW may be harvested in water depths ranging between 5-50 m [95]. Despite China's plan of having 5 GW of offshore wind installed capacity by 2015 and 30 GW by 2020 [93], nowadays only approximately 10% have been commissioned [16]. The Chinese plans for the offshore wind industry are approximately three years behind schedule and hence, the goal is no longer possible to achieve by 2015, but possibly by 2020 [92, 95–97].

Currently there are 414.8 MW of offshore wind power installed and approximately 850 MW under construction (see Table 2.5). Approximately 75% of the existing capacity is installed in intertidal projects, value which will drop to 60% once the projects currently under construction are commissioned. This demonstrates that the Chinese offshore wind industry is starting to increase its campaign in true offshore waters.

Table 2.5 shows that the top turbine suppliers for the Chinese offshore market are Siemens, Goldwind and Sinovel. All manufacturers are presently developing larger turbines, with higher rated capacities and improved reliability [97]. The XEMC Darwind company, originally Dutch [98], has commissioned a 5 MW turbine and is supplying 50 more turbines for the Putian Pinghai project. The turbine of the Suizhong project is located 70 km from the cost but it is connected to an offshore oil platform located 5.5 km aside.

Table 2.5: Project details of the Chinese commissioned and under construction intertidal and OWFs [16].

Name	Turbine manufacturer	Power [MW]	# of turbines	Water depth	Distance to shore	Support Structure	Commission date
Intertidal							
Dafeng	Shanghai Electric	2	1	N/A	N/A	Gravity	2009
DDHI	N/A	2.5	1	N/A	N/A	Suction bucket	2010
Longyuan Rudong	Several	32	16	N/A	5	Several	2010
Rudong 1	Sinovel, Siemens	99.3	38	0-4	4.5	Monopile, Jacket	2012
Rudong 2	Goldwind, Haizhuang	55	21	0-4	4.5	Monopile, High-rise pile cap	2012
Zhongmin Fujian	XEMC Darwind	5	1	0-5	0.001	High-rise pile cap	2012
Tianjin Gagang Binhai	Guodian	33	22	N/A	N/A	N/A	2014
Xiangshui	Golwind, Shanghai Electric	12.5	5	N/A	N/A	High-rise pile cap	2011-13
Rudong 3	N/A	50	20	0-4	4.5	Monopile	2013
Hydropower Rudong 1	Haizhuang	20	10	0-4	6.5	Gravity	2014
Hydropower Rudong 2	N/A	80	32	0-4	6.2	High-rise pile cap	UC
Longyuan Rudong 2	Several	49.2	12	0-5	5	Monopile, Jacket	UC
Rudong 4	Siemens, Envision	200	50	0-4	6.5	Monopile, Multi-pile	UC
Offshore							
Suizhong	Goldwind	1.5	1	30	70	Jacket	2007
Donghai Bridge 1	Sinovel	102	34	10	8	High-rise pile cap	2010
CGN Rudong	Siemens	152	38	8	25	Monopile, Jacket	UC
Donghai Bridge 2	Shanghai Electric	102.2	28	8	8	High-rise pile cap	UC
Longyuan	Siemens	16	4	6	13.5	High-rise pile cap	UC
Putian Pinghai	XEMC Darwind	50	10	13	8.3	High-rise pile cap	UC
Zhuhai Guishan	Guodian, Mingyang	198	66	8	13.4	Monopile, Jacket	UC

N/A - Data not available; *UC* - Under construction.

The Chinese offshore wind industry faces several key challenges which have to be addressed before it may reach the installed capacities already registered by the northern European countries:

- Lack of experience - connecting OWFs to shore is a challenge due to the low capabilities and experience of the utility companies. The problem will be aggravated once the offshore wind industry moves towards further offshore locations and higher installed capacities. Furthermore, the lack of expertise in installation and O&M procedures, suitable vessel fleet and highly-qualified personnel worsens the situation [92];

- Ports - hitherto, existing ports were adapted and used by the offshore wind industry due to the lack of specialized ports for turbine transportation and installation [92]. However, new port will be required since the existing ones will not be able to withstand the demand when the installation pace increases;

- Electricity prices - the investment cost per MW of OWFs is estimated to be 1.5-3 times higher than onshore [28]. The incentive rates were set as 110 € /MWh for projects in inter-tidal areas with waters up to 5 m deep, and 125 € /MWh for projects with waters deeper than 5 m [97]. Nonetheless, although the electricity prices are low [92], they may be enough to attract developers since the return rates for the projects may be as much as 8.2 and 10.3%, respectively [97];

- Reliability - the reliability of the Chinese turbines is lower than the world's average, with the gearbox seeming to be the root of most problems [27]. Some turbine developers are testing gearless solutions which bring many new challenges concerning weight and cost of fabrication and installation. Furthermore, corrosion and heat are also challenges due to meteorological conditions at the Chinese coast;

- Turbine support structures - the Chinese seabed, differently from the European one, is composed of soft and silty soils. Such characteristic brings challenges regarding the foundation and installation solutions. Hence, selecting the most appropriate support and foundation technologies will be key. So far, several types of support structures, e.g. high-pile rise cap, suction bucket and jackets, have been installed in China (see Table 2.5). Nonetheless, there has not been selected the most suitable support structure type;

- Project development - offshore wind developers are required to begin the construction phase within two years after the consent approval. This means that the Chinese developers are reducing the development phase by 2-4 years when compared to Europe [92]. Such strategy may lead to financial benefits if properly conducted. However, there are substantial risks associated since many important decisions are made during this phase, e.g. technology assessment, layout of the OWF, which may result in sub-optimized systems with lower profitability [99, 100].

Japan

Although, the Japanese economy is the 3rd largest and very energy efficient compared to the OECD [101], it is still one of the largest CO_2 emitters in the world [102]. In 2011, after the Fukushima nuclear incident, all nuclear power plants on the east coast were closed, leaving Japan highly dependent on fossil fuels [103]. This led to a rise in the electricity prices since Japan, due to its limited fossil fuel resources [101], had to import liquid natural gas paying approximately € 92 million each day [104]. Realizing that the situation was unsustainable, the Japanese government is aiming at the reduction its fossil fuel dependency and increase of renewable sources, especially the exploitation of offshore wind. Currently, the onshore wind industry is suffering geographical and social problems due to visual impact and low frequency noise [102]. Japan has set the ambitious target of having 37 GW of offshore wind installed (18 and 19 GW with floating and grounded turbines, respectively) power by 2050 [102].

The costs of the offshore wind industry are specially high in Japan due to the lack of suitable infrastructure and experience. In this way, there is a need for extra governmental incentives to encourage private investments in the sector, as well as, funding of new technologies to reduce costs. The Japanese government announced plans to allocate € 63 million to the development of offshore technologies [105]. Since 2014, Japan has the highest feed-in tariff (FIT) for offshore wind (280 € /MWh), surpassing the 180 € /MWh for onshore wind. Nonetheless, there is a believe that a FIT of at least 380 € /MWh is required to attract private investors [106].

Japan has the world's 9th largest EEZ which is approximately twelve times bigger than its land area [10]. Its offshore wind potential is estimated to be approximately 1600 GW with 80% located in waters more than 100 m deep [107]. It is anticipated that only 600 GW may be harvested using grounded (15%) and floating (85%) turbines [102]. Figure 2.21 shows that the highest mean wind speeds registered in Japanese waters are in the north and eastern parts of the coast.

Currently, Japan has 50 MW of offshore wind installed capacity using 28 turbines at 8 locations (see Table 2.6). Although, most of the turbines use ground support structures, Japan is the world's leader in floating developments, having currently three turbines using this technology.

Table 2.6 shows that most of the Japanese turbines have been installed near-shore, with distances up to 3 km and in water depths up to 14 m. The first turbines were erected in 2004 and used high-rise pile caps, technology commonly used onshore [102]. In 2010, the first turbines using monopiles were installed in the prefecture of Ibaraki, whereas in 2013, gravity-based turbines were commissioned 3 km offshore. Although, monopile foundations have the highest European market share [33], they may be vulnerable to seismic activity. Gravity-base foundations are expected to perform better under such circumstances, while jacket foundations suffer lower loads from ocean currents and tsunamis. For this reasons, a hybrid support structure between gravity based and jacket was used to support a wind turbine in the Kitakyushu project in 2013. Even though these near-shore projects do not allow to learn about the true offshore industry, they have provided valuable information of the technical challenges ahead.

Table 2.6: Details of the commissioned and under construction Japanese projects [15–17, 108].

Name	Prefecture	Power [MW]	# of turbines	Water depth	Distance to shore	Support Structure	Commission date
Grounded							
Setana	Hokkaido	1.32	2	13	0.7	High-rise pile cap	2004
Sakata	Yamagata	10	5	4	0.001	High-rise pile cap	2004
Kamisu 1	Ibaraki	14	7	5	0.05	Monopile	2010
Choshi	Chiba	2.4	1	12	3	Gravity	2013
Kamisu 2	Kamisu	16	8	5	0.1	Monopile	2013
Kitakyushu	Ibaraki	2	1	14	1.4	Hybrid jacket-gravity	2013
Floating							
Wind Lens	Kyushu	0.006	2	3	4	Semi-sub	2012
GOTO FOWT	Kabashima	2	1	96	10	Spar floater	2013
Fukushima 1	Fukushima	2	1	125	20	Semi-sub	2013
Fukushima 2	Fukushima	14	2	125	20	Semi-sub & Spar	UC

UC - Under Construction.
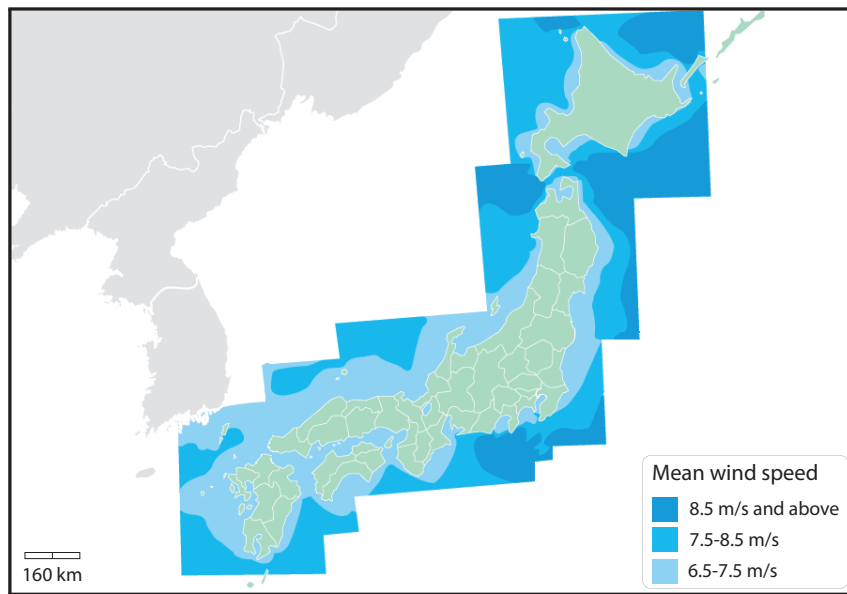
Figure 2.21: Mean wind speeds in Japanese waters [102].

There are plans to expand the near-shore projects Sakata and Kamisu to 37 MW an 250 MW, respectively. A consortium, leaded by Hitachi Zosen Corporation (Hitz), has been granted the possibility of assessing the feasibility of an offshore project in the prefecture of Niigata. The project is anticipated to have 44 Hitachi 5 MW turbines erected 2 km from shore and in water depths of 10-35 m. The construction is expected to begin in 2020 and it will cost € 800 million [109].

Since 2011, the Japanese industry has been doing an extreme push towards the development and testing of floating solutions for offshore turbines. As a result there are currently 3 floating projects operating. The Wind Lens project, led by the Kyushu University, commissioned in 2012 an 18 m diameter floating turbine platform with two 3 kW turbines and photovoltaic panels at 600 m from shore [110]. The next project phase aims at installing a 60 m diameter platform, 2 km from the shore, with 5 turbines and a total installed capacity of 1.3 MW. The first floating Japanese turbine, meanwhile decommissioned, was installed 1 km from the Kabashima Island (Goto City) in the Nagasaki Prefecture in 2012. It was a small-scale turbine (100 kW) and used a floating spar floater [108]. After the successful test, a 2 MW turbine was commissioned in 2013 (see Table 2.6) using also a spar floater, becoming the first full-scale-grid-connected floating turbine in Japan [16].

The Fukushima FORWARD project, carried out by the Japanese Ministry of Economy, Trade and Industry, was kick-started after the Fukushima incident in March 2011 and it has been the flagship testing project for floating wind in Japan [111]. At the first stage of the project, one 2 MW wind turbine was installed 20 km from the coast using a semi-submersible floater (see Table 2.6). At the same time, the world's first floating substation was installed 2 km away from the turbine [112]. It uses an advanced spar floater and a 25 MVA step-up transformer (22-66 kV) to increase the

transmission efficiency. Two 7 MW floating offshore turbines are currently under construction to be installed near the existing turbine [111]. The project is anticipated to be expanded to 1 GW of installed capacity in the far future [102].

As in any incipient technology not everything goes as planned: in December 2014, a hybrid floating turbine sunk 1.2 km off the coast of Kabe Island. This was the second incident since it sunk for the first time in 2013 [16]. Although, there is a steep learning curve for the Japanese industry, the current projects have already allowed for major cost reductions. The first phase of the Fukushima project cost approximately 15500 € /kW, whereas the second phase is expected to cost half. Nonetheless, this cost reduction might not suffice and another reduction of a factor of two seems necessary to allow floating structures to commercially compete wither their ground counterparts [113].

Hitherto, floating support structures are 4-6 times more expensive than their grounded counterpart. Hence, while the floating structures are not cost competitive, Japan is expected to invest in grounded support structure technology. In fact, the grounded support structures are expected to dominate the Japanese market until 2020-2025 [102]. Nonetheless, the existing floating projects have demonstrated technical feasibility and costs are now expected to be reduced. The increased know-how combined with a strengthened supply chain and manufacturing processes will be able to supply the floating structures to commercial-scale projects in the future.

The Japanese offshore industry has several regulatory, infrastructure and technical hurdles that need to be properly tackled to allow a sustained growth of its offshore wind installed capacity [107]:

- Environmental conditions - Japanese OWFs have to resist typhoons, lightning storms, tsunamis, earthquakes, high salinity and freezing temperatures [114]. Hence the design of the turbines has to be adjusted to endure such harsh conditions;

- Research & Development - Although different floating concepts are currently being tested, the most suitable technology to withstand the unique conditions in deep waters around Japan is not clear. Moreover, challenges related to mooring, wake effects, O&M strategies and data collection need to be mastered [107];

- Infrastructure - Despite the strong Japanese maritime industry and a high amount of ports, the port location, size and infrastructure does not perfectly align especially with the offshore wind industry needs. Hence, new port facilities are required to reduce vessels travel time to perform installation and O&M actions [106];

- Vessels - The current projects have been installed near the shore and with only a few turbines. Hence, the Japanese vessel fleet has not been challenged with large and deep offshore projects similar to the recent European projects [106];

- Grid reinforcement - Historically, the Japanese electricity market has been managed mostly at regional level. Hence, the network is not equipped to handle bulk power transmissions across the country and grid upgrades and reinforcement are necessary to allow an increased penetration of energy generated offshore [102];

- Mind-set - Japanese utility companies, used to operate nuclear power plants, are reluctant to a possible penetration increase of renewable sources due to their variable output. In order to motivate their acceptance, the electricity market reform is expected to liberalize the retail market and separate generation, transmission, and distribution roles by 2020 [102]. Furthermore, there are embryonic ideas of forcing utility companies to buy electricity from renewable sources [102];

- Lobbies - The fishing cooperations are very powerful in the Japanese market and hence may act as an impediment in the (long) consent phase of new projects [115]. To overcome this issue, wind developers may involve fishing associations in early project phases, as it as been demonstrated successfully in port projects such as Kabashima, Choshi, and Kitakyushu [114];

- Environmental Impact Assessments - Currently, EIAs are delaying the OWF granting process in Japan [113]. An EIA is typically requiring 3-4 years and is very expensive [102]. The Japanese government has announced that it will take measures to shorten EIA times to 1-1.5 years [102];

- Investment - Hitherto, the investment of the existing projects has comes mostly from the government. For example, the Kabashima project received € 46 million, whereas € 410 million were injected in the Fukushima Forward project by governmental institutions [102]. Nonetheless, the private investment is expected to increase due to the introduction of new FITs. For instance, a part of the funding of the projects Choshi and Kitakyushu came from the business sector [114]. A consortium intends to invest € 1.3 billion, without governmental support, in offshore wind during the next ten years [116].

USA

Although USA has the world's highest onshore wind energy generation [117], currently it has no commercial-scale OWFs in operation even though roughly 80% of all continental electricity demand originates from coastal states [118]. USA has the second world's largest EEZ, covering 11.351.000 km^2 [10] and estimates from the Department of Energy (DOE) indicate that the American offshore wind energy potential is more than 4000 GW along the country's coasts and the Great Lakes area, though only a small fraction can be explored in practice [119].

Despite investing over € 275 million in Research & Development between 2006 and 2014, currently the USA does not have a commercial OWF [119]. Nevertheless, 14 projects, which could potentially add circa 5 GW, are in advanced planning stages [120]. The Northeast States together account for eleven of these offshore development projects which lie in the Atlantic Ocean, whereas the remaining three projects lie off of the coasts of Ohio, Texas, and Oregon [120].

Out of the total ongoing projects, three projects – Fishermen's Energy, Dominion Virginia Power, and Principle Power Windfloat – were awarded up to € 43 million to complete their engineering and construction phases as part of the second stage of the DOE program Offshore Wind Advanced

Technology Demonstration [118]. Overall, the most advanced projects in the USA are the Cape Wind and the Deepwater Block Island projects, which are commencing the construction phase.

These two projects have already guaranteed energy contracts priced at 171 € /MWh for Cape Wind and 224 € /MWh for Deepwater's Block Island and both will have a 3.5% annual price escalation [120]. In comparison, as previously noted, Swedish company Vattenfall Vindkfrat A/S won a tender for Horns Rev 3 at a price of 103.1 EUR/MWh, which makes it the cheapest OWF in Europe. According to the DOE, expected CAPEX costs for a 500 MW farm in the USA are € 2.62 billion, or 5.23 € /MW [120]. Again in contrast, in the EU, in 2015, the median CAPEX of newly installed OWFs was € 1 billion for a median installed capacity of 288 MW, or 3.21 € /MW [15, 16]. This implies that the costs of offshore wind energy in the EU will be circa 33% cheaper than its American counterpart according to the DOE estimates, showing that the Northern EU countries experience has led to lower costs although more expensive technologies, such as HVdc transmission systems, are already being implemented (see Section 2.3.7).

The first American OWF, Cape Wind, was announced more than a decade ago and it has been surrounded by permitting issues, political obstacles, and legal protests [97, 121]. If built, the project, which has an area of 62 km^2 and is located 7 km offshore in the Massachusetts Federal waters off the coast of Cape Cod, will have a installed capacity of 468 MW from 130 Siemens 3.6-MW wind turbines installed with monopile foundations [122]. Although Cape Wind had public-private alliances with National Grid for 50% of its energy production and with the NSTAR utility for 27.5%, these contracts seem to have been terminated due to the offshore wind farm developers being unable to raise funding by the end of 2014 [121].

On the other hand, Block Island is now the first American OWF to secure funding (over € 265 million from French and American banks) and reach the financial close milestone [123]. Following this, Alstom Wind recently announced it had received a formal notice to proceed from Deepwater. As the USA enters the offshore market almost one decade after initial European developments, the average turbine size for commercial projects there is expected to be in the range of 5 MW [120]. The Block Island OWF, when finished, will have an installed capacity of 30 MW coming from five Alstom Haliade 150 6-MW offshore wind turbines [124].

The project is due to start operation in the last quarter of 2016 and installation of foundations is expected to start during 2015 [124]. Given its reduced distance from shore and power ratings, the Block Island export cable, which will be buried about 2 m under the ocean floor, will use MVac technology at 34 kV along its circa 30 km underwater route until the Scarborough State beach where the cable will then proceed to connect to a National Grid's substation in Wakefield [16, 123].

Nevertheless, there are still a few challenges that the American offshore wind industry must overcome before commercial projects become a reality in the USA. The top three identified barriers to the development of offshore wind have been identified as: cost-competitiveness of offshore wind energy, lack of infrastructure, such as offshore transmission assets, and regulatory challenges relating to uncertain and lengthy processes [120].

Regarding competitiveness, electricity prices in the USA have historically correlated to natural gas prices. Recent developments in the American shale-gas industry have driven spot market prices for US natural gas below 2.75 € /MMbtu which could hamper investment in other more expensive alternative generation sources such as wind and solar [125]. Nevertheless, the government plans to retire nearly 40 GW of old coal power plants could be an opportunity to substitute them with renewables sources [120].

The USA needs to provide policy certainty for allowing the development of its domestic offshore wind energy industry. Currently regulatory policies cover three general categories: site leasing processes, environmental and permitting processes and safety compliance [120]. Although federal policies, such as the Renewable Electricity Production Tax Credit (PTC) and the Business Energy Investment Tax Credit (ITC), expired for projects which did not begin construction by the end of 2013, the American government has recently passed an extension of both of these policies through 2015 [120]. However, since the extension maintained the same new definition of commencing construction, it is unlikely that the offshore wind energy industry will benefit from the extension. The importance of a stable and certain policy framework for renewable energy projects can be seen when the PTC expired in 2013: it caused a drop of 92% in new OWF compared to 2012 and a € 21 billion drop in private investment [126].

2.5.2   MTdc networks

Given the current trend of placing larger OWFs further away from shore (see Section 2.3.1), several countries, e.g. USA, China and the northern European countries, are considering the construction of Multi-Terminal dc (MTdc) networks [32, 73, 127–129]. Various initiatives, both in Europe and Asia, have pointed the importance of international electricity markets and of adequate cross-border transmission networks [130–132].

Several drivers promote the development of an offshore MTdc network in the North Sea including renewable energy integration (wind & ocean energy) [133–135], powering oil & gas platforms [136], interconnection of different electricity markets [7, 127, 137, 138] and support of ac grids with ancillary services [127, 139]. Furthermore, MTdc networks are also expected to improve the reliability of the OWFs interconnections to shore by having several connection points to the onshore electricity grids. Most existing OWFs use a single connection to shore, which when malfunctioning, might take the complete farm out of service [131, 140].

There are several crucial challenges that have to be addressed before the development of MTdc networks: system integration, protection mechanisms, dynamic behavior and power flow control [55, 56, 141]. System integration aspects of MTdc networks have been tackled in [127, 130]. The dynamic behavior of MTdc networks has also been extensively analyzed [1, 139, 142]. On the protection aspects, several works have focused on dc faults dynamics [143, 144], detection methods [145], HVdc switch breakers [146, 147] and other protection systems [148, 149]. The development of HVdc breaks is seen as a major drawback that has to be overcome before MTdc networks become a reality [145].

Like the development of the ac networks at the end of the XVIII century, HVdc networks will most likely start as simple grids, having their complexity increased throughout the time with an organic growth [1]. Therefore, standardization is required to allow early built dc transmissions to be integrated in a future MTdc network. For example, converter technology and the dc rated voltage must be similar in order to enhance system harmonization [139, 150]. Currently, there is already a lack of system harmonization between the German HVdc projects under construction: at least five different voltage levels ($\pm$150 kV, $\pm$250 kV, $\pm$300 kV, $\pm$320 kV and $\pm$600 kV) will be used. Technically, an offshore grid based on the same voltage is not necessary since intermediate dc-ac-dc stations could perform the required voltage transformation. However, this would mean higher investments, extra technical challenges and additional system losses [139].

Greenpeace has studied a 70 GW offshore network located in the North Sea which could be achieved between 2020–2030 (see Figure 2.22a). The offshore grid topology proposal aimed at maximizing the cross-border exchange between countries [151]. Figure 2.22b shows a ring-based proposal for a future MTdc network also located in the North Sea from the Dutch Office for Metropolitan Architecture (OMA) [152].

Expecting a similar trend as in Europe, in which the OWFs transmission distance and installed capacity grew steadily as projects developed, the USA is also planning to build an offshore MTdc to facilitate the interconnection of OWFs to the national grid [153]. Current efforts for developing offshore electricity networks, in the USA, are centered around the Atlantic Wind Connection, which will be built in three phases: the New Jersey Energy Link, the Delmarva Energy Link and the Bay Link (see Figure 2.22c) [153]. The grid, which is expect to take over a decade to be developed, will be able to transport 6 GW of offshore wind energy.

In the last years, several asian countries are evaluating the feasibility of an Asian Super Grid (ASG) which would interconnect, via HVdc technology, several countries, namely Japan, China, North and South Korea, Mongolia and Russia (shown in Figure 2.22d) [154]. The project is similar to the DESERTEC project which aims to deploy renewable energy plants in the Middle East and North African countries to meet domestic electricity demand and to export surplus electricity to Europe [155]. The ASG aims to interconnect via HVdc transmission lines locations of high energy demand – Shanghai, Seoul and Tokyo – with regions of large renewable energy potential, such as the Gobi Desert. The overall potential of solar and wind energy of the Gobi Desert is estimated to be 2600 TW [156]. Russia, China and Mongolia would profit by generating electricity inexpensively using fossil fuels and low-carbon renewable resources while North and South Korea and Japan would benefit from a secure energy supply despite their lack of natural resources [155].
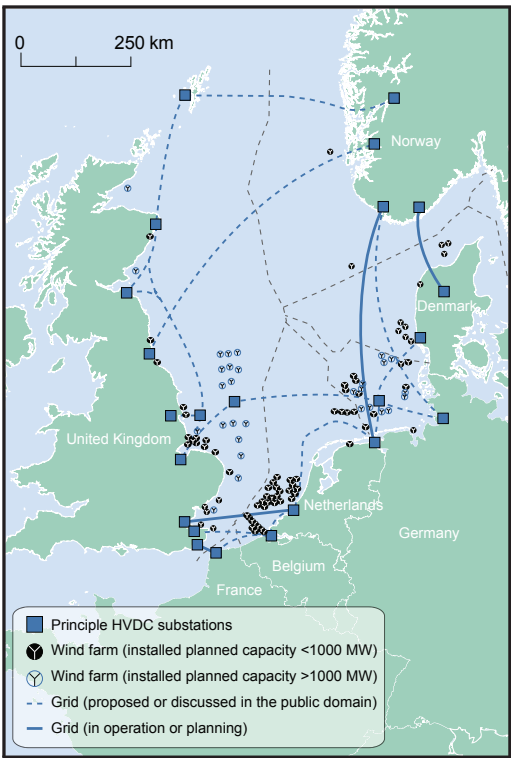
(a) Greenpeace's proposal [151].
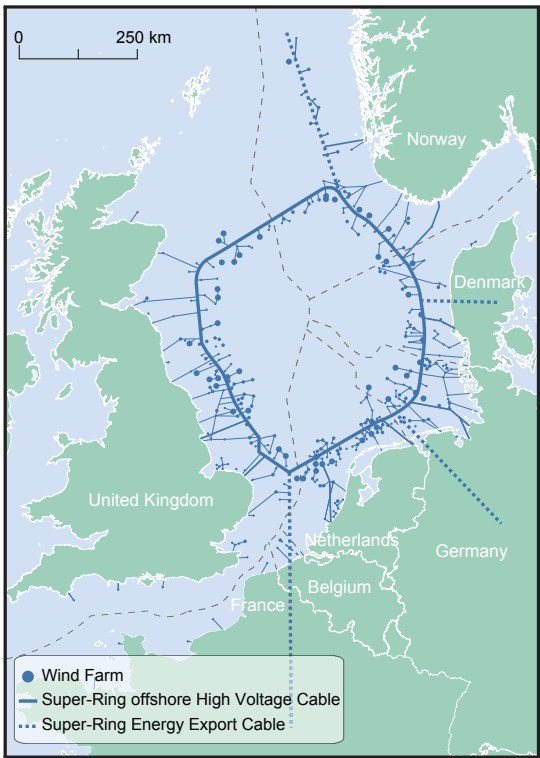
(b) OMA's vision [152].
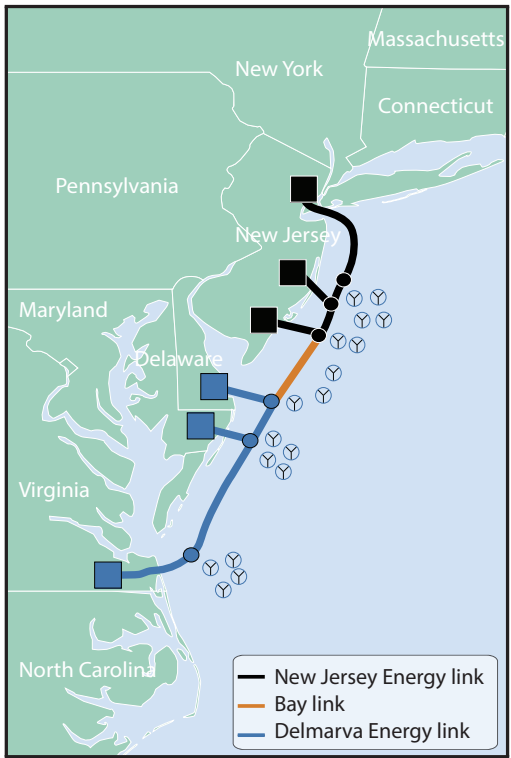
(c) Atlantic Wind Connection [153].

(d) Asian Super Grid [157].

Figure 2.22: Proposals for future MTdc networks.

2.6 Summary

In this paper it was presented the current situation of the offshore wind industry of the main players, as well as, the trends of the key characteristics of the commissioned and under construction European OWFs, namely: commissioning country, installed capacity, energy production, number of turbines, water depth, area, distance to shore, transmission technology and CAPEX.

The analysis showed that the initial OWFs mostly served as proof of concept. Hence, they were located in shallow waters close to shore and were composed of few wind turbines leading to low investment costs which were highly dependent on the number of turbines. Nowadays, commercial projects have higher installed capacities, are highly capital intensive and more complex to design, due to the larger seabed areas, higher number of turbines and longer distances to shore.

The conducted research revealed that the offshore wind installed capacity grew on average 36.1% per year since the first commercial OWF was built in 2001. Currently, there are 7748 MW installed and 3198 MW under construction in European waters representing a 273% growth of the commissioned capacity when compare to the values for 2010. This capacity is distributed among 76 OWFs which belong to ten European countries, with the highest share belonging to the northern European countries: the UK has 46% of the total installed capacity, Germany ranks second with 30%, while Denmark is third with 12%.

The analysis also showed that the projects' area is not increasing at the same pace of the installed capacity due to the release of new turbines with higher rated capacities which allow OWFs to increase their power nameplate without proportionally increasing the number of turbines. The average distance to shore and the water depth are both increasing throughout the years. Although the average investment cost per project is rising with the higher distances to shore and water depths (foundations, grid connection and installation), it is believed that the trend of building OWFs further offshore is to continue.

In the near future, the UK and Germany are expected to remain the largest European investors in offshore wind energy. Germany is building four large OWF clusters with a total installed capacity of 10.5 GW, whereas the UK launched, in 2008, its Round 3 programme for offshore development with a capacity of 28.9 GW. Asian countries have also taken their initial steps offshore, with China currently having 414.8 MW installed offshore and approximately 850 MW under construction. Although, the US has no OWFs, it is anticipated that it will play an important role in the long run.

Several countries are currently considering the construction of MTdc networks to integrate the energy generated offshore due to their advantages: renewable energy integration (offshore wind & ocean energy), powering oil & gas offshore platforms, interconnection of different electricity markets, support of ac grids with ancillary services and increase of the reliability of transmission systems. Nonetheless, several technological challenges gave to be overcome before such networks may become a reality. The EU and the EWEA have predicted 40 GW and 150 GW installed offshore by 2020 and 2030, respectively. These predictions may represent a plausible scenario since

they require a yearly increase rate of 29.6% and 19.1% to be satisfied, which are lower than the 36.1% annual growth average registered since 2001. In conclusion, although prospections for the offshore wind industry future may be difficult to make as they depend on momentary political and economical environments for legal support and financing, they all support the same main principle: the offshore wind exploitation is here to stay.

2.7 Nomenclature

ASG	Asian Super Grid
CAPEX	Capital Expenditure
CTL	Cascaded Two-Level
EEZ	Exclusive Economic Zone
EIA	Environmental Impact Assessment
DOE	Department of Energy
EU	European Union
EWEA	European Wind Energy Association
FIT	Feed-In Tariff
HVac	High-Voltage alternate current
HVdc	High-Voltage direct current
MMC	Modular Multi-level Converter
MTdc	Multi-Terminal direct current
MVac	Medium-Voltage alternate current
OWF	Offshore Wind Farm
O&M	Operation & Maintenance
OMA	Office for Metropolitan Architecture
UXO	UneXploded Ordnance
UC	Under Construction

References

[1] R. Teixeira Pinto, "Multi-terminal dc networks - system integration, dynamics and control," Ph.D. dissertation, Delft University of Technology, Delft, The Netherlands, 2014.

[2] I. E. Agency, "World energy outlook," IEA, Paris, Tech. Rep., 2012.

[3] EWEA, "Where's the money coming from? - Financing offshore wind farms," Tech. Rep., 2013.

[4] EWEA, "Pure power wind energy targets for 2020 and 2030," Tech. Rep., 2011.

[5] Council of the European Union. (2009) Last accessed 3rd August 2015. [Online]. Available: www.consilium.europa.eu/uedocs/cms_data/docs/pressdata/en/ec/110889.pdf

[6] EWEA, "Deep water - the next step for offshore wind energy," Tech. Rep., 2013.

[7] R. Green, and N. Vasilakos, "The economics of offshore wind," *Energy Policy*, vol. 39, no. 2, 2011.

[8] EWEA, "The european offshore wind industry - key trends and statistics 2013," Tech. Rep., 2014.

[9] AWS Truepower. [Last accessed 4th March 2015]. [Online]. Available: www.awstruepower.com/knowledge-center/maps/

[10] Sea Around Us Project. [Last accessed 18th March 2015]. [Online]. Available: www.seaaroundus.org

[11] Intergovernmental Oceanographic Commission and the Man and the Biosphere Programme, "Visions for a change," in *First International Workshop on Marine Spatial Planning*, Paris, France, Nov. 2006.

[12] United Nations. Part v - exclusive economic zone. [Last accessed 19th March 2015]. [Online]. Available: www.un.org/depts/los/convention_agreements/texts/unclos/part5.htm

[13] Belgian Science Policy, "A flood of space - towards a spatial structure plan for sustainable management of the north sea," GAUFRE, Kassel, Germany, Special Report, 2005.

[14] M. V. de Velde *et al.*, "Something is moving at sea...A marine spatial plan for the Belgian part of the North Sea," Belgian Federal Public Service Health, Food Chain Safety and Environment, Tech. Rep., March 2014.

[15] LORC. [Last accessed 1st March 2015]. [Online]. Available: www.lorc.dk/offshore-wind-farms-map/list

[16] 4C Offshore. [Last accessed 23rd March 2015]. [Online]. Available: www.4coffshore.com/windfarms

[17] The Wind Power. (2014) [Last accessed 1st March 2015]. [Online]. Available: www.thewindpower.net/windfarms_offshore_en.php

[18] S.-P. Breton, and G. Moe, "Status, plans and technologies for offshore wind turbines in europe and north america," *Renew. Energy*, vol. 34, pp. 646–654, 2009.

[19] P. Higgins, and A. Foley, "The evolution of offshore wind power in the United Kingdom," *Renew. and Sustainable Energy Reviews*, vol. 37, no. 0, pp. 599–612, 2014.

[20] A. Madariaga *et al.*, "Current facts about offshore wind farms," *Renew. and Sustainable Energy Reviews*, vol. 16, no. 5, pp. 3105–16, 2012.

[21] M. Bilgili, A. Yasar, and E. Simsek, "Offshore wind power development in europe and its comparison with onshore counterpart," *Renew. and Sustainable Energy Reviews*, vol. 15, no. 2, pp. 905–15, 2011.

[22] J. Kaldellis, and M. Kapsali, "Shifting towards offshore wind energy – Recent activity and future development," *Energy Policy*, vol. 53, no. 0, pp. 136–148, 2013.

[23] X. Sun, D. Huang, and G. Wu, "The current state of offshore wind energy technology development," *Energy*, vol. 41, no. 1, pp. 298–312, 2012.

[24] J. Wu, Z.-X. Wang, and G.-Q. Wang, "The key technologies and development of offshore wind farm in china," *Renew. and Sustainable Energy Reviews*, vol. 34, no. 0, pp. 453–462, 2014.

[25] Z.-Y. Zhao *et al.*, "Development route of the wind power industry in china," *Renew. and Sustainable Energy Reviews*, vol. 34, no. 0, pp. 1–7, 2014.

[26] Z. yu Zhao *et al.*, "A critical review of factors affecting the wind power generation industry in china," *Renew. and Sustainable Energy Reviews*, vol. 19, no. 0, pp. 499–508, 2013.

[27] X. Jin *et al.*, "A review on wind power industry and corresponding insurance market in china: Current status and challenges," *Renew. and Sustainable Energy Reviews*, vol. 38, no. 0, pp. 1069–1082, 2014.

[28] L. Hong, and B. Moller, "Feasibility study of china's offshore wind target by 2020," *Energy*, vol. 48, no. 1, pp. 268–277, 2012.

[29] A. C. Levitt *et al.*, "Pricing offshore wind power," *Energy Policy*, vol. 39, no. 10, pp. 6408–6421, 2011.

[30] M. Dicorato *et al.*, "Guidelines for assessment of investment cost for offshore wind generation," *Renew. Energy*, vol. 36, no. 8, pp. 2043–2051, 2011.

[31] M. I. Blanco, "The economics of wind energy," *Renew. and Sustainable Energy Reviews*, vol. 13, no. 6-7, pp. 1372–1382, 2009.

[32] EWEA, "The European offshore wind industry - key trends and statistics 2012," Tech. Rep., 2013.

[33] EWEA, "The european offshore wind industry - key trends and statistics 2014," Tech. Rep., 2015.

[34] N. Nikolaos, "Deep water offshore wind technologies," Master's thesis, University of Strathclyde, Scotland, 2004.

[35] P. Garrett. (2012, June) Can the uk's offshore progress continue? [Last accessed 20th March 2015]. Wind Power Monthly. [Online]. Available: www.windpowermonthly.com/article/1134082/uks-offshore-progress-continue

[36] T. Weaver, "Financial appraisal of operational offshore wind energy projects," *Renew. and Sustainable Energy Reviews*, vol. 16, no. 7, pp. 5110–20, 2012.

[37] J. H. Larsen, "The world's largest off-shore windfarm, middelgrunden 40 mw," Copenhagen Environment and Energy Office (CEEO), Tech. Rep., 2001.

[38] Renewables Map. [Last accessed 1st March 2015]. [Online]. Available: www.renewables-map.co.uk/windfarm.asp

[39] D. Weston. (2014, Sept.) Vattenfall's yttre stengrund decommissioned. [Last accessed 22nd March 2015]. Wind Power Offshore. [Online]. Available: www.windpoweroffshore.com/article/1313014/gallery-vattenfalls-yttre-stengrund-decommissioned

[40] E. Schroeder, "Turning offshore wind on," *California Law Review*, vol. 98, no. 5, pp. 1631–68, Oct. 2010.

[41] EWEA, "Positive environmental impacts of offshore wind farms," Tech. Rep., 2012.

[42] S. Mangi, "The Impact of Offshore Wind Farms on Marine Ecosystems: A Review Taking an Ecosystem Services Perspective," *Proc. of the IEEE*, vol. 101, no. 4, pp. 999–1009, April 2013.

[43] The Crown Estate, "Submarine cables and offshore renewable energy installations - proximity study," London, United Kingdom, Tech. Rep., 2012.

[44] The Crown Estate, "Energy and infrastructure outlook 2014-15 Offshore wind," London, United Kingdom, Tech. Rep., 2014.

[45] D. Roddier *et al.*, "WindFloat - A floating foundation for offshore wind turbines," *Renew. and Sustainable Energy*, vol. 033104, no. 2, pp. 1–34, 2010.

[46] Iberdrola, "Planning consent granted for east anglia one offshore windfarm," Iberdrola, Tech. Rep., 2014.

[47] The Stationery Office Limited, "The dogger bank creyke beck offshore wind farm order 2015," Tech. Rep. 318, Feb 2015.

[48] RWE , "Facts & figures - gwynt y mor offshore wind farm," RWE, Tech. Rep., 2014.

[49] GlobalTech1. [Last accessed 22nd March 2015]. [Online]. Available: www.globaltechone.de/en/about/

[50] European Environment Agency, "Europe's onshore and offshore wind energy potential - an assessment of environmental and economic constraints," European Environment Agency, Tech. Rep. 6, 2009.

[51] International Energy Agency, "Technology roadmap wind energy," Tech. Rep., 2013.

[52] Energy Numbers. (2014, Feb) Capacity factors at danish offshore wind farms. [Last accessed 4th March 2015]. [Online]. Available: www.energynumbers.info/capacity-factors-at-danish-offshore-wind-farms

[53] alpha ventus. (2014, Feb) First terawatt-hour offshore power. [Last accessed 4th March 2015]. [Online]. Available: www.alpha-ventus.de/index.php?id=80

[54] Gemini, "Gemini 600 MW Dutch offshore wind power," Tech. Rep., 2014.

[55] R. Teixeira Pinto *et al.*, "A novel distributed direct-voltage control strategy for grid integration of offshore wind energy systems through mtdc network," *IEEE Transactions on Industrial Electronics*, vol. 60, no. 6, pp. 2429–41, 2013.

[56] S. Rodrigues *et al.*, "Optimal Power Flow Control of VSC-based Multi-Terminal DC Network for Offshore Wind Integration in the North Sea," *IEEE Transactions on Emerg. and Selected Topics in Power Electronics*, vol. 1, no. 4, pp. 260–8, 2013.

[57] I. Erlich *et al.*, "Offshore Wind Power Generation Technologies," *Proc. of the IEEE*, vol. 101, no. 4, pp. 891–905, April 2013.

[58] The Crown Estate, "Offshore wind operational report 2014," London, United Kingdom, Tech. Rep., 2014.

[59] Loyens and Loeff, "North Sea offshore wind - Developments in Belgium and the Netherlands," Rotterdam, The Netherlands, Tech. Rep., Nov 2014.

[60] Alstom. (2014) [Last accessed 22nd March 2015]. [Online]. Available: www.alstom.com/Global/Power/Resources/Documents/Brochures/offshore-wind-turbine-6mw-robust-simple-efficient.pdf

[61] Danish Energy Danish. (2014, Sept.) New certainty for the danish offshore tenders - revised timeline for kriegers flak. [Last accessed 22nd March 2015]. [Online]. Available: www.ens.dk/en/supply/renewable-energy/wind-power/offshore-wind-power/large-scale-offshore-wind-tenders

[62] Danish Energy Agency, "New Offshore Wind Tenders in Denmark," Tech. Rep., Feb. 2013.

[63] Danish Ministry of Climate, Energy and Building. (2015, Feb.) Denmark gets cheaper power from offshore wind turbines. [Last accessed 16th March 2015]. [Online]. Available: www.kebmin.dk/en/news/denmark-gets-cheaper-power-from-offshore-wind-turbines

[64] Energinet.dk. (2015, March) Kriegers flak wind farm data. [Last accessed 16th March 2015]. [Online]. Available: www.energinet.dk/EN/ANLAEG-OG-PROJEKTER/Anlaegsprojekter-el/Kriegers-Flak-havmoellepark/Sider/data.aspx

[65] Danish Energy Agency. (2014, Sept.) New certainty for the danish offshore tenders - revised timeline for kriegers flak. [Last accessed 16th March 2015]. [Online]. Available: www.ens.dk/en/supply/renewable-energy/wind-power/offshore-wind-power/large-scale-offshore-wind-tenders

[66] Energinet.dk. (2015, Feb.) Kriegers flak wind farm grid connection. [Last accessed 16th March 2015]. [Online]. Available: www.energinet.dk/EN/ANLAEG-OG-PROJEKTER/Nyheder/Sider/200-km-kabler-til-nettilslutning-af-Kriegers-Flak-havmoellepark.aspx

[67] T. W. Overton. (2015, March) German offshore wind capacity surging. [Last accessed 16th March 2015].
POWER. [Online]. Available: www.powermag.com/german-offshore-wind-capacity-surging/

[68] E&E Publishing LLC. (2014, July) E.u. offshore wind targets look iffy as france and germany fall behind.
[Last accessed 16th March 2015]. [Online]. Available: www.eenews.net/stories/1060002437

[69] G. O. W. E. Foundation, "Current situation - offshore wind energy in germany," Tech. Rep., July 2014.

[70] Offshore-Windenergy.net. (2014, July) Wind farms. [Last accessed 16th March 2015]. [Online].
Available: www.offshore-windenergie.net/en/wind-farms

[71] L. Donat *et al.*, "Assessment of climate change policies in the context of the european semester -
country report the netherlands," Ecologic Institute and eclareon, Berlin, Germany, Tech. Rep., Jan.
2014.

[72] Netherlands Enterprise Agengy. (2015) [Last accessed 17th March 2015]. Berlin, Germany. [Online].
Available: www.rvothema4.pleio.nl

[73] Netherlands Enterprise Agency, "North sea 2050 spatial agenda," Ministerie van Economische Zaken,
The Hague, The Netherlands, Tech. Rep., Sept. 2014.

[74] Netherlands Enterprise Agency, "Rijksstructuurvisie windenergie op zee (in dutch)," Ministerie van
Economische Zaken, The Hague, The Netherlands, Tech. Rep., Sept. 2014.

[75] Netherlands Enterprise Agency, "Borssele wind farm zone project & site description," Ministry of
Economic Affairs, Tech. Rep., Dec. 2014.

[76] The Crown Estate, "Round 3 Offshore Wind Site Selection at National and Project Levels," London,
United Kingdom, Tech. Rep., 2013.

[77] The Crown Estate, "Wales highlights," London, United Kingdom, Tech. Rep., 2014.

[78] Forewind, "Fisheries update 3 - fisheries feedback helps shape dogger bank teesside a & b application,"
Forewind, Tech. Rep., 2014.

[79] Global Wind Energy Council, "Global Wind Report - Annual market update 2013," Tech. Rep., 2013.

[80] EWEA, "Squeezing wind energy: the financial crisis," Tech. Rep., 2012.

[81] European Commission. [Last accessed 1st March 2015]. [Online]. Available: www.eur-lex.europa.eu/
LexUriServ/LexUriServ.do?uri=CELEX:52008DC0768:EN:HTML

[82] EWEA, "Oceans of Opportunity - Harnessing Europe's largest domestic energy resource," EWEA, Tech.
Rep. September, 2009.

[83] EWEA, "2030 targets Bringing certainty," Tech. Rep., 2013.

[84] E. Ochieng *et al.*, "Future for offshore wind energy in the United Kingdom: The way forward," *Renew.
and Sustainable Energy Reviews*, vol. 39, no. 0, pp. 655–66, 2014.

[85] ANEEL. Capacidade de Geracao do Brasil (in Portuguese). [Last accessed 10th March 2015]. [Online].
Available: www.aneel.gov.br/aplicacoes/capacidadebrasil/capacidadebrasil.cfm

[86] D. Weston. (2015, Jan.) New brazilian energy minister looks to offshore wind. [Last accessed 19th
March 2015]. Wind Power Offshore. [Online]. Available: www.windpoweroffshore.com/article/
1328610/new-brazilian-energy-minister-looks-offshore-wind

[87] F. Pimenta, W. Kemption, and R. Garvine, "Combining meteorological stations and satellite data to evaluate the offshore wind power resource of Southeastern Brazil," *Renew. Energy*, vol. 33, no. 11, pp. 2375–2387, 2008.

[88] G. P. Ortiz, and M. Kampel, "Potencial De Energia Eolica Offshore Na Margem Do Brasil," in *V Simposio Brasileiro de Oceanografia*, 2011, pp. 1–4.

[89] Eolica Tecnologia. (2015) [Last accessed 10th March 2015]. [Online]. Available: www.eolica.com.br

[90] M. Storrer, P. Garcia, and E. E. Barbosa, "The Asa Branca offshore wind farm - A change for the creation of a new cluster for the supply of 10+ GW of multimegawatt wind turbines in Brazil," in *European Offshore Wind 2009 Conference & Exhibition*, Sweden, 2009.

[91] Tenproject. Offshore wind energy - progettazione, studi di fattibilita e studi paesaggistici (in italian). [Last accessed 10th March 2015]. [Online]. Available: www.tenproject.it/#!eolico-offshore/c1624

[92] S. Wyatt *et al.*, "Detailed appraisal of the offshore wind industry in china," Carbon Trust, London, United Kingdom, Tech. Rep., July 2014.

[93] KPMG China, "China's 12th five-year plan: Overview," KPMG, Tech. Rep., March 2011.

[94] J. Yang. (2015, March) [Last accessed 20th March 2015]. Wind Power Monthly. [Online]. Available: www.windpowermonthly.com/article/1338971/china-connect-215gw-new-capacity-2015

[95] L. Junfeng, and et. al., "China wind energy outlook," Tech. Rep., 2012.

[96] W. Qi. (2013, June) [Last accessed 20th March 2015]. Wind Power Monthly. [Online]. Available: www.windpowermonthly.com/article/1187293/analysis-china-unable-achieve-5gw-offshore-wind-goal-2015

[97] F. Shen. (2014, July) China three years late on installing offshore wind farms. [Last accessed 20th March 2015]. Bloomberg. [Online]. Available: www.bloomberg.com/news/articles/2014-07-16/china-three-years-late-on-installing-offshore-wind-farms

[98] XEMC Darwind. [Last accessed 20th March 2015]. [Online]. Available: www.darwind.nl

[99] J. F. Herbert-Acero *et al.*, "A review of methodological approaches for the design and optimization of wind farms," *Energies*, vol. 7, no. 11, pp. 6930–7016, 2014.

[100] S. Rodrigues *et al.*, "Wake losses optimization on offshore wind farms with moveable floating wind turbines," *Elsevier Energy Conversion and Management*, vol. 89, pp. 933–941, January 2015.

[101] R. S. Jones, and M. Kim, "Europe's onshore and offshore wind energy potential - an assessment of environmental and economic constraints," OECD Economics Department Working Papers, Tech. Rep. 6, 2013.

[102] A.-K. Govindji, R. James, and A. Carvallo, "Appraisal of the offshore wind industry in japan," Carbon Trust, Tech. Rep., Oct. 2014.

[103] Internation Energy Agency. (2012) [Last accessed 20th March 2015]. Internation Energy Agency. [Online]. Available: www.iea.org/statistics/statisticssearch/report/?country=JAPAN=&product=electricityandheat&year=Select

[104] M. D. Franco. (2013) [Last accessed 20th March 2015]. north america Wind Power. [Online]. Available: www.nawindpower.com/e107_plugins/content/content.php?content.11350

[105] D. Weston. (2015, Jan.) Japan budgets $68m for offshore. [Last accessed 19th March 2015]. Wind Power Offshore. [Online]. Available: www.windpoweroffshore.com/article/1329528/japan-budgets-68m-offshore

[106] Japanese Wind Power Association. (2014) Jwpa's opinion on the decision of fit for fy 2014. [Last accessed 22nd March 2015]. [Online]. Available: www.jwpa.jp/pdf/fitopinion_2014.pdf

[107] Carbon Trust, "Offshore wind japan project - mapping existing technology solutions to barriers identified in japan's offshore wind industry," London, United Kingdom, Tech. Rep., 2014.

[108] Main(e) International Consulting LLC, "Floating offshore wind foundations: Industry consortia and projects in the united states, europe and japan - an overview," Maine, USA, Tech. Rep., May 2013.

[109] M. Foster. (2015, Feb.) Analysis: Japan moves forward with offshore plans. [Last accessed 19th March 2015]. Wind Power Offshore. [Online]. Available: www.windpoweroffshore.com/article/1333241/analysis-japan-moves-forward-offshore-plans

[110] Y. Ohya. (2012) Highly efficient wind and water turbines with wind-lens technology & offshore floating energy farm. [Last accessed 20th March 2015]. [Online]. Available: www.japan.ahk.de/fileadmin/ahk_japan/events_2012/5_Kyush_Uni_Prof_Ohya.pdf

[111] Fukushima Offshore Wind Consortium, "Fukushima floating offshore wind farm demonstration project (fukushima forward)," Tech. Rep.

[112] Global Wind Energy Council, "Japan's offshore wind development speeding off," Tech. Rep., Sept. 2013.

[113] C. Watanabe. (2013, Nov.) Fukushima floating offshore wind project seeks to halve cost. [Last accessed 20th March 2015]. Bloomberg. [Online]. Available: www.bloomberg.com/news/articles/2013-11-28/fukushima-floating-offshore-wind-project-seeks-to-halve-cost

[114] NEDO, "Nedo offshore wind energy progress edition ii," New Energy and Industrial Technology Development Organization, Tech. Rep., July 2013.

[115] A. Bossler. (2013, Sept.) Floating turbines - japan enters the stage. [Last accessed 20th March 2015]. Wind Power Offshore. [Online]. Available: www.windpoweroffshore.com/article/1211680/floating-turbines---japan-enters-stage

[116] D. Thorpe. (2013) [Last accessed 20th March 2015]. global trader. [Online]. Available: www.gtglobaltrader.com/news/japanese-consortium-invest-%C2%A3962m-offshore-wind-power

[117] J. Walker. (2015, Jan.) A pleasant surprise: USA, not China, is 1 in Wind Energy. [Last accessed 23rd March 2015]. Into the Wind. [Online]. Available: www.aweablog.org/blog/post/a-pleasant-surprise-usa-not-china-is-1-in-wind-energy

[118] Energy.gov. Offshore wind advanced technology demonstration projects. [Last accessed 20th March 2015]. Office of Energy Efficiency & Renewable Energy. [Online]. Available: www.energy.gov/eere/wind/offshore-wind-advanced-technology-demonstration-projects

[119] Wind and Water Power Technologies Office, "U.s. department of energy wind and water power technologies office funding in the united states - offshore wind projects," Tech. Rep., July 2014.

[120] U.S. Department of Energy, "Offshore wind market and economic analysis 2014 annual market assessment," Tech. Rep. DE-EE0005360, Sept. 2014.

[121] J. O'Sullivan. (2015, Jan.) Two utilities opt out of cape wind. [Last accessed 20th March 2015]. The Boston Globe. [Online]. Available: www.bostonglobe.com/metro/2015/01/06/major-setback-for-cape-wind-project/kggnYeAXRj03PyfIUn2iIM/story.html

[122] Cape Wind. Cape wind project overview. [Last accessed 20th March 2015]. [Online]. Available: www.capewind.org/what/overview

[123] Deep Water Wind. (2015, March) Block island wind farm now fully financed. [Last accessed 20th March 2015]. Deep Water Wind. [Online]. Available: www.dwwind.com/news

[124] Alstom. (2015, March) Alstom announces a major milestone for deepwater's block island offshore wind project. [Last accessed 20th March 2015]. Alstom. [Online]. Available: www.alstom.com/press-centre/2015/3/alstom-announces-a-major-milestone-for-deepwaters-block-island-offshore-wind-project/

[125] U.S. Energy Information Administration. [Last accessed 20th March 2015]. [Online]. Available: www.eia.gov/naturalgas/weekly/

[126] A. W. E. Association. (2014, Dec.) Awea urges clean energy supporters in congress and white house to work to pass two-year extension of critical tax policies. [Last accessed 20th March 2015]. American Wind Energy Association. [Online]. Available: www.awea.org/MediaCenter/pressrelease.aspx?ItemNumber=7004

[127] EWEA, "Twenties project - final report," Tech. Rep., 2013.

[128] EWEA, "Wind in power: 2012 european statistics," Tech. Rep., 2013.

[129] Wind Energy, "Wind Energy - The Facts Part II Grid Integration," Brussels, Belgium, Tech. Rep., 2009.

[130] The North Seas Countries Offshore Grid Initiative, "Recommendations for guiding principles for the development of integrated offshore cross border infrastructure," Tech. Rep., 2012.

[131] OffshoreGrid, "Offshore Electricity Infrastructure in Europe," OffshoreGrid, Tech. Rep., October 2011.

[132] e Highway2050, "Modular development plan of the pan-european transmission system 2050," European Commission, Tech. Rep. WP 2 Developing the Grid architecture options as a function of the retained scenarios, 2012.

[133] J. F. Chozas, H. C. Soerensen, and M. Korpas, "Integration of Wave and Offshore Wind Energy in a European Offshore Grid," in *Proceedings of the Twentieth International Offshore and Polar Engineering Conference*, vol. 7, Beijing, China, 2010.

[134] Global Wind Energy Council, "Global Wind Report - Annual market update 2010," Tech. Rep., 2010.

[135] EAEM, "The UK Offshore Wind Industry," Tech. Rep., 2012.

[136] M. Hyttinen, J. O. Lamell, and T. F. Nestli, "New Application of Voltage Source Converter (VSC) HVDC to be Installed on the Gas Platform Troll A," in *CIGRÉ*, Paris, 2004.

[137] R. L. Hendriks *et al.*, "Developing a Transnational Electricity Infrastructure Offshore : Interdependence between Technical and Regulatory Solutions," in *Power and Energy Society General Meeting*, 2010.

[138] N. Ahmed *et al.*, "HVDC SuperGrids with modular multilevel converters - The power transmission backbone of the future," in *International Multi-Conference on Systems, Signals and Devices*, March 2012, pp. 1–7.

[139] S. Rodrigues, "Dynamic Modeling and Control of VSC-based Multi-terminal DC Networks," Master's thesis, Energy Department, Instituto Superior Técnico, Lisbon, Portugal, Dec 2011.

[140] The Crown Estate, "A guide to an offshore wind farm," London, United Kingdom, Tech. Rep., 2010.

[141] S. Rodrigues *et al.*, "Optimization of social welfare and transmission losses in offshore mtdc networks through multi-objective genetic algorithm," in *Power Electronics and Motion Control Conference (IPEMC)*, 2012, pp. 1287–1294.

[142] R. T. Pinto *et al.*, "Description and comparison of dc voltage control strategies for offshore mtdc networks: Steady-state and fault analysis," *European Power Electronics Journal*, vol. 22, no. 4, pp. 13 – 21, 2013.

[143] E. Kontos, R. Pinto, and P. Bauer, "Effect of power flow control methods on the dc fault response of multi-terminal dc networks," in *Industrial Electronics Society, IECON 2014 - 40th Annual Conference of the IEEE*, Oct 2014, pp. 2075–2081.

[144] Y. Zhang, N. Tai, and B. Xu, "Fault analysis and traveling-wave protection scheme for bipolar hvdc lines," *Power Delivery, IEEE Transactions on*, vol. 27, no. 3, pp. 1583–1591, July 2012.

[145] E. Kontos *et al.*, "Impact of hvdc transmission system topology on multiterminal dc network faults," *Power Delivery, IEEE Transactions on*, vol. PP, no. 99, pp. 1–1, 2014.

[146] J. Hafner, and B. Jacobson, "Proactive hybrid hvdc breakers - a key innovation for reliable hvdc grids," in *The electric power system of the future - Integrating supergrids and microgrids*, Bologna, 2011.

[147] C. Franck, "Hvdc circuit breakers: A review identifying future research needs," *Power Delivery, IEEE Transactions on*, vol. 26, no. 2, pp. 998–1007, April 2011.

[148] J. Suonan *et al.*, "Distance protection for hvdc transmission lines considering frequency-dependent parameters," *Power Delivery, IEEE Transactions on*, vol. 28, no. 2, pp. 723–732, April 2013.

[149] E. Kontos *et al.*, "Optimization of limiting reactors design for dc fault protection of multi-terminal hvdc networks," in *Energy Conversion Congress and Exposition (ECCE)*, 2014, pp. 5347–5354.

[150] R. Teixeira Pinto, and P. Bauer, "The Role of Modularity Inside the North Sea Transnational Grid Project - Modular Concepts for the Construction and Operation of Large Offshore," in *Renew. Energy World Europe Conference*, Italy, 2011.

[151] Greenpeace, "A North Sea electricity grid [R]evolution," Tech. Rep., 2008.

[152] The Office for Metropolitan Architecture. (2008) A masterplan for a renewable energy infrastructure in the north sea. [Last accessed 1st March 2015]. [Online]. Available: www.oma.eu/projects/2008/zeekracht

[153] Atlantic Wind Connection. Atlantic wind connection. [Last accessed 20th March 2015]. [Online]. Available: www.atlanticwindconnection.com/awc-projects/atlantic-wind-connection

[154] P. A. Kastmann *et al.*, "The transition to green energy in china, japan and korea," Innovation Norway, Tech. Rep., 2013.

[155] P. Elsner, "Desertec global grid corridor feasibility study," Birkbeck University of London, Tech. Rep., Aug. 2011.

[156] S. Mano *et al.*, "Gobitec and asian super grid for renewable energies in northeast asia," Fraunhofer, Tech. Rep., Jan. 2014.

[157] K. Byong-Chol. (2014, Aug.) Kepco wants grid linked to Japan. [Last accessed 23rd March 2015]. [Online]. Available: www.koreajoongangdaily.joins.com/news/article/Article.aspx?aid=2993919

Multi-Objective Optimization of Wind Farm Layouts

Currently, Offshore Wind Farms (OWFs) are designed to achieve high turbine density to reduce costs. However, due to wake interferences, densely packing turbines reduces energy production. Having insight into optimized trade-offs between energy production, capital investment and operational costs would be valuable to OWFs designers. To obtain this insight, the design of OWFs should be formulated as a multi-objective optimization problem. How to best solve a Multi-Objective Wind Farm Layout Optimization Problem (MOWFLOP) is however still largely an open question. It is however known that evolutionary algorithms (EAs) are among the state-of-the-art for solving multi-objective optimization problems. This work studies the different features that an MO Evolutionary Algorithm (MOEA) should have and which Constraint-Handling Techniques (CHTs) are suitable for solving MOWFLOP. We also investigate the relation between problem dimensionality/complexity and the degrees of freedom offered by different turbine-placement grid resolutions. Finally, the influence of problem size on algorithm performance is studied. The performance of two variants of the recently introduced Multi-Objective Gene-pool Optimal Mixing Evolutionary Algorithm (MOGOMEA) is compared with a traditional and a novel version of the Nondominated Sorting Genetic Algorithm II (NSGA-II). Five CHTs were used to assess which technique provides the best results. Results on a case study with different OWF areas demonstrate that one variant of MOGOMEA outperforms the NSGA-II for all tested problem sizes and CHTs.

3.1 Introduction

In 2007, the European Union (EU) targeted to generate 20% of its energy consumption through renewable sources and to improve the energy efficiency by 20% compared to 1990 levels, by 2020 [1]. Renewable energy sources are anticipated to help Europe meeting these targets. Among other renewable sources, such as hydro, solar and onshore wind, the northern European countries have been investing in Offshore Wind Farms (OWFs) for more than two decades due to higher and steadier mean wind speeds offshore compared to onshore and lower visual impact [2, 3].

The EU and the European Wind Energy Association (EWEA) estimated that the joint installed capacity of European OWFs will be 40 GW by 2020 and 150 GW by 2030 [1, 4, 5]. These predictions require a yearly increase rate of the offshore installed capacity of 29.6% and 19.1% to be satisfied, respectively [6]. Figure 3.1 shows that these predictions may represent plausible scenarios since the required growths are below the average European industry growth (36.1%) since 2002, when the first large-scale OWF was built [7, 8].

The European OWFs haver become larger throughout the years, with the average area reaching almost 60 km^2 in 2012 (see Figure 3.2a). Similarly, also the number of turbines per OWF has been increasing, as can be seen in Figure 3.2b. Projects commissioned from 2002 until 2011 had on average 39 turbines, whereas between 2012 and 2015, they have approximately 72 turbines.

Despite the important lessons learned by developers and technological advances achieved in recent years, the cost of energy generated offshore is not yet competitive. In fact, without encouragements and incentives from governments, the industry would probably not consider offshore wind [6, 9]. Since 2012, OWFs have been very capital intensive, costing on average € 1 billion (see Figure 3.2c). The Gwynt y Môr project, with an installed capacity of 576 MW and commissioned in 2015, is the second-largest OWF, costing € 2 billion (its layout is shown in Figure 3.3). It is a complex project due to the challenging seabed conditions and human-made constraints (a pre-existing pipeline crosses the project area, separating it into two zones). These high costs are mainly due to the larger seabed areas, large distance to shore, large water depth and large number of turbines [7, 8, 10].
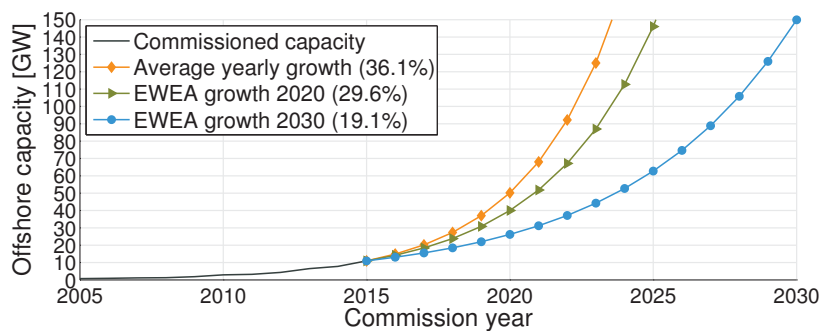
Figure 3.1: Joint installed capacity of offshore wind farms at different growth rates.

(a)

(b)

(c)
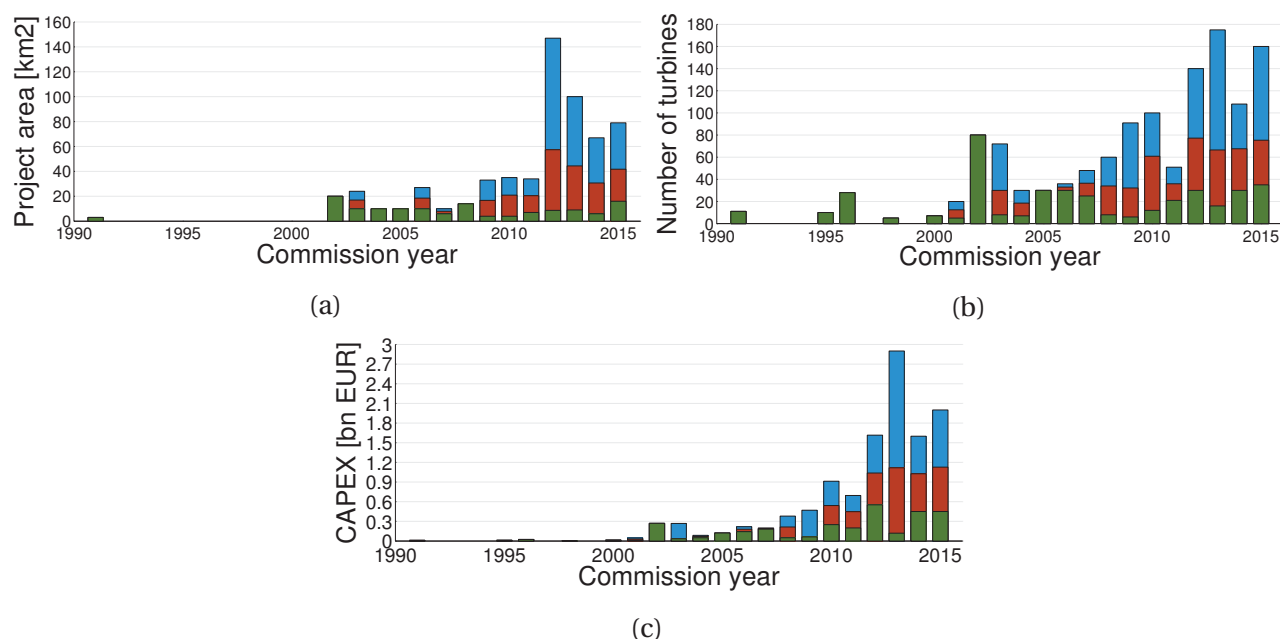
Figure 3.2: Yearly statistics of area, number of turbines and CAPEX of European OWFs with five or more turbines commissioned and under construction since 2002 [7, 8, 10–12].
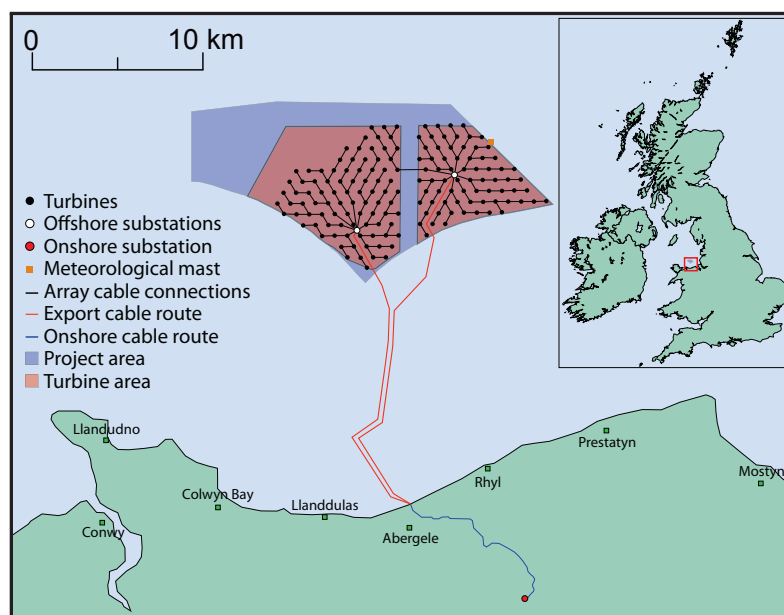
Figure 3.3: Layout of the British Gwynt y Môr OWF. Reproduced from [13].

One possible strategy to decrease the cost of energy of an OWF, is to increase its energy yield [9]. OWFs are usually designed with a high turbine density due to limitations on space and to reduce Capital Expenditure (CAPEX) on, for example, cables to interconnect the turbines [14]. However,

turbines induce wake interferences on other turbines. For example, the energy produced at the Danish OWF, Horns Rev 1, is 89% of what the same turbines together would produce if installed solitarily [15]. Therefore, wake effects are considered to be the strongest economical driver and designers create layouts that maximize the turbines' exposure to the prevailing wind direction to increase energy production [16, 17].

Designing the initial OWFs was simple because of the low number of turbines and homogeneity of depth and seabed soil properties. The layout was primarily defined by placing the turbines in regular structures with greater distances in the prevailing wind direction [18]. Optimizing the design of recent OWFs is a much more challenging task because it requires the analysis of sophisticated trade-offs between conflicting goals, most notably Annual Energy Production (AEP), CAPEX and Operational Expenses (OPEX). As previously noted, state-of-the-art OWFs are composed of a larger number of turbines and have more challenging seabed areas with depths and soil conditions that vary across the site [16]. Approximately 4% of the CAPEX of an OWF is allocated to the development phase [19]. In this phase, in addition to the layout, all the components and technologies to be used, have to be decided [20]. For such vast projects, automated optimization tools are crucial to ensure that optimized layouts are designed in this phase [21].

The Wind Farm Layout Optimization Problem (WFLOP) is a very difficult problem to solve [22]. It is non-linear, multi-modal, non-differentiable, non-convex, discontinuous and cannot be described analytically (without making vast simplifying assumptions) [18]. Moreover, due to various characteristics of the WFLOP, calculus-based approaches such as linear programming and gradient methods are not suitable to solve the problem [18, 23, 24]. The problem becomes even more complex if partial turbine wake shadowing is considered [22]. Although different modeling techniques have been introduced in the literature to reduce the computational burden of the WFLOP [25–28], it remains a very computationally demanding problem. Optimal solutions to the WFLOP can be confirmed only for small instances [22].

A solution that is widely used in academia, is to the solve the WFLOP with Evolutionary Algorithms (EAs), a type of optimization algorithm that belongs to the class of metaheuristics [22]. EAs are moreover among the most suitable methods to solve Multi-Objective (MO) problems [29]. Contrary to most (heuristic) optimization algorithms, these methods use a set of multiple solutions (also called a population) during optimization. EAs are moreover relatively simple to apply to solve optimization problems because only require a way to evaluate the objective functions of interest for them to work [29]. Several reviews of the different approaches for solving the WFLOP have appeared in literature [18, 22, 30–33]. The first work that used a metaheuristic, namely the classic Genetic Algorithm (GA), to solve the WFLOP was carried out in 1994 [34]. Several metaheuristics have been applied to the WFLOP and although EAs, like virtually all metaheuristics, do not guarantee to find the global optimum given a certain computational budget, EAs remain the most used type of optimization algorithm to solve the WFLOP [22].

The objective of this work is to address the following open research questions:

3.1.1 What characteristics should an optimization algorithm have to present optimized layouts?

Despite the fact that multiple studies on the (MO)WFLOP have appeared in literature, no fair comparison of different algorithms has been performed, i.e. employing the same settings for computational budget and using the same problem formulations and problem instances [22]. Rather, the different algorithms have been used in different scenarios, using different constraints and objectives. This limits the conclusions about the performance of algorithms that can be drawn from previously published work [22, 32]. Furthermore, no analysis has been carried out to understand what characteristics are required of an optimization algorithm to efficiently solve the MOWFLOP. Lastly, to correctly assess the optimization performance of EAs, multiple runs *have* to be done as these algorithms are stochastic in their operation. Nonetheless, statistics such as averages and variances over multiple runs have not presented in previous literature [22].

3.1.2 What is the best constraint-handling technique to ensure feasibility of the OWF layouts?

In WFLOP, if the formulation of the optimization problems allows placement of turbines closer to each other than the minimum distance required between turbines, the final design layouts may be infeasible [35]. For real-world problems, constraints that identify when a solution is feasible often have a key contribution to a problem's difficulty. Being able to handle these constraints efficiently and effectively to ensure that the final outcome of optimization is indeed a feasible solution, is therefore important. In metaheuristic optimization, such techniques are called Constraint-Handling Techniques (CHTs). It is known that different CHTs affect the performance of a MOEA differently (see, e.g. [36]). Hence, studying the performance under different CHTs is important and should be considered as an intrinsic part of the EA. Although several CHTs have been employed in the literature for solving the (MO)WFLOP, their impact on the performance of (MO)EAs has not yet been investigated [37].

3.1.3 How does the problem complexity scale with the number of variables?

The performance of metaheuristics, typically measured in the time required to reach an optimal solution or a solution of a certain quality level relative to the optimum (e.g. 95% of the optimum), is highly correlated with a problem's dimensionality (that is, assuming the problem itself can be scaled to larger dimensionalities) [29, 38]. Previous publications on (MO)WFLOP have not discussed the impact of increasing the number of design variables (which depends on the number of turbines, the number of grid positions, or both) on the performance of the EAs used [18].

3.1.4 What is the relation between problem dimensionality/complexity and the degrees of freedom offered by different turbine-placement grids?

In general, two approaches can be identified to model the positioning of turbines. Either the coordinates of a fixed number of turbines is given, or a grid is defined over the available area and turbines may be placed at grid points. One advantage of the latter approach is that it does not necessarily require specifying *a priori* the number of turbines to be placed. Instead, this number can be optimized together with the types of turbines to be placed and where to place them on the grid by making each grid point a decision variable. Because this flexibility on the number of turbines is a desirable design property, we adhere to the latter choice in this work. No work has however previously been published that studies the trade-off between problem dimensionality and the degrees of freedom offered by different grid resolutions according to which turbines can be placed. The usual strategy is to keep the number of optimization variables as low as possible in order to require less evaluations of the objective functions [39]. This would imply using a coarse grid. On the other hand, using a fine grid for the OWF area increases the design freedom since it is possible to obtain a larger number of different OWF layouts [35]. Using a finer grid however increases the complexity of the problem, even though it is still covering the same area, because the resolution of the grid is directly linked to the number of optimization variables. This in turn affects the rate of convergence and optimization performance of metaheuristic algorithms, especially when considering a fixed budget of computation time [18, 27].

The remainder of this work is organized as follows: Section 3.2 introduces the MOWFLOP in more detail. Section 3.3 describes the algorithms selected in this work as well as their main characteristics. The performance of these algorithms combined with different CHTs is tested on OWFs with different dimensions and grid-step sizes in Section 3.4. A discussion of the results is given in Section 3.5, while final conclusions, recommendations and future work are presented in Section 3.6.

3.2 Multi-Objective Wind Farm Layout Optimization Problem

The layout of an OWF is designed and optimized during the Front End Engineering Design (FEED) phase of the project [9]. The FEED phase is performed after initial feasibility studies and before investment decisions. The design options remain relatively flexible during the FEED phase. For example the number, model and location of the turbines is still not fixed [40, 41]. Furthermore, wind farm developers have to make a pre-selection of economically viable design concepts and associated key components during the FEED phase [9, 20]. The number of turbines and their locations have a strong impact on the overall efficiency of the project and hence, they may be considered to be one of the most important optimization variables in the WFLOP.

One of the most used objective functions used to formulate the WFLOP is the Net Present Value (NPV) [22], which may be calculated as:

$$NPV = \left(AED \cdot p_{kWh} - OPEX \right) a - CAPEX \qquad (3.1)$$

where a is the annuity factor ($a = (1 - (1+r)^{-n})/r$), r is the interest rate, n is the project lifetime and p_{kWh} is market energy price.

The NPV requires *a priori* economic values for the interest rate, wind farm lifetime and market energy price. If these values are changed, it is not guaranteed that the OWF layout that leads to the minimum NPV remains the same. Thus, if the designers wish to obtain a new layout for different economic parameters, another optimization run has to be performed, which, depending on the complexity of the models and the computational power available, may require a considerable amount of time. Using functions that depend on *a priori* determined economic values can be seen as converting a problem that is actually inherently multi-objective to a single-objective (SO) problem by the use of weighting factors. In doing so, developers will gain only limited insight into the problem and options for designing layouts because they are only given single layouts each time (one for every combination of economic values) instead of immediately being informed of all solutions that correspond to efficient trade-offs between the key aspects that are of importance, such as AEP, CAPEX and OPEX.

Although, more than 150 publications may be found in literature that have dealt with the WFLOP [22], only a few studies have investigated the trade-offs that emerge while designing a wind farm using a multi-objective formulation [31]. Table 3.1 presents the characteristics of the MOWFLOP as considered by relevant studies. The study carried out in [42] optimized the AEP with the problem constraints being considered as a second objective function. The AEP and the noise generated by the turbines were optimized in [44, 45]. Similarly, [47] optimized the AEP and the sum of the wind farm area and the number of turbines as second objective. Three simultaneous optimization goals were used in [49]: AEP, area used and collection system length.

The great majority of existing approaches, for both the WFLOP and its MO variant, have assumed either a fixed or a maximum number of turbines, despite the fact that the number of turbines is an important real-world optimization objective during the FEED phase [22]. An example of an exception to this is the work presented in [52], in which both the locations and number of turbines were used as design parameters to optimize the AEP and the sum of CAPEX and OPEX.

The energy production was used as an objective in all approaches that studied the MOWFLOP (see Table 3.1). In fact, the energy production is the most common objective function used both in academia and in commercial software [22]. In order to realistically approximate the amount of energy produced by an OWF it is necessary to consider wake effects due to the close proximity of turbines. Next, an overview of wake losses modeling is given and the model that we chose to employ, is described.

Table 3.1: Existing approaches for the MOWFLOP.

References	Optimization Variables	Design Objectives	Wake Model	Constraint Handling	Variables Domain	MOEA
Kusiak et al [42]	Turbine locations	Energy generation, Problem constraints	Katic / Jensen	Extra Objective	Continuous	SPEA [43]
Zhang et al [44, 45]	Turbine locations	Energy generation, Noise level	Jensen	—	Continuous	NSGA-II [46]
Veeramachaneni et al [47]	Turbine locations	Energy generation, Cost	Katic / Jensen	Repair	Continuous	MO-PSO [48]
Tran et al [49]	Turbine locations	Energy generation, Collection system length, Wind farm area	Katic / Jensen	—	Continuous	NSGA-II [46], SPEA2 [50], IBEA [51]
Sisbot et al [52]	Turbine locations and quantity	Energy generation, Cost	Katic / Jensen	Repair / Penalty	Discrete	MOGA [29]

3.2.1 Wake losses

Currently, there is a wide variety of models to calculate, with different accuracy levels, the wind deficits due to wake losses in wind farms [53–57]. Examples of low-fidelity engineering models to describe wake losses include the Katic-Jensen model [58, 59], the Eddy viscosity model [60], the Frandsen et al. model [61], the deep-array wake model [62] and the Larsen model [63]. These models, due to their simplified wake-speed deficit approach, can be evaluated in only little computation time and can provide a preliminary description of the far wake regime [64].

Other models were built to provide medium-fidelity results, such as the Dynamic Wake Meandering model [65] and several other approaches based on the actuator disk model [66, 67]. At the high-fidelity end, Computational Fluid Dynamics (CFD) models are found [55]. The highest of fidelity is obtained using models based on Large Eddy Simulations (LES). Although of value in their own right, one evaluation of such a model may take several weeks to complete [68].

CFD and LES models may be used for detailed studies such as: interactions between a turbulent flow and a rotor blade; the interaction between multiple wakes; or validation and calibration of simpler models [15, 68]. However, for wind farm layout optimization, the huge computational requirements of these models make them prohibitive to use because during optimization many evaluations of these models are typically required, especially in case of large OWFs [69].

For this reason, a commonly adopted design methodology (see, e.g. [39, 70, 71]) is to tackle the WFLOP with simplified and computationally light models. The solutions obtained by doing so provide a first, and often already quite insightful, assessment of the potential solutions to the problem and their quality because although the simpler models may not be as accurate as the ones with the highest fidelity, they do differentiate the performance of one wind farm layout versus another. A designer may then choose a few solutions from the optimized set and further evaluate them with more detailed models to get more accurate figures for the expected performance of these solutions. In this work, the Katic-Jensen model was employed during the optimization experiments. A description of the model is given next.

Katic-Jensen wake model

The Jensen model, originally proposed in 1983, is a simplified and fast manner of calculating the wind speed inside the wake of a turbine [58]. The model, further developed by Katic *et al* in 1986 [59], has been widely adopted in wind farm modeling due to its ease of implementation and low computational requirements [18, 22, 30, 72–74]. All the MO approaches presented in Table 3.1 used the Katic-Jensen model (with the exception of [44, 45] which used the original Jensen model). According to the Katic-Jensen model, the wind speed seen by the j-th turbine is given by:

$$U_j = U_0 \left(1 - \textit{deficit}\right) \tag{3.2}$$

where U_0 is the ambient wind speed and *deficit* is the velocity decrease caused by wake effects.

The wake expansion is considered to be linear [58, 59]:

$$R_{kw} = R_k + \alpha d_{kj} \tag{3.3}$$

where R_{kw} is the wake front radius, R_k is the turbine rotor radius, α is the momentum entrainment or wake decay coefficient and d_{kj} is the distance between the turbines (displayed in Figure 3.4).

The value of α may be calculated according to [75]:

$$\alpha = \frac{A}{\log\left(\frac{h_{hub}}{z_0}\right)} \tag{3.4}$$

where A is a constant (0.5), h_{hub} is the turbine hub height and z_0 is the surface roughness height, which, for offshore environments, is usually considered to be 0.0005 [76].

The interference of an upstream k-th turbine on a j-th turbine may be calculated as [59]:

$$U_{kj} = \frac{1 - \sqrt{1 - C_{T_k}}}{\left(1 + \frac{\alpha d_{kj}}{R_j}\right)^2} \frac{A_{kj}}{A_j} \tag{3.5}$$

where C_{T_k} is the k-th turbine thrust coefficient at a given wind speed, A_j is the j-th turbine rotor area and A_{kj} is the j-th turbine rotor area influenced by the upstream turbine k.

If the wake front affects entirely the j-th turbine, $A_{kj} = \pi R_j^2$ whereas if the wake front does not impact the j-th turbine, $A_{kj} = 0$. If the wake wave affects partially the turbine rotor sweep area (Figure 3.4), A_{kj}, is given by [25, 26, 77]:

$$A_{kj} = \frac{1}{2}\left(R_{kw}^2\left(2\arccos\left(\frac{R_{kw}^2 + c_{kj}^2 - R_j^2}{2R_{kw}c_{kj}}\right) - \sin\left(2\arccos\left(\frac{R_{kw}^2 + c_{kj}^2 - R_j^2}{2R_{kw}c_{kj}}\right)\right)\right)\right) + \\ \frac{1}{2}\left(R_j^2\left(2\arccos\left(\frac{R_j^2 + c_{kj}^2 - R_{kw}^2}{2R_j c_{kj}}\right) - \sin\left(2\arccos\left(\frac{R_j^2 + c_{kj}^2 - R_{kw}^2}{2R_j c_{kj}}\right)\right)\right)\right) \tag{3.6}$$
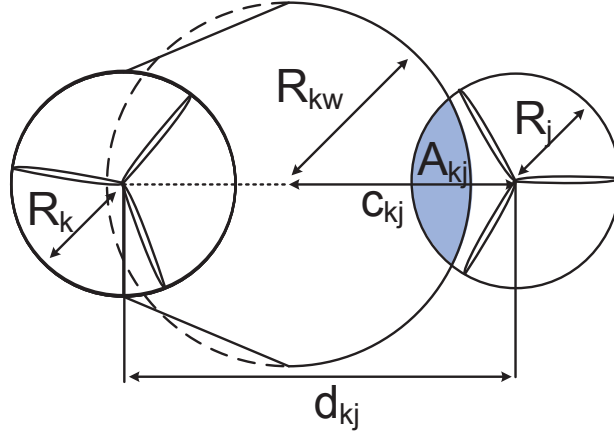
Figure 3.4: Turbine partially affected by the wake of an upstream turbine.
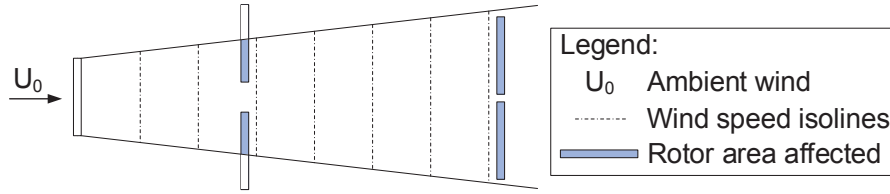
Figure 3.5: Wake growth and wind speed decrease according to the Katic-Jensen model.

To account for multiple interferences from upstream turbines (see Figure 3.5), the deficit term is calculated as [59]:

$$deficit = \sqrt{\sum_{k=1}^{n} U_{kj}^2} \qquad (3.7)$$

where U_{kj} is the contribution of each upstream turbine.

Assumptions

The Katic-Jensen wake model assumes, among other simplifications [22], that the wind speed inside the wake front is axisymmetric, decreases linearly, and that the wake front starts to expand after the turbine rotor. The fact that the wake front is assumed to be axisymmetric and that the wind speed reduction is assumed to be linear means that different layouts will have similar performance according to the model. For example, the turbines inside the wake front of Figure 3.5 have the same energy production according to the Katic-Jensen model (the ones at the same distance from the first turbine).

3.2.2   Constraint-handling

Similar to most real-world problems, the WFLOP has constraints. To obtain feasible wind farm layouts different constraints have to be respected [18]:

- *wind farm boundaries:* the turbines have to be placed inside the wind farm area [78];

- *infeasible areas:* there may be some areas that are not available to install turbines due to human-imposed constraints (e.g. unexploded ordnances, pre-existing cables, shipwrecks) or nature-imposed constraints (e.g., unappropriate type of soil material, cliff areas, soil areas with insufficient bearing capacity, large seabed gradients) [17];

- *minimum clearing distance:* a minimum distance between neighboring turbines is required to guarantee proper functioning and to safeguard their structural integrity [74];

- *number of turbines:* the number of turbines that may be installed has to be within the range specified in the Development Consent Order (DCO) [40].

In the following, several CHTs, previously used in literature for the WFLOP, are described.

No constraints

Various approaches avoid the use of CHTs:

- In the first work that used an EA for the wind farm layout design problem, the wind farm area was divided using a grid with a step size large enough to allow turbines to be placed on grid points without ever violating proximity constraints [34]. Similar approaches have been used in recent literature [39, 79–81]. This approach has a further benefit that the search space of the problem is relatively small because of the relatively large grid spacing, which may lead to faster convergence speeds of optimization algorithms. A big drawback of the approach however is that it oversimplifies the problem, prohibiting finding of better solutions that require more intricate layouts;

- In [49, 82] new variation operators were developed that guarantee that the new layouts remained feasible;

- The proximity constraints were not explicitly used in [44, 45]. Instead, the authors expected the algorithm to converge to the feasible space because of inherent characteristics of the problem, e.g. two turbines placed in close vicinity will generate less energy. Although generally true, this does not guarantee that the required minimum distance, which may differ from the minimum efficient distance in terms of energy production, will be respected.

Resample

In [69] the wind farm layout was replaced by an entirely new feasible, but randomly generated, layout whenever a turbine violated the proximity constraint. This strategy has the drawback that it disrupts the progressive evolution of knowledge acquired by the optimization algorithm. Consequently, this may mislead algorithms that employ variation operators that span multiple

generations to learn about the problem structure and exploit this information [36, 83]. Furthermore, this approach fails, or at least takes a long time, when it is hard to obtain a feasible solution through a random process [84].

Penalty term

The WFLOP has also been transformed into an unconstrained problem by computing a measure of how badly constraints have been violated, and by adding this measure to the objective function [52, 85]. This method, known as the penalty-function method, transforms the search space of the problem, which may increase the roughness of the search space. This may lead the optimization algorithm to local minima in the new search space [86], which may still correspond to infeasible solutions. Furthermore, it is difficult to create a generic penalty function that is optimal for all problems and that does not over- nor under-penalize the infeasible solutions [84, 86, 87]. On the other hand, if the penalty term is properly designed, the penalty-function method may work quite well, allowing the optimization algorithm to also explore the infeasible search space, which may act as a bridge between different feasible areas of the search space [86].

Constraint domination

In several publications, problem constraints have been tackled by the use of the so-called constraint-domination technique [25, 26, 39, 88–90]. Similar to the penalty-function method, a measure of how badly constraints are violated, is computed. When comparing wind farm layouts, the one with the lowest measure of constraint violation is then always preferred. The main drawback of this approach is that it may be difficult for an algorithm to achieve layouts that are located close to infeasible areas of the search space [84]. Furthermore the method negatively effects diversity in the population, which is important in EAs [87].

Repair mechanism

Repair mechanisms ensure that solutions are always in the feasible space by repairing any solution that has been generated and is infeasible [84]. In several studies of the WFLOP, turbine removal has been used [14, 27, 52, 91, 92]. Two different approaches were introduced in [47]: removal of the first turbine that is too close to another turbine and removal of the turbine that has the most conflicts with its neighbors. Although the second strategy presented slightly better results, it did not outperform by much the former approach [47].

Extra optimization goal

The sum over all constraints of the measure of constraint violation was considered as a separate minimization goal in [42]. Although effective, this approach increases the complexity of the problem by adding another objective goal. Moreover, it does not guarantee that the algorithm will return any feasible solution [84].

3.2.3 Domain of Optimization Variables

Different representations of solutions to the WFLOP problem have been considered, including real-valued variables, discrete variables and combinations of both. Next, each of these representations is described.

Real-coded

A real-valued, also referred to as continuous, representation of wind farm layouts, encoding the coordinates of turbines, was considered for the first time in [93]. Thereafter, many recent works have considered a real-valued representation (see Table 3.1 for MO examples). However, the wake models used actually do not offer sufficient resolution for the high precision of a real-valued representation to be of added value (see Section 3.2.1). Moreover, as stated previously, the number of turbines is an important optimization parameter. However, it is difficult to simultaneously optimize the number of turbines with a real-coded optimization algorithm since the turbine number is discrete. Furthermore, given the same number of problem variables and the same inherent underlying problem complexity, continuous optimization problems typically take longer to solve than discrete problems because of the larger variable-domain size of continuous variables.

Mixed-integer

A possible solution is to tackle the WFLOP as a mixed-integer optimization problem, in which both discrete variables, e.g. the number of turbines, and continuous variables, e.g. turbine positions, may be employed. However, tackling a mixed-integer problem is very hard, presenting many optimization challenges which do not arise in purely real or discrete optimization problems [94]. Moreover, straightforward encodings with many turbine locations and integer variables describing how many and/or which of these turbines to actually use, are highly redundant, which have a negative effect on optimization performance. Furthermore, simple wake models would still be required for computational efficiency reasons and hence the insufficient fidelity problem of the wake model also arises with this approach. The WFLOP has also previously been transformed into a mixed-integer *linear* optimization problem [95, 96]. Differently from heuristic methods, algorithms that solve optimization problems formulated as so-called linear programs guarantee that the optimal solution will be found [96]. However, the WFLOP needs to be linearized to this end, which strongly diminishes the extent to which the problem, and consequently its solutions, relate to the real-world scenario.

Discrete

Representations using discrete variables have also been considered. Typically, a grid is placed over the designated area and grid points correspond to (variables encoding) potential locations for turbines. This makes it straightforward to optimize both the number and locations of turbines. All the constraints presented in Section 3.2.2 may be automatically respected if the positions are encoded as discrete variables [39]. Furthermore, the location of a turbine may be described by a

single parameter in a discrete approach, whereas two coordinates have to be used in a continuous domain. It is furthermore known that if a hexagonal or a regularly spaced packing is optimal, optimization based on a discrete grid may yield a solution that is close to the continuous optimum for a bounded area [97]. Finally, the general trend of the offshore wind industry has been to place the turbines in regular structures, with greater distance turbine separation in the prevailing wind direction. Even in current state-of-the-art OWFs, turbines were placed in a grid-based layout (see Figure 3.3). For this reason, it is likely that the use of discrete turbine locations leads to layouts that may be more easily accepted by the offshore wind industry. A potential drawback is that a grid has to be defined *a priori* [22, 98].

3.3 Optimization Algorithms for the Multi-Objective Wind Farm Layout Optimization Problem

Although only few published works have dealt with the MOWFLOP, different MOEAs have already been used in these works (see Table 3.1). The Strength Pareto Evolutionary Algorithm (SPEA) [43] was used in [42], whereas in [47] the Multi-Objective version of the Particle Swarm Optimization (MO-PSO) algorithm was employed [48]. The well-known Nondominated Sorting Genetic Algorithm II (NSGA-II) algorithm has been used in several of the existing works [44, 45, 49]. Finally, only [49] has performed a basic comparison between three algorithms: NSGA-II, SPEA2 and Indicator Based EA (IBEA). It was concluded that IBEA was the most adequate algorithm for the MOWFLOP even though the NSGA-II and SPEA2 found trade-offs with a greater spread [49].

3.3.1 Definitions for MO optimization

We assume to have m objective functions $f_i(\vec{x})$, $i \in \{1, 2, \ldots, m\}$ that, without loss of generality, all need to be *minimized*. A solution $\vec{x}^1$ is said to (Pareto) *dominate* a solution $\vec{x}^2$ (denoted $\vec{x}^1 \succ \vec{x}^2$) if and only if $f_i(\vec{x}^1) \leq f_i(\vec{x}^2)$ holds for all $i \in \{1, 2, \ldots, m\}$ and $f_i(\vec{x}^1) < f_i(\vec{x}^2)$ holds for at least one $i \in \{1, 2, \ldots, m\}$. A *Pareto set* of size n is a set of solutions $\vec{x}^j$, $j \in \{1, 2, \ldots, n\}$ for which no solution dominates any other solution, i.e. there are no $j, k \in \{1, 2, \ldots, n\}$ such that $\vec{x}^j \succ \vec{x}^k$ holds. A *Pareto front* corresponding to a Pareto set is the set of all m-dimensional objective function values corresponding to the solutions, i.e. the set of all $\vec{f}(\vec{x}^j)$, $j \in \{1, 2, \ldots, n\}$. A solution $\vec{x}^1$ is *Pareto optimal* if and only if there exists no other $\vec{x}^2$ such that $\vec{x}^2 \succ \vec{x}^1$ holds. Further, the *optimal Pareto set* is the set of all optimal Pareto solutions and the *Optimal Pareto Front* (OPF) is the Pareto front that corresponds to the optimal Pareto set.

3.3.2 Characteristics

The key features that a MOEA should have to adequately solve the MOWFLOP are described next.

Clustering

Standard MOEAs steer the population towards the OPF while trying to preserve diversity in the population through different mechanisms, e.g. use of the crowding distance in NSGA-II [46], use of the environmental selection in SPEA2 [50] or use of the hypervolume in MO-CMA [83]. However, it has been shown that these mechanisms are insufficient to achieve good scalability [99]. Furthermore, selection based on the domination criterion tries to exploit all objectives simultaneously, thus reducing the pressure in the direction of the OPF [99]. For this reason, handling different parts of the objective space differently is of major importance. Finally, solutions along the OPF are typically very different, especially for the extreme regions of the front. The use of clusters to divide the objective space into smaller areas allows the MOEA to specialize variation to meet the specific requirements to find improvements in narrower areas of the search space, leading to better results, for both continuous and discrete problems [36, 38, 99].

Single-objective Optimization

Having a mechanism that puts extra pressure on exploiting individual objectives can be highly beneficial because nondominated selection may not provide enough pressure to find the extreme solutions (i.e. solutions that optimize a single objective) [99]. This is of special importance if one of the optimization goals is much harder to solve than the others since the algorithm may converge prematurely and discover only a small subset of the OPF [36]. Moreover, in some problems the number of available solutions in the extreme regions can be much smaller than in the middle regions of the front [100]. The benefit of adding SO optimizers to specifically obtain solutions in extreme regions of the front has been shown to improve the performance of MOEAs [36, 38, 101].

Problem structure exploitation

A key property of EAs is their ability to juxtapose partial solutions or substructures from different solutions to create improved solutions. This mixing is only efficient when key substructures are not disrupted too often by the variation operators [102]. In GAs, subsets of variables of two solutions are exchanged. However, it has been shown that without detecting and exploiting the dependencies between problem variables, EAs cannot solve some decomposable problems efficiently [38]. When enough knowledge of the problem is available, mixing can be made efficient by designing the variation operation in an appropriate way. However, for black-box optimization problems nothing is known of the problem structure a prior. For such problems, this knowledge has to be inferred from the population of solutions by identifying groups of variables that together make an important contribution to the quality of a solution [102]. Such information is commonly referred to as *linkage information*.

A general linkage model that can be used to capture the interactions between the l optimization variables is called the Family Of Subset (FOS) [102]. A FOS $\mathcal{F}$ consists of subsets that contain decision variables, i.e. $\mathcal{F} = \{\vec{F}^0, \vec{F}^1, \ldots, \vec{F}^{|\mathcal{F}|-1}\}$ where $\vec{F}^i \subseteq \{0, 1, \ldots, l-1\}$, $i \in \{0, 1, \ldots, |\mathcal{F}|-1\}$. Every

subset $\vec{F}^i$ is called a linkage subset and represents a group of variables which exhibit some degree of joint dependency and hence should be copied together during variation.

In this work, two algorithms are used: the well-known NSGA-II [46] and a variant of the recently introduced Multi-Objective Gene-pool Optimal Mixing Evolutionary Algorithm (MOGOMEA) [38], which was designed by combining the Gene-pool Optimal Mixing Evolutionary Algorithm (GOMEA) [102] with a MO framework [101]. Both algorithms as well as two slightly modified variants are presented in the following subsections.

3.3.3 MOGOMEA

Figure 3.6 shown a flowchart of the MOGOMEA and a description of the algorithm is given next.

Population initialization

The n_i initial wind farm layouts are created with a nearest neighbor heuristic to select turbine locations from the available locations that are spread as well as possible. Specifically, first, the initial number of turbines, m, is randomly generated between one and the maximum number of turbines that may be installed for the given area. The location of the initial turbine is randomly chosen from all the possible locations. The distance of the remaining locations is computed to the first turbine and the most distant one is chosen for the second turbine. The distances for the remaining locations are updated by checking whether the distance to the new turbine is smaller than the currently stored distance (the shorter distance is kept). The procedure is repeated in total m times or until a turbine violates the proximity constraint. In this way, it is guaranteed that feasible wind farm layouts are generated, similarly to several previous works [69, 82, 91].

k-leaders

The same nearest-neighbor heuristic as in the previous step is used to select k solutions, also called cluster leaders, from the nondominated solutions of the population that are spread as well as possible. This is done to bias the leaders towards the best solutions of the population.
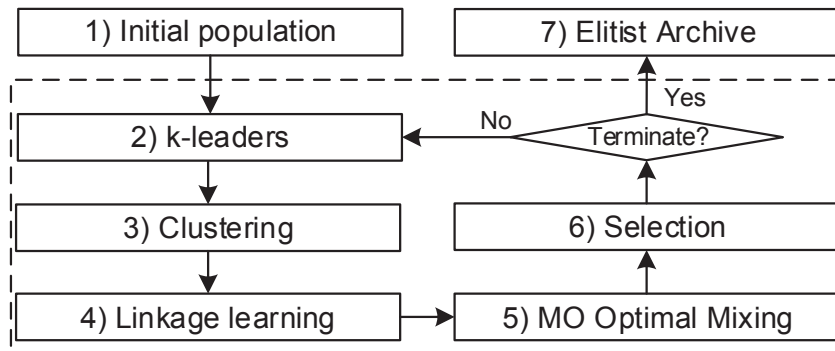
Figure 3.6: Flowchart of the MOGOMEA variant used in this work.

Differently from the previous step, a solution with a minimum value for a randomly chosen objective is chosen to be the first leader to increase the probability of having leaders at the extremes of the Pareto front. The distances are measured in the objective space. The heuristic is then repeated until all the necessary cluster leaders are selected (see Figure 3.7).

Clustering

Next, the c closest solutions (including the leader solutions themselves) to each leader are clustered together. Because the assignment is done independently for each cluster, some solutions may be assigned to multiple clusters while other solutions may not be clustered. To reduce the probability of this happening we increased the probability of clusters overlap by setting $c = \frac{2}{k} \lfloor \tau n \rfloor$ as proposed in [103]. This increases the probability of finding a good, uniform spread of solutions with a MOEA faster [103]. The clustering is performed on *normalized* objective values to remove the influence of differently scaled objectives.

Linkage learning

A linkage model $\mathcal{F}_j$ is learned for each cluster $\mathcal{C}_j$ to distinguish different regions along the Pareto Front and allow a different, objective-space region-specific, exploitation bias to be formed for each of them. Although different FOS structures may be used [104, 105], the linkage tree (LT) structure is used here since it has been demonstrated to result in the best and most reliable performance of the GOMEA framework on several benchmark functions [102, 104, 106].

A LT captures all decision variables as being fully independent in singleton (leaf nodes) subsets ($\vec{F}^i = \{i\}, i \in \{1, \ldots, l\}$). Furthermore, it organizes combinations of variables in a tree-like fashion. A branch node of the LT is a multivariate subset $\vec{F}^i$, which is the combination of two subsets $\vec{F}^j$ and $\vec{F}^k$ such that $\vec{F}^j \cap \vec{F}^k = \emptyset, |\vec{F}^j| < |\vec{F}^i|, |\vec{F}^k| < |\vec{F}^i|$ and $\vec{F}^j \cup \vec{F}^k = \vec{F}^i$. The LT FOS has $2l - 2$ linkage subsets because the root node is discarded since it contains all the variable indices and hence it does not generate a different offspring solution. Note that a variable can be part of multiple
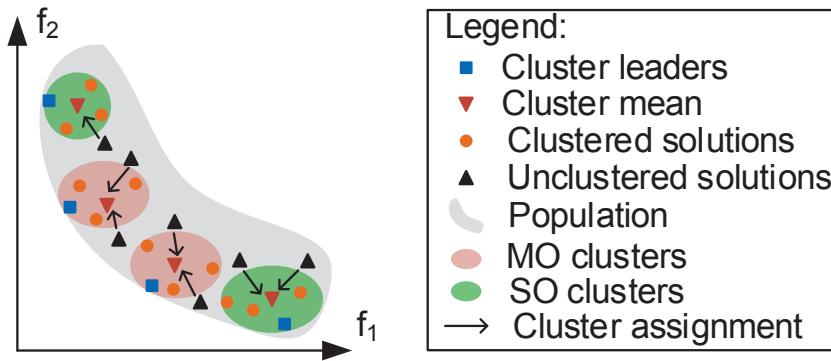
Figure 3.7: Selection of k leaders and cluster assignment.

subsets of the LT. Therefore, any two variables may be dependent according to some subsets, but independent according to others [107].

The LT is constructed using a pairwise measure of distance between sets of variables known as the Unweighted Pair Grouping Method with Arithmetic-mean (UPGMA [108]). Constructing an LT can be conceptually considered to start from the leaf nodes and creating branch nodes by consecutively combining two closest groups until the root node is obtained. An efficient implementation that takes a slightly different approach, but results in the same LT, has a computational complexity of only $\mathcal{O}(cl^2)$ [108] where c is the cluster size. To compute similarity between two variables as a foundation for the UPGMA method, various measures may be used. In this work, we use Mutual Information (MI), since it has demonstrated to lead to the most efficient performance on several benchmark problems [109]. MI is a dimensionless quantity and can be thought of as the reduction in uncertainty about one random variable given knowledge of another. A high MI value represents a large reduction in uncertainty, a lower value constitutes a low reduction of uncertainty and a null MI value means that the two variables are independent.

To illustrate the notion of a LT, Figure 3.8a shows the LT that resulted from clustering the turbine positions of the wind farm area shown in Figure 3.12b. The clusters of turbine positions, which show that neighboring positions are clustered together first, are also indicated in Figure 3.8b.

MO Gene-pool Optimal Mixing

The main operator of variation in MOGOMEA is called Multi-Objective Gene-pool Optimal Mixing (MOGOM) and it is applied to every solution in the population. For this reason, it is necessary to determine which cluster a solution belongs to since a separate LT is learned for

(a)   (b)
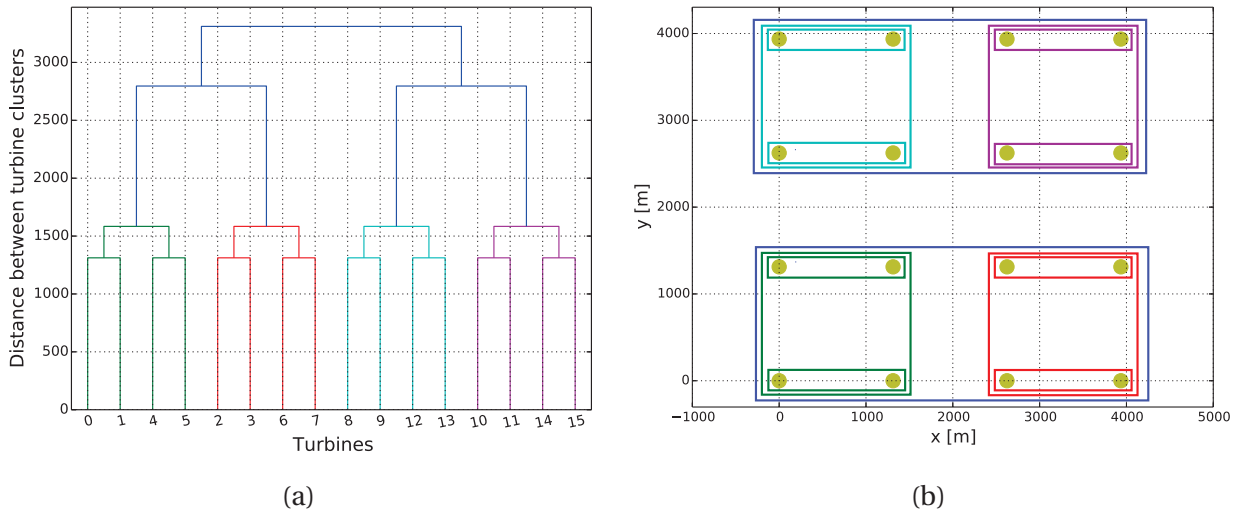
Figure 3.8: Figure (a) shows the LT learned offline based on the distances between the possible locations. The turbines are numbered from left to right and from bottom to top. Figure (b) shows the respective clustering of the positions in the wind farm.

each cluster. Solutions that have not been assigned to a cluster by the clustering algorithm are now assigned to the cluster with the nearest mean value (see Figure 3.7). In case of multiple cluster assignments, ties are broken randomly. Thereafter, every solution $\vec{x}$, also called the parent solution, is incrementally changed into an offspring solution. Firstly, the offspring solution $\vec{o}$ and a backup $\vec{b}$ are created by cloning $\vec{x}$. The linkage groups in FOS $\mathscr{F}_j$ are then enumerated in a random order. For every $\vec{F}^i \in \mathscr{F}_j$, a donor solution $\vec{d}$ is randomly chosen from the same cluster C_j. The optimization variables whose indices are indicated by the linkage group $\mathscr{F}_i$ are copied from the donor $\vec{d}$ to $\vec{o}$. Recent literature has demonstrated the need for mutation to reliably solve certain types of problems [38]. Therefore, in our version of MOGOMEA we use a simple bit-flipping mutation with probability $1/l$. Hence, when the copy occurs, the variables may be altered via mutation. If the copy generated a new offspring solution, the objective values of $\vec{o}$ are evaluated and compared with the backed-up solution $\vec{b}$. The changes are accepted and $\vec{b}$ is updated if: $\vec{o}$ dominates $\vec{b}$ ($\vec{o} \succ \vec{b}$); is equally good ($\vec{f}(\vec{o}) = \vec{f}(\vec{b})$); is a side step, i.e. $\vec{o}$ does not dominate $\vec{b}$ but it is also not dominated by any elitist solution $\mathscr{A} \nsucc \vec{o}$ (introduced later). Otherwise, the changes are rejected and $\vec{o}$ is reverted to the backed-up state $\vec{b}$. Pseudo-code is given in Figure 3.9.

The number of consecutive generations that the elitist archive (introduced later) has remained unaltered is called the No-Improvement Stretch (NIS). A routine called Forced Improvement (FI), which was introduced in previous literature [38, 104], is triggered when the NIS exceeds a threshold of $1 + \lfloor \log_{10}(n) \rfloor$. FI is a second round of MOGOM in which the donor solutions are randomly chosen from the elitist archive. Furthermore, in the FI phase, a mixing step is only accepted if the offspring dominates its parent (i.e. $\vec{o} \succ \vec{b}$) or if it is a new nondominated solution ($\mathscr{A}^t \nsucc \vec{o} \wedge \vec{f}(\vec{o}) \notin \vec{f}(\mathscr{A}^t)$). FI for a solution is stopped with the first accepted change [104]. If $\vec{o}$ is still unchanged after FI, it is replaced by a random solution from the elitist archive. Lastly, in every generation, the original SO version of GOM is used to perform variation in the cluster that has the largest mean value in objective i [105].

Survivor selection and automated population sizing

At the end of each generation, a selection procedure is used to create the next population. If the current elitist archive (introduced in the next step) is larger than the population size, n leaders are chosen from the archive. If the elitist archive is smaller than required, the solutions from the population and archive are combined, with duplicated solutions being discarded. If the size of this new combined population is still smaller than the population size, the remaining spots are filled with new randomly-generated solutions. If the size is larger than required, solutions from the best nondominated fronts are chosen. With this strategy one avoids the inherent problem of MOGOMEA that the new population may actually not be well spread over the currently known Pareto front since the MOGOM procedure only keeps the last modified version of a solution in the population, whereas all the solutions that were allowed into the elitist archive do not necessarily remain in the population. In every generation, the population is increased by its initial size, n_i, by adding new randomly-generated solutions to the population.

$\text{MOGenepoolOptimalMixing}(\vec{x}, \mathscr{C}, \mathscr{F}, \mathscr{A}^t)$

1   $\vec{b} \leftarrow \vec{o} \leftarrow \vec{x}$; $\vec{f}(\vec{b}) \leftarrow \vec{f}(\vec{o}) \leftarrow \vec{f}(\vec{x})$; $changed \leftarrow false$
2   **for** $i \in \{0, 1, \ldots, |\mathscr{F}| - 1\}$ **do**
3     $\vec{d} \leftarrow \text{Random}(\mathscr{C})$
4     $\vec{o}_{\mathscr{F}i} \leftarrow MUT(\vec{d}_{\mathscr{F}i})$
5   **if** $\vec{o}_{\mathscr{F}i} \neq \vec{b}_{\mathscr{F}i}$ **then**
6      $\vec{f}(\vec{o}) \leftarrow \text{EvaluateFitness}(\vec{o})$
7      $\mathscr{A}^t \leftarrow \text{UpdateElitistArchive}(\vec{o})$
8   **if** $(\vec{o} \succ \vec{b})$ **or** $(\vec{f}(\vec{o}) = \vec{f}(\vec{b}))$ **or** $(\mathscr{A}^t \not\succ \vec{o})$ **then**
9       $\vec{b}_{\mathscr{F}i} \leftarrow \vec{o}_{\mathscr{F}i}$; $\vec{f}(\vec{b}) \leftarrow \vec{f}(\vec{o})$; $changed \leftarrow true$
10   **else**
11       $\vec{o}_{\mathscr{F}i} \leftarrow \vec{b}_{\mathscr{F}i}$; $\vec{f}(\vec{o}) \leftarrow \vec{f}(\vec{b})$
12   **if** $\neg changed$ **or** $t^{NIS} > 1 + \lfloor \log_{10}(n) \rfloor$ **then**
13     $changed \leftarrow false$
14   **for** $i \in \{0, 1, \ldots, |\mathscr{F}| - 1\}$ **do**
15      $\vec{d} \leftarrow \text{Random}(\mathscr{A}^t)$
16      $\vec{o}_{\mathscr{F}i} \leftarrow \vec{d}_{\mathscr{F}i}$
17   **if** $\vec{o}_{\mathscr{F}i} \neq \vec{b}_{\mathscr{F}i}$ **then**
18       $\vec{f}(\vec{o}) \leftarrow \text{EvaluateFitness}(\vec{o})$
19       $\mathscr{A}^t \leftarrow \text{UpdateElitistArchive}(\vec{o})$
20   **if** $(\vec{o} \succ \vec{b})$ **or** $(\mathscr{A}^t \not\succ \vec{o}$ **and** $\vec{f}(\vec{o}) \notin \vec{f}(\mathscr{A}^t))$ **then**
21        $\vec{b}_{\mathscr{F}i} \leftarrow \vec{o}_{\mathscr{F}i}$; $\vec{f}(\vec{b}) \leftarrow \vec{f}(\vec{o})$; $changed \leftarrow true$
22   **else**
23        $\vec{o}_{\mathscr{F}i} \leftarrow \vec{b}_{\mathscr{F}i}$; $\vec{f}(\vec{o}) \leftarrow \vec{f}(\vec{b})$
24   **if** $changed$ **then breakfor**
25   **if** $\neg changed$ **then**
26     $\vec{d} \leftarrow \text{Random}(\mathscr{A}^t)$; $\vec{o} \leftarrow \vec{p}$; $\vec{f}(\vec{o}) \leftarrow \vec{f}(\vec{p})$

Figure 3.9: Pseudo code for MO Gene-pool Optimal Mixing [38].

Elitist Archive

The algorithm is equipped with a secondary population, called the elitist archive, for storing the nondominated solutions found during the search [110]. The use of such an archive is extremely useful since the primary population may be smaller than the number of Pareto front solutions and therefore nondominated solutions may be rejected during the selection procedure [111]. Every new and feasible solution, which dominates or is nondominated compared to its parent, is checked to see if it can be added into the archive. If the new solution is dominated by any archive member, it is discarded. If it is a new nondominated solution, it is added to the archive and the archive members that are dominated by it are removed. In the case that there exists an archive member with the same objective values, the previously archived solution is replaced by the new one if it results in a diversity improvement for the archive in the decision-variable space. The solution which has a greater Hamming distance to its nearest archive neighbor is chosen [38].

New aspects

The MOGOMEA is based on previous work [38]. However, a few alterations were implemented:

- The k-means algorithm is not used because the clusters means tend to drift "inwards", leading to reduced search effort in the vicinity of the Pareto extremes. Instead, the clusters are grown directly around the leaders chosen from the selection set [36].

- Previously, the LTs were learned on selection sets that were obtained using tournament selection with tournament size 2. In the new approach, the LTs are learned with all the solutions from the clusters, which is expected to increase the gene diversity and decrease the fitness bias.

- The population size is a very important internal parameter of EAs that should be adjusted according to the instance of the WFLOP being solved [18, 27]. If the population size is too small, there may not be enough genetic variation available to reach parts of the OPF [38]. In this work, a new population-growing scheme is introduced. This makes the algorithm more robust because if a larger population size is needed than what is used initially, the algorithm will eventually reach this population size.

3.3.4   o-MOGOMEA

In each generation and for every cluster, a linkage model is learned in MOGOMEA by building a hierarchical cluster tree [106]. This is a key feature of the algorithm that makes it especially efficient for problems which have an exploitable linkage structure [38].

The MOWFLOP however is not a fully black-box optimization problem since it is known that turbines influence the energy production of neighboring turbines and that this influence might be considered negligible for turbines situated far enough apart [26, 27]. This knowledge about the underlying problem structure suggests that a slightly different variant of the MOGOMEA may be designed that does not require structure learning. Although learning a LT is relatively efficient compared to various alternative models in literature, especially for large problems this is still a potentially time-consuming part of the algorithm. For this reason, we consider a version of MOGOMEA in which the LT is predetermined and kept fixed. To build this LT, the geographical distance between the potential turbine positions is used as a distance metric. The underlying problem structure is thus learned offline. Hence, we refer to it as offline MOGOMEA (o-MOGOMEA).

3.3.5 NSGA-II

A flowchart of the NSGA-II is shown in Figure 3.10 and a description of the algorithm is given next.

Population initialization

The population initialization scheme used for the MOGOMEA is also employed in the NSGA-II.

Ranking and Crowding

Initially, the solutions of the population are ranked. Rank one is assigned to all solutions that are not dominated by any other solution. Rank two is given to the solutions which are only dominated by rank one solutions. The procedure is then repeated until all solutions are ranked.

The crowding distance is used to compare solutions in the same rank and acts as a diversity operator. It measures the cuboid size defined by the locations of the closest neighbors (from the same rank) of a solution in the objective space, as shown in Figure 3.11. Larger values for the cuboid are preferred as this indicates that the solutions are located in areas of the search space that are not crowded.

Parents Selection

Two solutions are randomly chosen from the population and compared. The one with the lowest rank is selected. If they have the same rank, the one with the largest cuboid is chosen. The procedure is repeated until n parents are chosen.

Sampling

In this step, an offspring population is created. To do so, two parents are taken from the parent population, mixed via a classic crossover operator and mutated to generate two new solutions. The procedure is then repeated until all offspring are created.
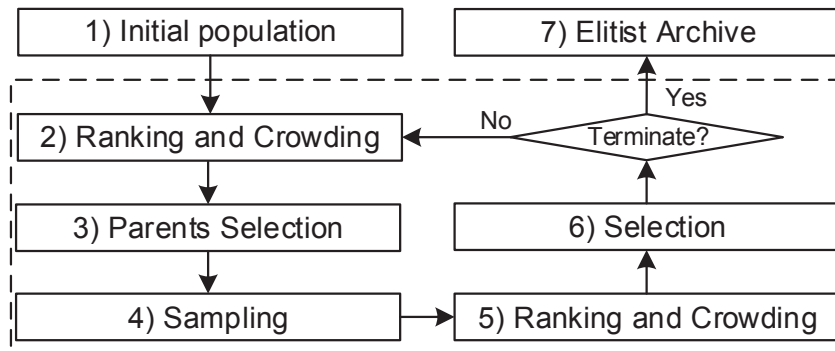
Figure 3.10: Flowchart of the NSGA-II.
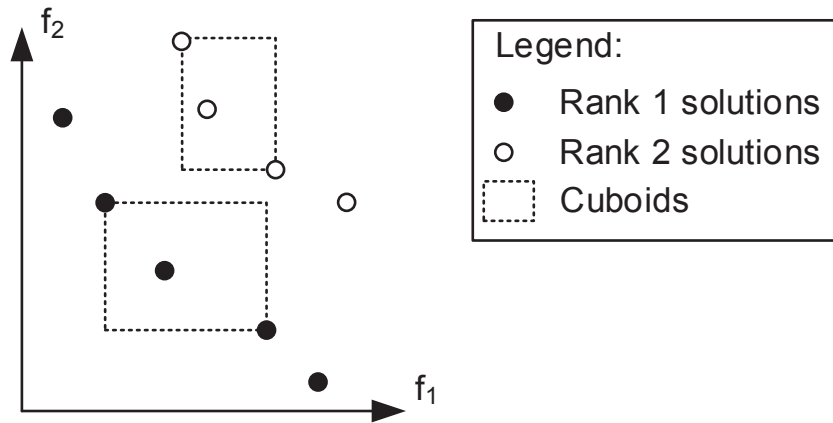
Figure 3.11: Nondominated ranking and crowding distance [46].

Ranking and Crowding

The same procedure is used as in step two. However, this is now performed in a set composed of the parent and offspring solutions.

Selection

The selection procedure of the MOGOMEA is used to create the new population. However, for the sake of making a fair comparison, the population size was not increased at the end of all generations because MOGOMEA uses far more fitness evaluations per generation than the NSGA-II. Hence, the population size of the NSGA-II-based algorithms was only increased after a number of generations that corresponds to an equivalent number of evaluations as would have been performed in MOGOMEA after one generation.

Elitist Archive

Although the original NSGA-II did not make use of an elitist archive [46], it has been shown that its performance is enhanced if it is equipped with one [38, 112, 113]. Therefore, in this work the NSGA-II uses a similar elitist archive as the one used in MOGOMEA.

3.3.6 c-NSGA-II

In the default version of the NSGA-II the solutions selected for mating are randomly chosen from the entire population. To test the influence of using the clustering strategy for the MOWFLOP, we designed a new variant of NSGA-II: clustering NSGA-II (c-NSGA-II). The same principle as used in MOGOMEA is employed: solutions are recombined only if they are in the same cluster cluster. The remainder of the algorithm is the same as the standard NSGA-II.

Table 3.2: Characteristics of the MOEAs under study.

Algorithm	Clustering	SO optimizers	Problem structure
NSGA-II	No	No	No
c-NSGA-II	Yes	No	No
o-MOGOMEA	Yes	Yes	Offline
MOGOMEA	Yes	Yes	Online

3.3.7 Overview of the algorithms

Table 3.2 provides a comparison of the characteristics of the algorithms under study. The original implementation of NSGA-II does not have any of the characteristics that are being investigated, whereas the c-NSGA-II, due to clustering, differentiates variation along the Pareto front. The o-MOGOMEA includes inherent SO optimization in its extreme clusters and uses information of the WFLOP to learn the FOS offline. Finally, the MOGOMEA has all the characteristics and also learns the FOS structure throughout the optimization run.

3.4 Case Study

This section provides the details of a case study. Specifically, the turbine and wind resource, wind farms, optimization goals, algorithm parameter settings, CHTs and performance indicators used are described in the following.

3.4.1 Turbine and wind resource

The selected wind turbine was the Vestas 8MW [114] whose power and thrust curves are given in Table 3.3. The turbine has an 164 m rotor diameter (RD) and a hug height of 107 m. The power and thrust curves were linearly interpolated and all turbines were considered to be similar.

The wind resource used (displayed in Table 3.4) is based on measurement data collected in the North Sea [115]. The wind behavior may be characterized by a Weibull distribution [18, 42]. Nonetheless, a discrete distribution was used during the optimization routine, in a similar fashion to other literature [34, 39, 79, 85, 88, 91, 92]. In this way, the computational cost to evaluate the energy production is low and, furthermore, the wake loss model used does not provide high-fidelity results, as stated previously (see Section 3.2.1).

Table 3.3: Turbine power and thrust curves.

Wind speed [m/s]	Power production [kW]	Thrust value
4	100	0.700000000
5	570	0.722386304
6	1103	0.773588333
7	1835	0.773285946
8	2858	0.767899317
9	4089	0.732727569
10	5571	0.688896343
11	7105	0.623028669
12	7873	0.500046699
13	7986	0.373661747
14	8008	0.293230676
15	8008	0.238407400
16	8008	0.196441644
17	8008	0.163774674
18	8008	0.137967245
19	8008	0.117309371
20	8008	0.100578122
21	8008	0.086883163
22	8008	0.075565832
23	8008	0.066131748
24	8008	0.058204932
25	8008	0.051495998

Table 3.4: Wind resource: average speed and annual frequency of occurrence.

Direction [°]	Mean wind speed [m/s]	Frequency [%]
0	9.77	6.3
30	8.34	5.9
60	7.93	5.5
90	10.18	7.8
120	8.14	8.3
150	8.24	6.5
180	9.05	11.4
210	11.59	14.6
240	12.11	12.1
270	11.90	8.5
300	10.38	6.4
330	8.14	6.7

3.4.2 Wind farms

We designed four different areas (see Figure 3.12a). All wind farms have a square area which is suitable for locations in which there is a predominant wind direction [35]. For each wind farm, three grid step sizes (2, 4 and 8 RD) were used to define possible turbine locations. The characteristics of the different wind farm areas are listed in Table 3.5. Note: the number of possible layouts includes infeasible layouts.
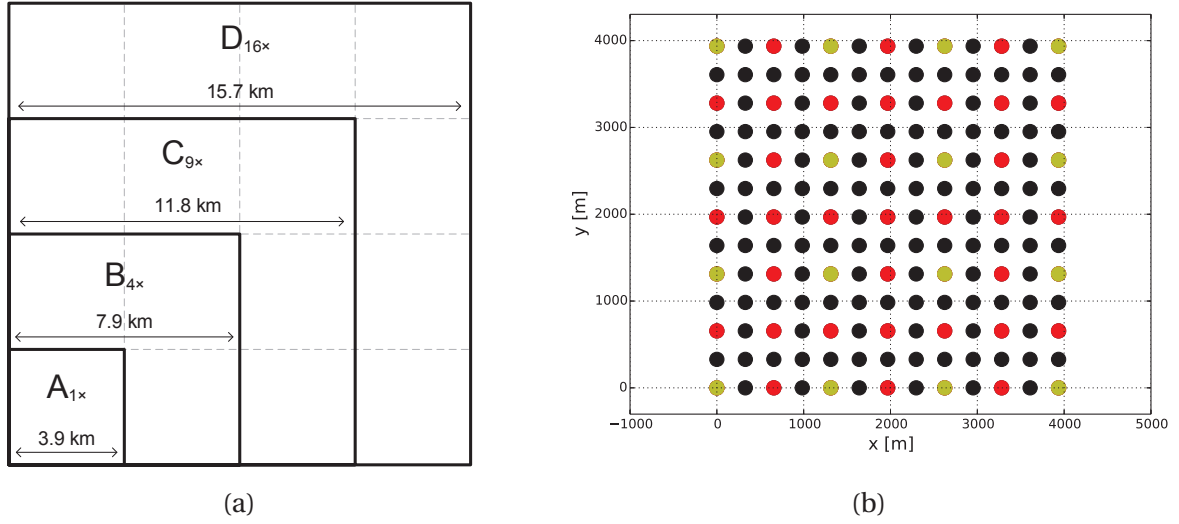
Figure 3.12: Figure (a) shows the dimensions of the areas considered in the case study. Figure (b) shows the turbine locations for wind farm A and three different grid steps: 2 RD spacing - all locations; 4 RD - red and yellow (every second location); 8 RD - yellow (every forth location).

Table 3.5: Characteristics of the wind farm areas under study.

Wind farm	Area (km^2)	Maximum packing	Step size (RD)	Number of variables	Number of possible layouts
A	15.49	16	8	16 (4^2)	65536
			4	49 (7^2)	5.6×10^{14}
			2	169 (13^2)	7.5×10^{50}
B	61.97	49	8	49 (7^2)	5.6×10^{14}
			4	169 (13^2)	7.5×10^{50}
			2	625 (25^2)	1.4×10^{188}
C	139.43	100	8	100 (10^2)	1.3×10^{30}
			4	361 (19^2)	4.7×10^{108}
			2	1369 (37^2)	1.3×10^{412}
D	247.89	169	8	169 (13^2)	7.5×10^{50}
			4	625 (25^2)	1.4×10^{188}
			2	2401 (49^2)	5.9×10^{722}

The maximum number of wind turbines, n_{pack}^{max}, is the number of positions available using an 8 RD grid step size. It should be noted that in our setup, the hexagonal packaging, the densest circle packing in a plane [116], is not possible. In fact, a grid step size of eight (or multiples) times smaller than the minimum distance is recommended to allow a hexagonal packaging [97].

3.4.3   Optimization goals

The two design objectives chosen for our case study, namely AEP and efficiency, are important design goals for wind farm designers. The optimization goals are described and the motivation for selecting them, is provided in the following.

Annual Energy production

The annual energy production (AEP) is one of the most commonly used optimization goals both in academia (all previous MO approaches shown in Table 3.1 used energy production as one of optimization goals) and in commercial software [22]. It is described by:

$$AEP = \frac{8760 \sum\limits_{i=1}^{\theta} \sum\limits_{j=1}^{turbs} P_j\left(\overline{wind_i}\right) \cdot f_i}{8760 \sum\limits_{i=1}^{\theta} n_{pack}^{max} \cdot P_{turb}^{ideal}\left(\overline{wind_i}\right) \cdot f_i} \tag{3.8}$$

where f_i is the wind frequency of occurrence for direction i, $\overline{wind}$ is mean wind speed for the i-th direction, $P_j\left(\overline{wind_i}\right)$ is the power production of the j-th turbine for the wind speed $\overline{wind_i}$, n_{pack}^{max} is the maximum packing of turbines for the wind farm area, 8760 is the number of hours in one year and P_{turb}^{ideal} is the energy production of a turbine without wake losses.

Efficiency

Efficiency is targeted at the maximization of the usage of the installed turbines. A common measure for this is the utilization factor, which is the fraction of the year required for the wind farm to produce its annual production if it produced energy at its full power all the time. This measure is also captured by the maximization of the wind farm efficiency [25, 26, 74, 89]. The ideal wind farm production is the power production of a single wind turbine (without wake losses) multiplied by the number of turbines in the wind farm. The wind farm efficiency is calculated by:

$$\eta_{wf} = \frac{\sum\limits_{i=1}^{\theta} \sum\limits_{j=1}^{turbs} P_j\left(\overline{wind_i}\right) \cdot f_i}{n_{turbs}^{wf} \cdot P_{turb}^{ideal}} \tag{3.9}$$

where η_{wf} is the wind farm efficiency and n_{turbs}^{wf} is the total number of turbines in the wind farm.

the wind farm energy production and efficiency are conflicting design goals. The wind farm energy production is increase by placing more turbines in the wind farm area. However, also the wake effects increase with the number of turbines. Only for very large wind farms it could happen that the energy generated by an extra turbine would not be enough to compensate for

the additional wake losses. The second design goal is maximized by reducing the wake effects between the turbines. However since the wake effects increase with the turbine number, this objective is maximized for layouts with only a few turbines that are placed far apart.

Motivation

The selected optimization goals solely depend on the energy production and wake losses. A more detailed WFLOP would need to use nested algorithms, e.g. an heuristic to design the collection system [117–120]. Although this is of importance to the final application, the use of nested algorithms also substantially increases runtime while it does not provide additional insight into the topics under study in this work. Therefore, this is omitted here.

3.4.4   Constraint-handling techniques

We use a minimum separation of 8 RD between neighboring wind turbines [49, 90]. Hence, the algorithms are required to handle this proximity constraint for layouts with 2 and 4 RD grid step sizes. All CHTs (except for the extra optimization goal strategy) previously used (see) Section 3.2.2) were implemented to assess their impact on the performance of the algorithms under study:

No constraints

The grid step size was selected as the minimum separation required for the turbines (8 RD). In this way, the algorithms may place turbines in any of the locations while guaranteeing that the wind farm layout remains feasible.

Constraint domination

The constraint violation value is the sum of the number of pairs of turbines which are placed closer than the minimum distance. During variation in MOGOMEA, a newly generated solution is directly compared with its parent (see Figure 3.9). Therefore, if a solution violates constraints, it is discarded before its fitness is evaluated. Since the initial population is guaranteed to be feasible (see Section 3.3.3), MOGOMEA does not cross into the infeasible part of the search space. In a similar fashion, the NSGA-II does not evaluate newly generated infeasible layouts and they are not present in the offspring population.

Penalty term

A penalty term was constructed as follows: for each pair of turbines that violate the proximity constraint, the energy production was reduced by what one turbine would produce if it were installed alone (P_{turb}^{ideal}). In this way, it is guaranteed that the solutions are not under-penalized since a turbine installed alone would not have any wake losses. This approach is called minimum penalty rule since the penalty is just above the limit where infeasible solutions are preferred [87]. The penalization weight increases with the number of turbine pairs that violate the proximity constraint because the penalization grows linearly, whereas the energy generation does not grow

proportionally due to the increase of wake losses. Hence, the penalty term behaves dynamically and is not only based on the number of proximity constraints which are violated, which has demonstrated to provide better results for benchmark functions [121]. Using a penalty term, all algorithms evaluate infeasible layouts. Although this might not be possible for some optimization problems, the wake losses model used is able to provide output. Nonetheless, these evaluations are not accurate since the Katic-Jensen model is a far-wake model [64].

Repair mechanism

To repair infeasible solutions, a turbine is randomly chosen to be removed from a pair of turbines that are too close. This strategy is expected to remove, half of the time, the turbine which most degraded the performance of the wind farm. The procedure is repeated until the layout becomes feasible.

Resample

With this approach, new layouts are resampled until a feasible one is created. For NSGA-II variants, the parent solutions are directly carried to the next population if the newly generated layouts are still infeasible after 100 trials. For MOGOMEA variants, a new donor is randomly chosen every time an infeasible solution is generated. If no feasible layout is created after 100 trials, the solution remains unaltered and the algorithm moves on to the next FOS subset.

3.4.5   MOEAs

MOGOMEA and o-MOGOMEA

Following recommendations from recent literature, we used five clusters [38]. Hence, two clusters are used to extend the Pareto front towards the two individual optimization goals while the remaining three clusters are responsible for finding good solutions in the center part of the OPF.

For cluster sizing, we initially set each cluster size to four, which is the minimal size with which MOGOMEA robustly solves the one-max zero-max problem [38]. This leads to an initial population of size 20, regardless of the dimensionality of the problem. This is however compensated by the population-increment mechanism which increases the population size every generation.

NSGA-II and c-NSGA-II

For variation, two-point crossover was used with probability 0.9 [38] and bit-flipping mutation with probability $1/l$, as originally proposed [46]. Five clusters were used in the c-NSGA-II in a similar fashion to the MOGOMEA variants.

3.4.6 Measuring performance

As previously noted, optimal solutions for the WFLOP can only be obtained for wind farms with a low number of potential turbine locations, given a limited budget of evaluations. Therefore, comparisons between EAs, for larger scenarios, may only be done on a relative basis [22]. We consider the elitist archive upon termination to be the approximation set (Figures 3.6 and 3.10). The elitist archive size was set large enough to accept all nondominated layouts for all cases, preventing oscillatory convergence of the archive [122].

To compare approximation sets, the hypervolume indicator was chosen since it is a commonly adopted useful indicator for evaluating the performance of algorithms on problems for which the OPF is unknown [123]. This performance indicator computes the search space covered by an approximation set (using a reference point). A higher hypervolume value is indicative of better performance. The hypervolume indicator captures both the diversity (even if all solutions are on the OPF, the indicator is not maximized unless the solutions are also spread out) and the proximity of the approximation set to the OPF.

The algorithms were given one million function evaluations (per objective) for all case study instances. However, if the hypervolume did not improve by at least 10^{-5} after $2 \times NIS$ generations, the algorithms were stopped. This means that further improvements might have been found if the algorithms were run longer but the convergence was deemed to be too slow [98]. Both optimization goals were normalized and the point $(0,0)$ was used as reference point to compute the hypervolume. As a result, the maximum hypervolume value is one. Note that this value cannot be achieved since it requires a layout with the maximum turbine packing and no wake losses.

3.5 Results

The experiments were run using Python implementations of the algorithms on a server computer with 16 cores (Intel Xeon ES-2690@2.9 GHz) running the 64-bit version of Ubuntu 12.04. The results were averaged over 10 independent runs. Next, we will address the open research questions presented in the introduction of the work.

3.5.1 What characteristics should an optimization algorithm have to present optimized layouts?

Although it is challenging to identify which feature has led to an improvement of the results, we try to breakdown and analyze each one of the characteristics under study.

Clustering

The results shown in Figure 3.13 show that the clustering scheme did not always improve the performance of the NSGA-II. Overall, both variants of the NSGA-II had similar performance.

SO Optimization

Figure 3.14 shows that, in general, NSGA-II variants did not extend the front as much as MOGOMEA variants did towards the highest energy production goal. A reason for this is that NSGA-II variants did not have any mechanism that puts extra pressure on individual objectives. As previously noted, these mechanisms can be highly beneficial if one of the goals is much harder to solve. In fact, finding the layout with the highest density pack of turbines in a pre-determined area is equivalent to the circle packing problem, which is a NP-complete problem [124, 125]. Furthermore, the number of available layouts in this extreme region of the OPF is much lower than in the middle section due to the lower number of available positions.

Problem internal structure

Using information on problem structure demonstrated to be beneficial since the MOGOMEA variants, on average, perform better than the NSGA-II variants as shown in Figure 3.13. In previous literature, it was shown that an online approach to learning linkage outperforms the offline approach for problems with an intricate interaction structure (and conversely in case of a straightforward structure) [106]. On the problems tested here, the *a priori* fixed model used in the o-MOGOMEA resulted in improved performance over MOGOMEA. It is important to point out that the same maximum number of fitness evaluations (one million, for each objective) was used for all wind farm areas and that the number of fitness evaluations, per solution, during the MOGOM procedure has a ceiling of $2l - 2$. For this reason, less generations were available to the MOGOMEA to learn linkage information online. A further reason for the improved performance of the offline learning variant is that the linkage structure in the MOWFLOP is largely dominated by the physical locations of the turbines, suggesting that the linkage structure of the MOWFLOP is not highly intricate and thus can well be exploited using an offline-learned structure.

3.5.2   What is the best CHT to ensure feasibility of the OWF layouts?

The MOGOMEA presented, on average, higher hypervolumes when equipped with the repair mechanism, especially in case of a grid resolution of 4 RD. The o-MOGOMEA exhibited superior performance when equipped with the resample approach. Both variants of NSGA-II showed the best average performances when using the constraint domination technique. Overall, no CHT has demonstrated to lead to superior performance in all problem instances.

3.5.3   How does the problem complexity scale with the number of variables?

We note that in this work we do not adhere to the common definition of scalability in experimental algorithmic design (i.e. how an algorithms' requirements such as memory, computing time or number of evaluations to reach the optimum increase as the problem size increases), but rather the impact of increasing the size of the problem on the performance of an algorithm under a predefined fixed budget of evaluations. As a final remark, although we are assessing the impact of the number of variables of the MOWFLOP on the computational time, the design phase of a

wind farm is a process that takes several months [126] and hence, it is an optimization problem that is not highly time-bounded in reality [98]. Therefore, the results obtained in this work should be mostly used as a guideline for the expected run times of the algorithms when equipped with different CHTs and applied to the MOWFLOP with different number of variables and wind farm sizes. Figure 3.15 shows the average run times of the algorithms.

First, it should be noted that algorithms may have been stopped before reaching the maximum number of evaluations. Second, there are multiple sources of influence on the time requirements. As a problem gets bigger (smaller grid spacing), the time requirements for model building (MOGOMEA) increase. However, for an algorithm to reach solutions of a similar quality on a larger problem, a higher number of evaluations is typically required. Since we have fixed the budget of function evaluations, final results are expected to be of lower quality for larger problems. This is especially of importance for wind farm D. Figure 3.15 shows that all algorithms, besides MOGOMEA, took on average less time to terminate for a 2 RD step. This means that the algorithms did not design wind farm layouts with high turbine densities. On the other hand, MOGOMEA took longer, on average, to terminate, due to the model building, which became the predominant component in the computing time.

The results further show that the model building of the MOGOMEA is not a major extra computational burden. In fact, the LT offline learned allowed o-MOGOMEA to find better results, i.e. more densely packed wind farm layouts, which almost always leads to requiring more computation time than does the fact that MOGOMEA has to learn a LT online every generation. Only for the biggest problem, Case D, requiring almost 2500 variables for a 2 RD grid resolution, a clear increase in required computation time for MOGOMEA versus o-MOGOMEA can be seen. On the other hand, it is important to realize that with longer runs, more densely packed wind farms would be found, ultimately increasing again the time spent performing function evaluations, potentially surpassing the time spent building linkage models.

Differently from the MOGOMEA, the run-time requirement of all remaining algorithms does not increase substantially with the number of optimization variables. This can be seen for the run times of case D. All the algorithms presented lower average runs when a 2 RD step size was employed. Once again, this is explained by the fact that the most packed layouts were not achieved. Regarding the impact of the CHTs, the use of the penalty term resulted in longer running times, for 4 and 2 RD grid resolutions, since infeasible layouts, packed with more turbines, were evaluated.

Consequently, the main influence on the running time is the evaluation of the wake losses, which becomes especially expensive if the layouts become dense. Ultimately, given a fixed time-budget rather than a number-of-evaluations budget (as would be likely in a real-world scenario), a big advantage could be the use of CHTs that do not allow evaluating infeasible layouts because the number of evaluations per second would thereby increase, thus allowing the optimization algorithms to progress further.

3.5.4 What is the relation between problem dimensionality/complexity and the degrees of freedom offered by different turbine-placement grids?

All algorithms were able to find similar Pareto fronts for all wind farm areas and CHTs when the 8 RD grid step size was used. The MOWFLOP with such a coarse grid becomes much easier to solve since it becomes an unconstrained problem with only few variables. All algorithms converged before one million evaluations for all instances of the 8 RD step size. Although relatively fast to compute, the real-world applicability is low because of the limited design freedom.

Smaller grid step sizes allow to find better wind farm layouts in the middle section of the Pareto front for problem instances A and B. However, for larger areas (C and D) the advantage of using the finest step size (2 RD) decreased within our limited budget of evaluations, since the problem complexity is highly increased (see Table 3.5), which is in line with previous literature [35].

Therefore, if wind farm developers aim at highly dense wind farms they should either use large grid spacings, manually create initial layouts to help the algorithms find good solutions in that area of the search space, let the algorithms run longer or start with a larger initial population size. The results obtained also indicate that it could be beneficial to use a Multi-Resolution (MR) scheme in which a large grid step is employed in the first optimization iteration to allow the algorithms to find densely packed wind farms with more ease [39]. Thereafter, these solutions would serve as an initial population for a second round of optimization in which a smaller grid step is used. In order to validate this assumption, we implemented a MR approach.

3.5.5 Multi-resolution

The algorithms start optimization with the 8 RD grid step and advance to the next smaller step size if the hypervolume did not increase at least 10^{-5} after NIS generations. The elitist archive is then mapped onto the finer grid and the new population is created through the same procedure used at the end of each run (see Section 3.3.3). When the algorithms advanced to a finer grid, all the new variables were set to zero since they were not mapped before. However, all algorithms create new offspring by exchanging subsets of variables between solutions. Hence, the only sources of new genetic material were the random solutions added at the end of each run and the mutation operator. To increase the impact of the latter, the mutation probability for the 8 RD step was kept constant, meaning that the rate is higher than previously for the 4 and 2 RD step sizes.

Figure 3.17 shows the results for the hypervolume and aggregated Pareto fronts for wind farm area B. The left plot shows the hypervolume of the MR approach for 4 and 8 RD step sizes. It can be seen that initially all the algorithms present similar hypervolume values since the same 8 RD step size is being used. Once the algorithms converge, they advance to the next grid resolution. This is accompanied with a higher design freedom and hence, better layouts are found. Both MOGOMEAs presented higher average hypervolumes with the MR scheme.

The right plot of Figure 3.17 shows the aggregated best Pareto fronts for all step sizes and the aggregated Pareto front found with the MR scheme. The MR approach allowed the algorithms to find Pareto fronts which cover the entire spectrum of wind farm densities. Both variants of MOGOMEA outperformed the NSGA-II implementations. Nonetheless, some parts of the new fronts are dominated by solutions found with the previous fixed grid schemes. The fact that the shown fronts are aggregated over multiple runs may explain this result.

3.5.6   Wind farm layouts

The Pareto fronts obtained for wind farm D with an 8 RD step size in the grid has a peculiarity: in the middle section there are several wind farm layouts with similar efficiency but with different energy production. If the number of turbines was fixed before optimization, wind farm designers would not find out that there are wind farm layouts with more turbines, and hence, more energy production, and similar wake losses. This demonstrates the advantage of using multi-objective optimization for the design of wind farms.

The results also show that the heuristic used for the initial populations (see Section 3.3.3) did not create solutions representing highly-packed layouts for the larger wind farm areas when the 4 and 2 RD grid spacings were used. Therefore, the optimization algorithms are required to find the more packed wind farm layouts, differently from previous literature in which a feasible solution with the maximum number of turbines was used as an initial layout [98]. Nonetheless, the heuristic had some effect in the performance of the algorithms. Similar to what was found in previous works [98], if the heuristic was able to find a layout with a high turbine density this could help the algorithms to extend the Pareto front in the first optimization goal.

Figure 3.13 shows that the hypervolume was lower for problem instances with larger wind farm areas. Such areas allowed layouts with more wind turbines and, hence, lower efficiencies. Furthermore, the impact of extending the front is much larger in the hypervolume indicator than improving the solutions in the middle of the front. This explains why the layouts with an 8 RD grid step size had, in general, a larger hypervolume indicator, despite their lower design freedom.

Figure 3.16 compares several wind farm layouts, composed of the same number of turbines, obtained with the o-MOGOMEA with a grid resolution of 8 RD and with the MR scheme. The algorithm, with an 8 RD step, optimized the layouts by placing more turbines at the edges of the farm and leaving wider spaces in the middle region. In this way, there is more free space for wake recovery and therefore, turbines in the wake of other turbines will receive higher mean wind speeds. On the other hand, with the MR scheme the free areas are evenly distributed throughout the farm and spread the turbines while preventing rows or columns from being formed. In fact, alignment of turbines only happened once it could not be avoided due to space limitations (see last plot of Figure 3.16). The layouts obtained with the MR scheme go against what has been done for most of the existing wind farms, in which the turbines were installed in grid-based layouts.
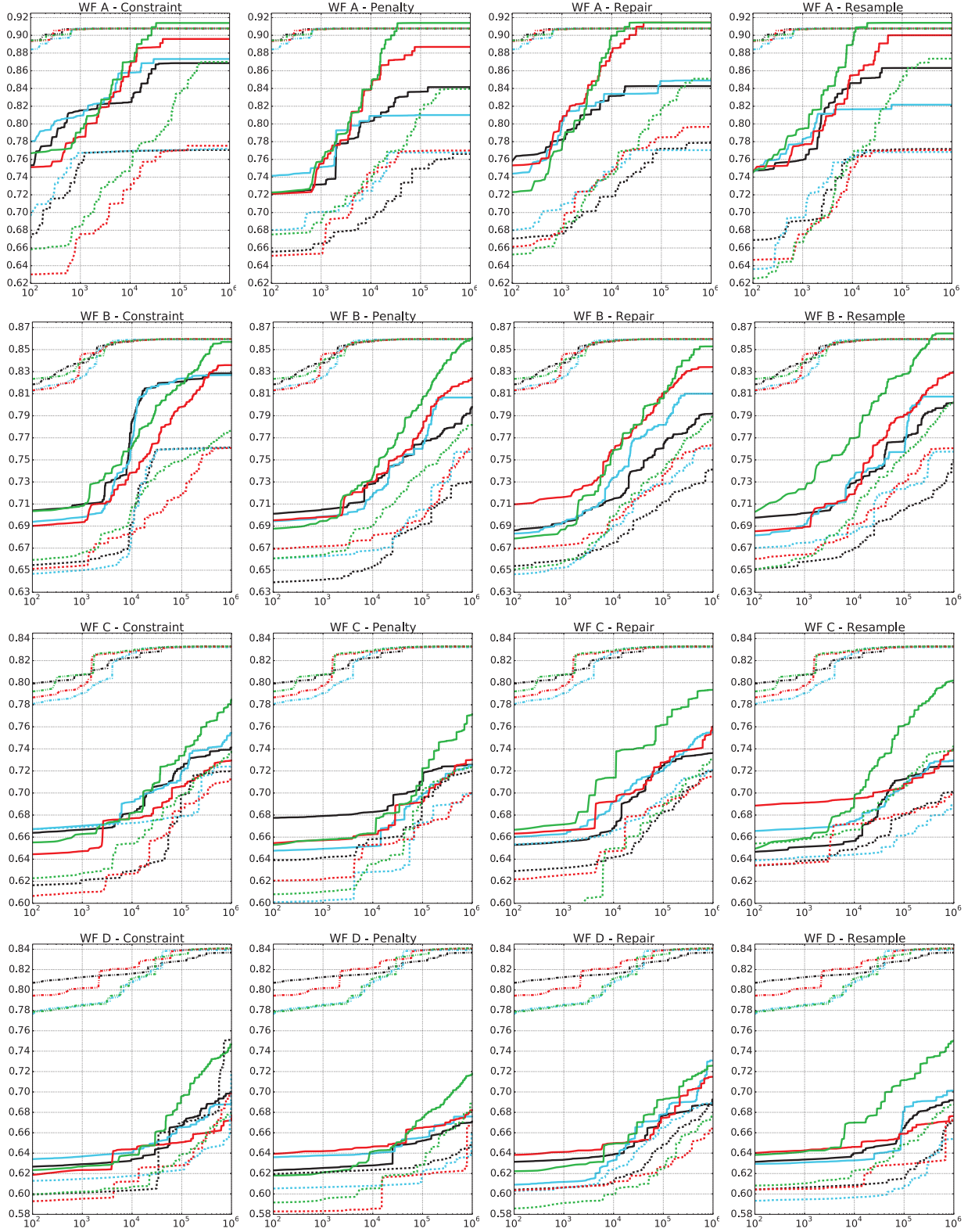
Figure 3.13: Averaged hypervolume obtained with the different algorithms, CHTs and grid step sizes. The x-axis shows the number of fitness valuations and the y-axis displays the hypervolume. MOGOMEA - red; o-MOGOMEA - green; NSGA-II - black; c-NSGA-II - blue. 8 RD grid spacing - dash-dotted lines; 4 RD - solid lines; 2 RD - dotted lines.
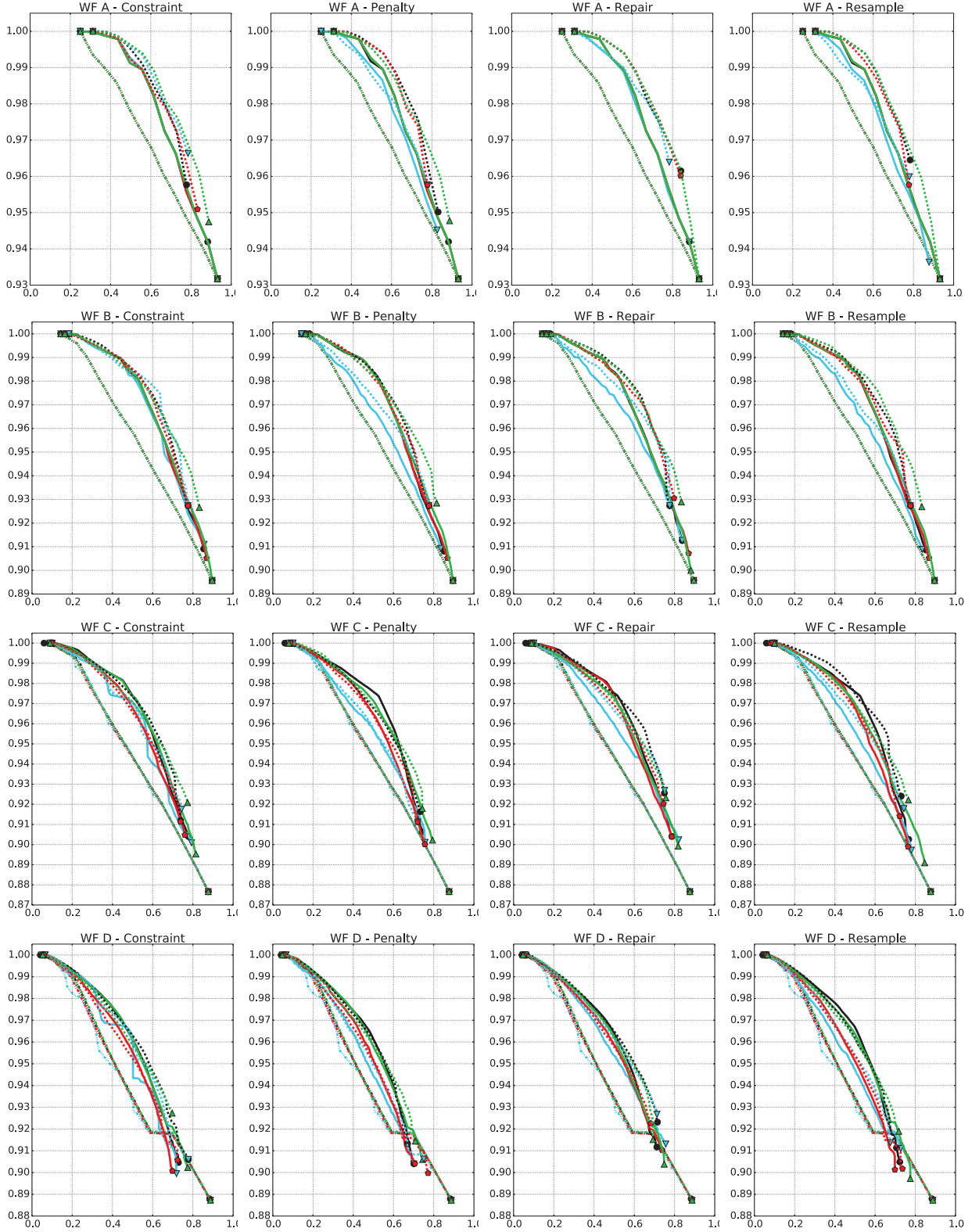
Figure 3.14: Aggregated Pareto fronts obtained with the different algorithms and CHTs. The x- and y-axes show the optimization goals, respectively. MOGOMEA - red; o-MOGOMEA - green; NSGA-II - black; c-NSGA-II - blue. 8 RD grid spacing - dash-dotted lines; 4 RD - solid lines; 2 RD - dotted lines.
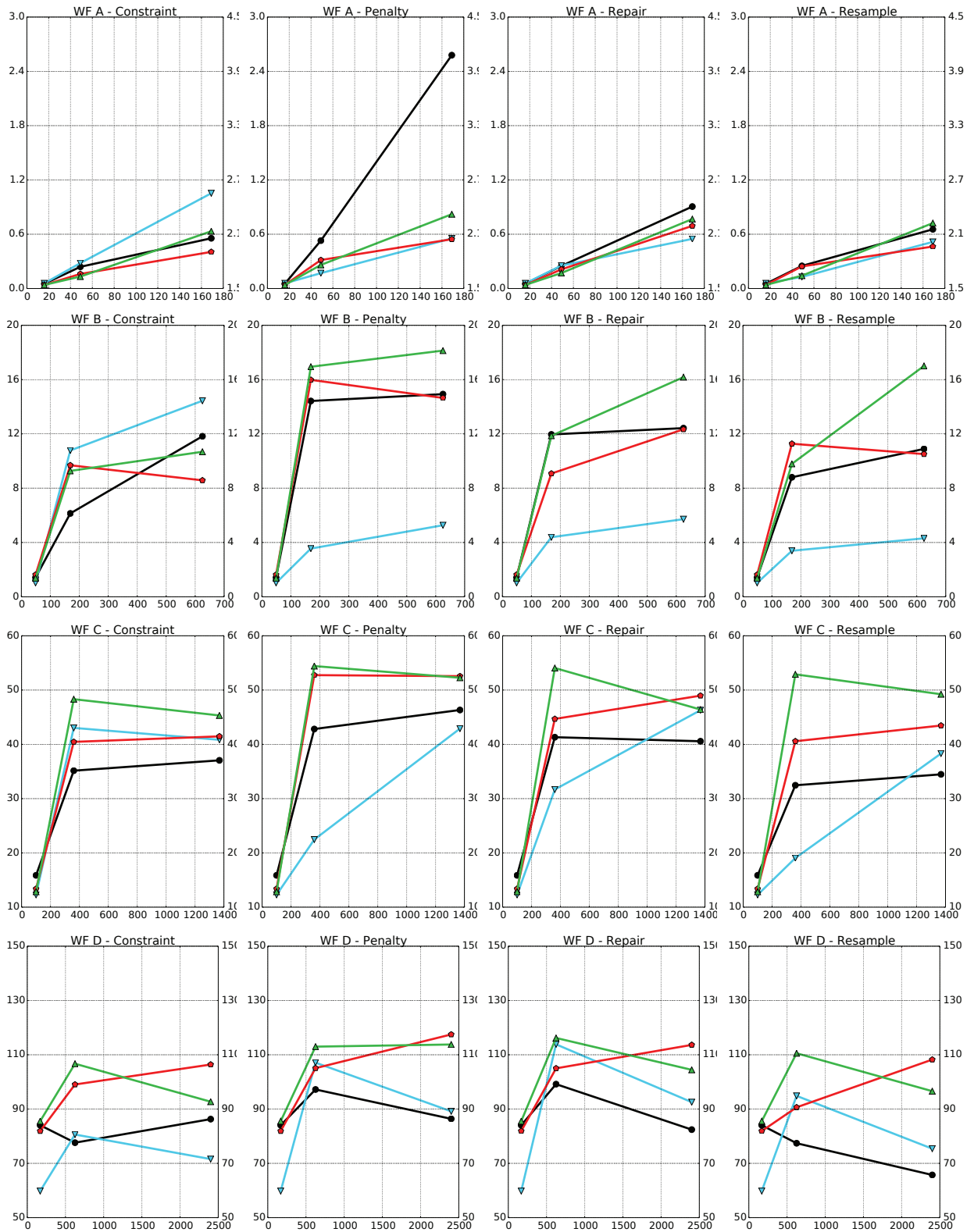
Figure 3.15: Time needed by each optimization algorithm to converge for the different constraint handling techniques. The x-axis shows the number of variables and the y-axis displays the average time, in hours, needed for termination. MOGOMEA - red; o-MOGOMEA - green; NSGA-II - black; c-NSGA-II - blue.
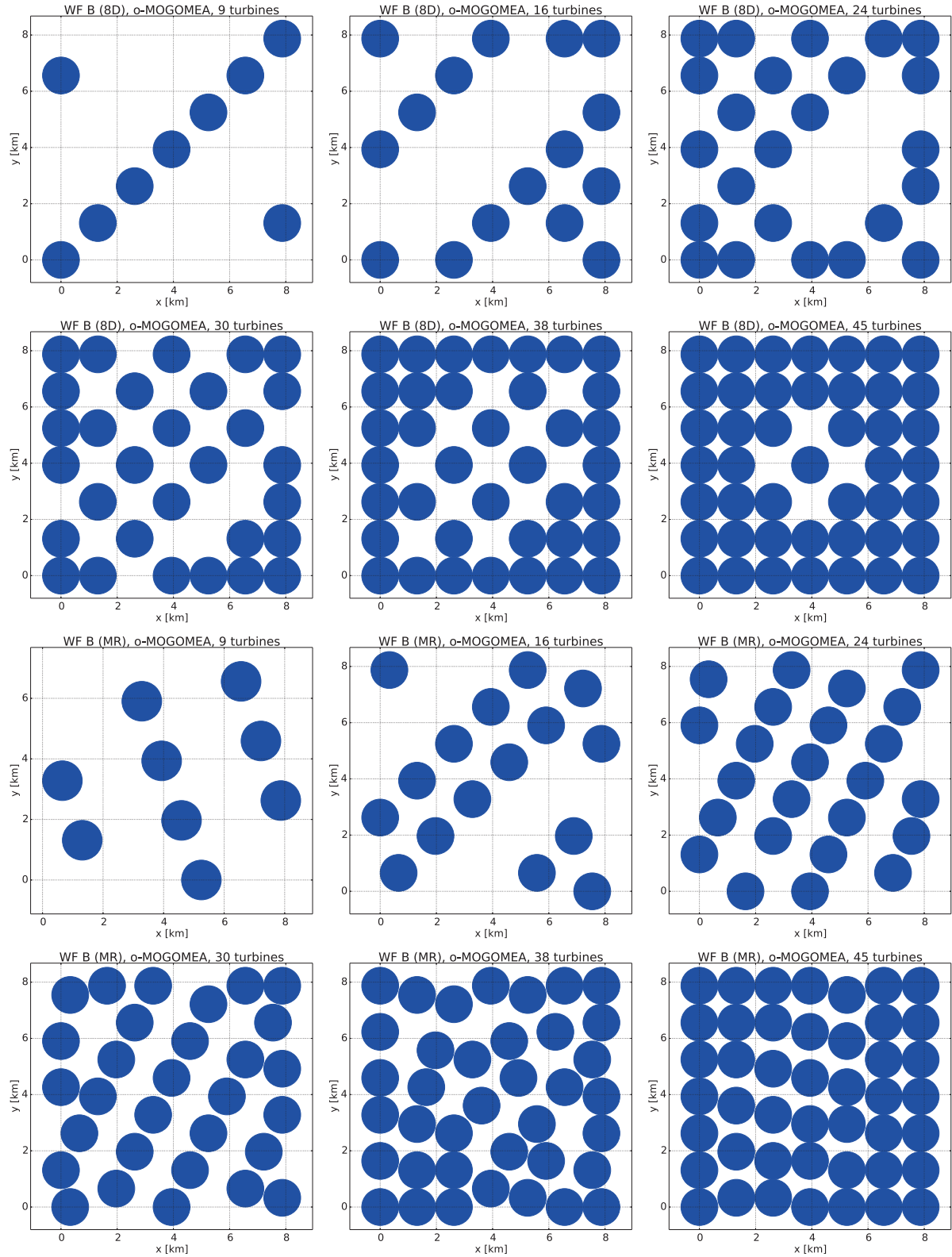
Figure 3.16: Layouts obtained with the o-MOGOMEA for an 8 RD step size and using the multi-resolution scheme. The turbines are located at the center of the circles, which represent the minimum separation between neighboring turbines.
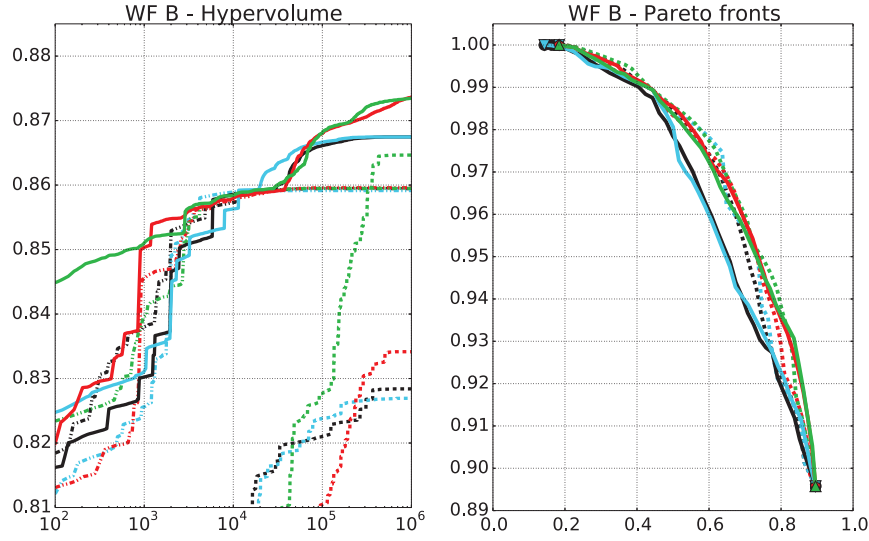
Figure 3.17: The left plot shows the average hypervolume obtained with the different algorithms with 8 RD (dash-dotted), 4 RD (dotted) and with the multi-step (solid) approach for wind farm area B. The x-axis shows the number of fitness valuations and the y-axis displays the hypervolume. The right plot shows the aggregated Pareto fronts between all the different step sizes (dotted) and the aggregated Pareto fronts obtained with the multi-resolution scheme (solid). The x- and y-axes show the optimization goals, respectively. For both plots: MOGOMEA - red; o-MOGOMEA - green; NSGA-II - black; c-NSGA-II - blue.

3.6 Conclusions

The main objective in this work was to address several important open questions in solving the WFLOP and more specifically, in its MO variant, which is arguably more relevant to real-world applications. The NSGA-II, the MOGOMEA and two variants of these algorithms were applied to solve the MOWFLOP, while considering different CHTs. Wind farms with different areas, discretized using three grid step sizes to identify potential turbine locations, were used to assess the performance of the MOEAs.

The two variants of the MOGOMEA obtained, on average, better wind farm layouts as well as areas with higher density of turbines and hence higher energy production. This result indicates that algorithmic characteristics specific to the MOGOMEA are important factors to obtain good trade-off solutions. The MOGOMEA combines wind farm layouts that are roughly similar (in objective space) to create new layouts. The MOGOMEA also actively searches for wind farm layouts that represent extreme trade-offs, i.e., that optimize only one objective. Finally, the MOGOMEA tries to identify and exploit the underlying variable-dependency structure of the problem.

No specific CHT demonstrated to have clear a advantage over the others for all algorithms. The resample approach was the best CHT for the o-MOGOMEA, whereas the repair mechanism was

the most suited for the MOGOMEA. Finally, the constraint domination technique presented better results for both variants of the NSGA-II. When used for real-world planning however, CHTs that first check constraints and prevent infeasible solutions from being evaluated, may present a potential advantage because they effectively increase the number of evaluations that can be performed per second.

Regarding the trade-off between problem dimensionality/complexity and design freedom, the results showed that, for all algorithms and small wind farm areas, finer grid step sizes allowed to find better wind farm layouts in the middle section of the Pareto front due to the larger degree of freedom in designing layouts. On the other hand, for larger areas, the advantage of using fine step sizes was reduced within the time we allowed the algorithms to run, due to increase of the problem complexity.

The results demonstrated that there is a trade-off between the computational time required for model building of the MOGOMEA and the evaluation time required to calculate the power production of the wind farm. The increase of the number of variables leads to higher computational requirements for model building. For very fine grid resolutions the time to build and exploit linkage models may overtake the time to evaluate the efficiency of wind farm layouts. However, for a problem such as MOWFLOP, we demonstrated that very good results can be obtained by fixing the linkage model to one that is learned *a priori*, i.e., offline, based on potential turbine locations since these locations are expected to have the most impact on the dependencies between problem variables in the MOWFLOP. This fully removes the potentially time-consuming overhead of model building as the problem size increases due to the use of finer grid resolutions.

Finally, designing wind farm layouts based on a multi-resolution approach whereby wind farms are first designed using a coarse grid, and over time are adjusted using finer grids, demonstrated to offer the best results when considering the same budget of function evaluations. The reason for this is that a wide trade-off is fairly easily obtained using a coarse grid resolution, which is then further improved along the entire front of trade-offs using finer grid resolutions.

For future work it would be interesting to assess the influence of smaller grid steps and wind farms with larger areas. It would also be interesting to test instances of the MOWFLOP with more than two optimization goals. Recent works introduced strategies to filter hierarchical linkage relations from the LT that may be superfluous leading to more concise linkage models without negatively effecting the performance [105]. Hence, it could be interesting to evaluate these filtering strategies in the MOWFLOP. The proposed population-sizing-free scheme has its drawbacks and other approaches may still work better, which is interesting to study further. Furthermore, the multi-step approach demonstrated to provide good results and hence, an in-depth study into the competences and a true (experimental) scalability of this approach that designates the required resources such as runtime required to reach the optimal Pareto front, should be carried out in future work.

3.7   Nomenclature

AEP	Annual Energy Production
CAPEX	Capital Expenditure
CFD	Computational Fluid Dynamics
c-NSGA	clustering NSGA
DCO	Development Consent Order
EA	Evolutionary Algorithm
EU	European Union
EWEA	European Wind Energy Association
FEED	Front-End Engineering and Design
FI	Forced Improvement
FOS	Family Of Subset
GA	Genetic Algorithm
GOMEA	Gene-pool Optimal Mixing
IBEA	Indicator Based EA
LES	Large Eddy Simulations
LT	Linkage Tree
MR	Multi-Resolution
MI	Mutual Information
MO	Multi Objective
MOEA	Multi Objective Evolutionary Algorithm
NIS	No Improvement Stretch
NSGA	Nondominated Sorting Genetic Algorithm
MOGOM	Multi-Objective Gene-pool Optimal Mixing
o-MOGOMEA	offline MOGOMEA
OPEX	Operational Expenditure
OPF	Optimal Pareto Front
OWF	Offshore Wind Farm
PSO	Particle Swarm Optimization
RD	Rotor Diameter
SO	Single Objective
SPEA	Strength Pareto Evolutionary Algorithm
UPGMA	Unweighted Pair Grouping Method Arithmetic
WFLOP	Wind Farm Layout Optimization Problem

References

[1] European Commission. [Last accessed 1st March 2015]. [Online]. Available: www.eur-lex.europa.eu/ LexUriServ/LexUriServ.do?uri=CELEX:52008DC0768:EN:HTML

[2] R. Green, and N. Vasilakos, "The economics of offshore wind," *Energy Policy*, vol. 39, no. 2, 2011.

[3] EWEA, "The european offshore wind industry - key trends and statistics 2013," Tech. Rep., 2014.

[4] EWEA, "Oceans of Opportunity - Harnessing Europe's largest domestic energy resource," EWEA, Tech. Rep. September, 2009.

[5] EWEA, "2030 targets Bringing certainty," Tech. Rep., 2013.

[6] S. Rodrigues *et al.*, "Trends of offshore wind projects," *Renewable and Sustainable Energy Reviews*, vol. 49, pp. 1114–1135, Sept. 2015.

[7] 4C Offshore. [Last accessed 23rd March 2015]. [Online]. Available: www.4coffshore.com/windfarms

[8] LORC. [Last accessed 1st March 2015]. [Online]. Available: www.lorc.dk/offshore-wind-farms-map/list

[9] The Crown Estate, "Offshore Wind Cost Reduction - Pathways Study," London, United Kingdom, Tech. Rep., 2012.

[10] The Wind Power. (2014) [Last accessed 1st March 2015]. [Online]. Available: www.thewindpower.net/windfarms_offshore_en.php

[11] Renewables Map. [Last accessed 1st March 2015]. [Online]. Available: www.renewables-map.co.uk/windfarm.asp

[12] M. Bilgili, A. Yasar, and E. Simsek, "Offshore wind power development in europe and its comparison with onshore counterpart," *Renew. and Sustainable Energy Reviews*, vol. 15, no. 2, pp. 905–15, 2011.

[13] RWE. [Last accessed 31st March 2015]. [Online]. Available: www.rwe.com/web/cms/en/1252456/rwe-innogy/sites/wind-offshore/under-construction/gwynt-y-mr/tech-and-spec/

[14] J. Serrano-Gonzalez *et al.*, "Overall design optimization of wind farms," *Renew. Energy*, vol. 36, no. 7, pp. 1973–1982, 2011.

[15] T. Sorensen, M. L. Thogersen, and P. Nielsen, "Adapting and calibration of existing wake models to meet the conditions inside offshore wind farms," EMD International A/S, Aalborg, Denmark, Tech. Rep., 2008.

[16] Anholt. [Last accessed 31st March 2015]. [Online]. Available: www.anholt-windfarm.com/en/the-project/project-site-and-scope

[17] The Crown Estate, "Submarine cables and offshore renewable energy installations - proximity study," London, United Kingdom, Tech. Rep., 2012.

[18] J. S. Gonzalez *et al.*, "A review and recent developments in the optimal wind-turbine micro-siting problem," *Renew. and Sustainable Energy Reviews*, vol. 30, no. 0, pp. 133–144, 2014.

[19] S. Wyatt *et al.*, "Detailed appraisal of the offshore wind industry in china," Carbon Trust, London, United Kingdom, Tech. Rep., July 2014.

[20] BVG Associates, "Value breakdown for the offshore wind sector," Tech. Rep., 2010.

[21] Wind Energy, "Wind Energy - The Facts Part I Technology," Brussels, Belgium, Tech. Rep., 2009.

[22] J. F. Herbert-Acero *et al.*, "A review of methodological approaches for the design and optimization of wind farms," *Energies*, vol. 7, no. 11, pp. 6930–7016, 2014.

[23] A. Tesauro, P.-E. Rethore, and G. Larsen, "State of the art of wind farm optimization," in *Proceedings of European Wind Energy Conference & Exhibition*, Copenhagen, Denmark, April 2012.

[24] C. N. Elkinton, J. F. Manwell, and J. G. McGowan, "Algorithms for Offshore Wind Farm Layout Optimization," *Wind Engineering*, vol. 32, pp. 67–84, 2008.

[25] S. Rodrigues, P. Bauer, and J. Pierik, "Modular approach for the optimal wind turbine micro siting problem through cma-es algorithm," in *Proceeding of the fifteenth annual conference companion on Genetic and evolutionary computation conference companion*, ser. GECCO '13 Companion.   New York, NY, USA: ACM, 2013, pp. 1561–1568.

[26] S. Rodrigues, P. Bauer, and J. Pierik, "A clustering approach for the wind turbine micro siting problem through genetic algorithm," in *39th Annual Conference IECON*, 2013.

[27] J. S. Gonzalez, M. Burgos Payan, and J. Riquelme Santos, "A new and efficient method for optimal design of large offshore wind power plants," *Power Systems, IEEE Transactions on*, vol. 28, no. 3, pp. 3075–3084, Aug 2013.

[28] A. G. Gonzalez-Rodriguez *et al.*, "Reducing computational effort in the calculation of annual energy produced in wind farms," *Renew. and Sustainable Energy Reviews*, vol. 43, no. 0, pp. 656–665, 2015.

[29] K. Deb, *Multi-Objective Optimization using Evolutionary Algorithms*, 1st ed.   Wiltshire, England: John Wiley & Sons, Ltd, 2001.

[30] S. Salcedo-Sanz *et al.*, "A review of recent evolutionary computation-based techniques in wind turbines layout optimization problems," *Central European Journal of Computer Science*, vol. 1, no. 1, pp. 101–107, 2011.

[31] S. Khan, and S. Rehman, "Computational intelligence techniques for placement of wind turbines: A brief plan of research in saudi arabian perspective," in *Energy Conference and Exhibition (EnergyCon), 2010 IEEE International*, Dec 2010, pp. 519–523.

[32] S. A. Khan, and S. Rehman, "Iterative non-deterministic algorithms in on-shore wind farm design: A brief survey," *Renew. and Sustainable Energy Reviews*, vol. 19, no. 0, pp. 370–384, 2013.

[33] S. Lumbreras, and A. Ramos, "Offshore wind farm electrical design: a review," *Wind Energy*, vol. 16, no. 3, pp. 459–473, 2013.

[34] G. Mosetti, C. Poloni, and B. Diviacco, "Optimization of wind turbine positioning in large windfarms by means of a genetic algorithm," *Journal of Wind Engineering and Industrial Aerodynamics*, vol. 51, no. 1, pp. 105–116, Jan 1994.

[35] F. Wang, D. Liu, and L. Zeng, "Study on computational grids in placement of wind turbines using genetic algorithm," in *World Non-Grid-Connected Wind Power and Energy Conference, 2009. WNWEC 2009*, 2009, pp. 1–4.

[36] S. Rodrigues, P. Bauer, and P. Bosman, "A novel population-based multi-objective cma-es and the impact of different constraint handling techniques," in *Proceedings of the sixteenth annual conference companion on Genetic and evolutionary computation conference, GECCO14*.   New York, NY, USA: ACM, 2014.

[37] P. Pardalos *et al.*, *Handbook of Wind Power Systems*.   Springer, 2013, no. IX.

[38] N. H. Luong, H. La Poutré, and P. A. Bosman, "Multi-objective gene-pool optimal mixing evolutionary algorithms," in *Proceedings of the 2014 Conference on Genetic and Evolutionary Computation*, 2014, pp. 357–364.

[39] P.-E. Rethore *et al.*, "Topfarm: Multi-fidelity optimization of offshore wind farm," in *ISOPE conference*, Hawaii, USA, 2011.

[40] RWE, "Galloper wind farm project environmental statement - chapter 5 project details," Tech. Rep., 2011.

[41] RWE, "Gwynt y mor offshore wind farm - environmental statement (non technical summary)," Tech. Rep., 2005.

[42] A. Kusiak, and Z. Song, "Design of wind farm layout for maximum wind energy capture," *Renew. Energy*, vol. 35, pp. 685–694, 2010.

[43] E. Zitzler, and L. Thiele, "Multiobjective evolutionary algorithms: a comparative case study and the strength pareto approach," *Evolutionary Computation, IEEE Transactions on*, vol. 3, no. 4, pp. 257–271, Nov 1999.

[44] P. Y. Zhang, "Topics in wind farm layout optimization: Analytical wake models, noise propagation, and energy production," Master's thesis, University of Toronto, 2013.

[45] W. Y. Kwong *et al.*, "Wind farm layout optimization considering energy generation and noise propagation," in *Proceedings of the ASME 2012 International Design Engineering Technical Conferences & Computers and Information in Engineering Conference*, Chicago, USA, Aug. 2012.

[46] K. Deb *et al.*, "A fast and elitist multiobjective genetic algorithm: Nsga-ii," *IEEE Transactions on Evolutionary Computation*, vol. 6, no. 2, pp. 182–197, 2002.

[47] K. Veeramachaneni *et al.*, "Optimizing energy output and layout costs for large wind farms using particle swarm optimization," in *IEEE Congress on Evolutionary Computation*, 2012, pp. 1–7.

[48] X. Li, "A nondominated sorting particle swarm optimizer for multiobjective optimization," in *Lecture Notes in Computer Science, Proceedings of Genetic and Evolutionary Computation GECCO 2003, Vol. 2723, Part I*, 2003, pp. 37–48.

[49] R. Tran *et al.*, "Fast and effective multi-objective optimisation of wind turbine placement," in *Proceedings of the 15th Annual Conference on Genetic and Evolutionary Computation*, 2013, pp. 1381–1388.

[50] E. Zitzler, M. Laumanns, and L. Thiele, "Spea2: Improving the strength pareto evolutionary algorithm," Tech. Rep., 2001.

[51] E. Zitzler, and S. Kunzli, "Indicator-based selection in multiobjective search," in *Parallel Problem Solving from Nature - PPSN VIII*, ser. Lecture Notes in Computer Science. Springer Berlin Heidelberg, 2004, vol. 3242, pp. 832–842.

[52] S. Sisbot *et al.*, "Optimal positioning of wind turbines on gokceada using multi-objective genetic algorithm," *Wind Energy*, vol. 13, no. 4, pp. 297–306, 2010.

[53] S. J. Andersen *et al.*, "Comparison of Engineering Wake Models with CFD Simulations," *Journal of Physics: Conference Series*, vol. 524, p. 012161, 2014.

[54] R. J. Barthelmie *et al.*, "Comparison of Wake Model Simulations with Offshore Wind Turbine Wake Profiles Measured by Sodar," *Journal of Atmospheric and Oceanic Technology*, vol. 23, no. 7, pp. 888–901, 2006.

[55] B. Sanderse, "Aerodynamics of wind turbine wakes - literature review," Energy Research Centre of the Netherlands (ECN), Petten, The Netherlands, Tech. Rep., 2009.

[56] A. Crespo, J. Hernandez, and S. Frandsen, "Survey of modelling methods for wind turbine wakes and wind farms," *Wind Energy*, vol. 2, no. 1, pp. 1–24, 1999.

[57] L. Vermeer, J. Sorensen, and A. Crespo, "Wind turbine wake aerodynamics," *Progress in Aerospace Sciences*, vol. 39, pp. 467–510, 2003.

[58] N. Jensen, "A note on wind generator interaction," Riso National Laboratory, Roskilde, Denmark, Tech. Rep. Riso-M-2411, 1983.

[59] I. Katic, J. Hojstrup, and N. Jensen, "A simple model for cluster efficiency," in *EWEC'86. Proceedings. Vol. 1*, 1986, pp. 407–410.

[60] F. F. Ainslie, "Calculating the flowfield in the wake of wind turbines," *Journal of Wind Engineering and Industrial Aerodynamics*, vol. 27, no. 1, pp. 213–224, 1988.

[61] S. Frandsen *et al.*, "Analytical modelling of wind speed deficit in large offshore wind farms," *Wind Energy*, vol. 9, no. 1–2, pp. 39–53, 2006.

[62] M. C. Brower, and N. M. Robinson, "The openwind deep-array wake model - development and validation," Tech. Rep., 2012.

[63] L. G. C., "A simple stationary semi-analytical wake model," Riso National Laboratory, Roskilde, Tech. Rep. Riso-R-1713(EN), 2009.

[64] J. Annoni *et al.*, "Evaluating wake models for wind farm control," in *Proceedings of the American Control Conference*, 2014, pp. 2517–2523.

[65] "Dynamic wake meandering modeling," Riso National Laboratory, Roskilde, Tech. Rep. Riso-R-1607(EN), 2007.

[66] R. Mikkelsen, "Actuator disc methods applied to wind turbines," Ph.D. dissertation, Technical University of Denmark, 2003.

[67] P. Torres, J.-W. van Wingerden, and M. Verhaegen, "Modeling of the flow in wind farms for total power optimization," in *International Conference on Control and Automation (ICCA)*, 2011, pp. 963–968.

[68] S. Ott, J. Berg, and M. Nielsen, "Linearised cfd models for wakes," Riso National Laboratory, Tech. Rep., 2011.

[69] M. Wagner *et al.*, "Optimizing the layout of 1000 wind turbines," in *European Wind Energy Association Annual Event*. Brussels, Belgium: European Wind Energy Association, 2011, pp. 1–10.

[70] P. Kumar, "A framework for multi-objective optimization and multi-criteria decision making for design of electrical drives," Ph.D. dissertation, Delft University of Technology, Delft, The Netherlands, 2008.

[71] Y. Zhou *et al.*, "Optimization of a hybrid wind park through a design approach - progressive design methodology," in *Power Electronics and Motion Control Conference, 2009. IPEMC '09. IEEE 6th International*, May 2009, pp. 1092–1098.

[72] Y. Eroglu, and S. U. Seckiner, "Wind farm layout optimization using particle filtering approach," *Renew. Energy*, vol. 58, no. 0, pp. 95–107, 2013.

[73] S. Turner *et al.*, "A new mathematical programming approach to optimize wind farm layouts," *Renew. Energy*, vol. 63, no. 0, pp. 674–680, 2014.

[74] S. Rodrigues *et al.*, "Wake losses optimization on offshore wind farms with moveable floating wind turbines," *Elsevier Energy Conversion and Management*, vol. 89, pp. 933–941, January 2015.

[75] S. Frandsen, "On the wind speed reduction in the center of large clusters of wind turbines," *Journal of Wind Engineering and Industrial Aerodynamics*, vol. 39, pp. 251–265, 1992.

[76] C. N. Elkinton, "Offshore wind farm layout optimization," Ph.D. dissertation, University of Massachusetts, Amherst, January 2007.

[77] J. Serrano-Gonzalez *et al.*, "Optimization of wind farm turbines layout using an evolutive algorithm," *Renew. Energy*, vol. 35, no. 8, pp. 1671–1681, 2010.

[78] H. Gu, and J. Wang, "Irregular-shape wind farm micro-siting optimization," *Energy*, vol. 57, no. 0, pp. 535–544, 2013.

[79] S. Grady, M. Hussaini, and M. Abdullah, "Placement of wind turbines using genetic algorithms," *Renewable Energy*, vol. 30, no. 2, pp. 259–270, 2005.

[80] D. Wilson *et al.*, "On learning to generate wind farm layouts," in *Proceedings of the 15th Annual Conference on Genetic and Evolutionary Computation*, ser. GECCO '13.   New York, NY, USA: ACM, 2013, pp. 767–774.

[81] A. Emami, and P. Noghreh, "New approach on optimization in placement of wind turbines within wind farm by genetic algorithms," *Renew. Energy*, vol. 35, no. 7, pp. 1559–1564, 2010.

[82] M. Wagner, J. Day, and F. Neumann, "A fast and effective local search algorithm for optimizing the placement of wind turbines," *Renew. Energy*, vol. 51, no. 0, pp. 64–70, 2013.

[83] C. Igel, N. Hansen, and S. Roth, "Covariance matrix adaptation for multi-objective optimization," *Evolutionary Computation*, vol. 15, no. 1, pp. 1–28, 2007.

[84] K. Harada *et al.*, "Constraint-handling method for multi-objective function optimization: Pareto descent repair operator," in *Evolutionary Multi-Criterion Optimization*, 2007, vol. 4403.

[85] C. Wan *et al.*, "Optimal micro-siting of wind farms by particle swarm optimization," in *Advances in Swarm Intelligence*, ser. Lecture Notes in Computer Science, Y. Tan, Y. Shi, and K. Tan, Eds.   Springer Berlin Heidelberg, 2010, vol. 6145, pp. 198–205.

[86] T. P. Runarsson, and X. Yao, "Constrained evolutionary optimization - the penalty function approach," 2002.

[87] C. A. C. Coello, "A survey of constraint handling techniques used with evolutionary algorithms," Laboratorio Nacional de Informatica Avanzada, Tech. Rep., 1999.

[88] S. Chowdhury *et al.*, "Optimizing the arrangement and the selection of turbines for wind farms subject to varying wind conditions," *Renew. Energy*, vol. 52, no. 0, pp. 273–282, 2013.

[89] S. Chowdhury *et al.*, "Unrestricted wind farm layout optimization (UWFLO): Investigating key factors influencing the maximum power generation," *Renew. Energy*, vol. 38, no. 1, pp. 16–30, 2012.

[90] Y. Eroglu, and S. U. Seckiner, "Design of wind farm layout using ant colony algorithm," *Renew. Energy*, vol. 44, no. 0, pp. 53–62, 2012.

[91] B. Saavedra-Moreno *et al.*, "Seeding evolutionary algorithms with heuristics for optimal wind turbines positioning in wind farms," *Renew. Energy*, vol. 36, no. 11, pp. 2838–2844, 2011.

[92] Y. Chen *et al.*, "Wind farm layout optimization using genetic algorithm with different hub height wind turbines," *Energy Conversion and Management*, vol. 70, no. 0, pp. 56–65, 2013.

[93] M. A. Lackner, and C. N. Elkinton, "An analytical framework for offshore wind farm layout optimization," *Wind Engineering*, vol. 31, pp. 17–31, Jan. 2007.

[94] K. Sadowski, D. Thierens, and P. A. Bosman, "Combining model-based eas for mixed-integer problems," in *Parallel Problem Solving from Nature – PPSN XIII*. Springer International Publishing, 2014, vol. 8672, pp. 342–351.

[95] P. Zhang *et al.*, "Solving wind farm layout optimization with mixed integer programmig and constraint programmig," in *Integration of AI and Techniques in Constraint Programming for Combinatorial Optimization Problems*, ser. Lecture Notes in Computer Science, C. Gomes, and M. Sellmann, Eds. Springer Berlin Heidelberg, 2013, vol. 7874, pp. 284–299.

[96] R. Archer *et al.*, "Wind turbine interference in a wind farm layout optimization mixed integer linear programming model," *Wind Engineering*, vol. 35, pp. 165–175, 2011.

[97] P. Fagerfjall, "Optimizing wind farm layout - more bang for the buck using mixed integer linear programming," Master's thesis, Gothenburg University, Gothenburg, 2010.

[98] U. A. Ozturk, and B. A. Norman, "Heuristic methods for wind energy conversion system positioning," *Electric Power Systems Research*, vol. 70, no. 3, pp. 179–185, 2004.

[99] M. Pelikan, K. Sastry, and D. E. Goldberg., "Multiobjective hboa, clustering, and scalability," in *Procedings of the Genetic and Evolutionary Computational Conference (GECCO)*, ACM, Ed., 2005, pp. 663–670.

[100] K. Sastry, M. Pelikan, and D. E. Goldberg, "Decomposable problems, niching, and scalability of multiobjective estimation of distribution algorithms." University of Illinois, Tech. Rep. 2005004, 2005.

[101] P. Bosman, "The anticipated mean shift and cluster registration in mixture-based edas for multi-objective optimization," in *Proceedings of the Genetic and Evolutionary Computation Conference - GECCO-2010*. New York: ACM Press, 2010, pp. 351–358.

[102] D. Thierens, and P. A. Bosman, "Optimal mixing evolutionary algorithms," in *Proceedings of the 13th Annual Conference on Genetic and Evolutionary Computation*, 2011, pp. 617–624.

[103] P. Bosman, and T. Alderliesten, "Incremental gaussian model-building in multi-objective edas with an application to deformable image registration," in *Proceedings of the Genetic and Evolutionary Computation Conference - GECCO-2012*. New York: ACM Press, 2012, pp. 241–248.

[104] P. A. Bosman, and D. Thierens, "Linkage neighbors, optimal mixing and forced improvements in genetic algorithms," in *Proceedings of the 14th Annual Conference on Genetic and Evolutionary Computation*, ser. GECCO '12. New York, NY, USA: ACM, 2012, pp. 585–592.

[105] P. A. Bosman, and D. Thierens, "More concise and robust linkage learning by filtering and combining linkage hierarchies," in *Proceedings of the 15th Annual Conference on Genetic and Evolutionary Computation*, ser. GECCO '13. New York, NY, USA: ACM, 2013, pp. 359–366.

[106] D. Thierens, and P. Bosman, "Predetermined versus learned linkage models," in *Proceedings of the 14th Annual Conference on Genetic and Evolutionary Computation*, ser. GECCO '12. New York, NY, USA: ACM, 2012, pp. 289–296.

[107] D. Thierens, and P. Bosman, "Evolvability analysis of the linkage tree genetic algorithm," in *Parallel Problem Solving from Nature - PPSN XII*, ser. Lecture Notes in Computer Science, 2012, vol. 7491, pp. 286–295.

[108] I. Gronau, and S. Moran, "Optimal implementations of UPGMA and other common clustering algorithms," *Information Processing Letters*, vol. 104, no. 6, pp. 205–210, 2007.

[109] P. Bosman, and D. Thierens, "On measures to build linkage trees in ltga," in *Parallel Problem Solving from Nature - PPSN XII*, Berlin, Germany, 2012, vol. 7491, pp. 276–285.

[110] N. Luong, and P. Bosman, "Elitist archiving for multi-objective evolutionary algorithms: To adapt or not to adapt," in *Parallel Problem Solving from Nature (PPSN XII)*. Berlin: Springer-Verlag, 2012, pp. 72–81.

[111] J. Knowles, and D. Corne, "Properties of an adaptive archiving algorithm for storing nondominated vectors," *Evolutionary Computation, IEEE Transactions on*, vol. 7, no. 2, pp. 100–116, April 2003.

[112] E. Zitzler, K. Deb, and L. Thiele, "Comparison of multiobjective evolutionary algorithms: Empirical results," *Evol. Comput.*, vol. 8, no. 2, pp. 173–195, Jun. 2000.

[113] P. Bosman, and D. Thierens, "The balance between proximity and diversity in multiobjective evolutionary algorithms," *Evol. Comput., IEEE Transactions on*, vol. 7, no. 2, pp. 174–188, April 2003.

[114] Vestas Wind Systems A/S, "Offshore v164-8.0 mw v112-3.3 mw," Tech. Rep., 2013. [Online]. Available: nozebra.ipapercms.dk/Vestas/Communication/Productbrochure/OffshoreProductBrochure/OffshoreProductBrochure/

[115] E. Berge *et al.*, "Modelling of offshore wind resources. Comparison of a mesoscale model and measurements from FINO 1 and North Sea oil rigs," in *European Wind Energy Conference and Exhibition (EWEC)* , 2009.

[116] H.-C. Chang, and L.-C. Wang, "A simple proof of thue's theorem on circle packing," Tech. Rep., 2010. [Online]. Available: arxiv.org/pdf/1009.4322.pdf

[117] J. Bauer, and J. Lysgaard, "The offshore wind farm array cable layout problem: a planar open vehicle routing problem," *Journal of the Operational Research Society*, vol. 66, pp. 360–368, 2014.

[118] S. Rodrigues, P. Bosman, and P. Bauer, "Collection network cable routing and wake losses optimization in offshore wind farms," in *Proceedings of the XIII Symposium of Specialists in Electric Operational and Expansion Planning*, Brazil, 2014.

[119] F. Gonzalez-Longatt *et al.*, "Optimal electric network design for a large offshore wind farm based on a modified genetic algorithm approach," *Systems Journal, IEEE*, vol. 6, no. 1, pp. 164–172, March 2012.

[120] "Algorithms for cable network design on large-scale wind farms," Tufts University, Medford, USA, Tech. Rep., 2011.

[121] J. T. Richardson *et al.*, "Some guidelines for genetic algorithms with penalty functions," in *Proceedings of the Third International Conference on Genetic Algorithms*, San Francisco, CA, USA, 1989, pp. 191–197.

[122] J. Fieldsend, R. Everson, and S. Singh, "Using unconstrained elite archives for multiobjective optimization," *IEEE Transactions on Evolutionary Computation*, vol. 7, no. 3, pp. 305–323, June 2003.

[123] E. Zitzler, and L. Thiele, "Multiobjective optimization using evolutionary algorithms - a comparative case study," in *Parallel Problem Solving from Nature (PPSN-V)*. Springer, 1998, vol. 1498, pp. 292–301.

[124] M. Hifi, V. T. Paschos, and V. Zissimopoulos, "A simulated annealing approach for the circular cutting problem," *European Journal of Operational Research*, vol. 159, no. 2, pp. 430–448, 2004.

[125] I. Castillo, F. J. Kampas, and J. D. Pinter, "Solving circle packing problems by global optimization: Numerical results and industrial applications," *European Journal of Operational Research*, vol. 191, no. 3, pp. 786–802, 2008.

[126] K. E. Thomsen, "Chapter three - project planning," in *Offshore Wind*, K. E. Thomsen, Ed. Boston: Elsevier, 2012, pp. 27–49.

Steady-State Loss Models for Optimization Purposes

The cost of offshore wind energy has not yet reached competitive levels despite the recent techno-logical improvements. Optimization tools designed to reduce the overall losses in Offshore Wind Farms (OWFs) may help to reduce its cost of energy. Hence, fast and accurate loss models are necessary for the optimization of the OWFs design. The aim of this work is the development of models to calculate the power losses in the offshore cables, transformers and converters of the collection and transmission systems. All the proposed models consider the main sources of losses during steady-state operation as well as their dependence on temperature and are computation-ally light. The cable model considers the type of soil surrounding it, whereas in the converter case, the IGBT datasheet information is used to compute the losses. The power production of a 640 MW OWF situated at 50, 100 and 150 km from shore is compared against the proposed models and models in which the operating temperature dependence is not considered for both the HVdc and HVac transmission options. Although the obtained break-even distances were similar in both models, higher efficiencies for both transmission technologies were obtained when considering the operating temperature correction factors. The higher accuracy of the proposed models may help designers to better predict the profitability of OWFs.

4.1 Introduction

Without governmental incentives the wind industry would probably not consider offshore projects due to their high energy costs [1, 2]. However, there are different measures to decrease offshore energy costs [1]. One of the possibilities is to optimize the offshore wind farm (OWF) layout and its electrical infrastructure to enhance the energy production. Since optimization algorithms require thousands of model evaluations, fast and reliable software tools are needed to obtain optimized OWF designs [3].

Differently from desired the cost of the offshore wind industry has stabilized in the last years. Furthermore, Figure 4.1a shows that the cost per MW installed in OWFs has increased since the initial projects. Figure 4.1b demonstrates that the offshore wind industry has chosen different transmission technologies according to the projects distance to shore and installed capacity.

Previous studies have calculated collection and transmission system losses as well as the Break-Even Distance (BED) between high-voltage ac (HVac) and high-voltage dc (HVdc) technologies (see Figure 4.2) [8–10]. However, the cable models did not considered the OWF site geographical properties (e.g. soil), converter (rectifier and inverter) models were highly simplified and temperature correction factors were disregarded [11].

Given the existing gap in the literature, the aim of this work is to develop better loss models for the electrical infrastructure of an OWF: the cabling systems, transformers and Modular Multilevel Converters (MMCs). To facilitate the integration with the optimization tools, the models need to capture the main sources of losses under steady-state, consider the operating temperature correction factors and soil properties, be computationally light and code based, i.e. without external simulation software. The remainder of the work is organized as follows: Sections 4.2, 4.3 and 4.4 introduce the proposed models, namely cables, converter and transformer, respectively. Afterwards, a case study is presented in Section 4.5, followed by the results Section 4.6. Final conclusions are given in Section 4.7.

(a) Cost per MW installed.

(b) Transmission technology.
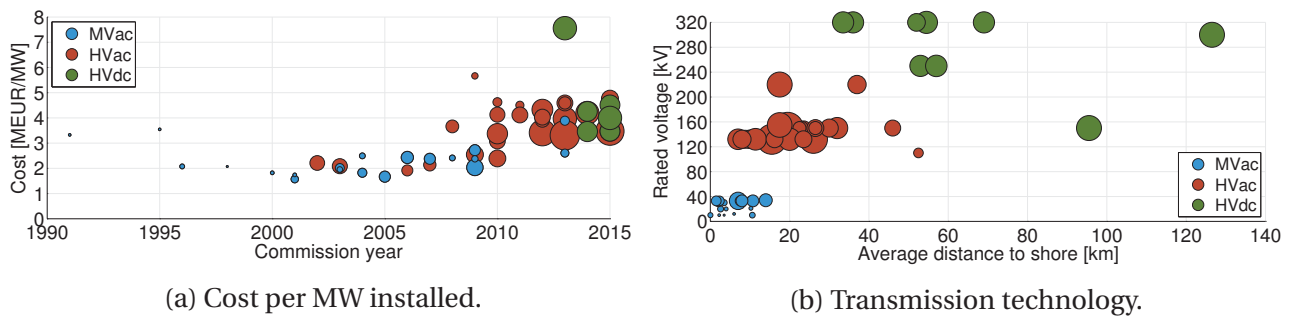
Figure 4.1: Influence of the distance to shore on project's transmission voltage level and technology for commissioned and under construction European OWFs composed of five or more turbines [4–7]. Bubble area represents the installed capacity of the OWFs.
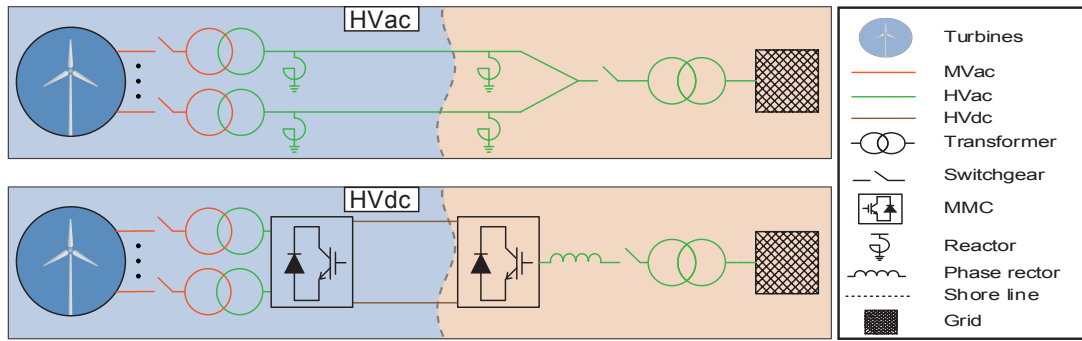
Figure 4.2: HVac and HVdc transmission system technologies.
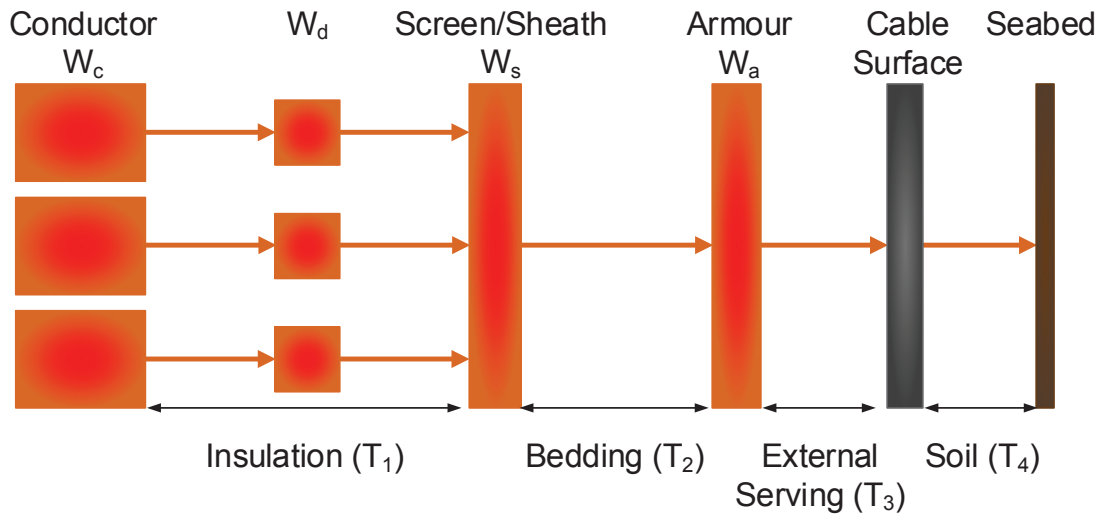
Figure 4.3: Heat dissipation in a three-core ac cable [11].

4.2 Cables

During the operation of an ac cable, heat is produced because of ohmic and dielectric losses. The losses at the conductors (W_c), the insulation (W_d) as well as the losses due to inducted circulating and eddy currents in the metallic sheath (W_s) and armour (W_a) of the cable generate heat. Then it dissipates the heat from the interior of the cable towards the surroundings. A graphical representation of this phenomenon for a three-core ac cable is presented in Figure 4.3.

In case of ac cables, a capacitance is created between the conductor and the screen/sheath due to the metallic screen around the conductor. When the cable is energized a charging current flows through it. The molecules of the material act as electric dipoles and realign each time the direction of the magnetic field changes. The work required for this realignment leads to consumption of power and subsequent heat generation [12]. This power loss is called dielectric loss and is given

by the following expression [13]:

$$W_d = 2\pi f C_p U_0^2 \tan\delta \tag{4.1}$$

where W_d is the dielectric loss per meter $[W/m]$, f is the system frequency $[Hz]$, C_p is the cable capacitance per meter $[F/m]$, U_0 is the phase voltage $[V]$ and $\tan\delta$ is the dielectric loss factor.

The generated heat and, consequently, the temperature of the conductor depend on the current flowing in the cable. Therefore, the maximum current through a cable is confined by its temperature limit which is usually imposed by the insulation material. In dc cables the heat generation is caused only by ohmic losses at the conductor since there are no sheath, armour or dielectric losses under dc loading.

According to the IEC 60287, the maximum current of an ac cable is given by the following expression, which also takes into account the possibility of drying out of the soil [13]:

$$I_{c,max} = \sqrt{\frac{\Delta\theta_{c,max} - W_d\left[\frac{1}{2}T_1 + n(T_2 + T_3 + \nu_x T_4)\right] + (\nu_x - 1)\Delta\theta_{cr}}{R_{ac}^{\theta_{c,max}}\,(T_1 + n(1+\lambda_1)T_2 + n(1+\lambda_1+\lambda_2)(T_3 + \nu_x T_4))}} \tag{4.2}$$

where $\Delta\theta_{c,max}$ is the maximum conductor temperature rise above the ambient temperature $[K]$, $I_{c,max}$ is the maximum current of conductor $[A]$, $R_{ac}^{\theta_{c,max}}$ is the ac resistance per meter of the conductor at $\theta_{c,max}$ °C $[\Omega/m]$, W_d is the dielectric loss per meter for the insulation surrounding one conductor $[W/m]$, T_1 is the thermal resistance per meter between one conductor and the sheath $[K\ m/W]$, T_2 is the thermal resistance per meter between the sheath and the armour $[K\ m/W]$, T_3 is the thermal resistance per meter of the external serving of the cable $[K\ m/W]$, T_4 is the thermal resistance per meter between the cable surface and the surrounding medium $[K\ m/W]$, n is the number of load-carrying conductors in the cable, λ_1 is the loss factor for the sheath or screen, λ_2 is the loss factor for the armour, ν_x is the ratio of dry over moist soil thermal resistivity and $\Delta\theta_{cr}$ is the critical drying soil temperature rise $[K]$. The thermal resistances T_{1-4} are calculated according to IEC 60287 [13].

For dc cables the same expression may be used by eliminating the ac specific parameters $(W_d, W_s, W_a, \lambda_1, \lambda_2 = 0)$, defining $n = 1$ and by replacing the ac resistance $R_{ac}^{\theta_{c,max}}$ by the dc resistance. These two resistances are related by:

$$R_{ac}^{\theta_c} = R_{dc}^{\theta_c}(1 + y_s + y_p) \tag{4.3}$$

where y_s is the skin effect factor and y_p is the proximity effect factor. The calculation of the skin and proximity effect factors for a three-core or three single-core cables are done according to [13].

Furthermore, the ac resistance of a conductor at a temperature θ_c can be derived by the following equation [13]:

$$R_{ac}^{\theta_c} = R_{ac}^{20}[1 + \alpha_{20}(\theta_c - 20)] \tag{4.4}$$

where α_{20} is the temperature coefficient of resistivity at $20\,°C$ (K^{-1}), θ_c is the temperature of the conductor (°C) and R_{ac}^{20} [Ω] is the resistance of the conductor at $20\,°C$.

The proposed cable model is based on the work presented in [14] and its core is given by the following expression:

$$W_t = W_d + W_{I,R}\left(\frac{I}{I_R}\right)^2 v_\theta \tag{4.5}$$

where W_t are the total cable losses [J], W_d are the cable dielectric losses [J], $W_{I,R}$ the rated cable ohmic losses [J], I_R is the rated rms current [A], I is the rms current [A] and v_θ is a correction temperature coefficient.

Figure 4.4 shows the procedure to calculate the cable losses. Although, the methodology is based on previous work [14], it does not require an external software to calculate the cable rated current neither to determine the occurrence of soil drying-out. An iterative procedure is used in the proposed model to avoid external software.

The rated current of the cable segment is calculated by an iterative method shown in Figure 4.5. Initially, an estimation for the rated current (e.g. manufacturer data) is used as a starting point. Then it is determined whether there is soil drying-out or not and the equation (4.2) is used. This new value of the rated current is used again to check if there is drying-out or not and the procedure starts again until it converges.

Consequently, the temperature of the conductor has to be calculated to estimate the total phase impedance (see Figure 4.4). The procedure is summarized in Figure 4.6. Initially the cable surface temperature is calculated for the rated current. If there is no drying-out for the rated current, then this is the case for the current I_c as well.
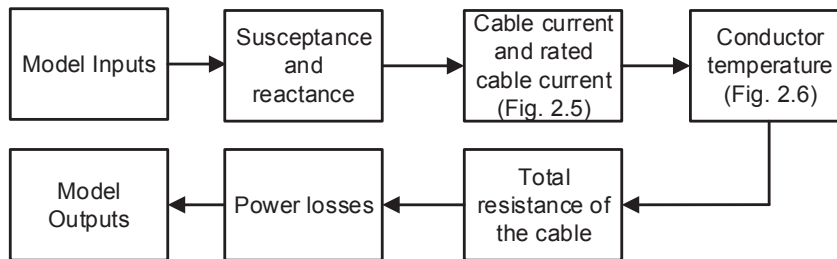
Figure 4.4: Power losses calculation of the cable model.
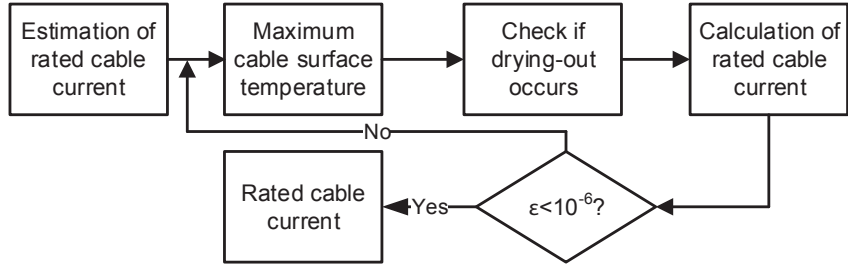
Figure 4.5: Calculation of the cable's rated current.
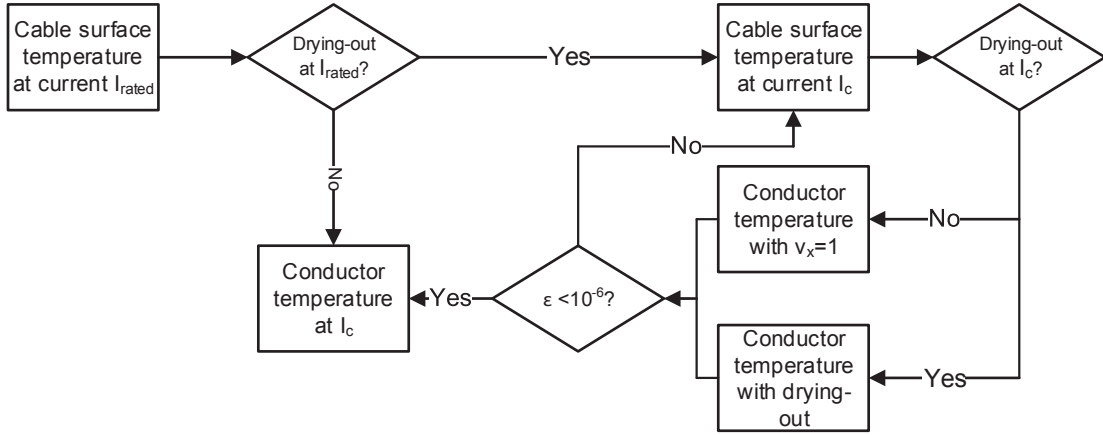
Figure 4.6: Calculation of the conductor temperature.

In case there is soil drying-out for the rated current, it has to be identified if there is drying-out for current I_c or not. The potential soil drying-out for current I_c is identified through equation (4.2) with $T_4 = 0$. The thermal resistance of the surrounding soil T_4 is not included and therefore the temperature rise $\Delta\theta_c$ corresponds to the difference between the conductor temperature and the external cable surface temperature. The temperature difference between the cable surface and the surrounding soil can be compared to the critical temperature difference above which drying-out occurs. Evidently, this calculation can be realized for the rated current since the conductor temperature for rated conditions is known.

Differently, the conductor temperature for I_c is not known before-hand. For this reason, the cable surface temperature for current I_c is determined using an iterative method. An estimation for the conductor temperature is made by [15]:

$$\theta_c = \theta_{c,Amb} + (\theta_{c,Max} - \theta_{c,Amb})\left(\frac{I_c}{I_{c,R}}\right)^2 \tag{4.6}$$

where θ_c is the conductor temperature [°C], $\theta_{c,Amb}$ is the ambient soil temperature [°C], $\theta_{c,Max}$ is the maximum operating temperature [°C] and I_R is the rated current of the cable [A].

(a) Losses.
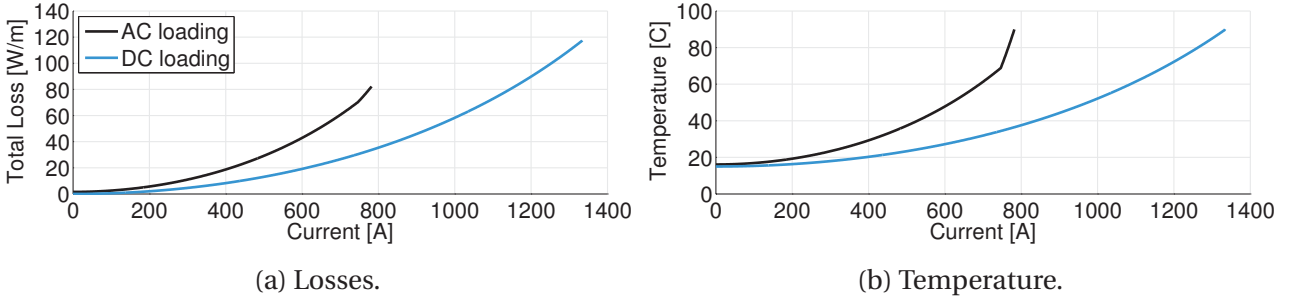
(b) Temperature.

Figure 4.7: Cable losses and temperature rise with the current.

The value of the conductor temperature is used for the determination of the cable surface temperature. Then it is determined whether drying-out occurs or not. Consequently, equation (4.2) is used for the conductor temperature and the calculation sequence is repeated until convergence is obtained. Having acquired a value for the conductor temperature, the total phase impedance can be determined using equation 4.4.

Figures 4.7a and 4.7b show the cable losses and temperature for ac and dc loadings, respectively. The conductor temperature is lower under dc loading due to the absence of the ac specific losses. In this example, differently from the ac case, it never exceeds the critical temperature above which soil drying-out occurs. Hence, the rated dc current is higher due to the lower heat generation.

4.3 Modular Multilevel Converter

Ac-dc converters are one the key components of a dc network. Due to the this recent steer towards dc networks, the Modular Multilevel Converter (MMC) introduced by Lesnicar and Marquardt back in 2003 is receiving a great deal of attention by both the research community and industry [16]. Figure 4.8 shows a three-phase n-level MMC composed of half-bridge Sub-Modules (SMs) and capable of producing n different voltage levels. The n voltage levels can be achieved by properly inserting or bypassing the SMs, which are usually composed of low voltage switches.

Currently, there are several models in the literature which calculate the power losses of a MMC. For example, in [17] the losses of the semiconductors are calculated in detail. However, the method becomes computationally intensive for a large number of SMs, which is typically the case for MMCs. Marquardt introduced a model that accounts for the losses caused by conduction and switching of a MMC via averaged current expressions for each semiconductor [18]. The advantages of this model are the exclusive use of code without the need for simulation software and the scalability with the number of SMs. However, it assumes that the semiconductors operate at maximum junction temperature and it does not consider the power losses of the inductors and cooling system. Furthermore, Marquardt's model assumes the switching losses to be linearly proportional to the current of the MMC which is not valid especially for low currents [19].
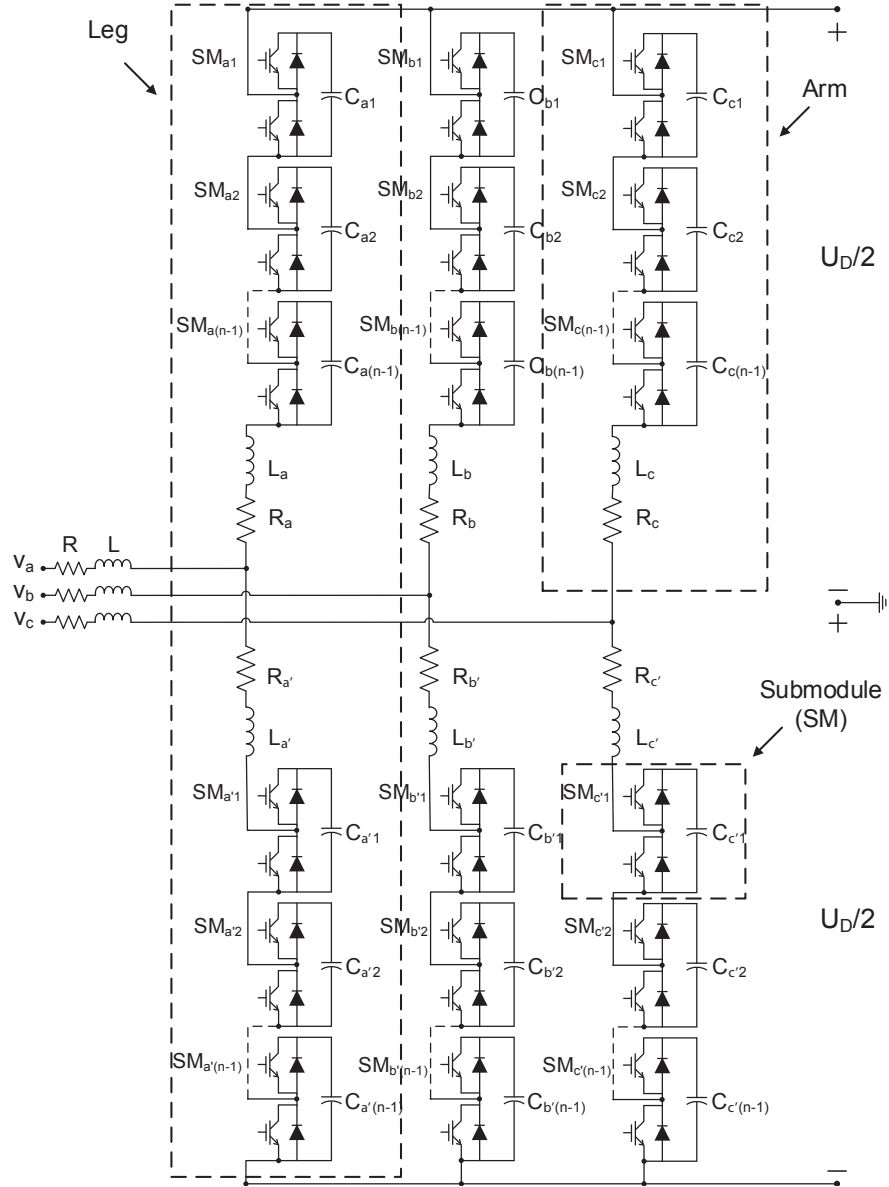
Figure 4.8: Three-phase n-level MMC [11].

4.3.1 Marquardt steady-state model

Allebrod, Hamerski and Marquardt have introduced a model for calculating the power losses of a MMC based solely on analytical expressions [18]. The model, which takes into consideration the conduction and switching losses of each semiconductor, is briefly described next.

Conduction losses

The conduction losses are determined for every semiconductor of a SM (shown in Figure 4.9) using the expressions [18]:

$$
\begin{cases}
P_{T1,2} = (V_{ce0} + R_{ce0} I^*_{eq})\bar{i} \\
P_{D1,2} = (V_{d0} + R_{d0} I^*_{eq})\bar{i}
\end{cases}
\tag{4.7}
$$

where V_{ce0} is the on-state zero-current collector-emitter voltage, V_{d0} is the on-state zero-current diode voltage, R_{ce0} is the on-state collector-emitter resistance, R_{d0} is the on-state diode resistance, I^*_{eq} is the equivalent on-state current and $\bar{i}$ is the arithmetic mean value of the current.

The $\bar{i}$ is obtained through the following expressions [18]:

$$
\begin{cases}
\bar{i}_{T1,D1} = \dfrac{1}{4} bx\overline{|I_{ac}|} \\
\bar{i}_{T2,D2} = \dfrac{1}{4} (1 - bx)\overline{|I_{ac}|} \pm \dfrac{1}{6}\bar{I}_{dc}\left(1 + \dfrac{1}{3m}\right)
\end{cases}
\tag{4.8}
$$

where I_{ac} is the ac current, m is the normalized ratio between the ac and dc currents, x relates to the dimensioning of the SM capacitors and b is the relative amplitude of the dc voltage controlled by the converter.
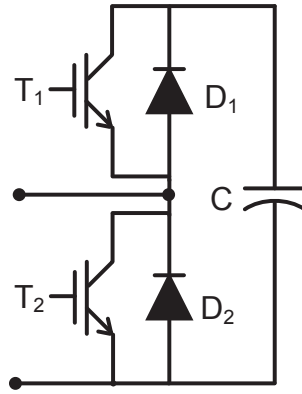
Figure 4.9: Half-bridge SM of a MMC.

Parameters m, x, b, k, and I_{eq}^* are respectively given by [18]:

$$
\begin{cases}
m = \dfrac{3\pi \left| \overline{I}_{ac} \right|}{4\overline{I}_{dc}}, |m| > 2 \\[2ex]
x = \left(1 - m^{-2} \right)^{3/2}, 0.65 < x < 1 \\[2ex]
b = \dfrac{V_{dc}}{2n\overline{V}_C}, 0 < b < 1 \\[2ex]
k = \dfrac{2}{m \cos(\varphi)}, 0 < k > 1 \\[2ex]
I_{eq,P,N}^* = \dfrac{\overline{I}_{dc}}{3} (m \pm 1) \dfrac{\pi}{4}
\end{cases}
\tag{4.9}
$$

where $\overline{I}_{dc}$ is the dc current, k is the modulation index, $\overline{V}_C$ is the average capacitor voltage and n is the number of SMs per arm and V_{dc} is the amplitude of the dc voltage. Subscript P corresponds to T_2 and D_1 while subscript N corresponds to elements T_1 and D_2 of the SM (see Figure 4.9).

Switching losses

The switching losses of each semiconductor can be derived through the expressions [18]:

$$
\begin{cases}
P_{T1,2} = f_c \left(\dfrac{W_{on} + W_{off}}{V_{ref} I_{ref}} \right) \overline{V}_C \overline{i}_{av} \\[3ex]
P_{D1,2} = f_c \left(\dfrac{W_{rec}}{V_{ref} I_{ref}} \right) \overline{V}_C \overline{i}_{av}
\end{cases}
\tag{4.10}
$$

where f_c is the carrier frequency of the semiconductors, W_{on} and W_{off} are the IGBT turn-on and -off losses, respectively, W_{rec} is the diode reverse recovery loss, V_{ref} and I_{ref} are references for voltage and current, respectively, and $\overline{i}_{av}$ is the arithmetic mean value of the arm current.

The current $\overline{i}_{av}$ may be calculated as:

$$
\overline{i}_{av,P,N} = \frac{1}{6} \overline{I}_{dc} \left(\frac{2m}{\pi} \pm 1 + \frac{1}{3m} \right)
\tag{4.11}
$$

where, once again, subscript P corresponds to T_2 and D_1 and subscript N corresponds to T_1 and D_2 of the SM.

Assumptions

The model assumes that the semiconductors are always at their maximum temperature of operation and that the switching losses are proportional to the current passing the MMC.

4.3.2 Proposed steady-state model

Derivation of the arm currents

The general expression for the current circulating in the MMC is given, for steady-state operation, by [20]:

$$i_{cc} = \frac{I_{dc}}{3} + \sum_{n=1}^{\infty} \widehat{I}_{cc,n} \cos(n\omega t + a_n) \tag{4.12}$$

where I_{dc} is the current at the dc side of the MMC, $\widehat{I}_{cc,n}$ is the amplitude of n-th harmonic of the ac current and a_n is the phase shift angle of n-th harmonic.

There are several methods of suppressing the harmonic component of the circulating current. Some approaches control the modulated voltage [21–23], others have used a passive filter [24, 25]. Furthermore, it has also been shown that the harmonics can be greatly suppressed by properly dimensioning the capacitance and the inductance of the MMC [26].

Due to the existence of several techniques to reduce the harmonic content, in this work it is assumed that there are no harmonics involved in the circulating current. Hence, the arm currents are given by the following expressions:

$$\begin{cases} i_{I,R}^{Uarm} = \pm\dfrac{I_{dc}}{3} \pm \dfrac{I_{ac}}{2}\cos\left(2\pi f t + \varphi\right) \\[2mm] i_{I,R}^{Larm} = \pm\dfrac{I_{dc}}{3} \mp \dfrac{I_{ac}}{2}\cos\left(2\pi f t + \varphi\right) \end{cases} \tag{4.13}$$

where $i_{I,R}^{Uarm}$ are the currents of the upper arm for inverter and rectifier operations, respectively, $i_{I,R}^{Larm}$ are the currents of the lower arm for inverter and rectifier operations, respectively, I_{ac} is the amplitude of the first ac current harmonic, f is the system frequency and φ is the power angle.

In order to obtain the arms currents it is necessary to know both I_{ac} and I_{dc}. However, since the power losses of the MMC are not known beforehand, only the current at the input side is known, i.e. the dc current for inverter operation and the ac current for rectifier operation. To overcome this deadlock an iterative procedure, shown in Figure 4.10, is employed.

Initially, it is assumed that the power losses are 1% of the input power, the power angle is zero degrees and both ac and dc voltages to be equal to their rated values. The dc, ac and rms values of the arm current are calculated, for inverter operation, according to:
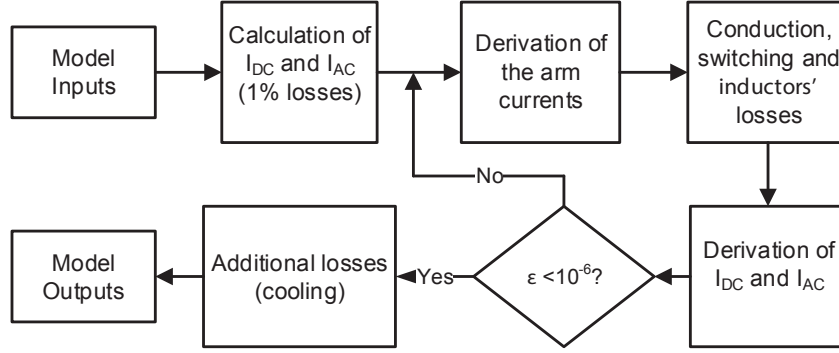
Figure 4.10: Iterative process to calculate the arm currents and power losses of the MMC.

$$\begin{cases} I_{dc} = \dfrac{P_{dc}}{V_{dc}} \\[2ex] I_{ac} = \dfrac{(1-0.01)P_{dc}}{\sqrt{3}V_{ac}\cos(\varphi)} \\[2ex] I_{arm,rms} = \sqrt{\left(\dfrac{I_{dc}}{3}\right)^2 + \left(\dfrac{I_{ac}}{2}\right)^2} \end{cases} \tag{4.14}$$

where P_{dc} is the power at the dc side of the converter, V_{dc} is the voltage at the dc side of the converter, V_{ac} is the line to line voltage at the ac side of the converter and $I_{arm,rms}$ is the rms value of the arm current of the converter.

Conduction losses

The power dissipated by an IGBT and its antiparallel diode during one period is obtained by:

$$\begin{cases} P_T = \dfrac{1}{T_f} \displaystyle\int_0^T K_{t,T}(V_{ce0}i_c + R_{ce0}i_c^2)\,dt \\[3ex] P_D = \dfrac{1}{T_f} \displaystyle\int_0^T K_{d,T}(V_{d0}i_d + R_{d0}i_d^2)\,dt \end{cases} \tag{4.15}$$

where $K_{t,T}$ and $K_{d,T}$ are the temperature correction factors for the IGBT and diode, respectively, i_c and i_d are the collector and diode instantaneous currents, respectively, V_{ce0} and V_{d0} are the on-state zero-current collector-emitter voltage and on-state zero-current diode voltage at maximum temperature, respectively, R_{ce} and R_d are the on-state collector-emitter resistance and on-state diode resistance at maximum temperature, respectively, and T_f is the duration of one period.

The temperature correction factors $K_{t,T}$ and $K_{d,T}$, which can be derived using the datasheet graphs shown in Figure 4.11, are determined by:

$$K_{t,T} = \frac{v_{ce,@T}}{v_{ce,@150^oC}} ; K_{d,T} = \frac{v_{d,@T}}{v_{d,@150^oC}} \tag{4.16}$$

where $v_{ce,@T}$ and $v_{d,@T}$ are the on-state collector-emitter voltage and the on-state diode voltage at operation temperature, respectively and $v_{ce,@150^oC}$ and $v_{d,@150^oC}$ are the on-state collector-emitter voltage and the on-state diode voltage at maximum temperature, respectively.

The junction's operation temperature of the semiconductors is required for the calculation of the correction factors $K_{t,T}$ and $K_{d,T}$. In this work, it is assumed that the junction's temperature varies with the square of the rms value of the arm current:

$$\theta_j = \theta_{m,Amb} + \left(\frac{I_{arm,rms}}{I_{arm,rms,nom}} \right)^2 (\theta_{m,Max} - \theta_{m,Amb}) \tag{4.17}$$

where $\theta_{m,Amb}$ is the ambient temperature, $\theta_{m,Max}$ is the maximum operating temperature of the IGBT module and $I_{arm,rms,nom}$ is the nominal arm rms current.

To calculate the conduction losses during one fundamental period for one of the converter arms, the current is sampled with a frequency two times higher than the number of voltage levels

(a) Collector current vs collector-emitter voltage   (b) Diode current vs diode voltage
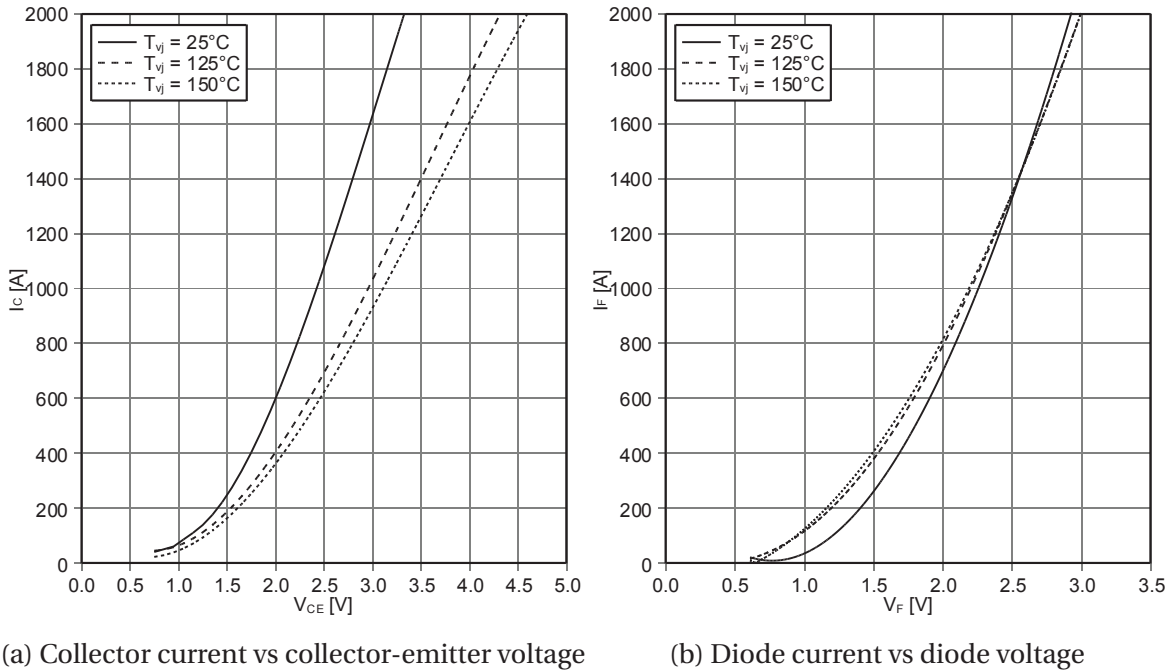
Figure 4.11: Datasheet curves used for the temperature correction factors $K_{t,T}$ and $K_{d,T}$ [19].

that the MMC produces [27]. At each time step, it is determined how many semiconductors are inserted or bypassed (see Figure 4.12).

The number of inserted SMs is determined using the direct modulation technique, in which the modulator tries to follow the amplitude of this reference signal as closely as possible (see Figure 4.13) and determines the number of SMs to be inserted in the upper and lower arms [28]:

$$n_{u,l} = \left\lceil N_{SM} \frac{1 \pm m_a \cos(\omega t)}{2} \right\rceil \tag{4.18}$$

where m_a is the modulation index, N_{SM} is the number of SMs per arm of the MMC and n_u and n_l are the number of inserted SMs in the upper and lower arms, respectively.

One fundamental period is then discretized and integrated. This value is then multiplied by the fundamental frequency to obtain the total conduction losses during one period.

Switching losses

In the proposed approach, the switching events are uniformly dispersed throughout one period, as shown in Figure 4.14. In this way, the calculation of the switching losses of the MMC is done

(a) SM inserted

(b) SM bypassed
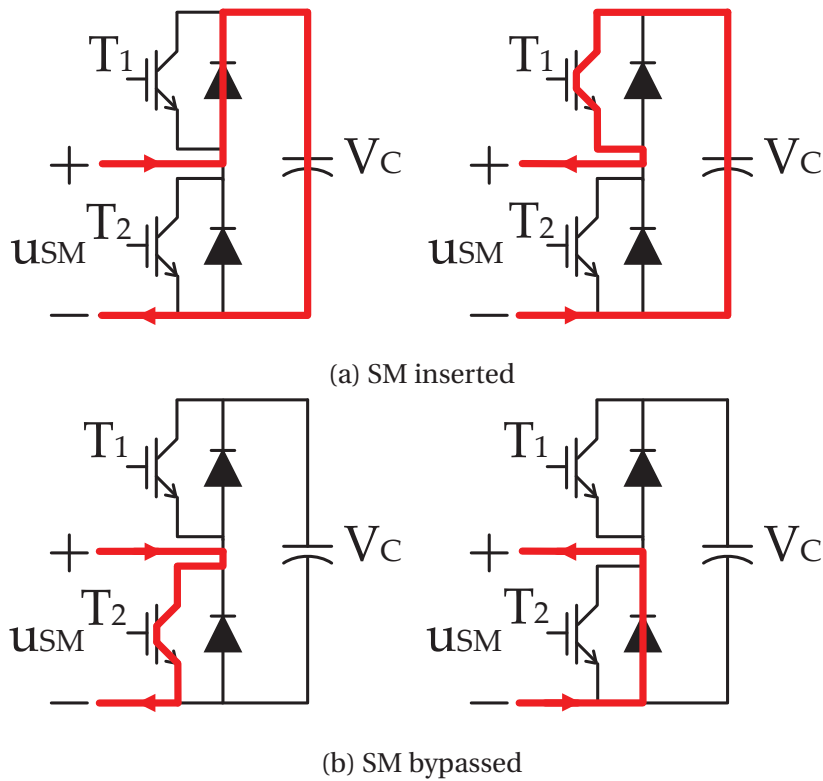
Figure 4.12: Operating states of the SMs.
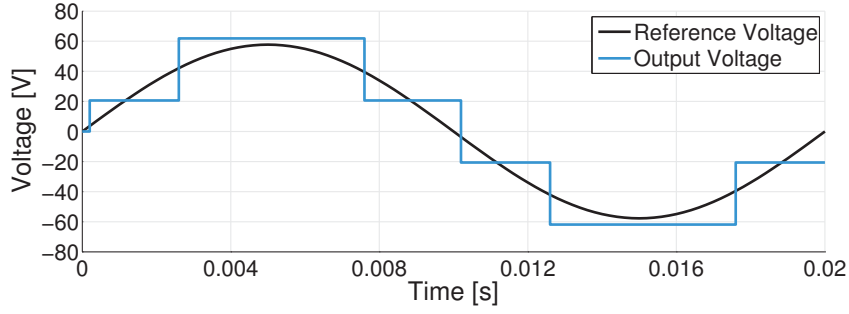
Figure 4.13: Direct modulation technique for four voltage levels.
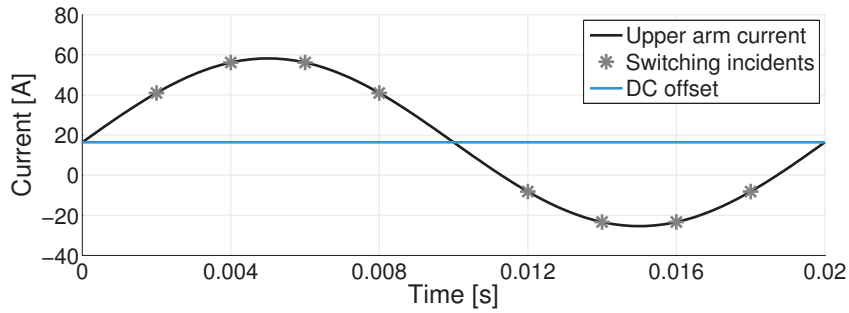
Figure 4.14: Switching events for a switching frequency of 200 Hz.

without knowing the exact moment when a switching occurs. This avoids a controller for the balancing of capacitors' voltages and hence, the switching events are obtained only with the switching frequency of the SMs.

Although the timing of the switching incidents is determined, the pattern gives no indication whether these are switch-ons or switch-offs. Therefore, the losses are averaged for two fundamental periods. For the first one, it is assumed that the first switching incident is a switch-on of the SM, whereas the first switching incident is a switch-off in the second period.

The switching energy losses are calculated using the following expressions:

$$\begin{cases} E_{on} = E_{on,150^oC}(I_{arm}) \, K_{t,T,on} \, K_{t,R_G,on} \, K_{V_{dc}} \\ E_{off} = E_{off,150^oC}(I_{arm}) \, K_{t,T,off} \, K_{t,R_G,off} \, K_{V_{dc}} \\ E_{rec} = E_{rec,150^oC}(I_{arm}) \, K_{d,T,rec} \, K_{d,R_G} \, K_{V_{dc}} \end{cases} \tag{4.19}$$

where E_{on}, E_{off} and E_{rec} are the IGBT's turn-on, turn-off and diode reverse recovery energies, respectively. The values of $E_{on,150^oC}$, $E_{off,150^oC}$ and $E_{rec,150^oC}$ are obtained from the manufacturer's datasheet and further scaled with correction factors for temperature (K_T), gate resistance (K_{R_G}) and applied dc blocking voltage ($K_{V_{dc}}$).

The temperature and gate resistance correction factors are calculated in a similar fashion to the temperature correction factors used in the conduction losses. Equation 4.17 is once again used to determine the junction temperature. The datasheet curves used for the temperature correction factors are shown in Figure 4.15, whereas the gate resistance correction factors are calculated using the graphs shown in Figure 4.16.

The graphs of the datasheet regarding the switching losses have been produced by applying a dc voltage of 1800 V to the collector-emitter [19]. Therefore, they have to be adjusted to the dc voltage that is applied during the MMC operation through the dc collector-emitter voltage correction factor, $K_{V_{dc}}$. This voltage is equal to the average SM capacitor's voltage divided by the number of switches that are connected in series:

$$K_{V_{cedc}} = \frac{V_C/N_{Series}}{V_{dc,Dts}}$$

(4.20)

where V_C is SM capacitor's voltage, N_{Series} is the number of IGBT modules in series composing a SM's switch and $V_{dc,Dts}$ is the datasheet collector-emitter dc voltage.

After the losses are averaged over two periods they are multiplied by the fundamental frequency to derive the switching power losses over one period.

(a) IGBT switching losses

(b) Diode reverse recovery losses
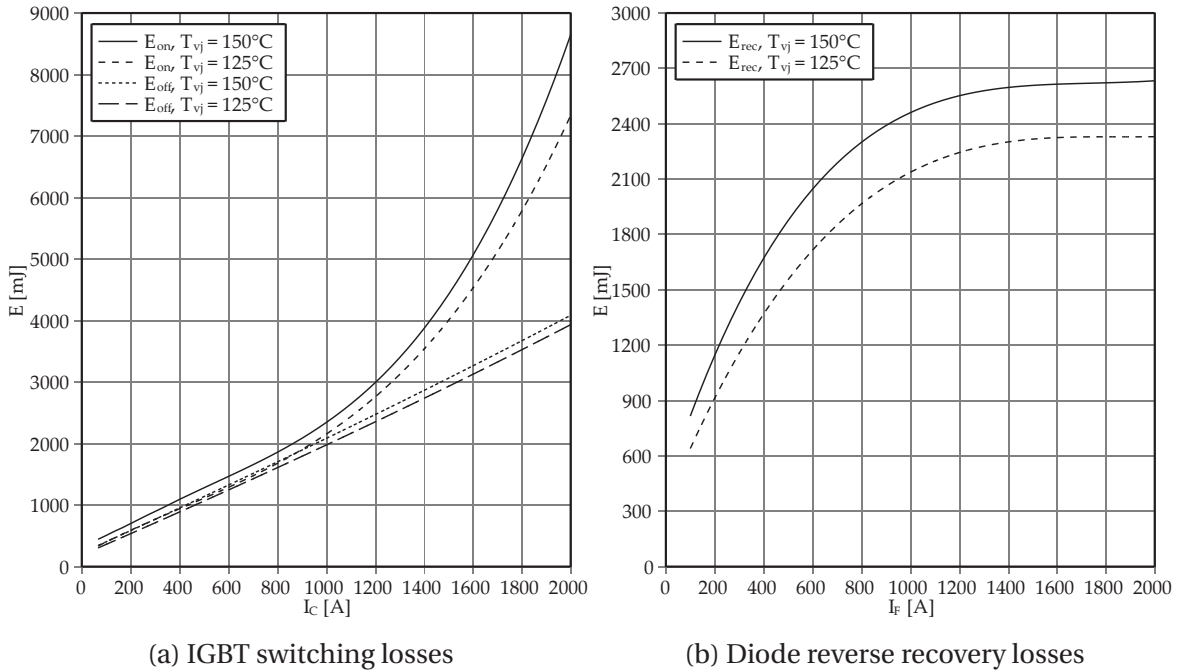
Figure 4.15: Datasheet curves for the IGBT switching losses and diode reverse recovery losses [19].

(a) IGBT switching losses

(b) Diode reverse recovery losses
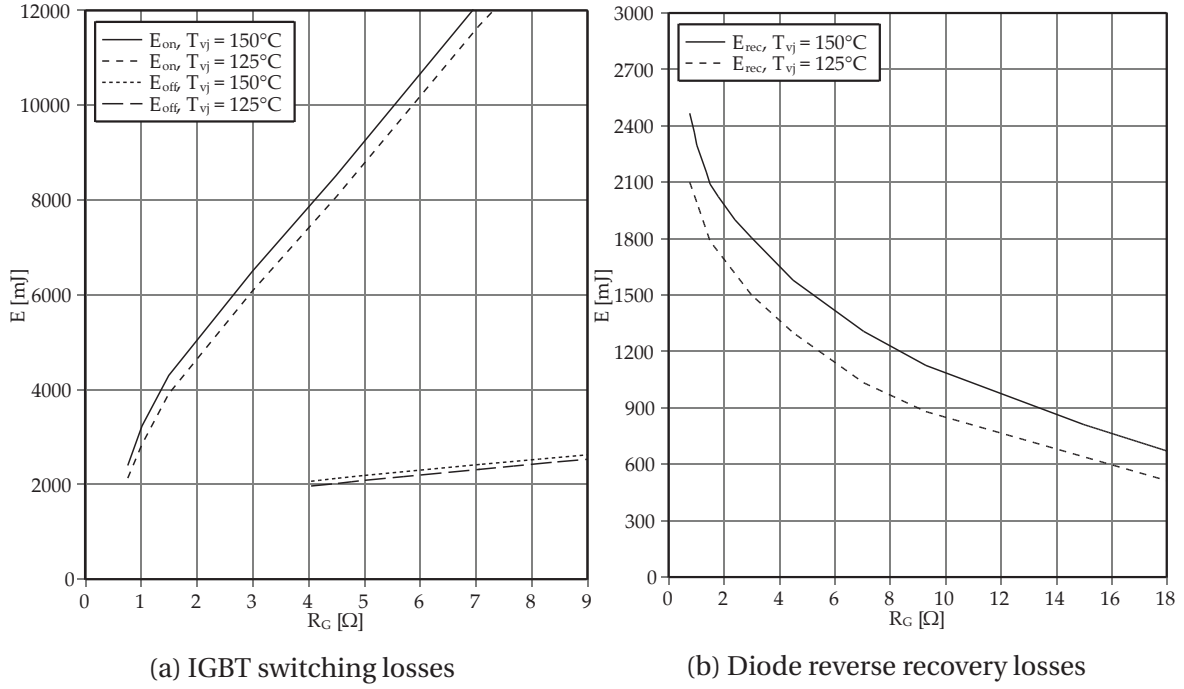
Figure 4.16: Datasheet curves for the gate resistance factors [19].

Inductors

The ohmic losses of an arm inductor are given by:

$$P_{ind} = R_{ind}^{\theta} I_{arm,RMS}^2 \tag{4.21}$$

where R_{ind}^{θ} is the ac (due to skin and proximity effects) and dc resistance of the arm inductor at $\theta\,^oC$ and $I_{arm,RMS}$ is the RMS current of the MMC arm.

In addition, the model takes into account the variation of the resistance with the temperature [13]:

$$R_{ind}^{\theta_i} = R_{ind}^{20}[1 + \alpha_{20}(\theta_i - 20)] \tag{4.22}$$

where α_{20} is the temperature coefficient of resistivity at 20 °C and θ_i is the temperature of the conductor which varies with the current of the MMC, in a similar fashion to the junction temperature (see Equation 4.17).

Cooling system

The additional losses of the cooling system are added to the conduction, switching and inductors losses to obtain the total losses of the converter. Large converters usually make use of liquid

cooling systems [11]. However, it is difficult to determine power requirements of a cooling system without knowing, among others, the power consumption of the pumps and the control scheme of the heat exchangers' fans. Hence the proposed method uses the coefficient of performance (COP) of the cooling system [11]. The COP is the ratio of the extracted heat over the power needed to achieve this extraction. In this work it is considered that COP=20 [29].

Assumptions

The proposed model considers that all SMs are identical and that the switching of the semiconductors is instantaneous. The capacitors' voltages are considered to be always balanced and equal to their rated value since there are several techniques to balance and distribute the dc voltage over the SMs [30, 31]. Similarly, and for the same reasons, it is assumed that the circulating currents have no harmonic content [21, 25, 26]. It is also considered that the resistance of the inductors varies linearly with their temperature according to the guidelines given in [13]. Finally, it is assumed that the inductors do not require additional cooling than passive air circulation.

Marquardt's assumptions - Proposed model vs Marquardt

A 650 MVA converter based on Infineon IGBTs [19] was used to compare the Marquardt and the proposed models. Table 4.1 shows the properties of the converter. The case study, whose details are given next, was run in an i7-laptop with 6 GB ram on Windows 7. The proposed model, coded in Python, took less than 1 s to provide the results.

Five different scenarios were carried out to compare both models in a gradual manner. In scenario 1, the proposed model is compared to Marquardt's model under the same assumptions. In scenario 2, the switching losses are calculated based on the datasheet information of the semiconductors. Thereafter, the additional features – variable operating temperature, inductors and cooling system losses – are gradually activated in scenarios 3, 4 and 5, respectively, to demonstrate their impact on the total efficiency of the MMC.

Table 4.1: Parameters of the MMC [11].

Parameter	Value
Rated power	650 MVA
Rated dc voltage	± 320 kV
Rated ac voltage	380 kV
Power factor	1
System frequency	50 Hz
Carrier frequency	600 Hz
Number of arm SMs	58
Arm resistance	0.07 Ω

Scenario 1 in this scenario the proposed model was tested with the same assumptions made by the Marquardt's model. Therefore, the switching losses of the IGBT were altered to be proportional to the current. In addition, the temperature impact was deactivated and no additional losses were computed. Figures 4.17b and 4.17d show that the efficiency curves of the proposed and Marquardt's models are identical under these circumstances.

Marquardt's model assumes that the switching losses are directly proportional to the current of the MMC. Figures 4.17a and 4.17c show that the switching losses start at zero and increase to approximately 0.7% at rated power.

Scenario 2 a more realistic relationship between the switching losses and the current was used in this scenario, hence the switching losses were not proportional to the current (see Figure 4.15). Figure 4.18 shows that this led to a significant drop in the efficiency of the converter for transmitted powers of up to 50% of the rated power.

Scenario 3 Figure 4.18 shows that when the impact of the temperature was incorporated in the proposed model it was observed an increase of the total efficiency of the converter. This was an expected result since previously the temperature was considered to be 150^oC and in scenario 3 the temperature ranged between $20-90^oC$.

Scenario 4 the losses of the inductors were added in this scenario. Figure 4.18 shows that the inductors did not contribute much to the power losses.

Scenario 5 the cooling system losses were incorporated in the final scenario. Figure 4.18 shows that these losses do not have a large impact on the total efficiency of the converter.

(a) Power losses breakdown for inverter operation

(b) Efficiency curves for inverter operation

(c) Power losses breakdown for rectifier operation

(d) Efficiency curves for rectifier operation
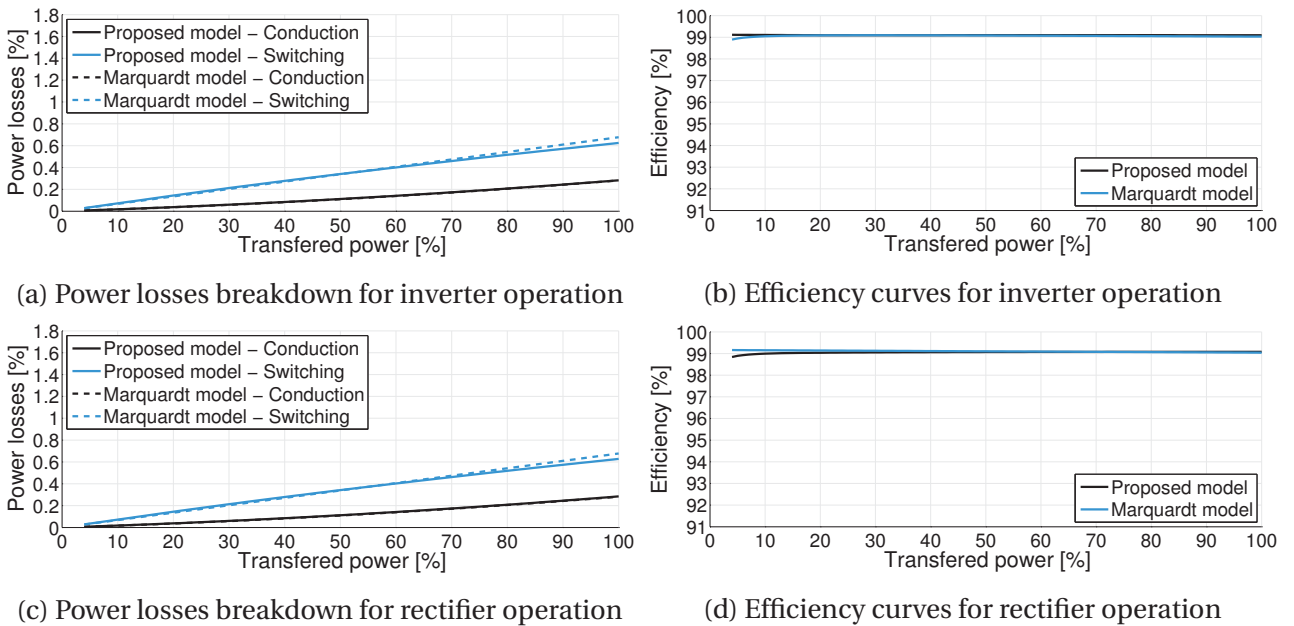
Figure 4.17: Marquardt and proposed model with Marquardt's assumptions.
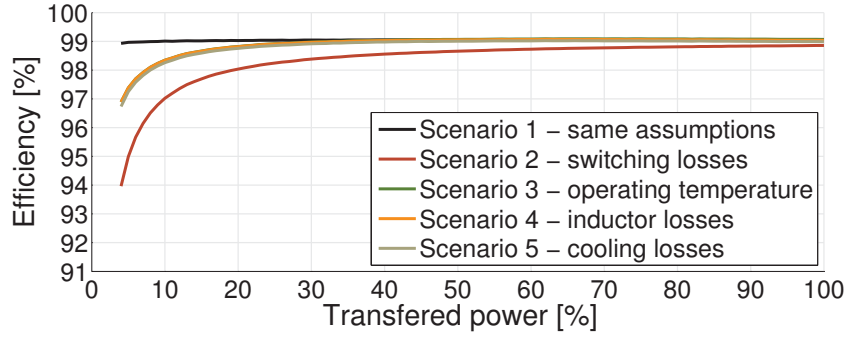
Figure 4.18: Efficiency curves of the proposed model for the different scenarios.

(a) Power losses breakdown

(b) Efficiency curves
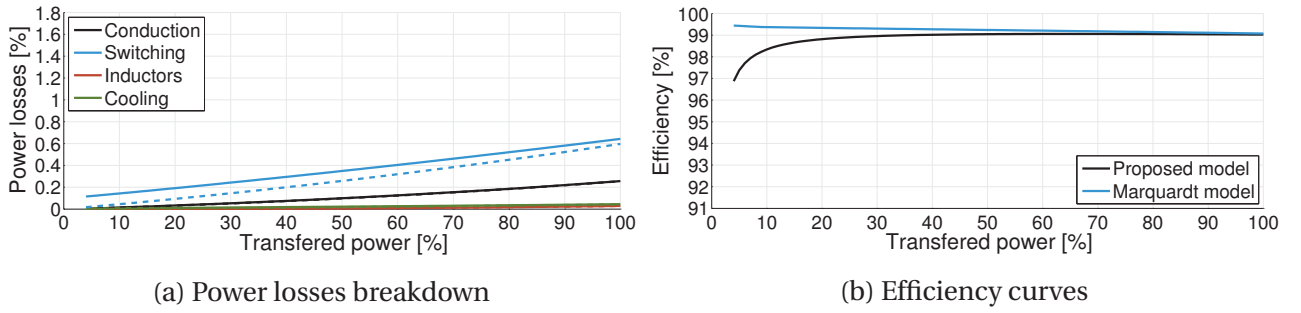
Figure 4.19: Marquardt and proposed model with our assumptions. Solid lines correspond to the proposed model and the dashed lines to Marquardt's model in the breakdown plot.

The efficiency curves of scenarios 1 and 5 differ and hence, the proposed model differs from Marquardt's model. The same datasheet correction factors for the semiconductors were implemented in Marquardt's model to verify if once again the models are in agreement. Figure 4.19 shows the losses breakdown and the efficiency curves obtained when both models were run with our assumptions. It can be seen that all losses are in agreement besides the switching losses. Although the correction factors were added to Marquardt's model, the switching losses are still proportional to the current of the MMC (see Equation 4.10).

4.3.3 Dynamic model

To further evaluate the accuracy of the proposed model, a comparison was made to a dynamic converter model. To this end, a half-bridge MMC model, which takes into account the switching behavior of the SMs and employs all the basic controllers that are used in practise, was designed using the SimPowerSystems library of Matlab/Simulink.

In the dynamic model, the converter specifications are the same as presented in Table 4.1. Additionally, SM capacitors of 20 mF and arm reactors of 10 mH were used. All the measurements are made with a sampling frequency of 20 kHz.

Figure 4.20 shows the control structure of the MMC, which is performed via PI controllers. In this case study, the converter station is directly controlling the dc link voltage, as well as the reactive power on the ac side. The active power is provided by a current-controlled source on the dc side of the converter. After obtaining the reference arm currents I^*_{dq}, the inner current controller (ICC) creates the reference voltage values at the arm reactors V^*_{convj}.

A circulating Current Suppressing Control (CSC) was implemented to suppress the circulating currents in the MMC. Circulating currents are the result of voltage imbalances between the phase legs and mainly consist of an ac part with double the fundamental frequency. These currents - if uncontrolled - contribute significantly to the converter conduction losses. Therefore, by controlling this second harmonic current to zero, the converter power losses can be minimized [32]. From the CSC another reference voltage is obtained ($U^*_{diff,j}$), which is then added or subtracted to obtain the upper and lower arm reference voltage for each phase, i.e., u^*_{Uj} and u^*_{Lj}.

The phase-shifted carrier-based pulse width modulation (PSC-PWM) technique was used to drive the IGBTs of each SM. By comparing the generated carrier signals to the reference voltage signals obtained from the previous control stage, the number of SMs that need to be inserted in series in each phase arm is calculated at each moment. This number is then provided to the SM capacitor balancing algorithm, which in turn generates the gate signals for the IGBTs.

Calculation of power losses

The currents and voltages are monitored both on the ac and the dc side, as well as at each arm of the converter. To determine the nominal dc current and the nominal rms current at each converter leg, the respective instantaneous values are monitored for P_{dc}=1 pu and averaged over 12 periods.

To obtain the efficiency curves the converter operation was simulated for all power levels (P_{dc}) starting from 0.04 pu up to 1 pu with a step of 0.01 pu. For power levels lower than 0.04 pu the results are not reliable, as the mean power level is comparable to the resulting ripple.

For each of the power levels, a first simulation is run to measure the rms value of the arm current.
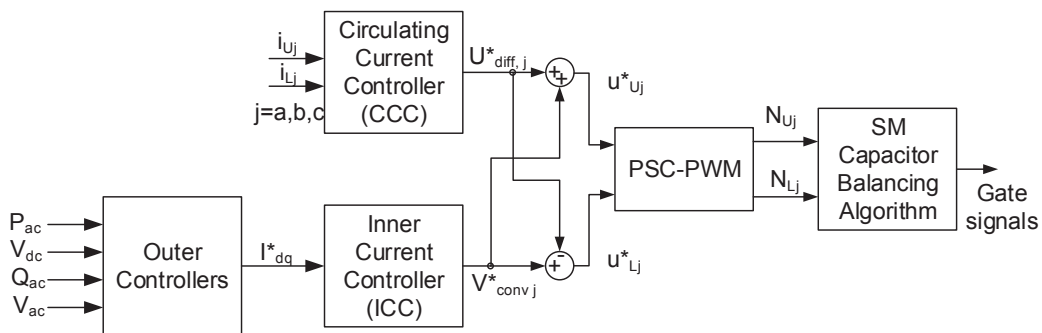
Figure 4.20: Control structure of the MMC station.

Based on this value, the equivalent on-state zero-current collector-emitter voltage of the IGBTs and the on-state zero-current voltage of the diodes, the resistance of the IGBTs and the resistance of the arm inductors are calculated.

The simulation for the specific operating point is run again with the updated resistance to obtain the voltage values and the capacitor voltages for each submodule, the circulating current, as well as the PWM signals for the switches.

Conduction losses

Due to limitations of the Simulink IGBT tunable parameters to calculate the conduction losses, it is assumed that the IGBT resistance is equal to the diode resistance. For each operating point, the equations of the proposed model are used to calculate the conduction losses, with the on-state zero-current voltage and resistance values for the IGBTs and the diodes obtained for the measured rms value of the arm current.

Switching losses

To calculate the switching losses of the converter, the equations of the proposed model are used. As input to the model, it is inserted the exact switching instants as obtained from the PWM signals of the dynamic model and the instantaneous values of the arm current that flows through the switches at each specific moment.

Inductor losses

Having obtained the instantaneous values of the arm current, as well as its rms value, the inductor losses are calculated using Equation 4.21.

Cooling losses

The total heat losses in the dynamic model are calculated as the sum of the conduction and switching losses. The cooling losses are calculated using the heat losses and the COP of the cooling system.

Model assessment 2 - Proposed model vs Dynamic

In the first comparison of the proposed model to the dynamic one, no capacitor balancing algorithm was implemented. Therefore, the gate signals were directly generated from the PSC-PWM. Table 4.2 shows that, as expected, the average switching frequencies are very close to the frequency of the PWM carriers.

Figure 4.21 shows that the models are in agreement for both the inverter and rectifier operation. The arm currents of phase a of the converters are very similar at full rated power (see Figs 4.21c and 4.21g). The proposed model uses a true sinusoidal for the arm current whereas the one from the dynamic model is the result of its control operation.

Table 4.2: Average switching frequencies (in Hz).

Balancing algorithm	Dynamic		Steady-State	
	Inverter	Rectifier	Inverter	Rectifier
None	587	592	600	600
Basic	1620	1756	1625	1750
Reduced	92	75	100	75

As previously noted, the voltages of the capacitors were considered to be always balanced and equal to their rated value in the steady-state model. Figure 4.21 also displays the values of these voltages in the dynamic implementation of the MMC. Nonetheless, it can be seen that, for the specific capacitor size, the voltage are always balanced and close to 1 pu.

Capacitor Balancing Control

To ensure the proper operation of the MMC and avoid unequal stresses on the power devices, the capacitors have to be kept at the same voltage level. Hence, a capacitors' voltage balancing control may be required. A generalized visual representation of how the modulation and capacitor voltage balancing operates is given in Figure 4.22.

Several strategies have been proposed on how to balance the voltages of the capacitors of the SMs. The most well-known strategies are the basic sorting algorithm [16] and the reduced switching algorithm [31]. Next, the results of the proposed and dynamic models are compared to assess the influence of the balancing strategy.

Basic sorting algorithm
According to this selection algorithm, in each control step, the voltages of the capacitors are measured and sorted in ascending order. The sign of the arm current and the number of arm SMs that have to be inserted dictate which SMs will be inserted in series. If the arm current is positive, the SMs with the lowest capacitor voltages will be inserted (if previously bypassed), whereas the inserted IGBTs are bypassed [30]. If the arm current is negative, the SMs with the highest capacitor voltages will be inserted, since the negative arm current discharges the capacitors (see Figure 4.12). With this strategy, the capacitors voltages are well balanced, in exchange for a higher switching frequency. Table 4.2 shows that the average number of switching events per fundamental period triplicated. After, the switching frequency of the proposed model was scaled up to match the dynamic model (see Table 4.2). Figure 4.23 shows that the results of the proposed model match with the dynamic model.

(a) Power losses breakdown for inverter operation

(b) Efficiency curves for inverter operation

(c) Arm current for inverter operation

(d) Capacitors' voltage for inverter operation

(e) Power losses breakdown for rectifier operation

(f) Efficiency curves for rectifier operation

(g) Arm current for rectifier operation

(h) Capacitors' voltage for rectifier operation
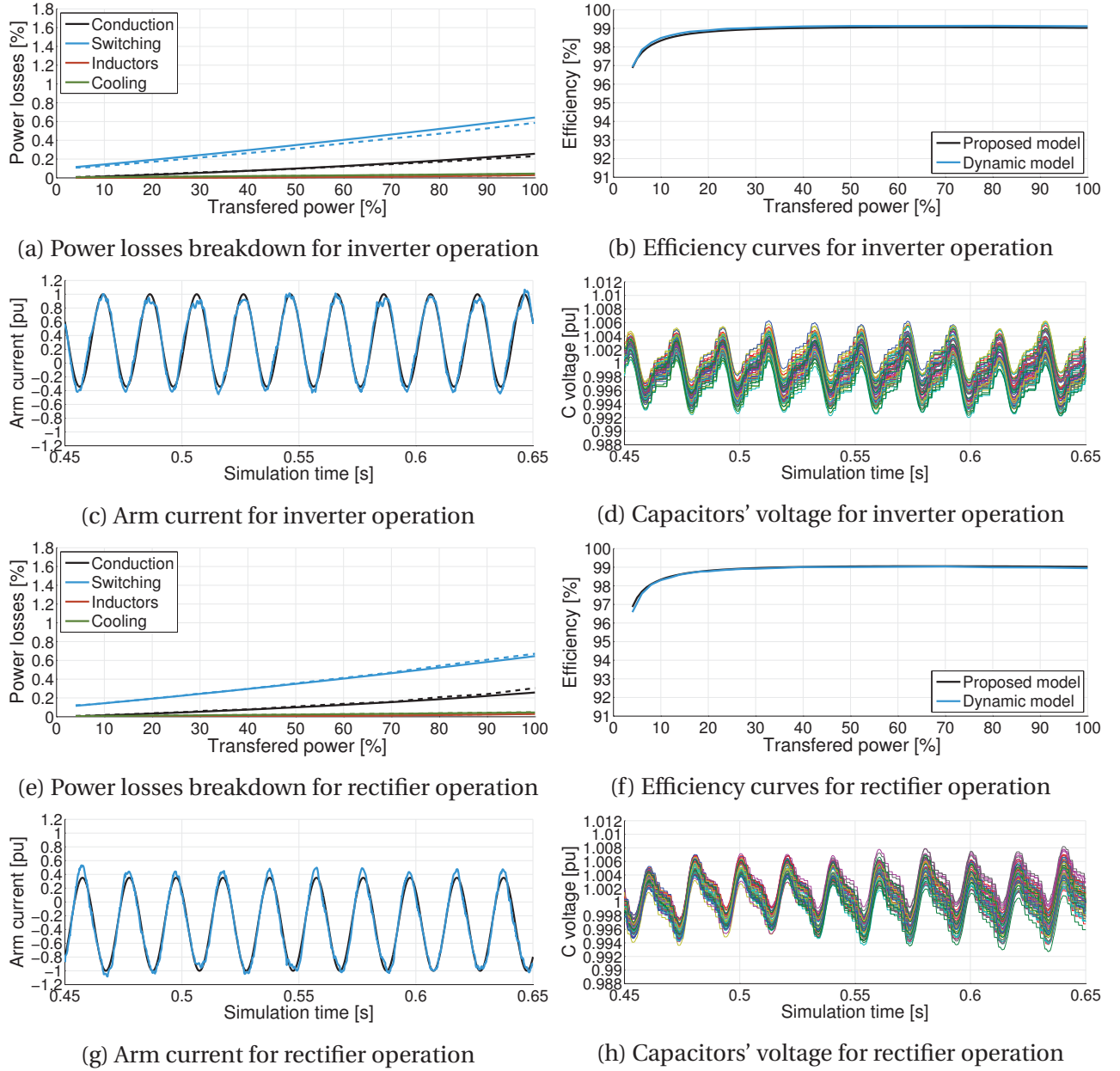
Figure 4.21: Results obtained with the proposed and dynamic models for both inverter (top plots) and rectifier operation (bottom plots). No capacitor balancing algorithm was used to balance the voltage of the capacitors. Solid lines correspond to the proposed model and the dashed lines to the dynamic model.

Reduced switching algorithm

The reduced switching algorithm is another approach for the capacitor balancing, which aims at reducing the effective switching frequency of the SMs [31]. When a SM needs to be inserted,
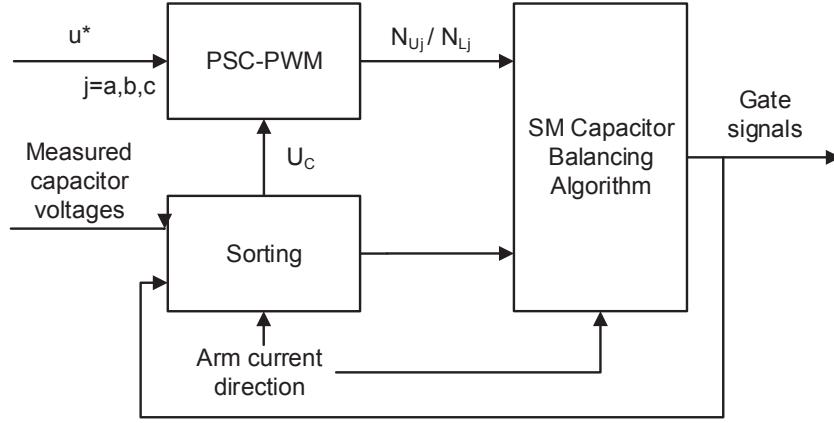
Figure 4.22: Modulation and capacitor balancing control [33].

(a) Power losses breakdown for inverter operation

(b) Efficiency curves for inverter operation

(c) Arm current for inverter operation

(d) Capacitors' voltage for inverter operation
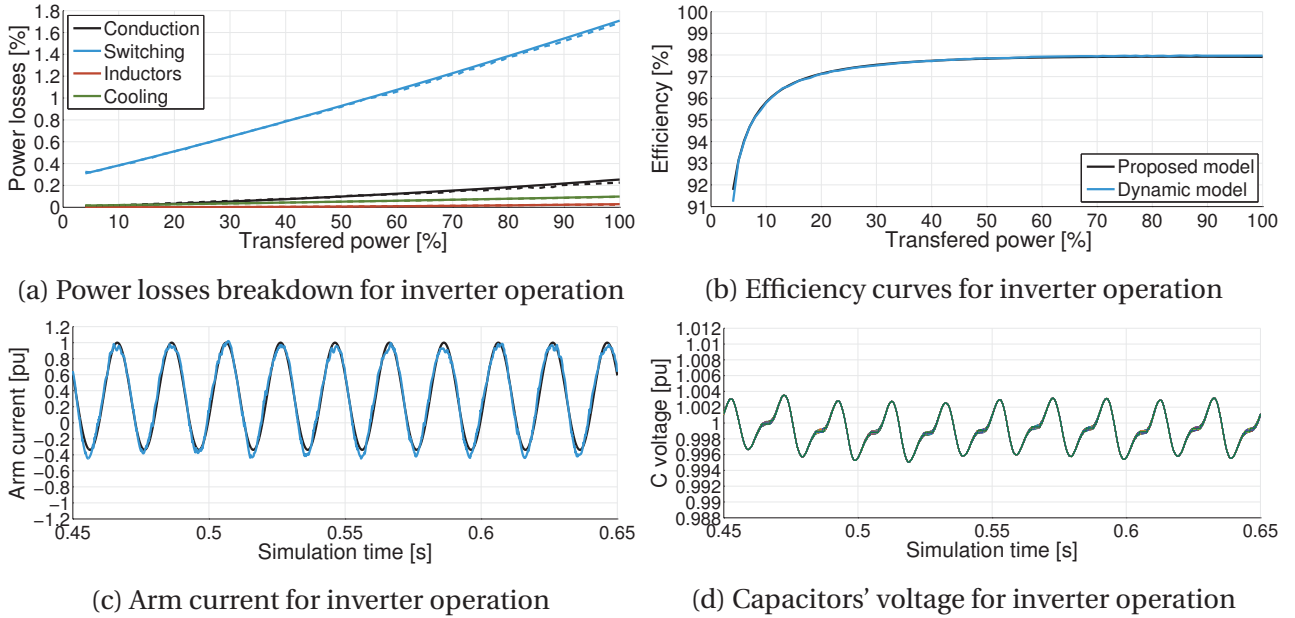
Figure 4.23: Results obtained with the proposed and dynamic models for inverter operation. The voltage of the capacitors were balanced with the basic sorting algorithm. Solid lines correspond to the proposed model and the dashed lines to the dynamic model.

the algorithm is only applied to the currently bypassed SMs. Accordingly, when a SM needs to be bypassed, the controller will take into consideration only the SMs that are inserted and will pick one to be bypassed. In this way, the average switching frequency of the SMs was reduced from 600 to 92 Hz and 75 Hz in inverter and rectifier operation, respectively (see Table 4.2). Once again the switching frequency of the proposed model was adjusted so that it would match as much as possible the dynamic model switching frequency. Figure 4.24 shows that the proposed and dynamic models are in concordance.

(a) Power losses breakdown for inverter operation

(b) Efficiency curves for inverter operation

(c) Arm current for inverter operation

(d) Capacitors' voltage for inverter operation
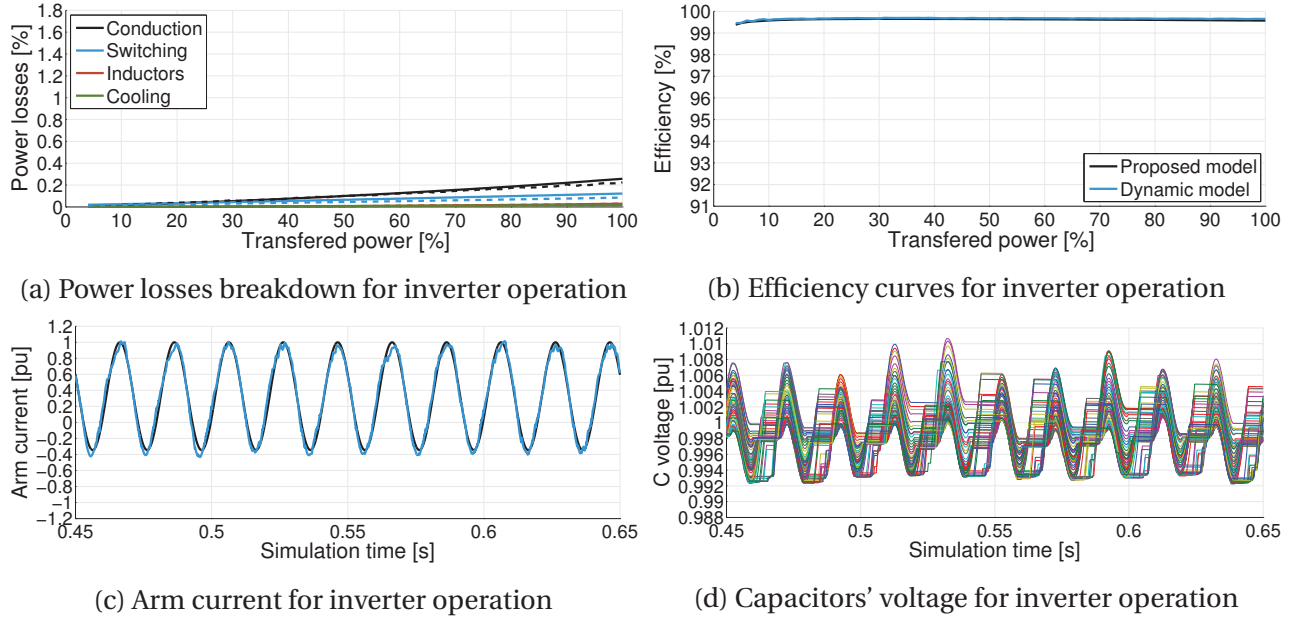
Figure 4.24: Results obtained with the proposed and dynamic models for inverter operation. The voltage of the capacitors were balanced with the reduced switching algorithm. Solid lines correspond to the proposed model and the dashed lines to the dynamic model.
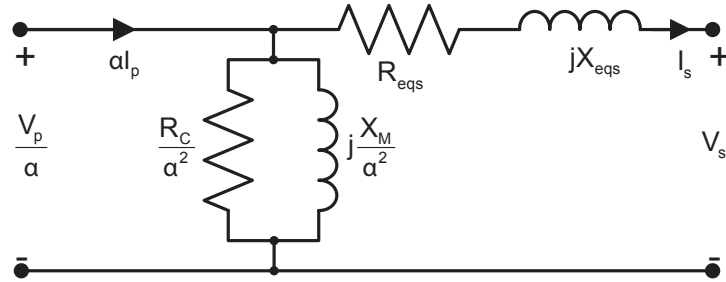
Figure 4.25: Simplified transformer equivalent circuit referred to the secondary voltage [34, 35].

4.4   Transformer

The transformer loss model is based on the equivalent circuit shown in Figure 4.25 [34, 35]. The main sources of losses in a transformer are the load (copper) and no-load (core) losses.

4.4.1   Mutual and leakage fluxes

The mutual magnetic flux is represented by X_M (Figure 4.25), whereas the leakage fluxes of the primary and secondary sides are represented by the equivalent series reactance X_{eqs}.

4.4.2 No-load (core) losses

The no-load losses are equal to:

$$P_{no-load} = 3\overline{V}_{in,Ph}^2 R_C^{-1} \tag{4.23}$$

where $\overline{V}_{in,Ph}$ is the input phase voltage referred to the secondary $[V]$ and R_C is the resistance of the excitation branch referred to the secondary $[\Omega]$.

4.4.3 Load (ohmic) losses

The load losses are calculated according to (4.24):

$$P_{load} = 3R_{eqs}^{\theta} I_s^2 \tag{4.24}$$

where I_s is the line current through the series impedance referred to the secondary $[A]$ and R_{eqs}^{θ} is the transformer equivalent resistance (primary and secondary resistances combined) at temperature θ $[\Omega]$.

The windings resistances and other stray resistances responsible for losses in the transformer windings and other metallic parts are included in R_{eqs}^{θ}. The winding resistance, which varies proportionally with temperature, represents around 85% of R_{eqs}^{θ}, whereas the stray resistances, which vary inversely with the temperature, represent 15% of R_{eqs}^{θ} [36]. Thus, R_{eqs}^{θ} may be expressed by:

$$R_{eqs}^{\theta} = 0.85 R_{eqs}^{\theta_{Test}} \left[1 + \alpha_{\theta_{Test}}(\theta - \theta_{Test})\right] + 0.15 R_{eqs}^{\theta_{Test}} \left[1 + \alpha_{\theta_{Test}}(\theta - \theta_{Test})\right]^{-1} \tag{4.25}$$

where $R_{eqs}^{\theta_{Test}}$ is the resistance $[\Omega]$ at temperature of the short circuit measurement and $\alpha_{\theta_{Test}}$ is the copper constant mass temperature coefficient.

4.4.4 Cooling losses

The cooling requirements of a transformer vary with respect to its rating, physical size and cooling system configuration [36]. Determining the power requirements of the transformers cooling system is not a straightforward task when exact figures are not available (e.g. power consumption of active components, control scheme). It is assumed that the cooling system power requirements vary linearly with the windings temperature. The cooling system consumes 20% of its rated power when the windings and ambient temperatures are equal (no-load losses dissipation) and it linearly reaches 100% rated power when the windings reach their maximum temperature. The model requires as input the rated installed power of the cooling system. The cooling fans for a high-power transformer is usually in the range of 35-40 kW [36].

4.4.5 Assumptions

The model assumes a constant voltage ratio (i.e. no tap changers) and that the windings temperature varies linearly with the transformer current rms value. Figure 4.26a shows the efficiency curves for three-phase transformers with Y/Y and D/Y connections, whose properties are shown on the right column of Table 4.3. It can be seen that the core losses are constant, whereas the load ohmic losses increase with the current (Figures 4.26b and c) and the cooling requirements do not contribute much to the total losses.

Table 4.3: Transformers data.

Variable	Unit	Offshore Transformers	Onshore Transformer
S_{Nom}	MVA	350	640
$V_{pr,Nom}$	kV	66	220
$V_{sec,Nom}$	kV	220	380
α	–	66/220	220/380
$R_{C,sec}$	pu	600	800
$X_{M,sec}$	pu	400	500
$R_{eq,sec}$	pu	0.005	0.003
$X_{eq,sec}$	pu	0.16	0.16
$P_{cool,Nom}$	kW	28	38
$\theta_{RiseMax}$	$°C$	65	65
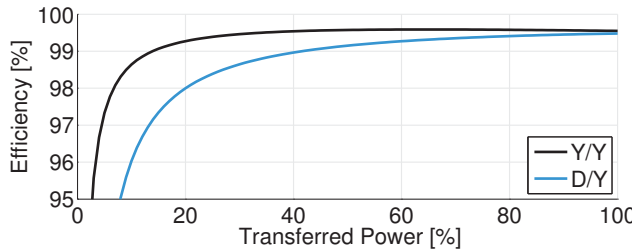
(a) Efficiency curves.
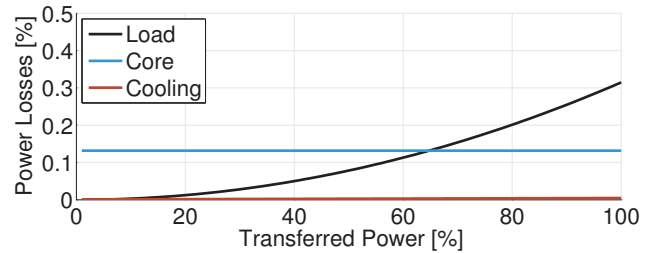
(b) YY Transformer.
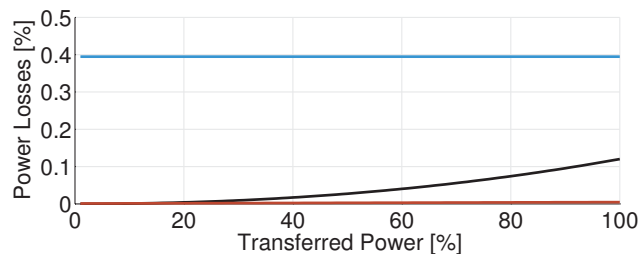
(c) DY Transformer.

Figure 4.26: Efficiency curves and power losses breakdown.

4.5   Case study

In the previous section the models for cables, MMC and transformer were introduced and assessed. These models were used for the final case study in which we assess the BED of an OWF according to the power losses of the collection and transmission systems. To this end an OWF composed of 80 wind turbines (WTs) with a rated power of 8 MW each was used. Half of the OWF is shown in Figure 4.27 (another symmetrical arrangement of 40 WTs and one offshore transformer substation is found at the offshore site).

The wind resource, shown in Figure 4.28a, is based on data collected from a measurement mast on the North Sea [37]. The OWF power production, which takes wake effects into account [38], was calculated with the FarmFlow software developed by the Energy Research Centre of the Netherlands (ECN) [39] (see Figure 4.28b).

The power flow inside the collection and transmission systems is obtained via a solver which guarantees that the mismatch equations are null in all the system nodes [40–42]. The power flow solver slack node is taken as the rectifier, in case of HVdc transmission, and as the onshore grid connection point in case of HVac transmission. The two transmission schemes are shown in Figure 4.2. The inverter of the HVdc system and the compensation reactors in the HVac system were controlled so that no reactive power was exchanged with the grid [43].

Figure 4.27: OWF layout.

(a) Wind resource.

(b) Wind farm energy production.
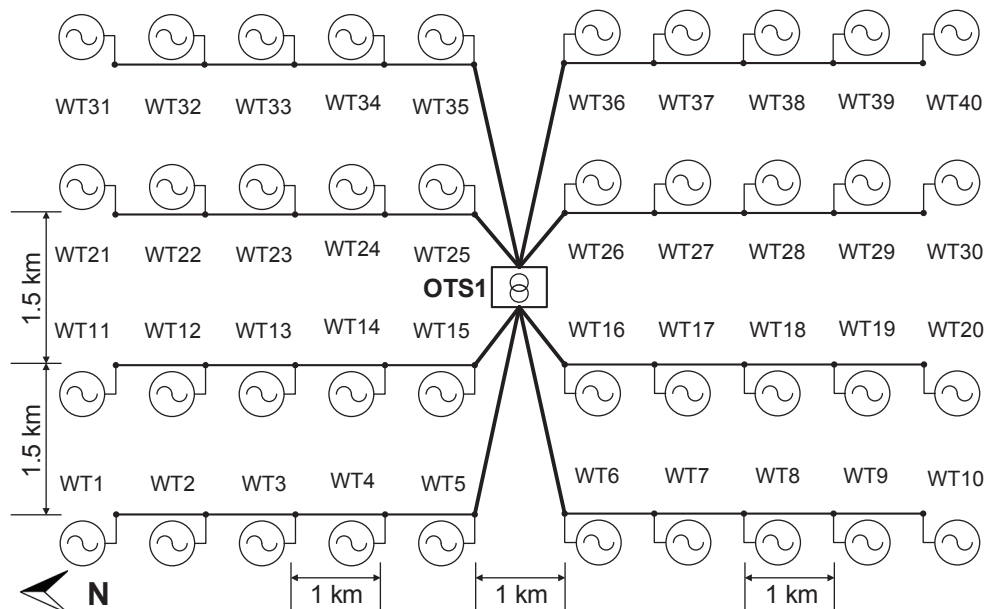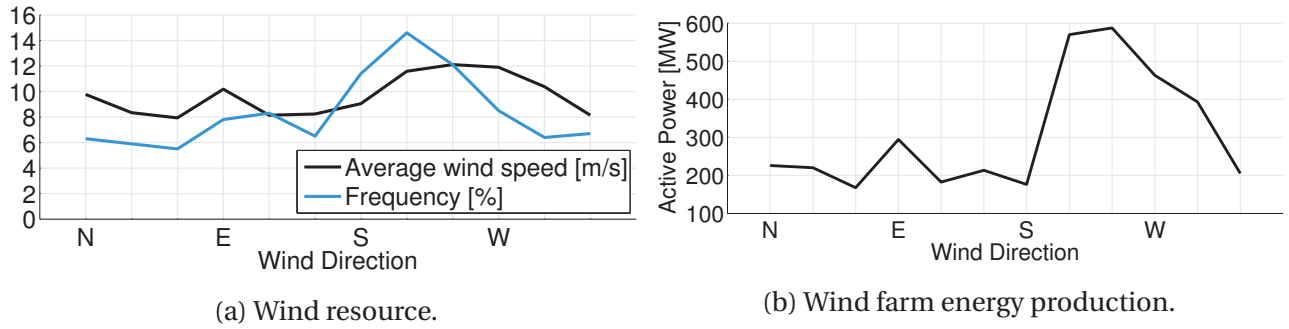
Figure 4.28: Wind turbine and wind farm characteristics with wind speed.
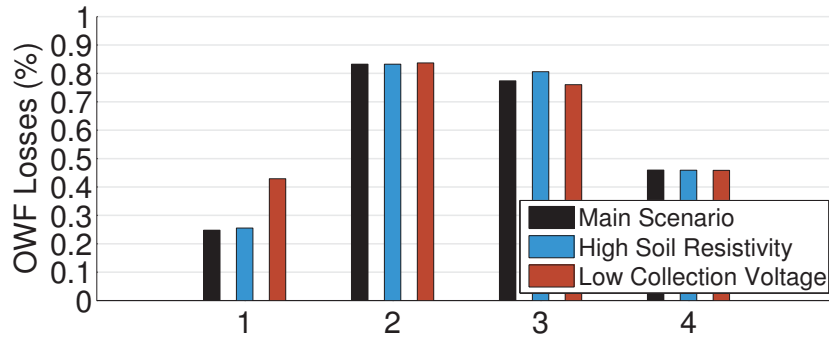
Figure 4.29: Losses for three scenarios. HVac losses: 1 - MVac cables, 2 - Offshore Transformers, 3 - HVac cables, 4 - Onshore Transformer. Distance to shore 50 km.

4.6   Results

4.6.1   Impact of the soil resistivity

Figure 4.29 shows the losses of the HVac transmission system per component for different soil resistivity. It can be seen that the type of soil surrounding the cables does not have a strong impact in their losses.

4.6.2   Impact of collection system voltage

The HVac scenario was also run for a collection system with a rated voltage of 33 kV (see Table 4.4). Figure 4.29 shows that, as expected, the low voltage collection system has almost double the power losses when compared to the main scenario which uses a 66 kV collection system.

4.6.3 Impact of the distance to shore

Figure 4.30a presents the power losses breakdown for three different distances to shore – 50, 100 and 150 km – for the HVac transmission technology, whereas Figure 4.30b presents the losses for the HVdc technology. The proposed models were also run without the temperature correction factors (at the maximum temperature) to assess the impact in the power losses.

Figure 4.30a shows that the HVac cables are the main contributors to the total losses. These losses rapidly increase with higher transmission distances to shore. The largest difference between the models which take into consideration the temperature of operation are seen in the HVac cables, whereas changes in the transformer losses are negligible.

Figure 4.30b shows that for HVdc systems, the converters and the offshore transformers represent most of the total losses and that cable losses are not predominant as in the HVac system. In addition, the cable losses increase linearly with the transmission distance. This phenomenon can be seen in Figure 4.30c which shows the wind farm efficiency for each wind direction. The efficiencies of the wind farms interconnected with the HVdc transmission system are very similar in the directions in which the energy production is low, whereas the efficiency drop is larger for directions with the largest energy production. Overall the efficiency of the transmission system is linear with the distance to shore. On the other hand, the efficiency of the HVac does not vary linearly with the distance as shown in Figure 4.30c.

Figure 4.31a shows a comparison between the two transmission schemes when the temperature of operation is not considered. It can be seen that for short transmission distances the HVac scheme is more efficient. However the HVdc scheme is less affected by the transmission length and becomes electrically more efficient at 115 km with an efficiency of 95.5%.

Table 4.4: Cables data used in the case study [13, 44].

Variable	Unit	MVac		HVac		HVdc
V	$[kV]$	30	66	220	220	320
A	$[mm^2]$	400	150	800	1400	630
C	$[\mu F/km]$	0.2900	0.1900	0.1700	0.2000	-
L	$[mH/km]$	0.3500	0.4100	0.4000	0.3500	-
R_{ac20}	$[\Omega/km]$	0.0494	0.1246	0.0246	0.0169	0.0273
$tan(\delta)$	$[-]$	0.0040	0.0010	0.0010	0.0010	-
θ_{max}	$[°C]$	90	90	90	90	90
λ_1	$[-]$	0.0339	0.0119	0.3101	0.5005	-
λ_2	$[-]$	0.1507	0.0587	0.2051	0.2832	-
T_1	$[K\ m/W]$	0.3253	0.4961	0.5028	0.4175	0.6643
T_2	$[K\ m/W]$	0.0525	0.0642	0.0408	0.0321	0.0329
T_3	$[K\ m/W]$	0.0455	0.0494	0.0313	0.0284	0.0388
$T_4 air$	$[K\ m/W]$	0.2126	0.2359	0.1310	0.1173	0.2511
$T_4 soil$	$[K\ m/W]$	0.5456	0.5582	0.4523	0.4375	0.5421

Figure 4.31b shows similar results for the case when the temperature of operation is considered. Although the losses with the proposed method are lower due to incorporation of the temperature of operation (0.5% higher at the BED), the BED was not altered.
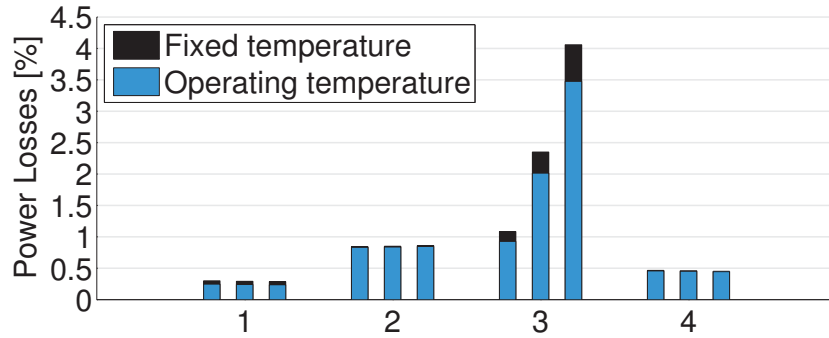
(a) HVac losses: 1 - MVac cables, 2 - Offshore Transformers, 3 - HVac cables, 4 - Onshore Transformer. Losses are shown in percentage of the rated power of each component. For each component: left bar - 50 km, middle bar - 100 km, right bar - 150 km.
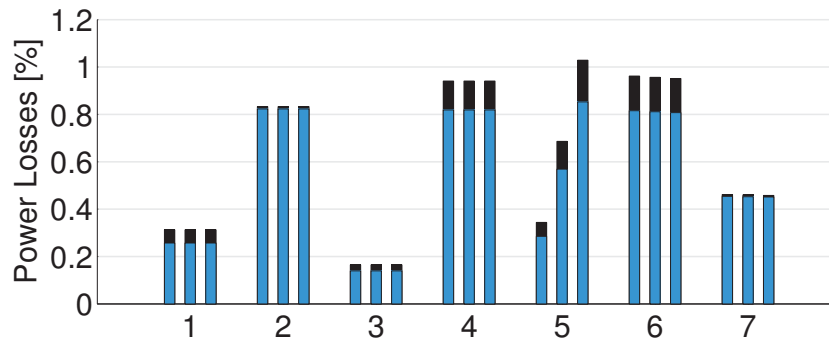
(b) HVdc losses: 1 - MVac cables, 2 - Offshore Transformers, 3 - HVac cables, 4 - Rectifier, 5 - HVdc cables, 6 - Inverter, 7 - Onshore Transformer. Losses are shown in percentage of the rated power of each component. For each component: left bar - 50 km, middle bar - 100 km, right bar - 150 km.
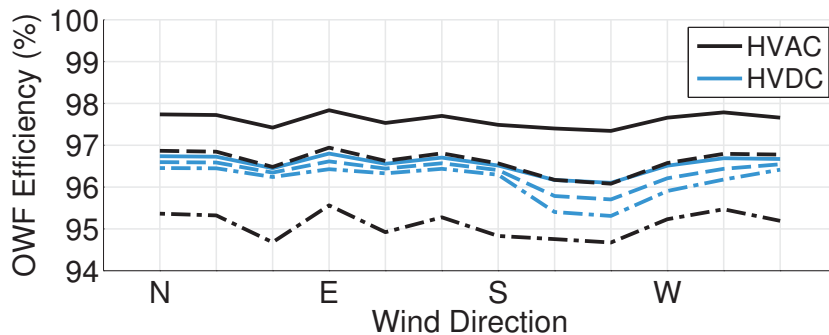
(c) Efficiency for each wind direction. Losses are shown in percentage of the energy produced by the turbines for each direction. Solid line - 50 km, Dashed line - 100 km, Dash-dotted line - 150 km.

Figure 4.30: Power losses breakdown for both transmission systems and considered distances.

(a) BED with no temperature variation. (b) BED with temperature variation.
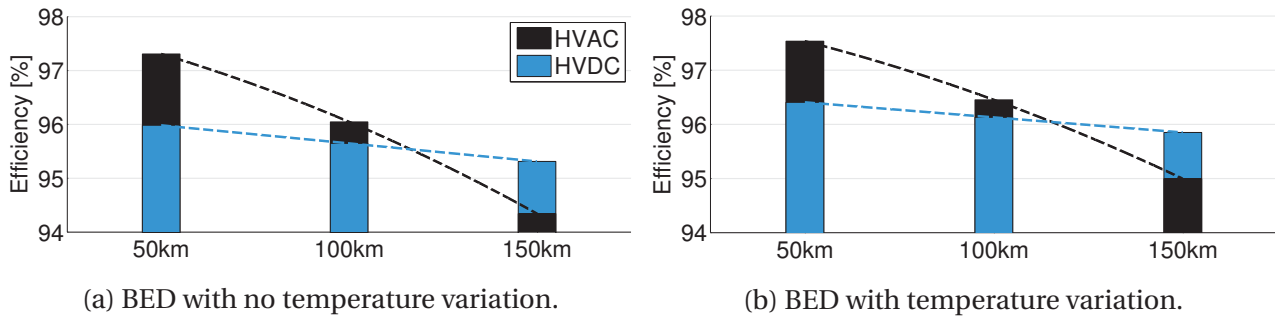
Figure 4.31: BEDs without and with temperature variation, respectively. Losses are shown in percentage of the energy produced by the turbines.

4.7 Conclusions

In this work, power loss models for ac and dc cables, MMC and transformers have been developed. They capture the main sources of losses under steady-state operation and are computationally light. The assumptions made for the models are reasonable since they will be used in the assessment of the efficiency of large OWFs during a 20-year period. The results show that the proposed models are able to capture the main sources of power losses, as well as, the main environmental factors, such as type of soil surrounding the cables and ambient temperature. Therefore, the proposed models are suitable to be used in the optimization phase of OWFs.

References

[1] The Crown Estate, "Offshore Wind Cost Reduction - Pathways Study," London, United Kingdom, Tech. Rep., 2012.

[2] S. Rodrigues *et al.*, "Trends of offshore wind projects," *Renewable and Sustainable Energy Reviews*, vol. 49, pp. 1114–1135, Sept. 2015.

[3] C. N. Elkinton, J. F. Manwell, and J. G. McGowan, "Algorithms for Offshore Wind Farm Layout Optimization," *Wind Engineering*, vol. 32, pp. 67–84, 2008.

[4] LORC. [Last accessed 1st March 2015]. [Online]. Available: www.lorc.dk/offshore-wind-farms-map/list

[5] 4C Offshore. [Last accessed 23rd March 2015]. [Online]. Available: www.4coffshore.com/windfarms

[6] The Wind Power. (2014) [Last accessed 1st March 2015]. [Online]. Available: www.thewindpower.net/windfarms_offshore_en.php

[7] Renewables Map. [Last accessed 1st March 2015]. [Online]. Available: www.renewables-map.co.uk/windfarm.asp

[8] S. Meier, and P. Kjor, "Benchmark of annual energy production for different wind farm topologies," in *Power Electronics Specialists Conference, 2005. PESC '05. IEEE 36th*, June 2005, pp. 2073–2080.

[9] N. B. Negra, J. Todorovic, and T. Ackermann, "Loss evaluation of HVAC and HVDC transmission solutions for large offshore wind farms," *Electric Power Systems Research*, vol. 76, no. 11, pp. 916–927, 2006.

[10] P. Bresesti *et al.*, "HVDC Connection of Offshore Wind Farms to the Transmission System," *IEEE Transactions on Energy Conversion*, vol. 22, no. 1, pp. 37–43, March 2007.

[11] A. Papadopoulos, "Modeling of collection and transmission losses of offshore wind farms for optimization purposes," Master's thesis, Electrical Sustainable Energy Department, Delft University of Technology, Delft, The Netherlands, Feb. 2015.

[12] G. J. Anders, *Rating of Electric Power Cables in Unfavourable Thermal Conditions*. John Wiley & Sons, 2005.

[13] International Electrotechnical Commission, *IEC 60287: Electric cables - Calculation of the current rating*, Switzerland Std., Rev. 1.2, 2006.

[14] G. J. Anders, and H. Brakelmann, "Improvement in Cable Rating Calculations by Consideration of Dependence of Losses on Temperature," *IEEE Trans. on Power Delivery*, vol. 19, no. 3, pp. 919–925, July 2004.

[15] A. Madariaga, and et al., "Effective Assessment of Electric Power Losses in Three-Core XLPE Cables," *IEEE Trans. on Power Systems*, vol. 28, no. 4, pp. 4488–4495, Nov. 2013.

[16] A. Lesnicar, and R. Marquardt, "An Innovative Modular Multilevel Converter Topology Suitable for a Wide Power Range," in *IEEE Power Tech Conference Proceedings, Bologna*, 2003.

[17] S. Rohner *et al.*, "Modulation, Losses, and Semiconductor Requirements of Modular Multilevel Converters," *IEEE Transactions on Industrial Electronics*, vol. 57, pp. 2633 – 2642, 2010.

[18] S. Allebrod, R. Hamerski, and R. Marquardt, "New Transformerless, Scalable Modular Multilevel Converters for HVDC-Transmission," in *Power Electronics Specialists Conference*, 2008, pp. 174 – 179.

[19] Infineon, *Technical Information of IGBT module FZ1000R33HL3*, Rotterdam, The Netherlands, 2013.

[20] K. Ilves *et al.*, "A New Modulation Method for the Modular Multilevel Converter Allowing Fundamental Switching Frequency," *IEEE Transactions on Power Electronics*, vol. 27, pp. 991 – 998, 2012.

[21] A. Antonopoulos, "Control, Modulation and Implementation of Modular Multilevel Converters," Master's thesis, Electrical Machines and Power Electronics Department, KTH, 2011.

[22] A. Antonopoulos, L. Angquist, and H. Nee, "On dynamics and voltage control of the Modular Multilevel Converter," in *13th European Conference on Power Electronics and Applications*, 2009.

[23] Q. Tu, Z. Xu, and L. Xu, "Reduced Switching-Frequency Modulation and Circulating Current Suppression for Modular Multilevel Converters," *IEEE Transactions on Power Delivery*, vol. 26, pp. 2009–2017, 2011.

[24] B. Jacobson *et al.*, "VSC-HVDC Transmission with Cascaded Two-Level Converters," in *43rd CIGRE*, 2010, pp. 1–8.

[25] K. Ilves, "Modeling and Design of Modular Multilevel Converters for Grid Applications," Master's thesis, Electrical Energy Conversion Department, KTH, 2012.

[26] M. Zygmanowski, B. Grzesik, and R. Nalepa, "Capacitance and Inductance Selection of the Modular Multilevel Converter," in *Power Electronics and Applications (EPE)*, 2013.

[27] Y. Zhang, N. Tai, and B. Xu, "Fault analysis and traveling-wave protection scheme for bipolar hvdc lines," *Power Delivery, IEEE Transactions on*, vol. 27, no. 3, pp. 1583–1591, July 2012.

[28] L. Angquist *et al.*, "Inner control of Modular Multilevel Converters - An approach using open-loop estimation of stored energy," in *International Power Electronics Conference (IPEC)*, 2010.

[29] Emerson Network Power, *Liebert CRV - Efficient Cooling for IT Equipment*, 2014.

[30] M. Saeedifard, and R. Iravani, "Dynamic performance of a modular multilevel back-to-back hvdc system," *Power Delivery, IEEE Transactions on*, vol. 25, no. 4, pp. 2903–2912, Oct 2010.

[31] Q. Tu, Z. Xu, and L. Xu, "Reduced switching-frequency modulation and circulating current suppression for modular multilevel converters," *Power Delivery, IEEE Transactions on*, vol. 26, no. 3, pp. 2009–2017, July 2011.

[32] J. Pou *et al.*, "Circulating current injection methods based on instantaneous information for the modular multilevel converter," *Industrial Electronics, IEEE Transactions on*, vol. 62, no. 2, pp. 777–788, Feb 2015.

[33] M. Guan, Z. Xu, and H. Chen, "Control and modulation strategies for modular multilevel converter based HVDC system," in *37th Annual Conference on IEEE Industrial Electronics Society (IECON)*, 2011.

[34] S. Chapman, *Electric Machinery Fundamentals*, 4th ed., 2005.

[35] S. Kulkarni, and S. Khaparde, *Transformer Engineering Design and Practice.* Marcel Dekker Inc, 2004.

[36] M. Heathcote, *J & P Transformer Book*, 13th ed. Newnes, 2007.

[37] E. Berge *et al.*, "Modelling of offshore wind resources. Comparison of a mesoscale model and measurements from FINO 1 and North Sea oil rigs," in *European Wind Energy Conference and Exhibition (EWEC)* , 2009.

[38] S. Rodrigues *et al.*, "Wake losses optimization on offshore wind farms with moveable floating wind turbines," *Elsevier Energy Conversion and Management*, vol. 89, pp. 933–941, January 2015.

[39] E. Bot, "Farmflow - improved near wake modelling and validation against four full scale wind farms," Energy Research Centre of the Netherlands, Tech. Rep., 2012.

[40] S. Rodrigues *et al.*, "Optimal Power Flow Control of VSC-based Multi-Terminal DC Network for Offshore Wind Integration in the North Sea," *IEEE Transactions on Emerg. and Selected Topics in Power Electronics*, vol. 1, no. 4, pp. 260–8, 2013.

[41] R. Teixeira Pinto *et al.*, "A novel distributed direct-voltage control strategy for grid integration of offshore wind energy systems through mtdc network," *IEEE Transactions on Industrial Electronics*, vol. 60, no. 6, pp. 2429–41, 2013.

[42] S. Rodrigues *et al.*, "Optimization of social welfare and transmission losses in offshore mtdc networks through multi-objective genetic algorithm," in *Power Electronics and Motion Control Conference (IPEMC)*, 2012, pp. 1287–1294.

[43] R. Teixeira Pinto *et al.*, "Grid code compliance of vsc-hvdc in offshore multi-terminal dc networks," in *39th Annual Conference IECON*, 2013.

[44] ABB, *XLPE Submarine Cable Systems - Attachment to XLPE Land Cable Systems - User's Guide*, Lyckeby, Sweden, 2010.

Multi-Objective Optimization Framework for Offshore Wind Farms

Current offshore wind farms (OWFs) design processes are based on a sequential approach which does not guarantee system optimality because it oversimplifies the problem by discarding important interdependencies between design aspects. This work presents a framework to integrate, automate and optimize the design of OWF layouts and the respective electrical infrastructures. The proposed framework optimizes simultaneously different goals (e.g. annual energy delivered and investment cost) which leads to efficient trade-offs during the design phase, e.g. reduction of wake losses vs collection system length. Furthermore, the proposed framework is independent of economic assumptions, meaning that no *a priori* values such as the interest rate or energy price, are needed. The proposed framework was applied to the Dutch Borssele areas I and II. A wide range of OWF layouts were obtained through the optimization framework. OWFs with similar energy production and investment cost to layouts designed with standard sequential strategies were obtained through the framework, meaning that the proposed framework has the capability to create different OWF layouts that would have been missed by the designers. In conclusion, the proposed multi-objective optimization framework represents a mind shift in design tools for OWFs which allows cost savings in the design and operation phases.

5.1 Introduction

Currently the offshore wind industry is aiming at reducing its levelized cost of energy (LCOE) [€/MWh] to breach the 100 €/MWh barrier as soon as 2020 [1–6] from the current 163 €/MWh [7]. Although the technologies used in offshore wind farms (OWFs) have greatly improved, the LCOE generated offshore is yet not competitive [8]. In fact, electricity generated offshore is currently approximately 50% more expensive when compared to onshore wind generation [9]. Figure 5.1a demonstrates that the cost of power (COP) [M€/MW] installed of OWFs has increased since the initial project and has not reduced in the last years [10, 11].

There are different measures that can decrease the costs of the energy generated offshore [2–6]. Key factors are, for example, exploitation of economies of scale and greater standardization, introduction of turbines with higher rated power and reliability and greater activity at the front end engineering and design (FEED) phase.

The design phase of an OWF is performed during the FEED phase (see Figure 5.2), after the initial feasibility studies have been done and permission has been granted, and before final investment decisions are made [2, 14]. FEED studies allow wind farm developers to make a pre-selection of economically viable design concepts and respective key components [3]. During the FEED phase, decisions have not yet been made regarding the number of turbines [15, 16], the support structures that will be used or the number of substations that will be built [15, 16]. In this phase, several layout concepts are preliminary designed, and although the final wind farm layout will be based on these designs, it may still differ considerably [15].

Several aspects have increased the need for a broader activity at the FEED stage [3]. The development phase of OWFs is time consuming due to the time needed to manually create several designs and the necessary cable routing [18–20]. In fact, circa 4% of the total capital expenditure (CAPEX) of an OWF are allocated to the development phase (see Figure 5.1b), in which all the components
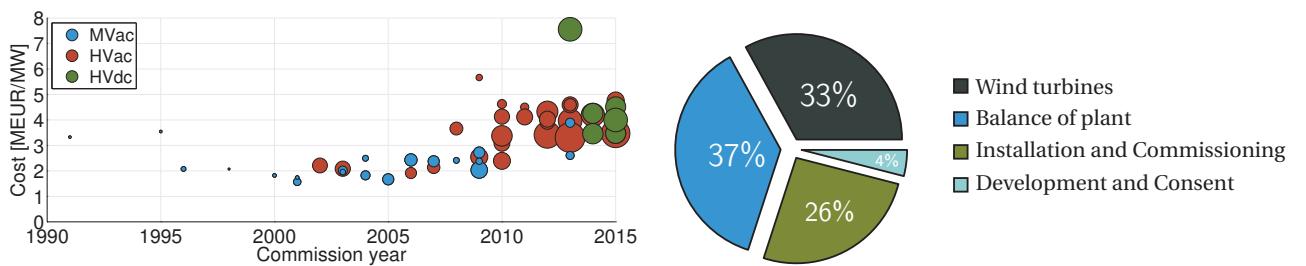
(a) COP of the European OWFs composed of five or more turbines [10, 11]. Circle size represents the installed capacity. The monetary values were updated considering a Eurozone inflation of 1.85% [12].

(b) Typical CAPEX breakdown of an OWF [13].

Figure 5.1: COP and CAPEX breakdown of OWFs.

Figure 5.2: Lifecycle of an OWF and location of the FEED phase [14, 17].

and technologies that lead to an optimized and feasible system must be assessed [13, 21]. Recent OWFs occupy larger areas, which often have variable water depth and seabed conditions [22] and are situated further from shore [22], leading to more complex constraints and design challenges on the grid connection. Finally, the large number of wind turbines leads to complex collection systems, which need to be carefully assessed to achieve wind farm layouts with higher efficiencies [2]. Figure 5.3 shows the difference in complexity between the first OWF, Vindeby, and the recent British Gwynt y Môr.

Additionally, current design processes are based on a sequential approach (or decoupled strategy) due to the complexity of designing an OWF [19, 23]. Such strategy does not guarantee system optimality because the interactions between different system components are disregarded. Moreover, early project decisions may become constraints in later stages [9]. Automated optimization is crucial to optimize wind farm layouts, since the design with standard tools is highly complex and time consuming [19]. A reduction of up to 10% in the LCOE is possible through more integrated design methods [9].

The increased difficulty in the design of modern OWFs comes from the fact that mostly all design aspects of an OWF influence both the energy production and costs [2]. For example, the energy production is increased by placing more turbines in the OWF area, however this also makes the costs rise. Also, interactions between turbines reduce the increase in energy production that results from more turbines being closed together. Hence, these design goals are conflicting, meaning that there is not a single solution for the problem but a set of solutions which represent the trade-off. In the multi-objective (MO) space, a layout is optimal if there is no other layout which is better in all objectives.

Although more than 150 research articles on the wind farm layout optimization problem (WFLOP) may be found in literature, few studies have investigated the inherent trade-offs of designing an OWF [25]. For example, the trade-off between the wind farm capacity factor and the power density within the project area was assessed in [26]. The authors analyzed the conflict between increasing the spacing between the turbines to increase energy production (via a decrease of wake losses) and the need for larger project areas.

(a) Vindeby wind farm [10].

(b) Gwynt y Môr wind farm [24].
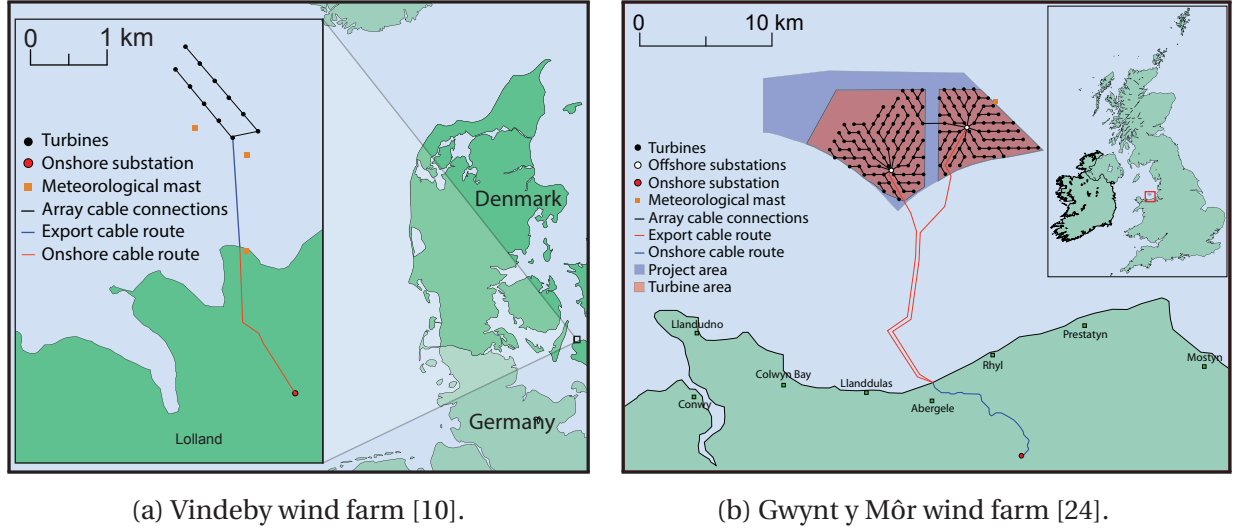
Figure 5.3: Differences in topology and design complexity between two OWFs.

Comprehensive studies that explicitly consider multiple goals during the optimization process are rare [27]. Table 5.1 presents the characteristics of the MO WFLOP (MOWFLOP) from previous studies. The work carried out in [28] optimized the annual energy production (AEP) [GWh/year] considering the problem constraints (minimum proximity constraint between wind turbines and area constraint which guarantees that all turbines are placed within the wind farm area) as a second objective function. The AEP and the turbine noise were optimized in [29, 30]. Similarly, the AEP was maximized and the sum of the wind farm area and number of turbines were treated as a second objective function in [31]. Three optimization goals were used in [32]: AEP, area used and collection system length. The work presented in [33] studied the features that a MO algorithm should have to efficiently solve the MOWFLOP. The optimization goals were the AEP and the system efficiency, while the optimization variables were the location and number of turbines.

A framework able to efficiently optimize, at once, both the wind farm layout and its respective electrical infrastructure for large OWFs is a highly desired tool by wind farm designers [20, 29]. However, none of the optimization frameworks displayed in Table 5.1 captured all the key aspects pertaining to the development of OWFs. In other words, as far as the authors knowledge goes a MO optimization framework – which is able to give general recommendations and trade-offs insight to OWF developers – has not yet been established.

To bridge this existing research gap, this work proposes a MO optimization framework to *integrate*, *automate* and *optimize* the design of OWF layouts and their electrical infrastructure. The most suitable and relevant optimization goals and design variables for the MOWFLOP will be identified. The optimization framework is then applied to the design of an OWF in a case study to demonstrate the advantages and differences of the proposed method.

Table 5.1: Existing approaches for the MOWFLOP.

References	Optimization Variables	Design Goals
Kusiak et al [28]	Turbine locations	Energy generation, Problem constraints
Zhang et al [29, 30], Sorkhabi et al [34]	Turbine locations	Energy generation, Noise level
Veeramachaneni et al [31]	Turbine locations	Energy generation, Cost
Tran et al [32]	Turbine locations	Energy generation, Collection system length, Wind farm area
Sisbot et al [35]	Turbine locations and quantity	Energy generation, Cost
Rodrigues et al [33]	Turbine locations and quantity	Energy generation, System efficiency

The work is organized as follows: Section 5.2 provides an overview of the relevant commercial and academic optimization methods for OWFs. Furthermore the most common economic functions used to assess the profitability of wind projects are introduced and explained. Thereafter, Section 5.3 presents the MO optimization framework for the design of OWF layouts and respective electrical infrastructures and its boundaries and selection criteria. Section 5.4 introduces the optimization variables considered in the framework as well as their boundaries, constraints and influences over the energy production and expenditures. The industrial trends of the different components of an OWF are also investigated. Section 5.5 then describes the case study used to demonstrate the usefulness of the proposed framework, followed by Section 5.6 in which the results obtained are discussed. Section 5.7 presents the main conclusions of the work.

5.2 Current Wind Farm Optimization Tools

5.2.1 Commercially Available Software

Currently, there are several software commercially available to optimize the design of wind farms. For example, WindPRO [36], WindFarmer [37] and WAsP [38] are among the most famous optimization tools. Table 5.2 presents the main features and limitations of the best-known available commercial software.

All the commercial wind farm design tools were specifically built for onshore environments and, therefore, consider some irrelevant design aspects for offshore areas such as visual impact (irrelevant for far offshore), shadow flickering, noise levels [34] and complex terrain elevations [42, 43]. Although it is possible to use them to design OWFs, none of them consider some of the important offshore aspects such as collection and transmission systems design, number and location of offshore substations and transmission technology. Furthermore, no commercial tool uses a MO algorithm to optimize the trade-offs between the chosen goals.

Table 5.2: Wind Farm Design Software Commercially Available.

Software	Optimization goals	Design parameters	Design Constraints	Design considerations	Limitations
OpenWind (AWS Truepower) [39]	Cost of Energy	Wind turbine coordinates	Site constraints for turbine placement, noise levels	Wake and turbulence losses, shadow flicker, visual impact, uncertainty analysis	Electrical losses are not considered
WAsP (DTU) [38]	None	Pre-defined wind turbine coordinates	None	Wake losses, different turbine models may be used simultaneously, estimation of loads in complex terrains	There is no optimization algorithm, electrical losses are not considered
WindFarmer (DNV Garrad Hassan's) [37]	Energy production	Wind turbine coordinates	Environmental constraints, wind farm boundaries, exclusion zones and set-back distances from boundaries, soil topography	Turbulence intensity, environmental and visual impacts, noise levels, shadow flicker, uncertainty analysis, wake loss, turbine loading, electrical losses calculation, reactive power production	No optimization of the collection system layout
WindPRO [36]	Energy production or Minimum production loss	Wind turbine coordinates	Minimum distances between turbines, site constraints for turbine placement	Noise levels, visual impact, shadow effects, Wake and turbulence losses, different turbine models may be used simultaneously, electrical losses calculation, uncertainty analysis	Restricted to geometrical layouts, addition of turbines incrementally
WindSim [40]	Wind project profit	Wind turbine coordinates	Environmental constraints, wind farm boundaries, exclusion zones for turbine placement, IEC Constraints	Optimum number of turbines, terrain features effects on the wind, wake and turbulence losses	No collection system design, electrical losses are not considered
WindFarm (ReSoft) [41]	Energy production or cost of energy	Wind turbine coordinates	Turbine separation, exclusion zones for turbine placement	Wake losses, visual impact, shadow flicker, noise levels, different turbine models may be used simultaneously	No collection system design, electrical losses are not considered

5.2.2 Academic Studies

On the other hand, several academic studies were specifically tailored to design OWFs. A brief description and the main drawbacks of some of these works are given next.

Offshore Wind Farm Layout Optimization (OWFLO) (2005)

The OWFLO project proposed a framework to design OWFs which uses the LCOE as the optimization goal. It includes turbine availability, wake and cable losses and cost models for the turbines, support structures, cables, operation expenditure (OPEX) [€ billion], installation and decommissioning [44]. With these models, the OWFLO tool captures key factors that influence the cost of energy: turbine size, water depth, distance to shore, soil types and wind and wave conditions.

The main goal of the OWFLO project was the development of an optimization software to provide insights into the trade-offs between cost and energy. However, even though both energy and cost models are used, wind farm developers are only presented with one solution at the end of the optimization routine. Hence, no information regarding the trade-offs is obtained. Furthermore, the design of the wind farm collection system, which is a key design aspect, was not considered.

Lackner and Elkington (2007)

The trade-offs inherent to OWFs design problems are identified in [45]. These trade-offs are captured by considering the LCOE as the optimization goal. However, by optimizing directly the LCOE, the wind farm designers are only presented with one final solution, hence, once again, no information regarding the trade-offs is obtained. Furthermore, the water depth and the wind speed are considered as functions of the distance to shore which does not depict reality.

Gribben et al. (2010)

This study presents an OWF layout design tool based on an engineering approach [46]. The authors also identify the multi-disciplinary nature of the problem and, although it is stated that it is important to make a selection of the significant design considerations since it is a highly complex problem, no selection criteria are provided. Moveover, there is no optimization routine implemented in the design approach and only a variation of the design parameters is carried out.

Trade-off insights are presented between, for example, energy yield and foundation costs. Nonetheless, similar to standard design strategies, the method is based on a sequential approach. Moreover, only geometrical layouts are considered and the turbine type is set beforehand.

Topology Optimization of Wind Farms (TopFarm) (2011)

The main goal of this EU-funded project, TopFarm, was the design of an optimization tool for wind farm developers [47]. The financial balance was used as the optimization goal, whereas the turbine coordinates were chosen as design variables. Relevance and relative cost basis were the

selection criteria for the cost models in the framework. TopFarm only considered costs which depend on the wind farm topology, since only these provide useful information to guide the search of the optimization algorithm.

Although TopFarm has a comprehensive number of modules, it still lacks key aspects for the optimization of OWF layouts. For example, the collection system routing was determined by solving the auxiliary road problem, i.e. interconnecting all turbines and assuming that the cables could transport the power connected to them. Furthermore, the TopFarm tool does not consider offshore substations or export cables, which are key factors for OWF developers.

5.2.3 Economic functions for Offshore Wind Projects

Investing capital in one project means that the same capital cannot be applied to another investment that is equally or more attractive. Therefore, before final investment decisions are made, wind farm designers create several wind farm designs during the FEED phase to evaluate them economically [2, 14].

The choice of which economic function to use is based on different factors, e.g. risk associated, financial structure, regulation, project size [48]. Due to the variety of factors, depending on the case some economic functions are more suitable than others. Therefore, different functions should be used to evaluate possible investments [49]. Table 5.3 presents the objective functions commonly used in the existing optimization frameworks as well as other economic functions which may be used to assess the profitability of OWFs. Next, a brief description of each function is given and their respective advantages and disadvantage are also discussed.

Annual Energy Delivered

Maximizing the AEP is among the most common goals [25] and aims at maximizing the production of the wind turbines. Another more comprehensive goal is to maximize the annual energy delivered (AED) [GWh/year] to the onshore electrical network. This goal covers the AEP but also the electrical losses of the entire system, e.g. transformers and cabling systems. Nonetheless, these goals do not take into consideration costs or the efficiency of the project.

Utilization Factor

The utilization factor (UF) [-], or capacity factor, of an OWF is the ratio between its AEP and its power production if working constantly at rated power, for the same period of time. This measure is also captured by the wind farm efficiency which is the ratio between the energy delivered over the energy produced without losses. The UF is maximized considering the AED and the efficiency of the system. However, the costs of the project are still neglected if designers use this measure.

Table 5.3: Economic functions for the WFLOP [48].

Function	Equation	Parameters
AED [GWh/year]	$8760 \sum\limits_{i=1}^{angle} \sum\limits_{j=1}^{bins} f_i^j \cdot \left(\left(\sum\limits_{k=1}^{turbines} T_k \left(\overline{wind}_i^j \right) \right) - \text{losses} \left(\overline{wind}_i^j \right) \right)$	f_i^j - wind frequency in direction i and wind bin j, $T_k \left(\overline{wind}_i^j \right)$ - power production of the k-th turbine, losses $\left(\overline{wind}_i^j \right)$ - system electrical losses
UF [-]	$\dfrac{AED}{8760 \sum\limits_{j=1}^{turbines} P_{rated}^j}$	P_{rated}^j - rated power of the j-th turbine
COP [M€/MW]	$\dfrac{CAPEX}{\sum\limits_{j=1}^{turbines} P_{rated}^j}$	
LCOE [€/MWh]	$\dfrac{1}{AED} \left(\dfrac{CAPEX}{a} + OPEX \right)$	a - annuity factor ($a = \dfrac{1-(1+r)^{-n}}{r}$), r - interest rate, n - wind farm lifetime, OPEX - annual operational expenditure
NPV [€ billion]	$\left(AED \cdot p_{kWh} - OPEX \right) a - CAPEX$	p_{kWh} - market energy price
IRR [%]	$\left(AED \cdot p_{kWh} - OPEX \right) \dfrac{1-(1+r_{IRR})^{-n}}{r_{IRR}} - CAPEX$	r_{IRR} - interest rate that zeroes the NPV equation
DPT [years]	$\dfrac{n \cdot CAPEX}{\left(AED \cdot p_{kWh} - OPEX \right) \cdot a}$	
ROI [-]	$\dfrac{\left(AED \cdot p_{kWh} - OPEX \right) \cdot a}{CAPEX}$	
BCR [€ billion]	$\dfrac{AED \cdot p_{kWh} \cdot a}{CAPEX + OPEX \cdot a}$	
AV [€ billion]	$AED \cdot p_{kWh} - OPEX$	

Cost of Power

Another approach is to minimize the COP installed which is the ratio between the CAPEX and the rated capacity of the project. In this way, the optimization tries to minimize the cost of the entire project. However, and specially in offshore environments, the OPEX also plays an important role in the total costs of the project. Hence, a better approach is to use economic functions which relate the AED, CAPEX and OPEX of the project through economic factors.

Levelized Cost of Energy

The LCOE is also one of the most common economic functions used to evaluate wind farm layouts [25]. The LCOE represents the minimum energy price that meets the desired interest rate by the designers [17]. The LCOE function requires the interest rate and the wind farm lifetime. However, it may not be straightforward to set a value for the interest rate since it is associated with the risk perceived by the investor and it also may change throughout the wind farm lifetime [50]. Furthermore, the LCOE is not suitable to choose between mutually exclusive options for OWF layouts since it does not capture the difference between investment sizes [48].

Net Present Value

The net present value (NPV) [€ billion] defines the total profit of the OWF. It considers both the cash outflows (costs) and inflows (revenues) [48]. Therefore, the NPV requires all the economic factors that the LCOE function requires as well as the price of energy. A positive NPV represents a good investment whereas a negative NPV value indicates that the income (with the interest rate chosen by the designers) is lower than the costs [48].

The NPV is suitable to evaluate and compare mutually exclusive projects because it can distinguish the difference in size of different OWFs [48]. Moreover, the NPV should also be used as an alternative measure to further validate the investment [48]. On the other hand, the NPV does not consider, for example, the time required to cover the investment costs, which may lead the designers to choose a layout that will require a long time to generate profit to the investors.

Internal Rate of Return

The internal rate of return (IRR) [%] is the interest rate that sets the NPV function equal to zero. The IRR function is usually used to approve or disapprove wind farm designs and allows to check if a minimum rate of return set by the designers is met [48]. Nonetheless, the IRR is not suitable to choose between exclusive alternative designs since it does not differentiate wind farm project sizes. Furthermore, the IRR may over predict the profitability of a project because it assumes that the interim revenues are reinvested at a similar rate to the IRR [48]. Finally, the IRR does not accurately distinguish the profitability of projects with different lifetimes.

Discounted Payback Time

The discounted payback time (DPT) [years] determines the time, in years, required to cover the CAPEX while taking into account the time value of the money. The use of the DPT is recommended when risk is an issue since it represents the period of time in which the capital invested was not recovered, and is therefore, still at risk [48].

The DPT is also not recommended to select one wind farm layout among a set of alternatives because it also does not discern wind farm project sizes. Furthermore, the DPT is not suitable to rank the different possibilities since it ignores the cash revenues after the payback time [48].

Return on Investment

The return on investment (ROI) [-] represents the revenues per unit invested. It is calculated by calculating the ratio between the cash revenue and the initial investment. The ROI is recommended to accepting or rejecting single projects [48]. The ROI is not suitable to choose among mutually exclusive wind farm designs for the same reasons presented for the IRR and LCOE.

Benefit to Cost Ratio

The benefit to cost ratio (BCR) [-] is similar to the NPV function but instead of subtracting the CAPEX to the revenues, it computes a ratio. Higher values for the BCR function represent better wind farm designs. Similarly to other functions the BCR function is recommended to accepting or rejecting single projects but not for selecting among mutually exclusive alternatives. However, it can be used to differentiate the size of the projects if the BCR ratio is obtained with incremental revenues and expenses [48].

To calculate the incremental ratio, the different projects are sorted by increasing CAPEX values and the BCR of the first project is calculated. Next, the incremental difference between the revenues and CAPEX of the second project to the first are obtained. The ratio of these values is then multiplied by the BCR of the first project. If the result is higher than one, the second project becomes the reference. The procedure is repeated until a ratio lower than one is obtained [48].

Annualized Value

The annualized value (AV) [€ billion] represents the annual revenues. The AV is constant if no escalation of the price of energy or the OPEX are considered [48].

5.2.4   Current Optimization Frameworks

Figure 5.4 shows the current optimization strategy used by wind farm designers. The main disadvantage of this approach is that, by varying the economic factors, e.g. interest rate and price of energy, of the objective functions, it is not guaranteed that the layout solution remains the most advantageous. In fact, optimization strategies that optimize economic functions such as the LCOE or the NPV, may be thought as weighted optimization procedures, in which a MO problem is simplified into a single problem one.

Current single-objective optimization frameworks only output one layout which is, often, pre-constrained due to decisionS taken before the optimization. An example of this practice is the choice of the wind turbine model or the number of turbines in the initial phase of the design process (see Section 5.1). However, the designers should not limit the design themselves beforehand but rather should explore all the designs and select the most suitable design only after a careful inspection of economic factors and high-level constraints.
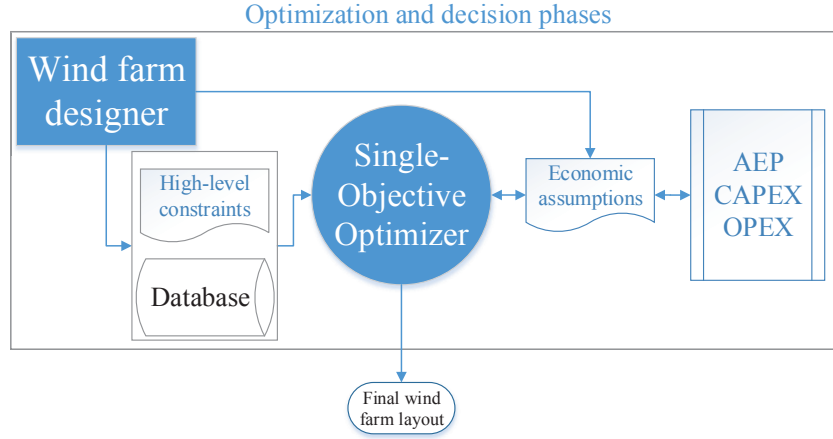
Figure 5.4: Flowchart of current single-objective optimization strategies. Dotted-line arrows represent input from the designer, solid-line arrows represent algorithm flow and dotted-point-line arrows represent component use.

5.3 Multi-Objective Optimization Framework

5.3.1 Optimization Goals

All economic functions used to evaluate the profitability of OWFs have the same backbone variables: the AED, CAPEX and OPEX. They were the chosen optimization goals because they retain their original function direction when optimizing any economic function. In other words, to optimize an economic function $f(AED, CAPEX, OPEX)$, the AED must be maximized and both the CAPEX and OPEX have to be decreased. In this way, it is possible to obtain optimized wind farm designs without setting *a priori* economic factors.

Although MO optimization is generally slower and computationally more demanding than single-objective optimization due to the larger problem search space (optimizing conflicting goals is more challenging than optimizing only one function), the former only requires one optimization routine because it optimizes all goals simultaneously, and therefore the optimization and decision phases are decoupled (see Figure 5.5). In this way, time is saved since only one optimization routine is run. Afterwards, all the possible results are presented to the designers. Nonetheless, the proposed framework still depends on component costs. The optimization strategy would be more flexible if it differentiated wind farm layouts solely on raw comparisons (e.g. cable length, number of turbines or support structures height) without relying on any costs. However, as for any optimization problem, adding many optimization goals is counter-productive as it raises the problem complexity and largely increases the required computational cost.

The optimization framework targets the FEED phase of an OWF. At this stage the farm layout is not yet decided, but the wind farm location is already defined [15]. Therefore, the macro siting optimization of the wind farm is out of scope. It is considered that the project location resulted
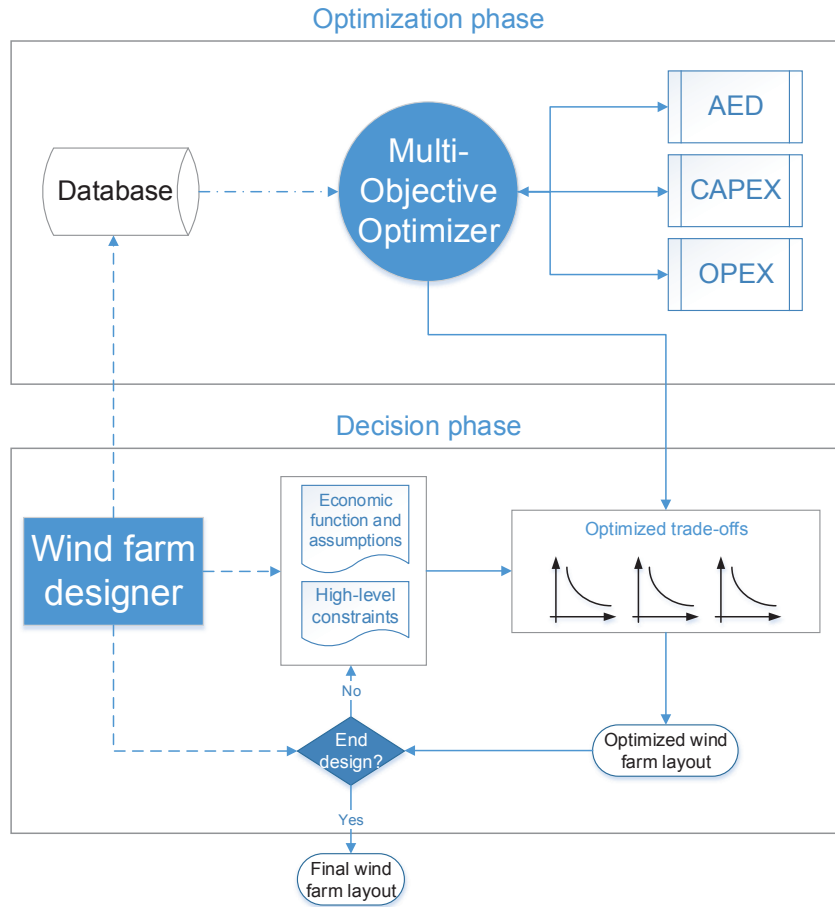
Figure 5.5: Proposed MO optimization framework for the design of OWFs and their electrical infrastructure. Dotted-line arrows represent input from the designer, solid-line arrows represent algorithm flow and dotted-point-line arrows represent component use.

from several factors that minimized environmental impacts such as bird and marine life, military activity, nature conservation, shipping and navigation, sub-sea cabling and pipelines, existing offshore industries and aviation [22].

Furthermore, it is assumed that the location has suitable wave and tidal conditions, soil properties, feasible water depths, as well as an economically viable wind resource. Although transportation and installation of wind farm components are not directly considered, part of these costs are captured in the framework by avoiding the most challenging seabed areas and by including an installation cost share in the price of turbines.

Finally, a pre-selection of components, e.g. wind turbines and cables, has been performed beforehand. In this way, the wind farm designers provide a database with information on these components to the optimization phase (see Figure 5.5).

Selection criteria

The following criteria were used to select the design aspects to be incorporated in the framework:

- Topic relevance - only design considerations that are relevant for OWFs should be included. For example, as mentioned in Section 5.2, visual impact, shadow flickering and noise are not relevant in offshore environments [15, 19, 51] although they are highly relevant when designing onshore wind farms.

- Impact - the optimization framework should include design features that play an important role in the wind farm layout. This is because the optimization algorithm needs to capture the difference between the wind farm layouts [47].

The trends of the different components will be assessed in the next section. Furthermore the trends of the components will also identify the important design characteristics, e.g. number, location and type of offshore substations, that need to be considered in the optimization framework.

5.4 Selected Design Aspects and Optimization Variables

This section presents the optimization variables and respective design aspects which, based on the aforementioned selection criteria, should be considered in the optimization of OWF layouts and their electrical infrastructure. The optimization variables and design aspects are presented separately for the main components of an OWF: turbines, offshore substations and cables (shown in Figure 5.6). Table 5.4 summarizes all the design aspects with their respective boundaries and constraints. Furthermore, it also shows the direct influences of the design variables over the AED and CAPEX. Next, the industrial trends of each optimization variable are given to assure that the optimization framework embraces all the important points of state-of-the-art OWFs.

5.4.1 Wind turbines

Figure 5.7 shows that the rated power, rotor diameter and hub height of offshore wind turbines is increasing since the initial projects. The average turbine rated power installed between 2012-2014 rounded the 4 MW mark (see Figure 5.8a) [53]. This means that, generally, the offshore wind industry prefers larger wind turbines.

The electrical systems of wind turbines have also evolved. Figure 5.8b shows that the first turbines used simple fixed-speed systems with asynchronous generators and with no power converters [55]. In a second technological step, pitch-controlled variable speed wind turbines technologies emerged as the preferred technologies and became the dominating type of wind turbines in the following years. Wind turbines equipped with doubly-fed induction generators (DFIGs) constitute approximately 25% of the offshore market [10]. Nowadays, most of the offshore wind

Table 5.4: Design variables: influences, boundaries and constraints.

Design variables	AED	Costs	Boundaries	Constraints
Wind turbines				
Number	Energy conversion, wakes losses	Turbine cost, collection cables cost	Maximum stated in the development consent order (DCO) or maximum turbine packing	Wind farm efficiency, capacity factor, installed capacity
Location	Wake losses	Support structure costs	Wind project area	Turbine separation, water depth, natural and man-made constraints [15]
Model	Energy conversion, wakes losses	Turbine costs	Pre-selected turbine models	Commercial and consistency reasons [15]
Offshore substations				
Number	Electrical losses	Components cost, substation cost, cabling costs	Maximum stated in the DCO	—
Location	Electrical losses	Support structure costs, cabling costs	Wind project area	Same as for the turbine locations [52]
Type	Electrical losses	Components cost, support structure costs, substation cost, cabling costs	Technologies allowed in the DCO	Same as for the turbine models
Collection cables				
Rated power	Electrical losses	Cabling costs	Pre-selected cables, Voltages allowed in the DCO	Turbines rated power
Rated voltage	Electrical losses	Cabling costs, reactive power compensation costs	Pre-selected cables	—
Transmission cables				
Rated power	Electrical losses	Cabling costs	Pre-selected cables	Project rated power (overplanting)
Rated voltage	Electrical losses	Cabling costs, reactive power compensation costs	Pre-selected cables, Voltages allowed in the DCO	—
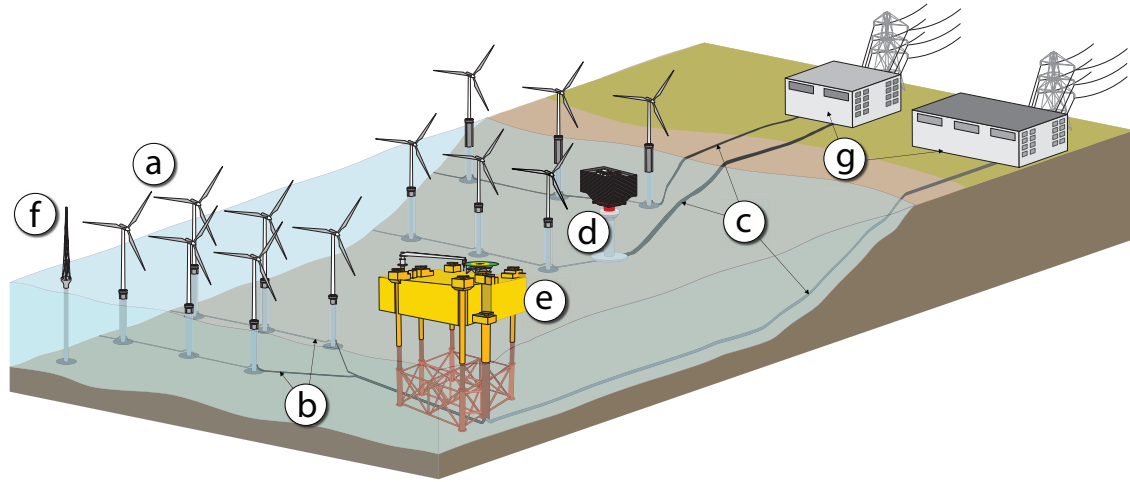
Figure 5.6: Main components of an OWF: a - Wind turbines; b - Collection cables; c - Export cables; d - Transformer station; e - Converter station; f - Meteorological mast; g - Onshore stations.
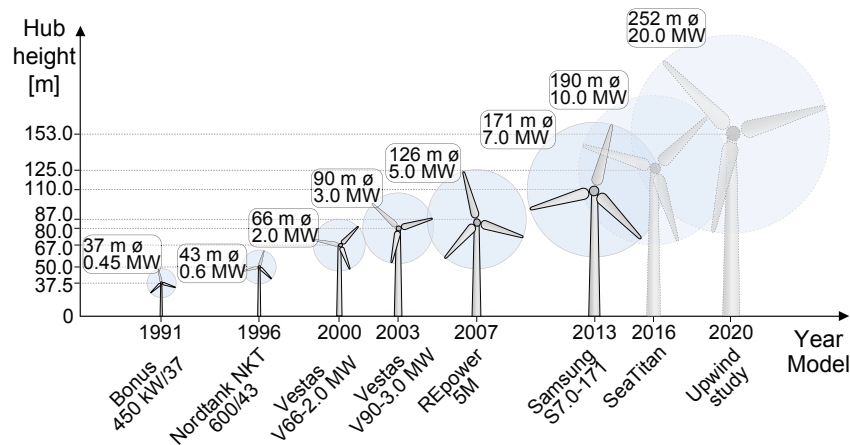
Figure 5.7: Hub height, rated power and rotor diameter of several wind turbine models and their commission year [10, 11].

turbines are equipped with fully-rated voltage source converters (VSCs) in a back-to-back configuration. These converters allow for enhanced controllability which helps to meet the challenging grid code requirements and the reduction in mechanical loads achieved with variable-speed operation [56].

Regarding the support structures, Figure 5.8c shows that the monopiles have the highest market share, although different grounded support designs, e.g. tripods, gravity based and jackets, have been tested. Figure 5.9 shows the most common support structures and two innovative designs: the suction bucket and the twisted jacket [57, 58]. Nonetheless, monopiles are expected

(a) Turbine rated power

(b) Turbine electrical configuration

(c) Turbine support structure

(d) Transmission technology

Figure 5.8: Statistics for commissioned and under construction European OWFs [10, 11, 54].

to maintain their market share for the coming years since efforts are being done to enhance the design of monopiles to be able to support 6-8 MW turbines in water depths up to 40 m [59].

In the far future, floating support structures are expected to obtain a fair share of the offshore wind market due to their use in deep waters [60]. Figure 5.9 shows several floating solutions which have been tested in the last years. However, much has to be done before floating solutions become economically more viable than monopiles [60].

Design variables, constraints and influences

The number, model and location of the turbines have to be simultaneously optimized to guarantee that enhanced layouts are obtained. The locations of the wind turbines have a strong impact on the overall efficiency of the wind farm. The turbines energy production is directly related to the turbines power curve and to the wind resource 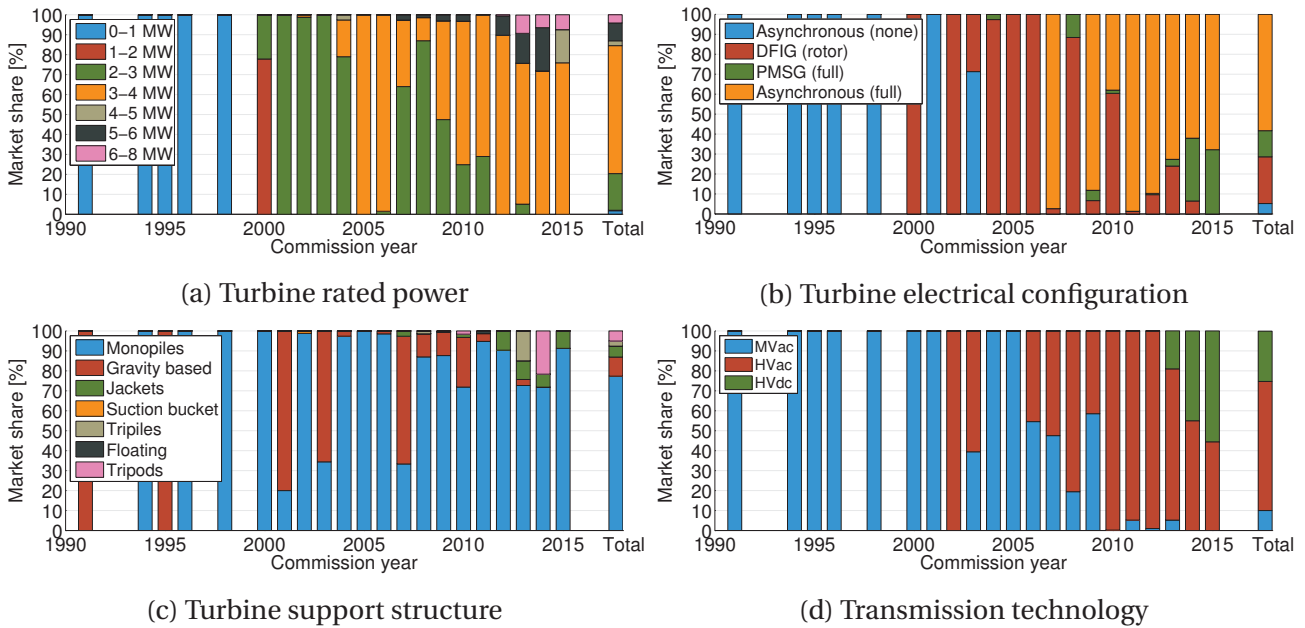specific from the wind farm area. Installing wind turbines close to each other causes interferences such as shadowing effects, which lead to reduced power production and, therefore, lower wind farm efficiencies. For example, the Danish Horns Rev OWF produces 11% less due to wake effects [65].

Different turbine models have distinct market prices, hence, it is important to evaluate the influence of the number and model of turbines in the CAPEX. Also the support structures have to be assessed since the turbine model and water depth and soil properties play a major role. Support structure costs are typically dominated by the steel price and the influence of the water depth and ground conditions on the structure design [13]. Therefore, costly support structures may be prevented if deep locations of the wind farm area are avoided. The proposed optimization framework needs to address the dependency of the support structure cost with the water depth.
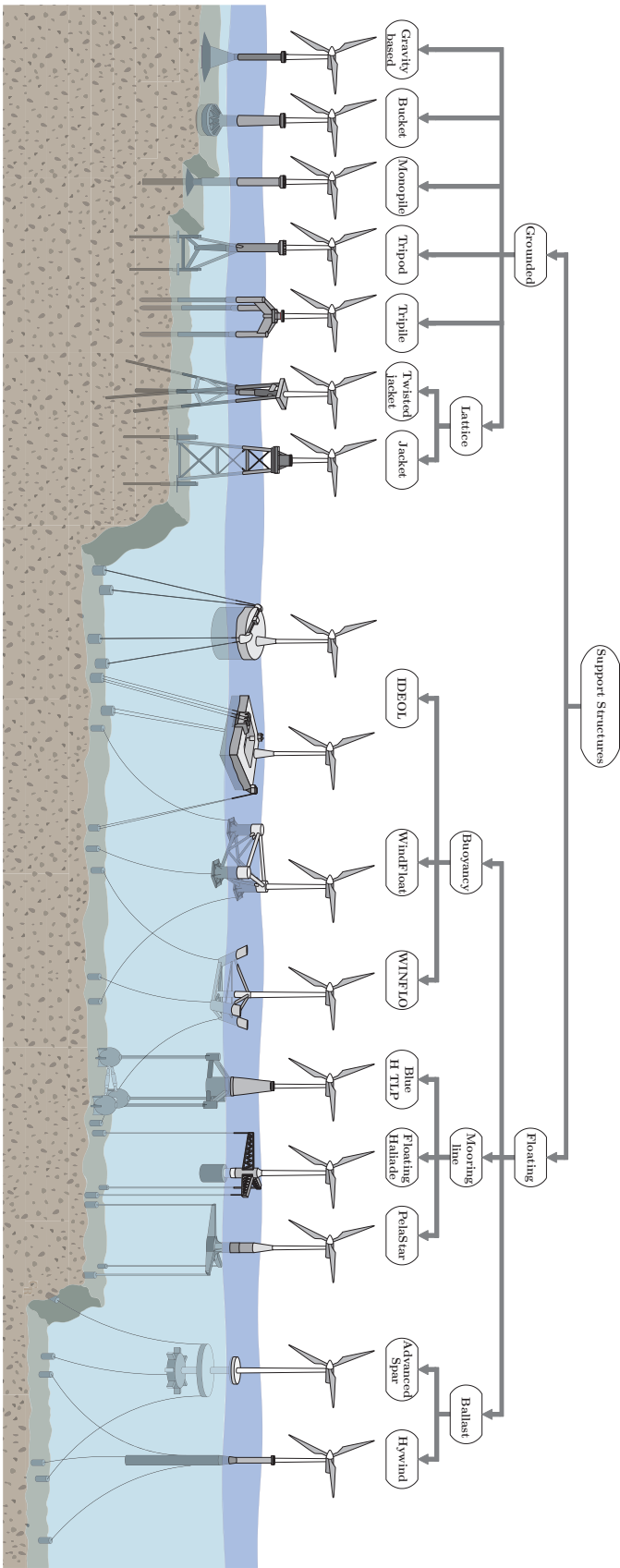
Figure 5.9: Most common grounded turbine support structures and several existing floating solutions [61–64].

5.4.2 Offshore substations

Since 2002 most of the OWFs make use of offshore substations to increase the voltage levels of the transmission system (see Figure 5.8d). Currently, there are two types of offshore substations: transformer substations, that simply increase the ac voltage to suitable transmission levels; and converter substations which perform ac to dc conversion (and viceversa).

Design variables, constraints and influences

The number and location of substations are important design aspects as they directly impact the total length of the collection system [66]. The number of substations has also a strong impact in the project CAPEX, as well as type of substation. Converter substations are much more expensive due to their larger size and weight, but also due to the extra components required to rectify ac into dc. Furthermore, the type of substation also defines the transmission technology, which plays an important role in the overall system cost and electrical losses [67].

Figure 5.10a shows that one external substation was commonly used in OWFs with a low number of turbines. When more turbines were installed, the substation started to be inside the wind farm to minimize the collection system length. Nowadays, large OWFs usually make use of two offshore substations as shown in Figure 5.3b [10, 11]. In this way, the optimization framework has to be able to place offshore substations both inside and outside the wind turbines as well as handle multiple offshore substations.

5.4.3 Collection cables

The collection cables interconnect different wind turbines and transport the energy generated to an offshore substation or to shore if no substation is present. More precisely, the collection cables connect the switchgear inside the turbines to the switchgears of the substation [19, 68].

(a) Number and location of offshore substations   (b) Number of different collection cables
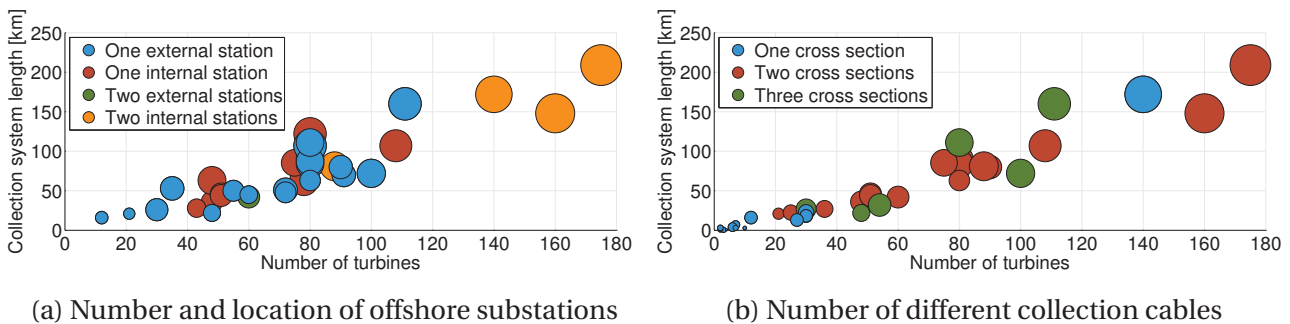
Figure 5.10: Statistics for commissioned and under construction European OWFs [10, 11, 54]. Circle size represents the installed capacity of the wind farms.

Design variables, constraints and influences

The main design variables of the collection cables are the rated voltage and their cross section which is related to their rated power. So far, 33 kV is the highest and most common voltage level in wind farm collection systems [10]. If a 66 kV collection system was used, the transmittable power would double but the costs would increase by 12% [69]. Therefore, the voltage level of the collection system has to be assessed to assure that optimized layouts are obtained.

The cable layout design is performed during FEED studies and several topologies may be used, e.g. radial, looped or branched arrays [15, 70–73]. The design of the collection system plays an important role in the electrical losses. For example, the use of branching may lead to shorter collection systems (Figure 5.3b shows an example of a branched collection system) and, hence, lower installation costs [74].

The usage of cables with different cross sections is another strategy to reduce the investment costs related to the cabling system. Figure 5.10b shows that, hitherto, the offshore industry has opted to use array cables with different cross sections only if the total array cable length was above 25 km (an exception is the British Greater Gabbard wind farm) [52]. This strategy allows for costs reduction because cables that carry the power of only a few turbines have lower cross sections and, therefore, need less raw material [75].

5.4.4 Transmission cables

Initial OWFs exported their energy production via medium-voltage ac (MVac) transmission systems since the transmission losses were low due to their low installed capacities (up to 100 MW) and close proximity to shore (shorter than 15 km) [22]. In 2002, the Danish Horns Rev 1 became the first project to make use of an offshore transformer station [10]. Thus far, the industry has used the high-voltage dc (HVdc) technology when distances higher than 50 km and installed capacities above 100 MW were considered [22].

Although HVac technology is used to transport 65% of the energy generated offshore and the HVdc technology accounts for 25% of the total installed capacity (see Figure 5.8d), currently it is still unclear if one technology will obtain a large share of the market or if several technologies will be used [22]. Therefore, it is desirable to obtain an optimization framework that includes for the different transmission technologies.

Design variables, constraints and influences

The type of cable has a direct impact in the overall system cost, as well as, in the transmission losses. Furthermore, also the cross section of the cables is directly linked with their power transfer capability. Finally, the rated voltage of the transmission system also relates with the power losses and with the allowed transmission distances [76]. This is of high importance when HVac systems are considered due to the large reactive power compensation needs [76–78].

5.5 Case Study

The key variables during the design of an OWF, the optimization goals and the need for MO optimization were introduced in the previous sections. Now, the proposed framework is applied to a case study to demonstrate the advantages and the design capabilities given to the designers.

5.5.1 Borssele Wind Farm

In 2013, the Netherlands defined an Energy Agreement which set as target to increase its renewable energy production by 14% until 2020 [79]. To achieve this target the government has allocated up to € 18 billion to subsidize the offshore wind industry. The Energy Agreement identified the need for an additional offshore capacity of 3.5 GW by 2023. For this purpose, 700 MW licences and respective subsidies will be tendered annually between 2015–2019 [80]. Furthermore, similarly to the Danish approach, governmental agencies will perform the initial site studies and surveys [81].

Several areas, shown in Figure 5.11, have been identified for the development of OWFs. The areas Borssele, IJmuiden Ver, Hollandse kust and Ten Noorden van de Waddeneilanden cover approximately 2900 km^2 (representing 5% of the Dutch EZZ [82]) and have a potential offshore wind capacity of 17.4 GW (assuming an average of 6 MW/km^2) [83].

The first two zones of the Borssele wind farm area are considered for the case study. The Dutch Borssele wind farm zone is situated 0.5 km away from the Belgian exclusive economic zone [84] and has a total area of 344 km^2 which is divided into four sites with a maximum installed power of 350 MW each (see Figure 5.12a) [84].

Two 700 MW platforms will be built in the Borssele area [80]. Each platform will connect two sites to the onshore grid via 220 kV ac cables [84, 85]. The developers have a maximum bid value of 0.124 €/kWh for areas I and II [84]. The collection system is planned to have a 66 kV rated voltage [84, 86].

The wind farm area, mean water depth and existing pipelines or telecom cables are shown in Figure 5.12a. The water depth ranges between approximately 16-38 m [84]. The presence of unexploded ordnances (UXOs), which are likely to be present at the site, are neglected since they will be removed if necessary by governmental agencies without additional costs to the wind farm developers [88, 89].

Although, most of the existing OWFs make use of a standard grid layout [10, 11], this is not the case for the Borssele wind farm area in which there are no restrictions regarding the placing of the turbines [90, 91].

The wind resource data (shown in Figure 5.12b) was measured at four different locations [92]. The measurement points are located between 15 and 82 km of the OWF and the measurement height varied between 21 and 315 m above sea level [92]. The measurement campaigns were carried between 5.5 months to 12 years [92]. The long-term mean wind speed at a hub height of
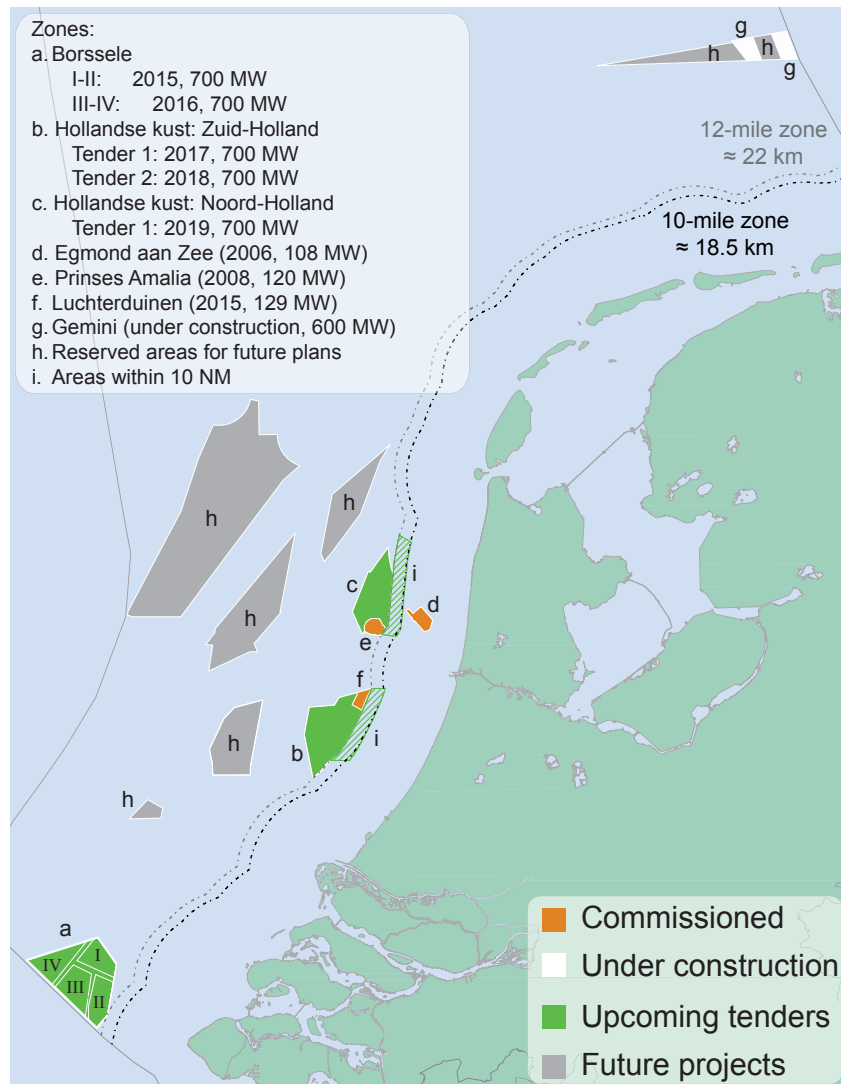
Figure 5.11: Dutch commissioned, under construction, planned and future OWF areas [82, 83].

100 m above sea level at the center of the Borssele zone is 9.6 m/s [92]. The wind speeds were extrapolated to the turbine hub heights to account for its vertical profile [93]. The mean wind speed at hub height of the Vestas turbine (107 m) is 9.67 m/s, whereas for the Darwind turbine (hub height of 92.5 m) a value of 9.52 m/s is obtained (the turbine are introduced next). Lastly, it was considered that the wind turbines could operate during 80% of the time for wind speeds higher than 18 m/s, i.e. during 80% of that time the wind speeds were lower than 25 m/s and, in this way, the turbines could operate. For wind speeds higher than 25 m/s the turbines have to be shut down for safety reasons (see Figure 5.13).

Lastly, the point of common coupling (PCC), situated in Borssele, is approximately 50 km away from the area [94] and the length of the export cables is considered to be 15% longer than the distance to shore to account for any necessary rerouting (see Figure 5.3b).

(a) Wind farm water depth [85].

(b) Annual wind rose at height of 90 m [87].
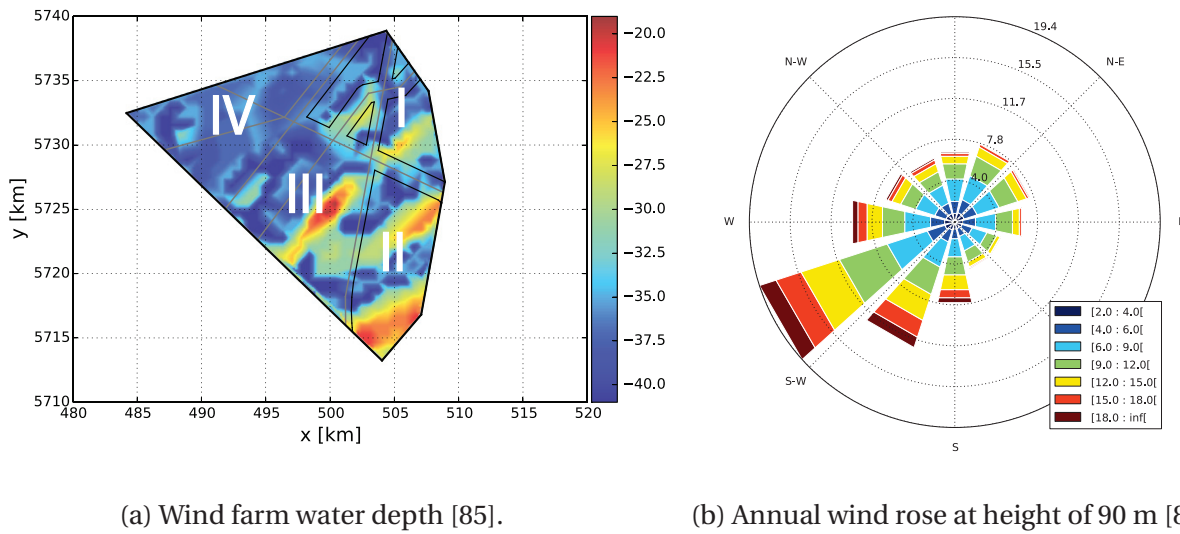
Figure 5.12: Description of the Borssele wind farm area, existing pipeline and telecom cables and water depth [85]. The color bar of the left figure represents the water depth in meters and the legend of the right figure presents the wind bins in m/s.

(a) Power curves
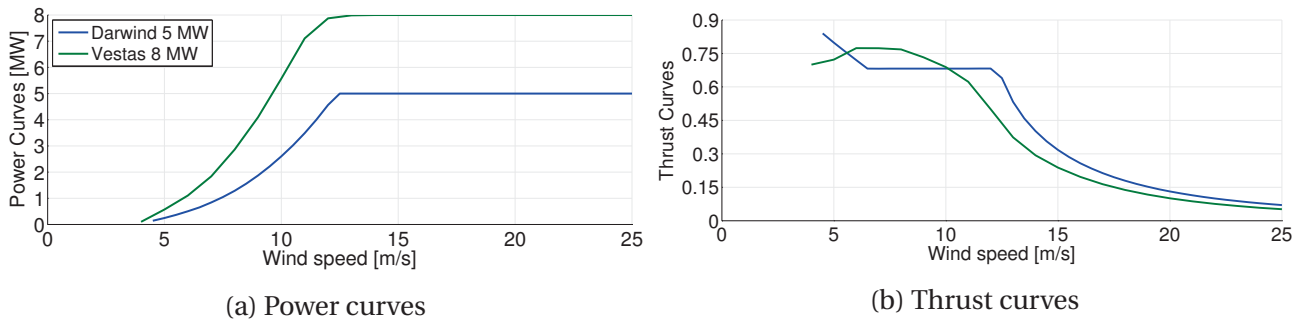
(b) Thrust curves

Figure 5.13: Power and thrust curves of the turbines used in the case study.

5.5.2   Component data

Turbines

The turbines considered in the case study are the Vestas 8 MW with a rotor diameter (RD) of 164 m and hub height of 107 m [95] and the Darwind 5 MW with a 115 m rotor diameter and a hub height of 92.5 m [96]. Figure 5.13 presents the power and thrust curves of both turbines. Since these curves represent the power delivered at the output of the turbine, it is not necessary to calculate the power losses in the turbine electrical system [25]. Both turbines makes use of full-rated power converters connected in back-to-back. A minimum separation between two wind turbines has to be respected [18]. In this case study a minimum distance of 4 RD was used [85].

Cables

All cables are modeled with a π-model which takes into consideration the type of soil surrounding the cables and the geometric dimensions of the cable according to the IEC standards 60228 and 60287 [97, 98]. For a thorough description of the cable model the reader is referred to [77, 99]. Table 5.5 presents the properties of the all the cables used in the case study. The 33 kV cables (240 or 500 mm^2 of cross section) are able to carry 5 or 8 Darwind turbines; and 3 or 5 Vestas turbines, respectively. Regarding the 66 kV cables, they can carry the power of 11 or 16 Darwind turbines; and 6 or 10 Vestas turbines, respectively.

Multi-level Modular Converters (MMCs)

A MMC steady-state model recently introduced in the literature is used in this work [77, 101, 102]. The model captures the conduction and switching losses of the semiconductors, the conduction losses of the arm reactors, the cooling system losses and the influence of the temperature of operation. The MMC is based on Infineon IGBTs and its properties are shown in Table 5.6 [103]. The MMC is considered to balance the voltage of the capacitors of the submodules through the reduced switching control strategy which lowers the switching losses and allows the efficiency of the MMC to be close to 99.5% [102].

Transformers

The transformers are modeled with a T-model which considers the core and ohmic losses (see Figure 5.14) [77, 99]. The transformer parameters (shown in Figure 5.14) are based on the three-phase transformer of the SimPowerSystems toolbox of MATLAB Simulink [77].
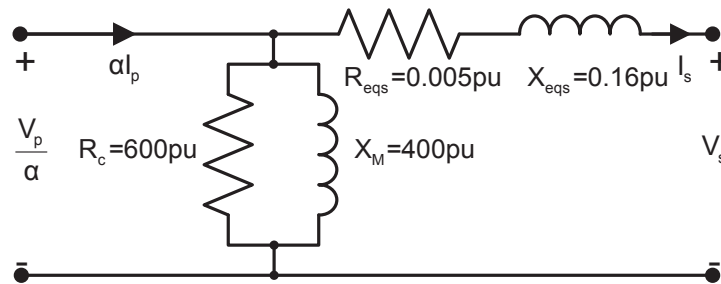
Figure 5.14: Transformer model [77, 99].

Table 5.5: Parameters of the cables used in the case study [97, 98, 100].

	MVac				HVac						HVdc							
Rated Voltage [kV]	33		66		132			220			±150				±320			
Cross section [mm²]	240	500	240	630	500	800	1000	500	800	1000	240	630	1200	2000	240	630	1200	2000
Rated Power [MVA or MW]	27.7	40	54.9	81.7	150	178	189	250	295	330	209	374	537	722	446	797	1147	1540
Current Rating (Copper) [A]	485	700	480	715	655	775	825	655	775	866	697	1246	1791	2406	697	1246	1791	2406
Resistance @20°C [mΩ/km]	80.4	44.7	85	41.4	51.3	37.4	34	39.1	24.6	21	75.4	28.3	15.1	9	75.4	27.3	15.1	9
Capacitance per phase [nF/km]	280	300	220	320	140	170	190	140	170	190	—	—	—	—	—	—	—	—
Inductance per phase [mH/km]	0.34	0.31	0.38	0.33	0.43	0.4	0.38	0.43	0.4	0.39	—	—	—	—	—	—	—	—
Cost [k€/km]	243	373	283	437	598	782	886	771	1009	1301	502	664	824	1005	502	677	1019	1405

Table 5.6: MMC parameters [76, 77, 101].

Parameter	Value
Rated power	>500 MVA
Rated dc voltage	±150 kV or ±320 kV
Rated ac voltage	380 kV
System frequency	50 Hz
Carrier frequency	100 Hz
Number of arm SMs	58
Arm resistance	$0.07\,\Omega$
Reactance phase reactor	0.1 pu
Resistance phase reactor	0.01 pu

5.5.3 Optimization goals

AED

Energy production

The energy generated is calculated based on the turbines power curves. The availability of the turbines is considered to be 97% which is envisioned to be obtained between 2015-2035 [104].

Wake losses

The Jensen model was used to calculate the wake interaction between turbines. The Jensen model, one of the most common models used, is a simplified and fast manner of calculating the wind speed inside the wake of a turbine [25]. More precisely it was used a later version of the model, which was developed by Katic *et al* [105]. All the MO approaches presented in Table 5.1 used the Katic-Jensen model (except [29, 30] which used the original Jensen model). For a description of the wake model the reader is referred to [105–107].

Collection system design

Finding the optimal branched infield cable topology for OWFs corresponds to the capacitated minimum spanning tree problem [108]. A savings heuristic approach is used since the optimization framework requires fast models. It is a hybrid between the heuristics Planar Open Savings [72] and Esau and Williams [109]. Furthermore, the possibility to use multiple cable capacities, the minimization of pipeline/cable crossings and the option to select the maximum number of cables branches per turbine are also included [75].

It is assumed that the collection system connects every turbine to one substation through one distinct cable. The inter-array cables cannot cross each other or the transmission lines of their substation. The maximum number of cable connections per turbine is considered to be four

due to space limitations inside the turbine tower [68, 86]. Finally, the crossings with existing pipelines and telecom cables should be minimized [66, 110]. For a more detailed explanation of the heuristic the reader is referred to [75].

Electric infrastructures

Three different transmission technologies (TT) are considered in this work: MVac, HVac and HVdc (see Figure 5.15). The MVac interconnects directly the turbines to the PCC, whereas the other two options make use of offshore substations.

Recent studies investigated the advantages of using an overplanting strategy. Such design strategy breaks the common rule used up to now of using a transmission system with the same power capacity of the wind farm. The main idea is to harvest energy from more turbines for low wind speeds and apply curtailment strategies when the wind speed is too high [111]. This idea is implemented in the HVdc scenario by setting the MMC rated power as the sum of the turbines rated power that are interconnected to it. Since the number of cables per MMC is fixed, it is assumed that if the chosen cables have not enough energy transport capacity, the algorithm upgrades them to have larger cross sections. If the cable with the highest cross section available is not able to carry all the power, the MMC caps the power that flows through it to its rated power and the rest is curtailed.

For the case of HVac technology if there is at least one power flow in which the chosen cable is not able to transport all the power, the number of cables of that substation is increased by one and the power flows are run once again. Lastly, the number of turbines that could be connected to each MVac cable is calculated assuming the turbines to operate with a power factor of 0.95 to allow for some reactive power transport [86].
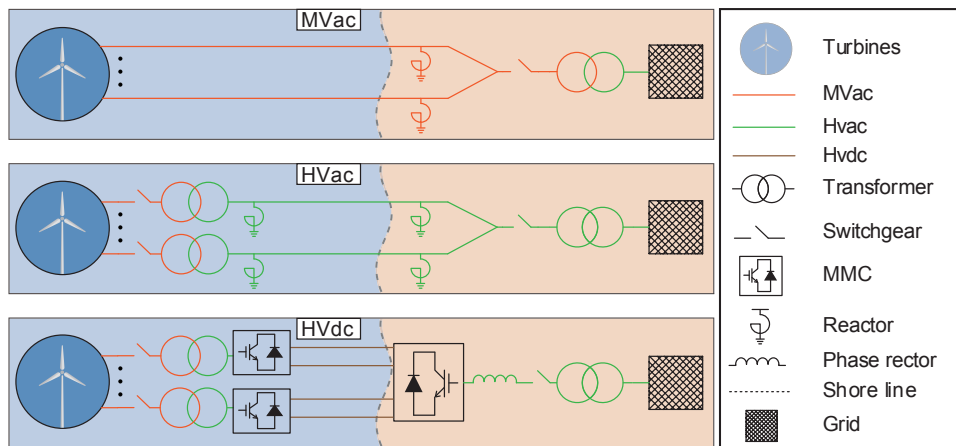

Figure 5.15: Electrical infrastructures considered in the optimization framework.

Power flows

The power flows from the turbines to the PCC are calculated using an optimal power flow solver library developed in the Python programming language called PyPower [112]. There are three possible types of nodes in a network: PQ, PV and slack nodes. A node PQ is a node in which the active and reactive power are known and the state variables are defined as the load angle (δ) and voltage. On a PV node the active power and voltage level are known but the reactive power and δ are unknown [76]. Finally, on slack nodes a reference angle and the voltage are set but the active and reactive powers are not determined before solving the load flow. Table 5.7 shows a comparison between the different types of network nodes.

The turbines are considered to be nodes of type PQ, i.e. the active power is set to the values obtained with the wake losses model and it is considered that the turbines are not producing any reactive power. In this way, the power flow equations determine the voltage and angle at the turbine nodes. Alternatively, the turbines could be set as PV nodes to help in the reactive power support. However, this is wind farm power control and it is out of the scope of this work.

The ac side of the MMCs and the onshore network nodes are defined as slack buses, i.e. the voltage is equal to 1 pu and the angle δ is set to zero degrees. The transformer nodes are considered to be of type PQ and with no net injection of active or reactive power flowing into their nodes. The sizing of the transformers is initially done by summing the turbines rated power which are connected to it. After running the power flows if the rated power of the transformers is surpassed, these become the new values and the power flow scenarios are repeated.

The reactors nodes (see Figure 5.15) are considered to be of type PV (see Table 5.7). It is considered that no active power flows to the reactors and that the voltage is equal to 1 pu. In this way, the reactors provide total reactive power compensation. The reactor sizing is based on the scenario in which no active power is produced at the turbines, since it represents the most demanding case for the reactive power compensation units [76].

CAPEX

The cost models used in this case study are based on several literature works [49, 74, 86, 113–116] and it is not the scope of this work to further develop or validate them. The cost values used are updated considering an annual Eurozone inflation of 1.85% [12].

Table 5.7: Comparison between the network node types [76].

Node type	Known variables	Unknown variables
PQ	Active power and Reactive power	Voltage and δ
PV	Active power and Voltage	Reactive power and δ
Slack node	Voltage and δ	Active power and Reactive power

Turbines

The prices for the turbines are obtained using the data in [74]. The cost of the Darwind turbine is €4.85 million and the Vestas 8 MW costs €6.39 million, including 10% extra for the transport and installation. If the 66 kV collection system is used, the cost of the turbines increases by 20% due to the extra costs of the turbine transformers and switchgears [86]. The cost to decommission the turbines is €1.05 million for the Darwind turbine and €1.68 million for the Vestas 8 MW [117].

Support structures

The cost of the monopile support structures and their transport and installation is given by [74]:

$$\text{C}_{ss} = 0.54 \cdot \text{P}_{\text{rated}}^{turb} \left(1 + 0.02\left(w_d - 8\right)\right) \left(1 + 0.8 \cdot 10^{-6}\left(h\left(\frac{RD}{2}\right)^2 - 10^5\right)\right) \tag{5.1}$$

where C_{ss} is the support structure cost [€ million], w_d is the water depth [m], h is the turbine hub height [m], RD is the rotor diameter [m] and $\text{P}_{\text{rated}}^{turb}$ is the turbine rated power [MW].

Cables

The cost values of the 33 kV collection cables are obtained from [74] and are shown in Table 5.5. The cost of the 66 kV cables is considered to be 15% more expensive than the 33 kV cables for similar cross sections [86]. The cost to install the MVac cables is considered to be 365 k€/km independently of the voltage level or the cable cross section [74, 86].

The costs of the HVac cables are based on values taken from [115] and are shown in Table 5.5. An additional cost of 720 k€/km is added to account for the installation of the cable [74]. The costs of the HVdc cables are based on [116] and are also shown in Table 5.5. Similarly to the HVac cables, the installation had an extra cost of 720 k€/km [74]. The cost to cross an existing pipeline or telecom cable is considered to be €0.1 million [75].

Switchgears

The switchgears for the 33 kV collection system cost 73.25 k€ and the 66 kV ones cost 101.25 k€ [115]. One MV switchgear is installed in each collection cable as shown in Figure 5.15. The HV switchgears cost €1.57 million for a rated voltage of 132 kV and €2.6 million for 220 kV [116].

Offshore substations

The cost of the HVac offshore substations is given by [115]:

$$\text{C}_{ss}^{HVac} = 2.8286 \text{ M€} + 0.099 P_{ss} \tag{5.2}$$

where P_{ss} is the sum of the rated power of the turbines connected to the substation [MW] and C_{ss}^{HVac} is the cost substat [€ million].

The same expression is used for the HVdc substations but with an 85% increase to account for the larger and heavier structure needed to house the extra components [118].

The cost of reserve diesel generators to run essential substation equipment is given by [74]:

$$C_{gen} = 0.0237 \text{ M€} + 0.0023 P_{ss} \tag{5.3}$$

where P_{ss} is the sum of the rated power of the turbines that connect to the substation [MW] and C_{gen} is the cost of the diesel generator [€ million].

Transformers

The transformer costs are expressed as [74]:

$$C_{trafo} = 0.0477 P_{trafo}^{0.7513} \tag{5.4}$$

where P_{trafo} is the rated power of the transformer [MVA] and C_{trafo} is the cost [€ million]. The minimum transformer rated capacity is considered to be 50 MW.

MMCs

The cost of the MMCs is given by the following expression [116]:

$$C_{MMC} = 61.3777 \text{ M€} + 0.0657 P_{MMC} \tag{5.5}$$

where P_{MMC} is the rated power of the MMC [MVA] and C_{MMC} is the cost of the MMC [€ million]. The minimum MMC rated capacity is 500 MVA.

Reactive power compensation

The 33 kV reactors are considered to have an efficiency of 98% [119] and cost 66% of what a transformer of the same rating would cost [115]. A 40% extra cost is added to the 66 kV reactors due to their higher volume and weight [86].

SCADA, Project development, Insurance

The SCADA system is considered to cost 0.75 M€/turbine [74], whereas the project development is estimated as 0.468 M€/MW [74]. The insurance and contingencies during the project phase are considered to be € 0.7 million per Darwind turbine and € 1.12 million for the Vestas turbines [117].

OPEX

The OPEX is an important component of OWFs and, hence, should be considered during the optimization phase. Inasmuch to use a more comprehensive OPEX calculation model, such as the OPEX Cost Estimator from ECN [120], a considerable amount of data is required, e.g. available vessels, crew members and detailed weather information.

Simpler approaches can be used to avoid this drawback. The OPEX may be considered as a percentage of the investment costs [44, 45] or monetized through a cost value per MWh produced by the farm [49, 121, 122]. Because the value of the OPEX is directly proportional to either the AED or the CAPEX, it is not included in the optimization process and is only calculated afterwards. In this way, the problem becomes bi-objective with the AED and CAPEX as optimization goals.

5.5.4 Multi-objective Gene-pool Optimal Mixing Evolutionary Algorithm

The Multi-objective Gene-pool Optimal Mixing Evolutionary Algorithm (MOGOMEA) was used in this work. The MOGOMEA, recently introduced in the literature [123], is a metaheuristic discrete MO optimization algorithm which demonstrated to outperform, i.e. obtain better optimized trade-offs, other state-of-the-art well-known MO optimization algorithms on standard combinatorial benchmark functions [123], as well as in real-world applications [33, 124] for a given budget of function evaluations. Although the MOGOMEA is capable of obtaining high-quality results, it does not guarantee that the global optimal solutions are found given a finite amount of evaluations of the optimization functions [123].

Since the MOGOMEA only uses discrete variables, it is straightforward to optimize the number and locations of turbines in simultaneous. Constraints on the location of turbines, such as minimum distance to existing power cables and shipwrecks, within the OWF area are automatically respected by not considering constrained places in the possible set of locations for the turbines [47]. Furthermore, the limited precision offered by the models used, such as the wake model, do not require the accuracy of continuous variables [33]. The location of a turbine may be described by a single parameter in a discrete approach, whereas a continuous domain demands two variables. Lastly, given the same number of problem variables and the same inherent underlying problem complexity, continuous optimization problems are typically slower to solve than discrete problems because of the larger variable-domain size of continuous variables [33].

MOGOMEA starts by initializing n solutions (the definition of a solution is introduced in equation 5.6) which are evaluated to obtain their objective values. The algorithm then alters solutions into offspring by exchanging variables between different solutions. The MOGOMEA clusters solutions that are in the same objective space vicinity and only performs variation within each cluster since solutions tend to be very dissimilar for different areas of the objective space [123].

The general variant of the algorithm uses the mutual information as measure to build a hierarchical linkage model to identify group of variables that are important to be copied together under black-box optimization, i.e. nothing is known about the optimization problems [125, 126].

However, it is known that turbines influence the energy production of neighboring turbines and that this influence might be considered negligible for turbines situated far enough apart [127, 128]. For this reason, in this work the distance between the possible locations is used as a measure of dependency instead of the standard statistical analysis used in MOGOMEA [33].

The population size used by the algorithm is an important internal parameter that should be adjusted according to the instance of the WFLOP being solved [128, 129]. A population-free sizing scheme of MOGOMEA is used, avoiding the need for the right population size to be assessed [33]. In this way, the population size is incrementally increased throughout the optimization [33]. This is done to allow new genetic material into the population since the algorithm performs a very intensive local-search strategy and hence, it may fail to design layouts that cannot be reached from the initial solutions (only through mutation) [123].

Although the MOGOMEA was initially designed to have a population of solutions that are sequentially altered to generate offsprings [123], the version of MOGOMEA employed evaluates the solutions in an asynchronous parallel manner. Currently, it is becoming important to move towards a parallel environment in which several CPU cores may be used simultaneously [130]. This is of high importance especially because the evaluation time of a solution varies with the complexity of the OWF layout it represents. For example, the wake loss evaluation highly depends on the number of turbines [127, 128] and wind directions [107], whereas the collection system design also depends on the number of turbines of the project [72, 75].

Optimization variables

A solution is composed as follows:

$$x = \begin{bmatrix} t_1 & \cdots & t_i & V_{HVac} & C_{HVac} & V_{HVdc} & C_{HVdc} & V_{MVac} \end{bmatrix} \tag{5.6}$$

where $t_1 \ldots t_i$ determine what is placed in each available position of the wind farm area. The following representation is used: 0 - Empty, 1 - Darwind 5 MW turbine, 2 - Vestas 8 MW, 3 - Transformer substation, 4 - Converter substation. The variables V_{HVac}, V_{HVdc} and V_{MVac} determine the voltage level of the HVac, HVdc and MVac cables, respectively. The variables C_{HVac} and C_{HVdc} identify the cross section of the cables.

Random wind farm layouts

An heuristic that aims at maximizing the distance between turbines is used to create random layouts. Firstly, the number of turbines of the wind farm, m, is randomly generated between one and the number of locations of the grid. The location of the initial turbine is randomly chosen from all the possible locations. After, the distances of the remaining possible locations are computed to the first turbine and the most distant location is chosen for the second turbine. The distances of the remaining locations are updated by checking whether the distance to the new turbine is smaller than the currently stored distance (the shorter distance is kept). The

procedure is repeated m times or until a turbine violates the proximity constraint. In this way, it is guaranteed that feasible wind farm layouts are generated, similarly to previous works [131–133].

Whenever a turbine is placed in the layout, the algorithm randomly selects a turbine model from the ones considered. At the end, the turbine model used in the OWF is the one that was assigned the most since, generally speaking, OWFs are composed of only one turbine type [10, 11]. Nonetheless, the framework was designed as is so that this constraint could be removed in the future, if desired.

A random number of substations is sampled between zero and three. Next, the k-means clustering algorithm is run with that same number [134]. The closest locations of the grid to the cluster centroids are chosen to represent the substations. Thereafter, another random number is sampled for each substation to decide if it represents either a converter or a transformer substation. In case there is at least one converter station, the algorithm considers that all substations perform ac-dc conversion, i.e. the transmission system uses the HVdc technology.

Multi-resolution

The results obtained in [33] indicate that it could be beneficial to use a multi-resolution scheme in which a large grid step is employed in the first optimization iteration to allow the algorithm to find highly packed wind farms easier. Thereafter, these solutions would serve as initial population for a second optimization routine with a smaller grid step. Therefore, the algorithm starts the optimization routine with the 4 RD grid step and advances to smaller step sizes of 2 RD and 1 RD. The layouts are then mapped onto the finer grid.

Internal parameters

The initial population size, n, is set to 32 since it corresponds to the number of CPU threads available. The algorithm groups the wind farm layouts into five clusters during the optimization process since this setting has proved to already provide improved results over using a single cluster in recent literature [123].

5.6 Results

The case study was performed with Python 2.7 on a server with 16 cores (Xeon ES-2690@2.9 GHz) running the 64-bit version of Ubuntu 12.04. The optimization framework was given 30 days to run. The largest grid step (4 RD) size was run for 6 days, whereas 12 days were given to each of the two remaining more refined grid steps (2 RD and 1 RD).

5.6.1 Optimized trade-off

Figure 5.16 shows the optimized trade-off obtained with the MO optimization algorithm (and for the two layouts designed by hand, which are introduced next) between the AED and CAPEX.

The trade-off, composed of 358 different OWF layouts, shows that three different transmission technologies were used. For small wind farms the 66 kV interconnection to shore was the best option. On the other hand, for AEDs higher than 4000 GWh/year, the HVdc transmission technology was used. In the right-hand extreme part of the trade-off curve the HVac technology was used. However, it came with much higher investment costs and did not increase the AED significantly.

Although the optimized trade-off shows a linear relationship between the goals up to an AED of approximately 7000 GWh/year, it is important to note that nothing guarantees that the layouts that are in a close vicinity in the objective space, are also similar in variable space, i.e. the layouts and technologies may vary considerably.

The framework could also use the Darwind 5 MW turbine; however, no layout of the trade-off used it. The results for the standard layouts also corroborate this result: although the wind farm layout composed of Vestas 8 MW turbines is situated in the trade-off, the OWF with Darwind 5 MW turbines performs worse than the other layouts. The Darwind 5 MW wind turbines produced less energy and, even though they are cheaper, this difference did not suffice for profitability.

The data gathered for this specific case study hinted that the Vestas turbine was the best one. However, this result is specific to this case study and should not be generalized since turbines with lower rated powers could be the best option under different circumstances. For example, the support structure costs, insurance costs, among others, do weight in the decision making. Although, one turbine demonstrated to be clearly superior for this case, for other scenarios, e.g. different wind farm area or distance to shore, the outcome could differ.

A more difficult situation would be when one could not have a direct hint from the specifications of the wind turbines. Under such scenario, the advantages of the proposed optimization framework would clearly stand out. Furthermore, the optimization framework is also able to select from more than two wind turbine types, which is a very difficult selection process to be manually performed.
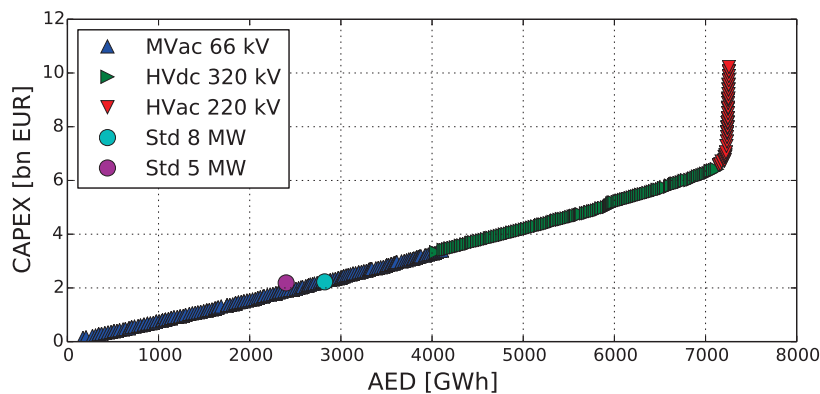

Figure 5.16: Optimized trade-off obtained between the optimization goals for areas I and II and standard layouts. The optimized layouts will be numbered from left to right.

5.6.2 Wind farm layouts designed with standard approaches

Two OWF layouts were hand-designed by taking into consideration the guidelines given to these areas [135]. In this way, 350 MW (352 MW for the 8 MW turbines) were placed in each wind farm area and all the turbines were interconnected to one 220-kV HVac offshore substation placed in the exact location where it will be built [84]. It is important to note that some optimization was used during the design of these layouts. The wind turbines were placed in the grid that maximized the distance between them. Furthermore, as shown in Figure 5.17, the turbines have a larger distance between them in the main wind direction (see Figure 5.12b). Finally, the collection systems were designed with the heuristic algorithm presented in [75].

The grid step sizes used in the standard layouts are different from the ones that the optimization framework had access to. This difference may explain why no layouts that export the power to shore via HVac technology were found in the vicinity of the trade-off shown in Figure 5.16. Nonetheless, the layout with 8 MW wind turbines did not dominate (was not superior in any way) the layouts of the optimized trade-off.

5.6.3 Economic functions

Figure 5.18 shows how the layouts of the optimized trade-off perform according to the economic functions presented in Table 5.3. Table 5.8 presents the economic values and general characteristics of the layouts (shown in Figure 5.19) that demonstrated to be the best according to the different economic functions. The results were obtained with the following assumptions:

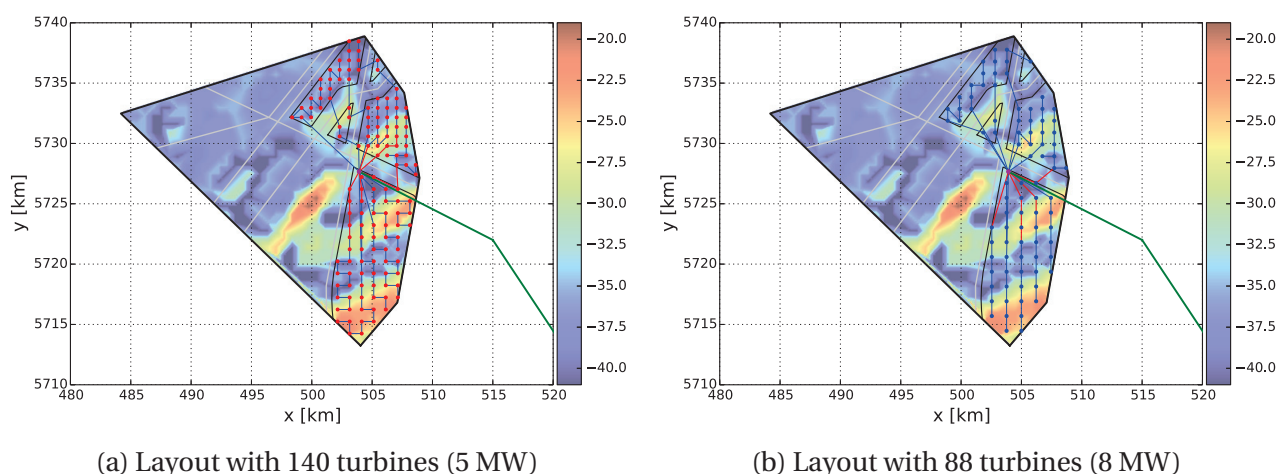(a) Layout with 140 turbines (5 MW)　　　　(b) Layout with 88 turbines (8 MW)

Figure 5.17: Layouts obtained with standard design philosophies and restricted to the design specifications [135]. Red and blue circles represent the 5 MW and 8 MW turbines, respectively. Gray lines are existing pipelines and telecom cables, blue and red lines are the collection system cables and green lines are the exporting HVac cables. The purple circles represent the substations.

interest rate of 7% [70], wind farm lifetime of 20 years, annual OPEX of 2% of the respective CAPEX [44, 45, 136] and price of energy of 0.124 €/kWh, which is the highest bid for the Borssele areas I and II [84]. In Section 5.6.4 the impact of these parameters will be assessed. Although fixed annual values were used, distinct annual values could have been applied in a straightforward manner to simulate, for example, the financial incentives that the energy generated at OWFs obtain in the first years of exploration [137].

AED

Figure 5.19f shows the layout with the highest AED, whereas some of its characteristics are given in Table 5.8. The layout uses the concept of distributed substations in which several small offshore substations housing a single transformer and one reactor for compensation of the export cable are used [138]. This concept, as shown in Figure 5.19f and Table 5.8, leads to a significant reduction in the total collection system length (CSL) since this layout has 110 km less array cables than layout number 248, which has 55 turbines less. The electrical losses are reduced and the usage of array cables with high cross sections is also minimized in layout number 358. Furthermore, this concept leads to fewer crossings with existing pipelines and telecom cables. On average, there are approximately nine turbines (72 MW) connected to each substation.

The AED function is fully biased towards energy production maximization, hence, designers should be cautious when applying it in case there are no constraints over the installed power or a maximum project CAPEX. Moreover, the economic values obtained for this layout clearly demonstrated that. This layout obtained a negative NPV, a DPT of almost 28 years and a ROI value lower than one, meaning that the investment would not be able to generate profit for the wind farm developers, despite its very high AED.

Utilization factor

The layout which presented the highest UF value, shown in Figure 5.19a, was composed of only eight 8-MW turbines. Since the objective is to minimize the losses one might initially think that a layout with only one turbine would provide the best results. However, not only the wake losses are being considered but all the power losses until the PCC. In this way, the layout with eight turbines demonstrated to also make a better use of the MVac cable. The turbines were placed far apart from each other and in shallow areas. The same layout would present the best result if the efficiency of the system would have been used instead of the UF [33].

The standard layout with 5-MW turbines presented worse results than its counterpart composed of Vestas turbines in all functions but the UF. This means that despite the lower AED, the 5-MW turbines are slightly better used and it would be the best layout if the UF was the deciding factor.

LCOE

The LCOE values of the optimized layouts are shown in Figure 5.18a. Values between approximately 80 to 105 €/MWh were found for MVac and HVdc transmission technologies. On the other
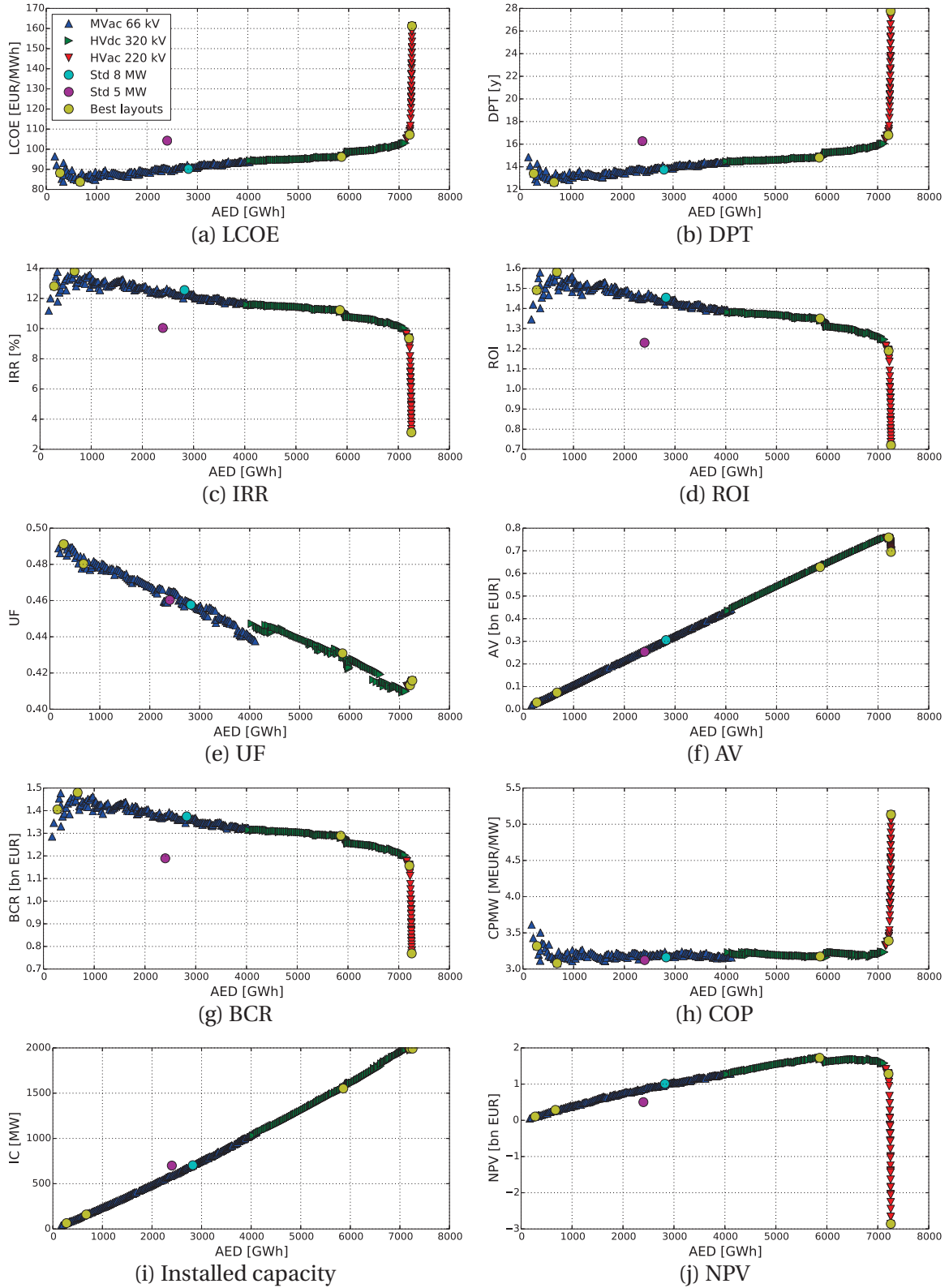
Figure 5.18: Results obtained for the different economic functions of the layouts of the optimized trade-off. The values obtained with the standard layouts are also shown.

Table 5.8: Economic values and general characteristics of the best layouts.

Layout nr.	NPV [bn €]	LCOE [€/MWh]	COP [M€/MW]	UF	IRR [%]	DPT [years]	ROI	AV [bn €]	BCR	AED [GWh/year]	CAPEX [bn €]	IC [MW]	TT	CSL [km]	NSS
3	0.10	88.22	3.32	**0.49**	12.80	13.41	1.49	0.03	1.41	275	0.21	64	MVac	76.13	0
5	0.14	83.91	3.11	0.48	13.78	12.67	1.57	0.04	**1.48**	340	0.25	80	MVac	74.53	0
18	0.28	**83.79**	**3.08**	0.48	**13.81**	**12.64**	**1.58**	0.07	1.47	673	0.49	160	MVac	182.45	0
248	**1.73**	96.18	3.17	0.43	11.23	14.81	1.35	0.63	1.29	5858	4.93	1552	HVdc	281.54	1
322	1.28	107.20	3.39	0.41	9.35	16.80	1.19	**0.76**	0.76	7210	6.76	1992	HVac	181.30	8
358	-2.86	161.21	5.13	0.42	3.12	27.77	0.72	0.69	0.77	**7256**	10.23	1992	HVac	170.65	28
Std 8 MW	1.01	90.19	3.16	0.45	12.55	13.75	1.45	0.31	1.37	2822	2.23	704	HVac	138.31	1
Std 5 MW	0.50	104.24	3.12	0.46	10.04	16.26	1.23	0.25	1.19	2399	2.19	700	HVac	163.79	1

(a) Layout number 3

(b) Layout number 5

(c) Layout number 18

(d) Layout number 248
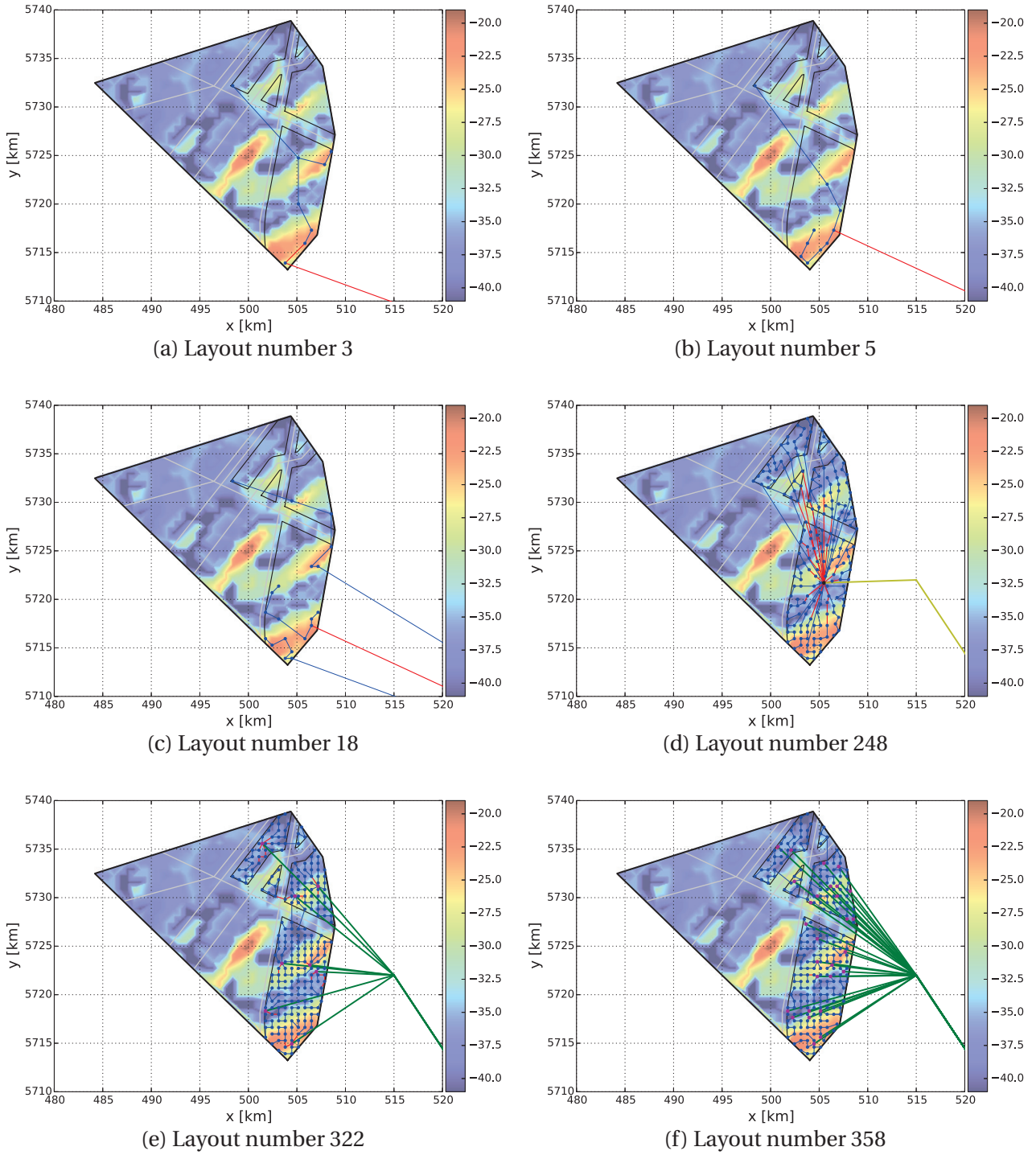
(e) Layout number 322

(f) Layout number 358

Figure 5.19: Layouts obtained with proposed optimization framework. Blue, purple and black circles represent, respectively, the 8 MW turbines, HVac and HVdc substations. Gray lines are existing pipelines and telecom cables, blue and red lines are the collection system cables and green and yellow lines are the exporting HVac and HVdc cables, respectively.

hand, the layouts based on HVac technology presented higher LCOE prices due to their higher CAPEX values.

The layout which presented the lowest LCOE (83.79 €/MWh) was composed of 20 turbines as shown in Figure 5.19c. Although the turbines were placed far apart to minimize wake losses, they were also placed in regions of shallow waters to minimize the cost of support structures. Furthermore, the turbines were also placed in the wind farm area closest to shore, minimizing the cabling system cost and the electrical losses.

IRR, ROI, COP, BCR and DPT

The same layout that had the lowest LCOE also presented the best values for the IRR, DPT, COP, BCR and ROI functions. Although these economic indicators present different values, they did not alter the ranking between layouts, i.e. if a certain layout performs best at one of these economic functions it also turns out to be the best according to the remaining ones.

AV

The AV equation is biased towards larger wind farms since it measures the annual revenue. The layout that maximized the AV equation is shown in Figure 5.19e and it is very similar to layout number 358, shown in Figure 5.19f. The only difference is that it makes use of eight offshore HVac substations to interconnect the 249 turbines to shore.

Incremental BCR

According to the incremental BCR economic analysis, the wind farm layout number 5 (see Figure 5.19b) was the preferred choice. It is composed of ten 8 MW turbines and, therefore, makes full use of the 66 kV cable with the largest cross section (see Table 5.5), thus minimizing the ratio between the AED and the investment costs.

NPV

The wind farm layout with the highest NPV value (Figure 5.19d) has one HVdc offshore substation that interconnects 194 turbines to shore.

5.6.4 The influence of economic factors

In this section, the influence of the economic factors over the wind farm layout design is investigated. To this end, different parameters, such as the interest rate, wind farm lifetime and price of energy, were altered to analyze the resulting implications. Initially, the LCOE is analyzed, followed by the NPV function.
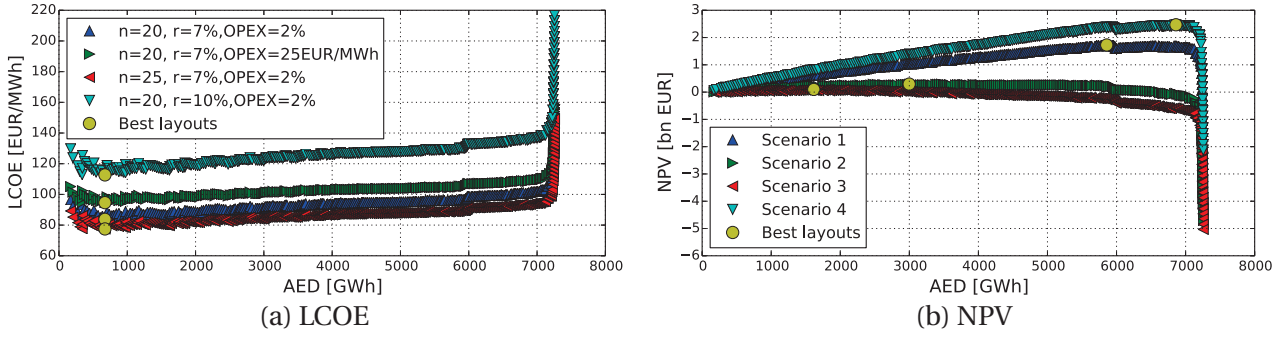
Figure 5.20: LCOE and NPV values for different economic factors.

LCOE

Assuming the OPEX to be a percentage of the investment costs [44, 45], p_{CAPEX}, the LCOE clearly becomes a ratio between the CAPEX and the AED:

$$LCOE = \frac{CAPEX}{AED} \left(\frac{1}{a} + p_{CAPEX} \right) \tag{5.7}$$

This equation shows that both an alteration to the interest rate and wind farm lifetime or a different percentage of the CAPEX for the OPEX, will affect in the same way all the wind farm layouts since it only shifts the ratio between the CAPEX and the AED.

Another possibility, in the absence of a more refined OPEX model, is to monetize the OPEX through a cost value per MWh, c, delivered by the OWF [49, 121]:

$$LCOE = \frac{1}{AED} \left(\frac{CAPEX}{a} + c \cdot AED \right) = \frac{CAPEX}{a \cdot AED} + c \tag{5.8}$$

Once again, all the layouts will be affected in the same way if the value c is changed. This means that, if the OPEX is somewhat directly dependent on either the CAPEX or the AED, the LCOE function is insensitive to the variation of its economic factors. Figure 5.20a shows that the order of the layouts of the optimized trade-off remained unaltered, hence, the wind layout number 18 remained the one with the lowest LCOE value.

NPV

Differently from the LCOE function, the variation of the economic parameters will influence the cash flows of the NPV equation even if the OPEX is proportional to one of the other goals (see Figure 5.20b). In this way, the economic parameters play an important role as weighting factors in the outcome of the NPV function. Table 5.9 presents the characteristics of the four layouts (shown in Figure 5.21) with the highest NPV value for different economic parameters. Figure 5.20b shows

(a) Layout number 57

(b) Layout number 115

(c) Layout number 248
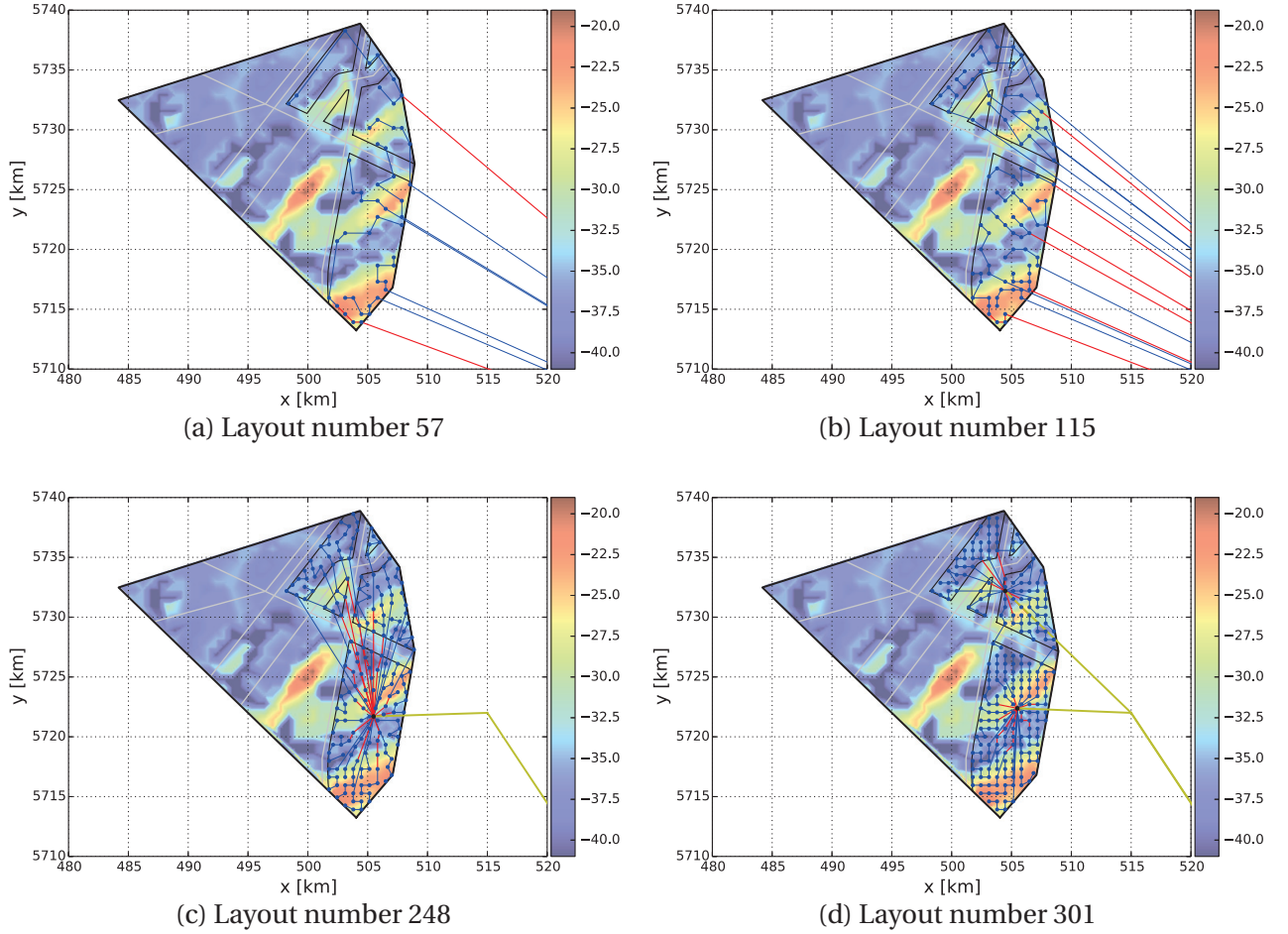
(d) Layout number 301

Figure 5.21: Layouts with the best NPV values for different economic factors. Blue, purple and black circles represent, respectively, the 8 MW turbines, HVac and HVdc substations. Gray lines are existing pipelines and telecom cables, blue and red lines are the collection system cables and yellow lines are the exporting HVdc cables.

that OWFs with higher installed capacities (IC) correspond to higher revenues, either through a higher price of energy or via a longer exploration of the site.

If the designers used an energy price of 0.1 €/kWh, which is the target for energy generated offshore by 2020 (see Section 5.1), a layout with an IC of 752 MW presents the highest NPV (see Figure 5.21b). This is the only layout of the optimized trade-off curve that has a similar capacity to the 700-MW guideline which demonstrated to be advantageous at some point.

If the lifetime operation of the OWF is considered to be 25 years [139, 140], it is more beneficial, according to the NPV function, to install more turbines to increase the AED and take advantage of the extra time of operation (Figure 5.21d).

Table 5.9: Influence of the economic factors on the NPV function.

Scenario nr.	Lifetime [years]	Interest rate [%]	Energy price [€/kWh]	NPV [bn €]	Layout nr.	AED [GWh/year]	CAPEX [bn €]	IC [MW]	TT	CSL [km]	NSS
1	20	7	0.124	1.726	**248**	5858	4.93	1552	HVdc	281.54	1
2	20	7	**0.1**	0.29	**115**	2998	2.38	752	MVac	821.98	0
3	20	**12**	0.124	0.097	**57**	1617	1.22	392	MVac	418.91	0
4	**25**	7	0.124	2.468	**301**	6860	6.04	1904	HVdc	230.63	2

5.6.5 Discussion

The optimized trade-off curve was obtained in 30 days with the proposed framework, which is relatively fast if compared to the design phase of a state-of-the-art OWF which takes several months [141]. The optimization strategy also demonstrates that designers would have missed other wind farm designs that could lead to similar AED and CAPEX values. For example, Figure 5.22 shows a layout with 88 Vestas 8 MW turbines connected to shore via 66-kV cables, which has similar values for the AED and CAPEX as the standard layout of Figure 5.17b. If, for example, there would be a risk associated with building structures offshore (e.g. substations, or reliability values for the different components of the system), the layout obtained with the algorithm would be preferable to the standard HVac-based one.

No high-level constraints were applied to the case study, e.g. maximum installed capacity. Although these will have an influence on the choice of the layout, the basis of the framework holds since the designers are only required to firstly discard the layouts which do not meet the high-level constraints and then apply the economic functions over the remaining ones.

The optimization phase can still be an iterative process of refining the optimization goals and constraints because the MO algorithm is powerful enough to exploit peculiarities in an optimization goal that actually still gives undesired results. For example, in the case study there was no restriction regarding the maximum number of export cables or a preference towards layouts which used offshore substations. In this way, even though the layouts shown in Figures 5.17b and 5.22 have similar AED and CAPEX values, the latter, found with the optimization framework, may not be desired by the designers due to the high amount of cables connected to shore.

The proposed MO optimization framework provides the designers with important information that could not easily be obtained with single-objective alternatives. For example, the optimized trade-off shown in Figure 5.16 shows to the designers the best transmission technology and voltage level for the different range of ICs. Furthermore, the trade-off also informs the designers about any possible important point of transition in the problem design space, i.e. it shows when increasing the IC does not lead to much better designs but mostly to more expensive layouts. For example, this is the case for the right part of the optimized trade-off of Figure 5.16. Even though the layouts have higher AED, this comes with a dramatic increase of the CAPEX. Therefore, this alerts the designers that such layouts may not represent the best solution.

The discovery of key points of transition in the problem search space (Figure 5.16) is also directly applicable to the economic functions shown in Figure 5.18. The designers are informed when the layouts do not present interesting economic figures in a straightforward manner.

The multi-objective optimization approach also provides designers with layouts that were optimized without using economic parameters. This allows the designers to iterate over the layouts with different economic parameters without the need to rerun the optimization (see Section 5.6.4).
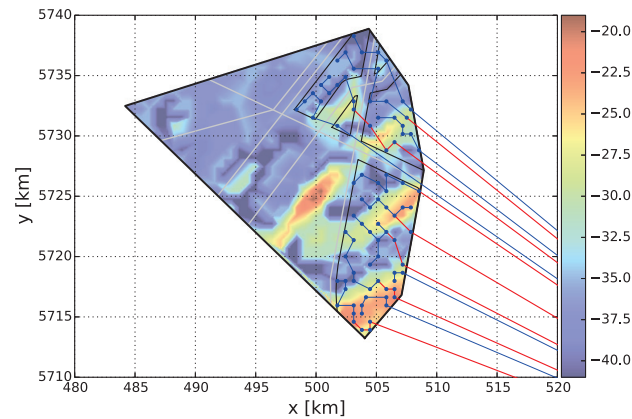
Figure 5.22: Layout with similar AED and CAPEX values as the standard layout with 8 MW turbines.

5.7 Conclusions

A review of existing commercial and academic optimization tools showed their drawbacks and gaps to be twofold: first, the optimization processes are based on a sequential approach and, second, *a priori* economic assumptions need to be made for the optimization phase. To solve these issues, a MO optimization framework to automate, integrate and optimize the design of OWFs was presented in this work.

The design aspects of existing OWFs, e.g. number and location of offshore substations and collection system design, were analyzed. Furthermore, also the industrial trends of the components was investigated. In this way, it was assured that the optimization framework captured all the important design aspects and the industrial trends of the components used in state-of-the-art OWFs. Also, the important optimization variables of the wind farm layout optimization problem were assessed.

A state-of-the-art multi-objective optimization algorithm, so-called MOGOMEA, was used in this work. More specifically, a variant of the algorithm tailored for the wind farm layout optimization problem was employed. The algorithm and the optimization framework were then applied to a case study in the Dutch offshore Borssele area. The framework found several wind farm layouts that represent an optimized trade-off of between the design goals, the annual energy delivered to the onshore electrical network and the investment costs.

Distinct wind farm layouts demonstrated to be the most profitable choice depending on the economic function used. The economic factors, e.g. interest rate and price of energy, demonstrated to play an important role in the outcome of the best layout. These results show that wind farm designers should not decide the layout of the wind farm based solely on one economic function such as the NPV or LCOE. Instead, designers should carefully inspect the performance of the layouts at hand using several economic functions.

The proposed framework helps the designers to perform such analysis since all efficient trade-offs are presented to them. This way, designers may iterate over the optimized trade-offs to select which layout is the most suitable without rerunning the optimization tool, accelerating the decision phase and reducing costs. Moreover, the framework designed layouts that performed similarly to layouts based on existing design strategies, e.g. placement of turbines in a standard grid. This result indicates that designers may be missing other design concepts that lead to similar performances. Nonetheless, the selection of the wind farm layout has to undergo a selection to assure that it is the one that most meets the desire of the designers.

Although the work here presented incorporated a comprehensive collection of models and data, there are several extensions that can be further researched in future work:

- External and future wake effects, caused respectively by existing and future neighboring OWFs, should also be considered during the design of wind farm layouts due to the decreasing space between projects [142–144]. For example, in the case study it would have been beneficial if the wind data from the Belgium wind farms had been considered in the wind resource assessment [145];

- Simplified OPEX cost models were used in this work (percentage of CAPEX or as a fixed cost per MWh). If a more detailed OPEX model which is not directly related to neither the AED not the CAPEX (e.g. the OPEX Cost Estimator from ECN [120]) the optimization goals would have been the AED, CAPEX and OPEX and the optimization framework would have provided a three-dimensional trade-off;

- The grid step size was refined throughout the optimization. However it could be interesting to investigate the benefits of allowing dynamic grid step sizes and rotation of the grid [146].

Abbreviations/Nomenclature and Units

AED [GWh/year]   Annual Energy Delivered
AEP [GWh/year]   Annual Energy Production
AV [€ billion]   Annualized Value
BCR [-]   Benefit to Cost Ratio
CAPEX [€ billion]   Capital Expenditure
COE [M€/MWh]   Cost of Energy
COP [M€/MW]   Cost of Power
CSL [km]   Collection System Length
DCO   Development Consent Order
DFIG   Doubly-Fed Induction Generator
DPT [years]   Discounted Payback Time
FEED   Front-End Engineering and Design
HVac   High-Voltage alternate current
HVdc   High-Voltage direct current
IC [MW]   Installed Capacity
IRR [%]   Internal Rate of Return
LCOE [€/MWh]   Levelized Cost of Energy
MMC   Modular Multi-level Converter
MO   Multi-Objective
MOGOMEA   Multi-Objective Gene-pool Optimal Mixing Evolutionary Algorithm
MVac   Medium-Voltage alternate current
NPV [€ billion]   Net Present Value
NSS   Number of Substations
OPEX [€ billion]   Operational Expenditure
OWF   Offshore Wind Farm
PCC   Point of Common Coupling
PMSG   Permanent-Magnet Synchronous Generator
RD [m]   Rotor Diameter
ROI [-]   Return on Investment
TT   Transmission Technology
UXO   UneXploded Ordnance
UF [-]   Utilization Factor
VSC   Voltage-Source Converter
WFLOP   Wind Farm Layout Optimization Problem

References

[1] B. Christensen, "The Road to Below 10 ct EUR/kWh - Siemens response to the challenge," in *EWEA Offshore*, Copenhagen, Denmark, March 2015.

[2] BVG Associates, "Future renewable energy costs: offshore wind - how technology innovation is anticipated to reduce the cost of energy from european offshore wind farms," KIC InnoEnergy, Eindhoven, The Netherlands, Tech. Rep., 2014.

[3] The Crown Estate, "Offshore Wind Cost Reduction - Pathways Study," London, United Kingdom, Tech. Rep., 2012.

[4] Offshore Wind Cost Reduction Task Force, "Offshore wind cost reduction task force report," Tech. Rep., June 2012.

[5] Offshore Renewable Energy Catapult, "Cost reduction monitoring framework," Glasgow, Scotland, Tech. Rep., Feb. 2015.

[6] Offshore Wind Programme Board, "Sharing good practice in the supply chain to facilitate cost reduction," Tech. Rep. Rev 03.

[7] D. Milborrow. (2015, Jan.) [Last accessed 15th September 2015]. [Online]. Available: http://www.windpowermonthly.com/article/1330525/onshore-wind-competitive-ever

[8] The Wind Power. (2015) [Last accessed 1st June 2015]. [Online]. Available: www.windpowermonthly.com/article/1337352/ewea-offshore-offshore-cost-competitive-2023

[9] DNV GL, "Project FORCE - Offshore Wind Cost Reduction through Integrated Design," Hovik, Norway, Tech. Rep., 2014.

[10] LORC. [Last accessed 1st March 2015]. [Online]. Available: www.lorc.dk/offshore-wind-farms-map/list

[11] 4C Offshore. [Last accessed 23rd March 2015]. [Online]. Available: www.4coffshore.com/windfarms

[12] Trading Economics. [Last accessed 8th August 2015]. [Online]. Available: www.tradingeconomics.com/euro-area/inflation-cpi

[13] BVG Associates, "Value breakdown for the offshore wind sector," Tech. Rep., 2010.

[14] Scottish Enterprise, "Offshore wind fact overview of a wind farm project," Glasgow, Scotland, Tech. Rep., March 2010.

[15] RWE, "Galloper wind farm project environmental statement - chapter 5 project details," Tech. Rep., 2011.

[16] RWE, "Gwynt y mor offshore wind farm - environmental statement (non technical summary)," Tech. Rep., 2005.

[17] M. C. Ebbesen, "Seeing the big picture - Finding the optimal conceptual design," in *EWEA Offshore*, Copenhagen, Denmark, March 2015.

[18] M. D. Esteban *et al.*, "Why offshore wind energy?" *Renewable Energy*, vol. 36, no. 2, pp. 444–450, 2011.

[19] Wind Energy, "Wind Energy - The Facts Part I Technology," Brussels, Belgium, Tech. Rep., 2009.

[20] R. S. Clausen, "Optimising Wind Farm Layouts - Weighing Costs Against Benefits," in *EWEA Offshore*, Copenhagen, Denmark, March 2015.

[21] S. Wyatt *et al.*, "Detailed appraisal of the offshore wind industry in china," Carbon Trust, London, United Kingdom, Tech. Rep., July 2014.

[22] S. Rodrigues *et al.*, "Trends of offshore wind projects," *Renewable and Sustainable Energy Reviews*, vol. 49, pp. 1114–1135, Sept. 2015.

[23] S. Lumbreras, and A. Ramos, "Offshore wind farm electrical design: a review," *Wind Energy*, vol. 16, no. 3, pp. 459–473, 2013.

[24] RWE. [Last accessed 31st March 2015]. [Online]. Available: www.rwe.com/web/cms/en/1252456/ rwe-innogy/sites/wind-offshore/under-construction/gwynt-y-mr/tech-and-spec/

[25] J. F. Herbert-Acero *et al.*, "A review of methodological approaches for the design and optimization of wind farms," *Energies*, vol. 7, no. 11, pp. 6930–7016, 2014.

[26] W. Tong *et al.*, "Multi-objective wind farm design - exploring the trade-off between capacity factor and land use," in *10th World Congress on Structural and Multidisciplinary Optimization*, Florida, USA, May 2013.

[27] S. Khan, and S. Rehman, "Computational intelligence techniques for placement of wind turbines: A brief plan of research in saudi arabian perspective," in *Energy Conference and Exhibition (EnergyCon), 2010 IEEE International*, Dec 2010, pp. 519–523.

[28] A. Kusiak, and Z. Song, "Design of wind farm layout for maximum wind energy capture," *Renew. Energy*, vol. 35, pp. 685–694, 2010.

[29] P. Y. Zhang, "Topics in wind farm layout optimization: Analytical wake models, noise propagation, and energy production," Master's thesis, University of Toronto, 2013.

[30] W. Y. Kwong *et al.*, "Wind farm layout optimization considering energy generation and noise propagation," in *Proceedings of the ASME 2012 International Design Engineering Technical Conferences & Computers and Information in Engineering Conference*, Chicago, USA, Aug. 2012.

[31] K. Veeramachaneni *et al.*, "Optimizing energy output and layout costs for large wind farms using particle swarm optimization," in *IEEE Congress on Evolutionary Computation*, 2012, pp. 1–7.

[32] R. Tran *et al.*, "Fast and effective multi-objective optimisation of wind turbine placement," in *Proceedings of the 15th Annual Conference on Genetic and Evolutionary Computation*, 2013, pp. 1381–1388.

[33] S. Rodrigues, P. Bauer, and P. A. Bosman, "Multi-objective optimization of wind farm layouts - complexity, constraint handling and scalability," *submitted to Renewable and Sustainable Energy Reviews (2nd review round)*.

[34] S. Sorkhabi *et al.*, "Constrained multi-objective wind farm layout optimization - introducing a novel constraint handling approach based on constraint programming," in *Proceedings of International Design Engineering Technical Conference*, Boston, USA, August 2015.

[35] S. Sisbot *et al.*, "Optimal positioning of wind turbines on gokceada using multi-objective genetic algorithm," *Wind Energy*, vol. 13, no. 4, pp. 297–306, 2010.

[36] WindPRO. [Last accessed 20th April 2014]. [Online]. Available: www.emd.dk/WindPRO

[37] GHWindFarmer. [Last accessed 20th April 2014]. [Online]. Available: http://www.gl-garradhassan. com/en/software/GHWindFarmer.php

[38] WasP. Wind resources for energy production of wind turbines. [Last accessed 20th April 2014]. [Online]. Available: http://www.wasp.dk/wasp

[39] OpenWind. [Last accessed 20th April 2014]. [Online]. Available: http://www.awstruepower.com/solutions/products/openwind/

[40] WindSim. [Last accessed 20th April 2014]. [Online]. Available: http://www.windsim.com/

[41] ReSoft. [Last accessed 20th April 2014]. [Online]. Available: http://www.resoft.co.uk/

[42] N. A. Kallioras *et al.*, "Optimum layout design of onshore wind farms considering stochastic loading," *Advances in Engineering Software*, vol. 88, pp. 8–20, 2015.

[43] M. Song *et al.*, "Optimization of wind turbine micro-siting for reducing the sensitivity of power generation to wind direction," *Renewable Energy*, vol. 85, pp. 57–65, 2016.

[44] C. N. Elkinton, J. F. Manwell, and J. G. McGowan, "Offshore wind farm layout optimization (OWFLO) project: an introduction," in *In Proceedings of the European Offshore Wind Conference & Exhibition*, Copenhagen, Denmark, Oct. 2005.

[45] M. A. Lackner, and C. N. Elkinton, "An analytical framework for offshore wind farm layout optimization," *Wind Engineering*, vol. 31, pp. 17–31, Jan. 2007.

[46] B. J. Gribben, N. Williams, and D. Ranford, "Offshore wind farm layout design - a systems engineering approach," in *Ocean Power Fluid Machinery*, London, United Kingdom, Oct. 2010.

[47] P.-E. Rethore *et al.*, "Topfarm: Multi-fidelity optimization of offshore wind farm," in *ISOPE conference*, Hawaii, USA, 2011.

[48] W. Short, D. J. Packey, and T. Holt, "A manual for the economic evaluation of energy efficiency and renewable energy technologies," National Renewable Energy Laboratory, Golden, Colorado, Tech. Rep. NREL/TP-462-5173, March 1995.

[49] C. N. Elkinton, "Offshore wind farm layout optimization," Ph.D. dissertation, University of Massachusetts, Amherst, January 2007.

[50] W. S. de Oliveira, and A. J. Fernandes, "Investment Analysis For Wind Energy Projects," *Revista Brasileira de Energia*, vol. 19, no. 2, pp. 239–285, 2013.

[51] I. Erlich *et al.*, "Offshore Wind Power Generation Technologies," *Proc. of the IEEE*, vol. 101, no. 4, pp. 891–905, April 2013.

[52] Greater Gabbard Offshore Winds Ltd, "Greater gabbard offshore wind farm non technical summary," Tech. Rep., 2005.

[53] EWEA, "The european offshore wind industry - key trends and statistics 2013," Tech. Rep., 2014.

[54] The Wind Power. (2014) [Last accessed 1st March 2015]. [Online]. Available: www.thewindpower.net/windfarms_offshore_en.php

[55] H. Polinder *et al.*, "Trends in wind turbine generator systems," *Emerging and Selected Topics in Power Electronics, IEEE Journal of*, vol. 1, no. 3, pp. 174–185, Sept 2013.

[56] R. Teixeira Pinto *et al.*, "Grid code compliance of vsc-hvdc in offshore multi-terminal dc networks," in *39th Annual Conference IECON*, 2013.

[57] L. B. Ibsen, M. Liingaard, and S. A. Nielsen, "Bucket Foundation, a status," in *Copenhagen Offshore Wind*, 2005.

[58] P. de Villiers, "Demonstrating keystone engineering's innovative inward battered guide structure (ibgs) offshore foundation concept at hornsea - best practice for private-public cooperation," Carbon Trust, Tech. Rep., April 2012.

[59] J. Gengenbach *et al.*, "Design challenges of XL monopiles," in *EWEA Offshore*, Copenhagen, Denmark, March 2015.

[60] A.-K. Govindji, R. James, and A. Carvallo, "Appraisal of the offshore wind industry in japan," Carbon Trust, Tech. Rep., Oct. 2014.

[61] EWEA, "Deep water - the next step for offshore wind energy," Tech. Rep., 2013.

[62] D. Roddier *et al.*, "WindFloat - A floating foundation for offshore wind turbines," *Renew. and Sustainable Energy*, vol. 033104, no. 2, pp. 1–34, 2010.

[63] Main(e) International Consulting LLC. (2013) Japan's floating offshore wind projects: An overview. [Last accessed 24th August 2014]. Maine, USA.

[64] Main(e) International Consulting LLC, "Floating offshore wind foundations: Industry consortia and projects in the united states, europe and japan - an overview," Maine, USA, Tech. Rep., May 2013.

[65] T. Sorensen, M. L. Thogersen, and P. Nielsen, "Adapting and calibration of existing wake models to meet the conditions inside offshore wind farms," EMD International A/S, Aalborg, Denmark, Tech. Rep., 2008.

[66] The Crown Estate, "Submarine cables and offshore renewable energy installations - proximity study," London, United Kingdom, Tech. Rep., 2012.

[67] S. Rodrigues, P. Bauer, and J. Pierik, "Comparison of offshore power transmission technologies: A multi-objective optimization approach," in *Power Electronics and Motion Control Conference (EPE/PEMC), 15th International*, 2012.

[68] J. Schachner, "Power connection for offshore wind farms," Master's thesis, Delft University of Technology, Delft, The Netherlands, Jan. 2004.

[69] Carbon Trust. Offshore wind accelerator - driving down the cost of offshore wind. [Last accessed 1st May 2014]. London, United Kingdom. [Online]. Available: carbontrust.com/media/105322/electrical_presentation_jm_-dec_2011.pdf

[70] J. Pierik *et al.*, "Dowec Electrical System Baseline design," Energy Research Centre of the Netherlands (ECN), Petten, The Netherlands, Tech. Rep. DOWEC 045 rev. 2, Feb. 2002.

[71] "Algorithms for cable network design on large-scale wind farms," Tufts University, Medford, USA, Tech. Rep., 2011.

[72] J. Bauer, and J. Lysgaard, "The offshore wind farm array cable layout problem: a planar open vehicle routing problem," *Journal of the Operational Research Society*, vol. 66, pp. 360–368, 2014.

[73] A. Tesauro, P.-E. Rethore, and G. Larsen, "State of the art of wind farm optimization," in *Proceedings of European Wind Energy Conference & Exhibition*, Copenhagen, Denmark, April 2012.

[74] M. Dicorato *et al.*, "Guidelines for assessment of investment cost for offshore wind generation," *Renew. Energy*, vol. 36, no. 8, pp. 2043–2051, 2011.

[75] G. Katsouris, "Infield cable topology optimization of offshore wind farms," Master's thesis, Delft University of Technology, Delft, The Netherlands, Feb. 2015.

[76] R. Teixeira Pinto, "Multi-terminal dc networks - system integration, dynamics and control," Ph.D. dissertation, Delft University of Technology, Delft, The Netherlands, 2014.

[77] A. Papadopoulos, "Modeling of collection and transmission losses of offshore wind farms for optimization purposes," Master's thesis, Electrical Sustainable Energy Department, Delft University of Technology, Delft, The Netherlands, Feb. 2015.

[78] S. Rodrigues, "Dynamic Modeling and Control of VSC-based Multi-terminal DC Networks," Master's thesis, Energy Department, Instituto Superior Técnico, Lisbon, Portugal, Dec 2011.

[79] L. Donat *et al.*, "Assessment of climate change policies in the context of the european semester - country report the netherlands," Ecologic Institute and eclareon, Berlin, Germany, Tech. Rep., Jan. 2014.

[80] Loyens and Loeff, "North Sea offshore wind - Developments in Belgium and the Netherlands," Rotterdam, The Netherlands, Tech. Rep., Nov 2014.

[81] Netherlands Enterprise Agengy. (2015) [Last accessed 17th March 2015]. Berlin, Germany. [Online]. Available: www.rvothema4.pleio.nl

[82] Netherlands Enterprise Agency, "North sea 2050 spatial agenda," Ministerie van Economische Zaken, The Hague, The Netherlands, Tech. Rep., Sept. 2014.

[83] Netherlands Enterprise Agency, "Rijksstructuurvisie windenergie op zee (in dutch)," Ministerie van Economische Zaken, The Hague, The Netherlands, Tech. Rep., Sept. 2014.

[84] Netherlands Enterprise Agency, "Borssele wind farm zone project & site description," Ministry of Economic Affairs, Tech. Rep. 2, Aug. 2015.

[85] Netherlands Enterprise Agency, "Borssele Wind Farm Zone - Project & Site Description," Tech. Rep., 2014.

[86] DNV GL, "66 kV Systems for Offshore Wind Farms," TenneT, Arnhem, The Netherlands, Tech. Rep. 113799-UKBR-R02, Rev. 2, March 2015.

[87] Deltares, "Metocean study for the Borssele Wind Farm Zone," Delft, The Netherlands, Tech. Rep., Feb. 2015.

[88] Netherlands Enterprise Agency. (2015) Uxo removal/clearance. [Last accessed 28th December 2015]. [Online]. Available: http://offshorewind.rvo.nl/questions/view/41293422/uxo-removalclearance-09-12-2015

[89] Netherlands Enterprise Agency, "Borssele Wind Farm Zone Wind Farm Sites I and II Project and Site Description ," Tech. Rep., 2015.

[90] Netherlands Enterprise Agency. (2015) Wind farm layout - location turbines. [Last accessed 23th August 2015]. [Online]. Available: http://offshorewind.rvo.nl/questions/view/32317252/wind-farm-layout-location-turbines-22-05-2015

[91] Netherlands Enterprise Agency. (2015) Wind farm layout. [Last accessed 23th August 2015]. [Online]. Available: http://offshorewind.rvo.nl/questions/view/33205612/wind-farm-layout-07-07-2015

[92] Ecofys, "Site Studies Wind Farm Zone Borssele - Wind Resource Assessment," Utrecht, The Netherlands, Tech. Rep., Sept. 2015.

[93] S. A. Hsu, E. A. Meindl, and D. B. Gilhousen, "Determining the power-law wind-profile exponent under near-neutral stability conditions at sea," *J. Appl. Meteor.*, vol. 33, pp. 757–765, 1994.

[94] Tennet, "Offshore grid connection system borssele - scoping document (notitie reikwijdte en detail-niveau)," Den Haag, the Netherlands, Tech. Rep., March 2015.

[95] Vestas Wind Systems A/S, "Offshore v164-8.0 mw v112-3.3 mw," Tech. Rep., 2013. [Online]. Available: nozebra.ipapercms.dk/Vestas/Communication/Productbrochure/OffshoreProductBrochure/OffshoreProductBrochure/

[96] XEMC Darwind. Xd115-5mw. [Last accessed 20th March 2015]. [Online]. Available: www.darwind.nl/Wind-turbines/XD115-5MW

[97] International Electrotechnical Commission, *IEC 60228: Electric cables - Conductors of insulated cables*, Std., 2004.

[98] International Electrotechnical Commission, *IEC 60287: Electric cables - Calculation of the current rating*, Std., Rev. 1.2, 2006.

[99] A. Papadopoulos *et al.*, "Collection and transmission losses of offshore wind farms for optimization purposes," in *IEEE ECCE USA*, 2015.

[100] ABB, *XLPE Submarine Cable Systems - Attachment to XLPE Land Cable Systems - User's Guide*, Lyckeby, Sweden, 2010.

[101] A. Papadopoulos *et al.*, "A fast steady-state loss model of a modular multilevel converter for optimization purposes," in *ECCE Asia, 2015 IEEE*, 2015.

[102] S. Rodrigues *et al.*, "Steady-state loss model of half-bridge modular multilevel converters," *Industry Applications, IEEE Transactions on*, vol. PP, no. 99, pp. 1–1, Jan. 2016.

[103] Infineon, *Technical Information of IGBT module FZ1000R33HL3*, Rotterdam, The Netherlands, 2013.

[104] A. C. Levitt *et al.*, "Pricing offshore wind power," *Energy Policy*, vol. 39, no. 10, pp. 6408–6421, 2011.

[105] I. Katic, J. Hojstrup, and N. Jensen, "A simple model for cluster efficiency," in *EWEC'86. Proceedings. Vol. 1*, 1986, pp. 407–410.

[106] N. Jensen, "A note on wind generator interaction," Riso National Laboratory, Roskilde, Denmark, Tech. Rep. Riso-M-2411, 1983.

[107] S. Rodrigues, P. Bauer, and J. Pierik, "Modular approach for the optimal wind turbine micro siting problem through cma-es algorithm," in *Proceeding of the fifteenth annual conference companion on Genetic and evolutionary computation conference companion*, ser. GECCO '13 Companion. New York, NY, USA: ACM, 2013, pp. 1561–1568.

[108] A. Amberg, W. Domschke, and S. Voß, "Capacitated minimum spanning trees: Algorithms using intelligent search," 1996.

[109] L. R. Esau, and K. C. Williams, "On teleprocessing system design: part ii a method for approximating the optimal network," *IBM Systems Journal*, vol. 5, no. 3, pp. 142–147, 1966.

[110] The Crown Estate, "Subsea cables uk guideline no 6 the proximity of offshore renewable energy installations & submarine cable infrastructure in uk waters," London, United Kingdom, Tech. Rep., 2012.

[111] "Money does grow on turbines - Overplanting Offshore Windfarms," in *Global Offshore Wind Conference*, Glasgow, UK, June 2014.

[112] PYPOWER. (2011) [Last accessed 1st May 2015]. [Online]. Available: http://rwl.github.io/PYPOWER/index.html

[113] O. Barten, "What is the ideal powercurve?" Master's thesis, Delft University of Technology, Delft, The Netherlands, March 2012.

[114] S. Georgios, "Techno-economical analysis of dc collection grid for offshore wind parks," Master's thesis, University of Nottingham, Nottingham, United Kingdom, 2010.

[115] S. Lundberg, "Performance comparison of wind park configuration," Master's thesis, Chalmers University of Technology, Goteburg, Sweden, 2003.

[116] J. R. Lluch, "Power transmission systems for offshore wind farms technical-economic analysis," Master's thesis, Universitat Politcnica de Catalunya, Barcelona, 2015.

[117] FLOW Offshore Wind Cost Model. [Last accessed 28th August 2015]. [Online]. Available: http://flow-offshore.nl/page/flow-offshore-wind-cost-model

[118] B. van Eeckhout, "The economic value of vsc hvdc compared to hvac for offshore wind farms," Master's thesis, Katholieke Universiteit Leuven, Leuven, Belgium, 2007.

[119] Z. Gajic, B. Hillstrom, and F. Mekic, "HV Shunt Reactor Secrets for Protection Engineers," in *30th Western Protective Relaying Conference*, Spokane, Washington, Oct. 2003.

[120] H. Braam *et al.*, "Properties of the O&M Cost Estimator (OMCE)," ECN, Petten, The Netherlands, Tech. Rep. ECN-E–11-045, July 2011.

[121] Deloitte, "Establishing the investment case Wind power," Copenhagen, Denmark, Tech. Rep., April 2014.

[122] K. Cory, and P. Schwabe, "Wind levelized cost of energy - a comparison of technical and financing input variables," National Renewable Energy Laboratory, Golden, Colorado, Tech. Rep. NREL/TP-6A2-46671, Oct. 2009.

[123] N. H. Luong, H. La Poutré, and P. A. Bosman, "Multi-objective gene-pool optimal mixing evolutionary algorithms," in *Proceedings of the 2014 Conference on Genetic and Evolutionary Computation*, 2014, pp. 357–364.

[124] N. H. Luong *et al.*, "Scalable and practical multi-objective distribution network expansion planning," in *Proceedings of the IEEE PES General Meeting*, Denver, USA, July 2015.

[125] P. Bosman, and D. Thierens, "On measures to build linkage trees in ltga," in *Parallel Problem Solving from Nature - PPSN XII*, Berlin, Germany, 2012, vol. 7491, pp. 276–285.

[126] D. Thierens, and P. A. Bosman, "Optimal mixing evolutionary algorithms," in *Proceedings of the 13th Annual Conference on Genetic and Evolutionary Computation*, 2011, pp. 617–624.

[127] S. Rodrigues, P. Bauer, and J. Pierik, "A clustering approach for the wind turbine micro siting problem through genetic algorithm," in *39th Annual Conference IECON*, 2013.

[128] J. S. Gonzalez, M. Burgos Payan, and J. Riquelme Santos, "A new and efficient method for optimal design of large offshore wind power plants," *Power Systems, IEEE Transactions on*, vol. 28, no. 3, pp. 3075–3084, Aug 2013.

[129] J. S. Gonzalez *et al.*, "A review and recent developments in the optimal wind-turbine micro-siting problem," *Renew. and Sustainable Energy Reviews*, vol. 30, no. 0, pp. 133–144, 2014.

[130] R. de Bokx, "Parallelizing the Linkage Tree Genetic Algorithm and Searching for the Optimal Replacement for the Linkage Tree," Master's thesis, Delft University of Technology, Delft, The Netherlands, 2015.

[131] B. Saavedra-Moreno *et al.*, "Seeding evolutionary algorithms with heuristics for optimal wind turbines positioning in wind farms," *Renew. Energy*, vol. 36, no. 11, pp. 2838–2844, 2011.

[132] M. Wagner *et al.*, "Optimizing the layout of 1000 wind turbines," in *European Wind Energy Association Annual Event*.   Brussels, Belgium: European Wind Energy Association, 2011, pp. 1–10.

[133] M. Wagner, J. Day, and F. Neumann, "A fast and effective local search algorithm for optimizing the placement of wind turbines," *Renew. Energy*, vol. 51, no. 0, pp. 64–70, 2013.

[134] J. MacQueen, "Some methods for classification and analysis of multivariate observations," in *Proceedings of the Fifth Berkeley Symposium on Mathematical Statistics and Probability, Volume 1 Statistics*. Berkeley, Calif.: University of California Press, 1967, pp. 281–297.

[135] Netherlands Enterprise Agency, "Borssele wind farm zone project & site description," Ministry of Economic Affairs, Tech. Rep., Dec. 2014.

[136] B. Bulder *et al.*, "Dutch Offshore Wind Energy Converter Task 12 - Cost Comparison of the Selected Concepts," Energy Research Centre of the Netherlands (ECN), Petten, The Netherlands, Tech. Rep. ECN-C–01-080, March 2000.

[137] Carbon Trust, "Offshore wind power: big challenge, big opportunity maximising the environmental, economic and security benefits," London, United Kingdom, Tech. Rep., 2008.

[138] S. F. Ahrenfeldt, "Distributed Substations - A cost-efficient multi-platform topology," in *EWEA Offshore*, Copenhagen, Denmark, March 2015.

[139] P. Smith. (2014, Nov.) [Last accessed 5th September 2015]. [Online]. Available: windpowermonthly.com/article/1320109/question-week-offshore-projects-built-last

[140] European Wind Energy Association (EWEA), "The economics of wind energy," Tech. Rep., March 2009.

[141] K. E. Thomsen, "Chapter three - project planning," in *Offshore Wind*, K. E. Thomsen, Ed.   Boston: Elsevier, 2012, pp. 27–49.

[142] DNV Kema, "Framework for the Categorisation of Losses and Uncertainty for Wind Energy Assessments," Tech. Rep., Feb. 2013.

[143] K. Hansen, and et al., "Simulation of wake effects between two wind farms," *Journal of Wind Engineering and Industrial Aerodynamics*, vol. 625, no. 1, pp. 1–12, Jan 2015.

[144] C. B. Hasager *et al.*, "EERA Design Tool for Offshore Wind Farm Cluster (DTOC)," in *EWEA Offshore*, Copenhagen, Denmark, March 2015.

[145] B. Bulder *et al.*, "Quick scan wind farm efficiencies of the Borssele location," Energy Research Centre of the Netherlands (ECN), Petten, The Netherlands, Tech. Rep. ECN-X–14-098, June 2014.

[146] F. Wang, D. Liu, and L. Zeng, "Study on computational grids in placement of wind turbines using genetic algorithm," in *World Non-Grid-Connected Wind Power and Energy Conference, 2009. WNWEC 2009*, 2009, pp. 1–4.

Wake Losses Optimization of Offshore Wind Farms with Movable Floating Wind Turbines

In the future, floating wind turbines could be used to harvest energy in deep offshore areas where higher wind mean speeds are observed. Currently, several floating turbine concepts are being designed and tested in small scale projects; in particular, one concept allows the turbine to move after installation. This article presents a novel layout optimization framework for wind farms composed of movable floating turbines. The proposed framework uses an evolutionary optimization strategy in a nested configuration which simultaneously optimizes the anchoring locations and the wind turbine position within the mooring lines for each individual wind direction. The results show that maximum energy production is obtained when movable wind turbines are deployed in an optimized layout. In conclusion, the framework represents a new design optimization tool for future offshore wind farms composed of movable floating turbines.

6.1 Introduction

The need for steadier and higher mean wind speeds has been pushing the wind industry towards areas located further offshore [1]. In fact, the average distance to shore and water depth of offshore wind farms (OWF) have been increasing since the industry first steps (Figure 6.1). However, current grounded support structures are only economical viable till certain water depths [2].

With the desire of moving to locations with deeper water depths, in an economically viable way, floating wind turbines concepts have appeared in the last years. Currently, there are several floating turbine concepts being developed and tested in pilot projects [2, 8]. One of these floating turbine concepts is developed by the IDEOL company [9]. This specific design takes another advantage from the fact that a flowing turbine is not bottom-fixed to the seabed: it allows the turbine to have a certain mobility freedom even after its installation [9].

To reduce costs, e.g. cabling and area rental costs, turbines tend to be packed in wind farms. However, installing turbines close to each other causes interferences such as wake losses through shadowing. For example, the efficiency of the Danish Horns Rev I OWF is 89% of what the same turbines would produce if installed alone [10]. Thus, it is important to reduce the wake losses in far and large OWFs. A possible strategy to reduce wake losses is to optimize the wind farm layout.

The wind farm layout optimization problem has been intensively studied in the last years [11–20]. More specifically, the first work that dealt with the wind farm layout problem was carried out back in 1994 [21]. The wind farm area was grid-discretized and the optimizer was set to obtain layouts that would increase the wind farm efficiency. The first work that considered the wind farm space as a continuous space was carried out in [22], whereas the first optimization approach tailored for offshore environments was presented in [23].

Although a great deal of research has been conducted in the wind farm layout optimization problem, all investigations solely considered the possibility of optimizing the turbine locations before construction. Hence, so far no strategy has been developed which considers the possibility of moving the wind turbines after the project commissioning. This work presents a novel optimization framework for OWFs composed of movable wind turbines.
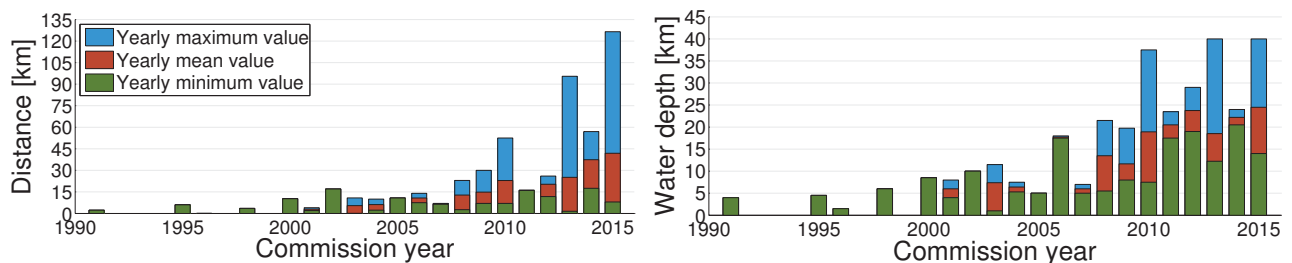

Figure 6.1: Yearly statistics of the distance to shore and water depth of commissioned and under construction European OWFs composed of five or more turbines [3–7].

The work is organized as follows: the next section introduces the different types of floating wind turbines that currently exist, followed by a detailed explanation of the movable wind turbine concept. Thereafter, in Section 6.3, the novel optimization framework is proposed. Section 6.4 presents the wake loss models used in this work, whereas Section 6.5 presents a case study specifically designed to evaluate the proposed approach. In Section 6.6 the results are presented and an analysis is carried out. The article closes with general conclusions and recommendations for offshore wind and future research.

6.2   Floating Wind Turbines

Existing commercial-size OWFs make use of grounded substructure concepts to support their turbines. Such substructures become very expensive and difficult to engineer as the water depth increases. Hitherto, water depths higher than 50 m require floating support structures. In fact, as shown in Figure 6.2, only a few projects used grounded support structures with average water depths higher than 40 m [8].

Many countries have a limited number of suitable sites in sufficiently shallow water to allow economically viable fixed substructures [24]. Within Europe, much of the Mediterranean and Atlantic basins as well as Norway face this difficulty [25]. In the long term, it is anticipated that floating structures will become prominent in the offshore wind market [25]. There are several advantages for using floating turbines:

- access to previously inaccessible places where there is stronger yet less turbulent winds [26];

- more flexible construction and installation phases [25];

- possible commissioning and assembly at the quayside, avoiding the need for heavy-lift jack-up or dynamic positioning vessels, further reducing the cost and risk of deployment activities [26];
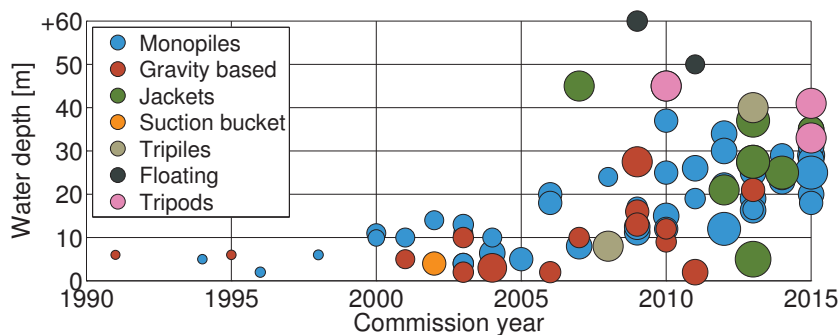

Figure 6.2: Average water depth per offshore project [3, 4].

- avoiding piling activities during installation and an easier decommissioning processes lead to reduced environmental impacts and sea life disturbance;
- geotechnical requirements are reduced since core sampling is only needed at the anchor positions, as opposed to the necessity of deep core sampling at every pile site [26].

Nonetheless, there are several challenges related to floating wind turbines. For example, the increased wind and wave-induced motion, the added complexity of the design process, electrical infrastructure design and costs (in particular the flexible cable), construction, installation and operation & maintenance (O&M) procedures [25]. However, increased know-how and standardization practices will contribute to overcoming these challenges. Furthermore, it is also expected that a higher energy production will be achieved since the floating turbines will be deployed at sites with higher mean wind speeds. Currently the existing floating concepts may be categorized in three main types [27]:

- Buoyancy: employs a barge type device with catenary mooring lines;
- Mooring Line: under water chains or tethers connect the buoyant body to a counterweight that lies on the seabed [2]. With the buoyant body semi-submerged in the water, the necessary uplifting force is created, keeping the chains constantly tensioned [28];
- Ballast: uses spar buoy platforms with catenary mooring anchors.

6.2.1 Movable Wind Turbine Concept

IDEOL developed a new floating turbine concept, which allows the structure to move along its mooring lines [9]. Figure 6.3a shows the basic version of a movable turbine, which only allows for linear movements (one degree of freedom). This system is easier to operate since the turbine position is set by only one parameter, e.g. the distance from one the anchoring positions. Figure 6.3b illustrates a more complex design which, by rearranging the anchoring positions, allows the turbine to cover a triangular area. This new anchoring configuration gives two degrees of freedom to the turbines, thus it allows them to move in two directions. Although, this system results in a higher maneuverability of the turbine, it increases the control complexity since two coordinates have to be set to position the turbine.

With this mobility, it becomes possible to optimize the wind farm layout based on different environmental data, e.g. wind and tidal direction. Hence, this solution allows for wake losses reduction, leading to an increased annual energy production (AEP). On the other hand, this concept is more complex than a similar floating concept due to the extra mobility machinery and attached complexity. Furthermore, they are logistically more complex, since it requires a system operator to move the turbines according to the wind direction. Nonetheless, reducing wake losses through a real-time wind farm layout optimization according to the wind direction may bring energy gains which overcome the shortcomings.

The wind direction is a key factor for the turbine mobility approach. Since the turbine mobility is somehow limited, the layout adjustment may be limited to more persistent wind direction

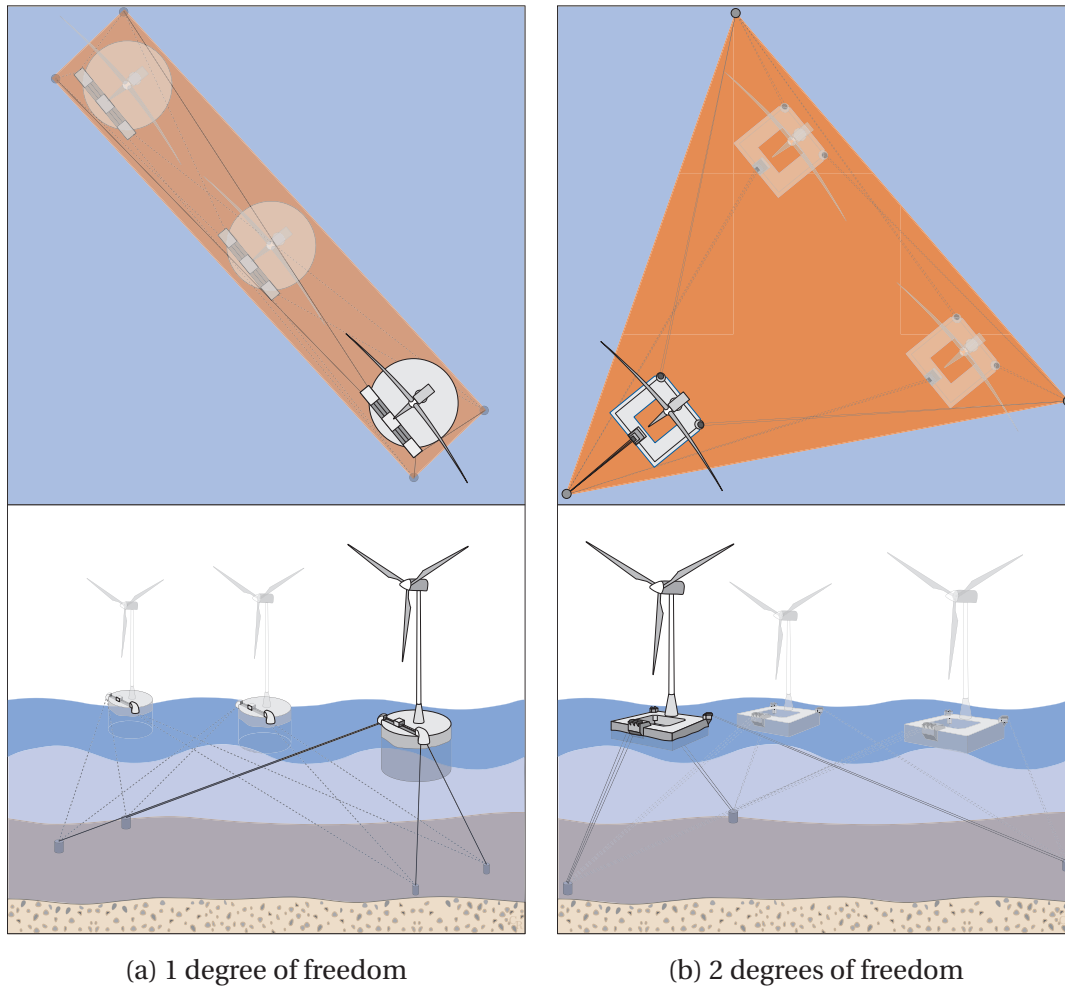(a) 1 degree of freedom (b) 2 degrees of freedom

Figure 6.3: Two IDEOL concepts for a movable and floating wind turbine [9]. The figures show three different turbine positioning for both concepts.

alterations while disregarding fast wind direction transients. Therefore, the decision of moving the turbines should be based on data from meteorological masts and weather forecast to guarantee that there is an energy generation benefit to the repositioning.

6.3 Wind Farm Layout Optimization Framework

The proposed optimization framework here presented makes use of the advantaged brought by movable wind turbines: it optimizes the turbines real-time location according to the wind direction. The framework has an integrative design strategy since it optimizes the positions of the turbine within their mooring lines and the turbines anchoring locations.

Current OWFs are composed of dozens of turbines [3], which makes the optimization variables increase rapidly (e.g. the turbine locations). In fact, solving the wind farm layout optimization

problem to optimality is very difficult since it falls under the combinatorial optimization problem class [29]. Therefore, the wind farm layout problem is not suitable to be solved through deterministic algorithms [29]. A solution, widely use in academia, is the use of stochastic algorithms, where randomness is included in the process [30].

An evolutionary strategy called Covariance Matrix Adaption (CMA-ES) was used. The CMA-ES is one of the most powerful evolutionary algorithms for real-valued single-objective optimization of non-linear and non-convex functions [13, 31] and it has been applied in different fields of engineering [13, 32]. Figure 6.4 presents a flowchart of the CMA-ES algorithm.

6.3.1 Nested optimization

One might optimize first the locations of the turbines and after optimize the positions within the mooring lines for each wind direction; however, such approach represents a simplification which may create constraints in the solution space. The optimal solution for each individual problem is not necessarily the optimal solution for the complete problem.

A nested optimization framework is proposed in this work to simultaneously optimize the turbine positioning. An outer optimization loop is responsible for first establishing the turbines anchoring positions, whereas an inner loop optimizes the turbine location within its mooring lines for each wind direction. Figure 6.5 shows the interactions between the two nested CMA-ES algorithms and both optimization loops are explained next.

Outer optimization loop

The CMA-ES of the outer optimization loop is set to optimize the anchoring locations. To do so, the optimization variables of this problem are the central point of the anchoring locations and the rotation angle.

The encoded solutions have the following structure:

$$X_{loop}^{outer} = \begin{bmatrix} x_1 & \cdots & x_n & y_1 & \cdots & y_n & \theta_1 & \cdots & \theta_n \end{bmatrix} \tag{6.1}$$
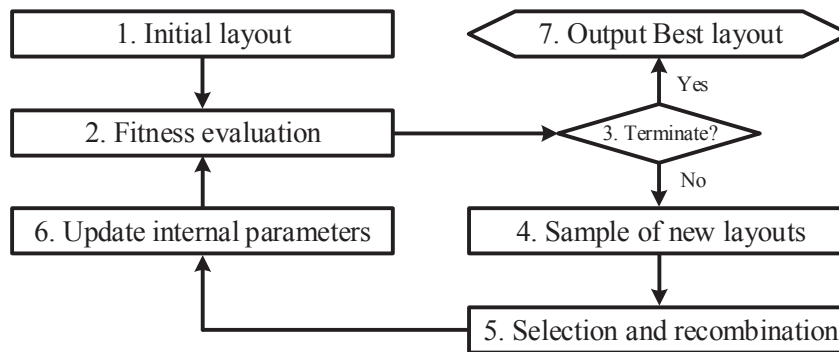

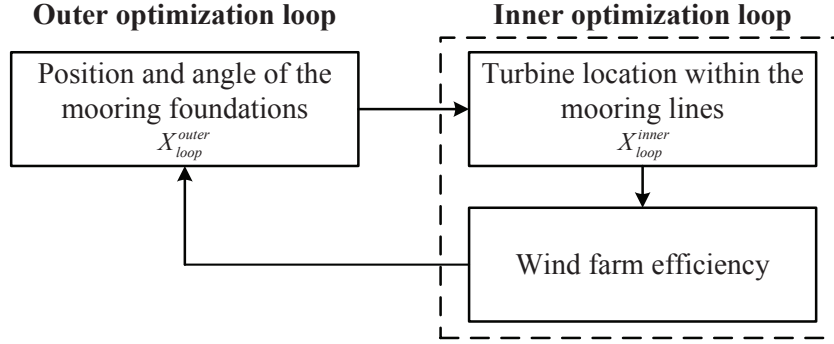Figure 6.4: Flowchart of the CMA-ES algorithm.

Figure 6.5: Proposed nested optimization approach in which both the mooring line positions and the turbines locations are simultaneously optimized.

where (x_1, y_1, θ_1) and (x_n, y_n, θ_n) correspond to the central points and angles of the anchoring locations of the first and $n\text{-}th$ turbines, respectively.

Inner optimization loop

The inner loop CMA-ES receives as input the position and angles of the anchoring locations. Thereafter, it optimizes the locations of the turbines within the mooring lines to reduce wakes losses. The inner loop solutions are encoded as:

$$X_{loop}^{inner} = \begin{bmatrix} a_1 & \cdots & a_n & b_1 & \cdots & b_n \end{bmatrix} \tag{6.2}$$

where (a_1, b_1) and (a_n, b_n) correspond to the coordinates within the mooring lines of the first and $n\text{-}th$ turbines, respectively.

Figure 6.6 depicts the optimization variables for a $k\text{-}th$ turbine with one and two degrees of freedom. In Figure 6.6a, it can be seen that outer optimization loop defines the location of the turbines, giving the inner loop only the possibility of optimizing the turbine location along a straight line. On the other hand, with two degrees of freedom, the inner loop optimizes the location of the turbine within an area (see Figure 6.6b).

6.3.2   Optimization goal

The maximization of the wind farm production is one of the most common optimization goals and it has been widely used in academia and in commercial software [23, 33, 34]. This work uses a similar optimization goal, the maximization of the wind farm efficiency, which is calculated as the ratio between the wind farm production with and without wake losses [12, 35]. The wind farm production is computed as the mean power output for all wind directions and then scaled to account for a given wind direction frequency of occurrence. The ideal wind farm production is
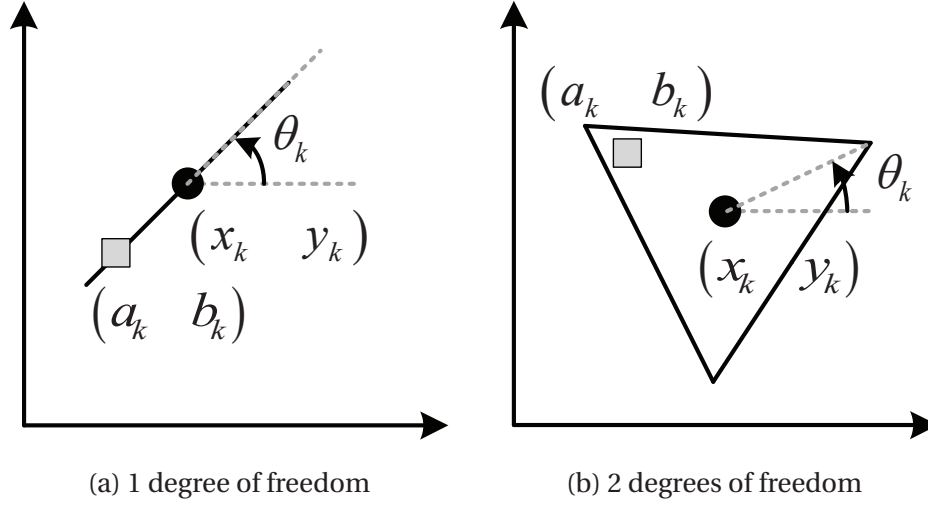
(a) 1 degree of freedom   (b) 2 degrees of freedom

Figure 6.6: Optimization variables used to obtained improved wind farm layouts for a $k\text{-}th$ turbine

obtained as the power production of a single wind turbine (without wake losses) multiplied by the number of turbines in the wind farm. Finally, the wind farm efficiency is calculated by:

$$\eta_{WF} = \frac{P_{farm}}{n \times P_{turb}^{ideal}} \tag{6.3}$$

where η_{farm} is the wind farm efficiency, P_{farm} is the farm total power production and $n \times P_{turb}^{ideal}$ represents the power produced by n turbines without shadowing effects.

6.3.3   Constraints

To obtain feasible wind farm layouts, the following constraints – displayed in Figure 6.7 – were implemented:

- A minimum distance between neighboring turbines is required at all times – including both the default central locations and the optimized layouts – to guarantee the well-function and integrity of the turbines. In this work, the minimum separation is considered equal four times the turbines rotor diameter, however, this value is turbine dependent and should be provided by the manufacturer;

- The turbines have to be placed inside the farm area. For the mobile turbines case, the central point of the manoeuvrable area has to be located within the wind farm area. Nevertheless, the turbines are allowed to temporarily move to external positions.
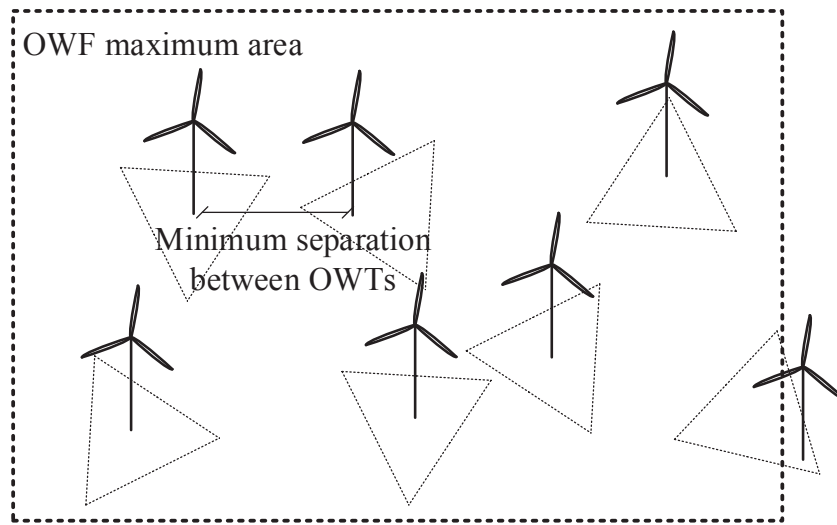
Figure 6.7: Constraints taken into consideration to guarantee the feasibility of the layouts.

6.4 Wake Losses Modeling

Installing turbines in closes vicinities causes interferences such as wake losses through shadowing. For example, the Danish Horns Rev I OWF produces circa 89% of the energy that the same turbines would produce if no wake losses occurred [10]. Hence, it is important to analyze and reduce the wake losses in far and large OWFs.

Currently, there is a wide variety of models to calculate, with different accuracy levels, the wake losses inside wind farms [36–42]. Examples of wake losses models to calculate the wind deficits due to wakes inside wind farms include the Jensen model (also known as Park model) [43], Eddy viscosity model [44], Frandsen et al. model [45], deep-array wake model [46] and the Larsen model [47]. These engineering models, due to their simplified wake speed deficit approach, offer fast calculation times and are able to provide a preliminary description of the far wake regime (4-6 rotor diameters) [40]. Other models were built to provide medium-fidelity results, namely the Dynamic Wake Meandering model [48] and several other approaches based on the actuator disk model [49, 50].

Computational fluid dynamics (CFD) models stand in the high-fidelity end [39]. The CFD models solve the parabolized Navier-Stokes equations which that may take various hours to compute in a large wind farm. Examples of CFD models are the Simulator for Offshore Wind Farm Applications (SOWFA), a modular and open-source tool developed by NREL [51], the EllipSys3D developed by DTU and Risø [36] and FarmFlow developed by the Energy Research Centre of the Netherlands (ECN) [52]. Finally, high-resolution models based on large eddy simulations (LES) models offer the highest fidelity but may take several weeks to complete [53].

CFD and LES approaches represent the most accurate tools to calculate turbine wakes and may be used for detailed studies such as: interactions between a turbulent flow and a rotor blade; the interaction between multiple wakes; or validation and calibration of simpler models [10, 53]. However, a major disadvantage of such high-fidelity simulations is the excessive computational burden. Such drawback is further heightened when these models are employed to optimize the design of a large OWF, which requires a great deal of evaluations of the AEP [13].

Two models which sit in both extremes of the spectrum are used in this work to calculate the wake losses inside an OWF. The Jensen model is employed during the optimization routine, whereas FarmFlow is used to verify the efficiency of the optimized wind farm layouts. A brief description of both models is provided next.

6.4.1 Katic-Jensen model

The Jensen model, one of the most common models used, is a simplified and fast manner of calculating the wind speed inside the wake of a turbine [54]. More precisely it was used a later version of the model, which was developed by Katic *et al* [55]. This model, due to this ease of implementation and fast computation has been widely adopted in wind farm modeling [35,56–61].

6.4.2 FarmFlow

FarmFlow, which is an improved version of the UPMWAKE model [62], solves the parabolized Navier-Stokes equations in all three dimensions, while the turbulent processes in the wake are modeled with a k-ϵ turbulence model. The performance of FarmFlow has been evaluated and compared to the commonly used models for predicting wind speed decrease inside turbines wakes [38, 42].

6.5 Case Study

6.5.1 Wind farm

The proposed optimization framework was tested in a medium-sized OWF of 180 MW installed power and a square-shaped area with 5 km per side. The farm is composed of 36 identical turbines with a rated power of 5 MW. The turbines have a hub height of 90 m and a 126 m rotor diameter. Figure 6.8 presents the turbine power curve and thrust coefficient for the operational wind speeds.

In the initial default wind farm layout the wind turbines were placed in a grid with 1 km distance between them and the angles for the mooring lines were set to the reference value (see Figure 6.6). The wind farm was considered to be a continuous space, whereas the mooring lines are considered to be 50% longer than the turbine rotor diameter.
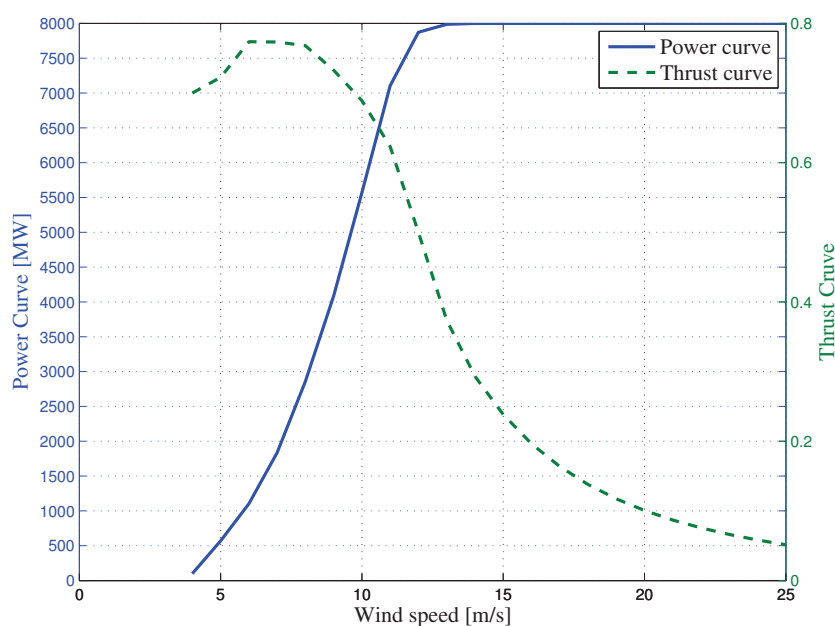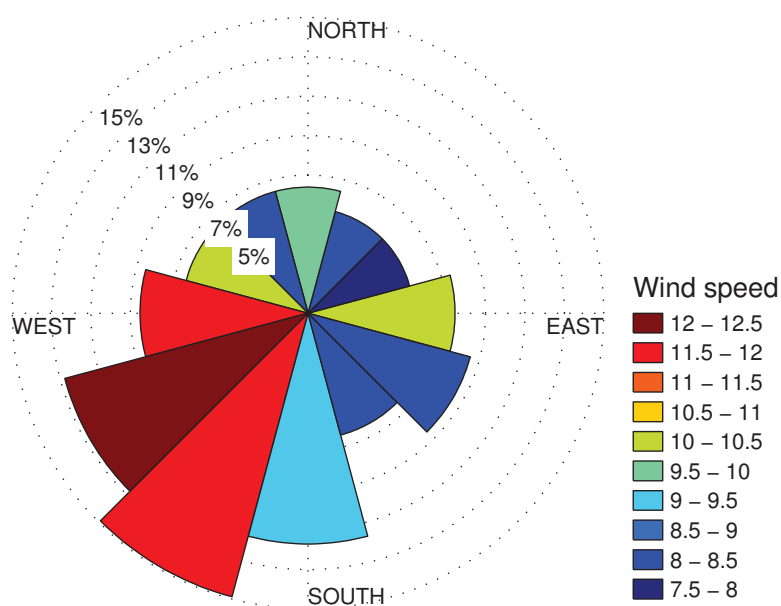
Figure 6.8: Wind turbine power and thrust curves.

Figure 6.9: Wind rose with average wind speeds and frequencies. North is the zero degree direction for the wind rose.

6.5.2 Wind rose

The proposed framework relies on the wind resource existing at the offshore site to obtain optimized layouts. The wind resource used – displayed in Figure 6.9 – is based on measurement data collected during four years at the offshore platform Fino 1, located in the North Sea [63].

Table 6.1: Case study scenarios

Scenario	Optimized locations	Movable turbines	Degrees of freedom
1	No	No	0
2	Yes	No	0
3	No	Yes	1
4	No	Yes	2
5	Yes	Yes	1
6	Yes	Yes	2

6.5.3 CMA-ES

The outer loop CMA-ES was run for 24 h, whereas the inner loop was given 100 iterations per wind direction. All remaining parameters of the CMA-ES algorithm were set to their default values [64].

6.5.4 Scenarios

Six different scenarios were considered for the case study. Scenario 1 represents a standard grid-based wind farm project. The turbines locations are not optimized neither have the ability to move after installation. In Scenario 2, the turbine locations are optimized but no turbine mobility is considered. Contrarily, Scenarios 3 and 4 use the standard grid layout but make use of the movable wind turbine. Finally, for Scenarios 5 and 6, an integrative optimization approach is used which encompasses both the turbines anchoring positions and the turbines location within the mooring lines. Table 6.1 summarizes the characteristics of each scenario.

6.6 Results

This section presents the results obtained for the six different scenarios. Figure 6.10 shows the optimized layouts, whereas Figure 6.11 depicts the overall wind farm efficiencies for the difference scenarios. The wind farms' efficiency, for each wind direction, is shown in Figure 6.12.

6.6.1 Katic-Jensen model

According to the Katic-Jensen model, the regular layout has the lowest efficiency (Figure 6.11). Figure 6.12 (a) shows that the standard grid layout has very low efficiencies for the directions where the wind is aligned with the turbine rows. The wind farm layout composed of fixed turbines and optimized layout has the second highest efficiency, only surpassed by Scenario 6. For Scenarios 3 and 4, where the turbines are positioned in the grid layout, the optimization was able to decrease the wake losses for the directions where the wind is aligned with the turbine rows, while it also increased the energy capture for the other angles (Figure 6.12 (a)).

(a) Scenario 1

(b) Scenario 2

(c) Scenario 3
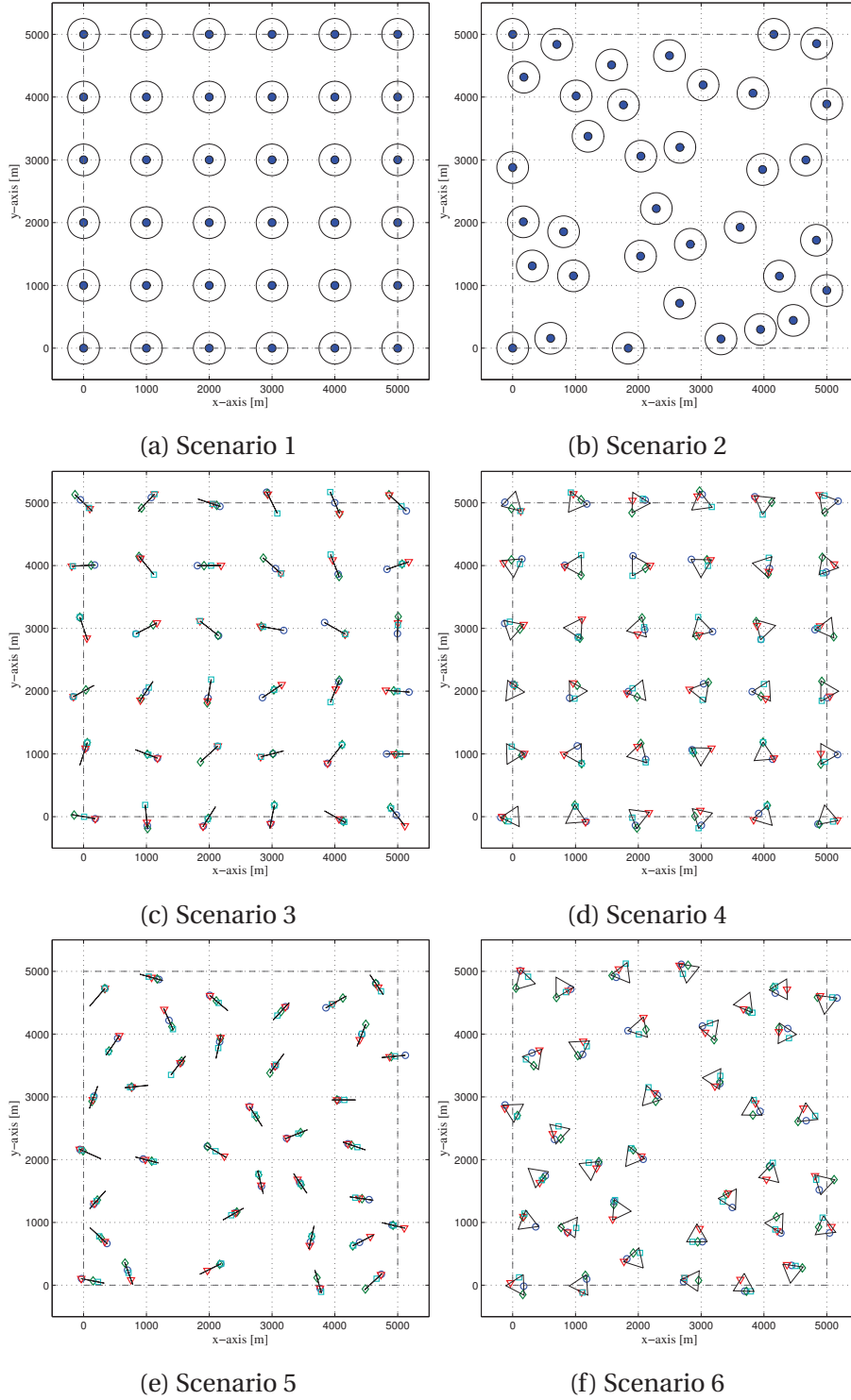
(d) Scenario 4

(e) Scenario 5

(f) Scenario 6

Figure 6.10: Optimized wind farm layouts. Legend — (a) and (b) figures: blue circle represents the turbines whereas the black circle represents half of the minimum distance between turbines; (c), (d), (e) and (f) figures: turbines locations for four different wind directions examples - blue circle: 0 degrees, green diamond: 90 degrees, red triangle: 180 degrees, cyan square: 270 degrees.
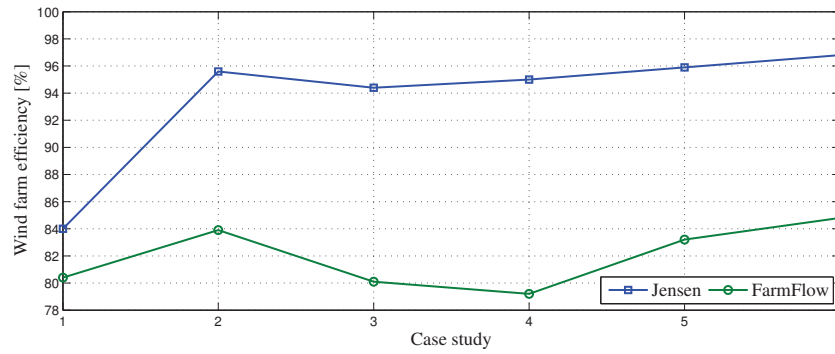
Figure 6.11: Wind farm efficiency for both models and all scenarios.

(a) Jensen model
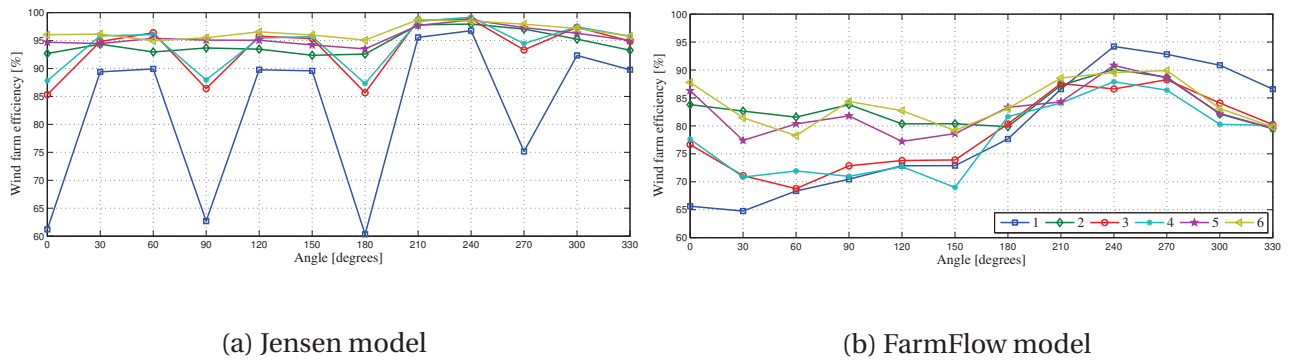
(b) FarmFlow model

Figure 6.12: Wind farm efficiency per wind direction for all scenarios and wake models.

6.6.2 FarmFlow

According to FarmFlow, Scenario 1 has the highest efficiency between 240-330 degrees (Figure 6.12 (b)). This may be explained by the fact that the highest mean wind speeds are felt in these directions and therefore, the impact of turbines for the wake generation is the weakest (due to the lower thrust coefficients, Figure 6.8). Furthermore, the grid layout benefits from the fact that the turbines have greater spacings for these angles. Hence, a lower wind farm efficiency is expected in case the main wind section is aligned with the turbine rows.

Scenarios 3 and 4 presented the lowest efficiencies of the case studies according to FarmFlow, whereas Scenarios 2, 5 and 6 had not only the highest energy productions (Figure 6.11) as well as the lowest efficiency variabilities according to both models (Figure 6.12).

Figure 6.11 shows that there is an absolute difference of the wind farm efficiencies according to the two wake models. Furthermore, there were also some relative differences between them. The highest discrepancies between the models have occurred in case studies 3 and 4. According to the Jensen model, all optimized layouts performed better than the standard layout, whereas FarmFlow gave a lower efficiency for these two cases.

In these scenarios, the wind turbines are placed in a grid layout, hence, the distances between the

turbines vary much less than in scenarios 2, 5 and 6. Figure 6.12 (b) shows that Scenarios 1, 3 and 4 have lower efficiencies for the wind directions with lower mean speeds (0-150 degrees) and yet they yield comparable efficiencies with the other scenarios in the main wind directions (180-330 degrees). By comparing the results of both models in Figure 6.12, it is possible to observe that the Jensen model did not accurately depicted the wake losses for scenarios 3 and 4 for the wind directions in the 0-150 degrees range. Differently, in the scenarios in which the wind farm layout is also optimized, both models are in a higher concordance. Therefore, one might conclude that the Jensen model offers a poorer accuracy for this specific range of distances in combination with lower mean wind speeds (higher turbine shadowing effect).

The accuracy of different wake models has been the object of several previous studies. For example, Andersen et al. [36] conducted a comparison of different engineering wake models (including the Jensen model) and CFD simulations. They demonstrated that the highest discrepancies between the Jensen and the CFD models were observed around distances of 4-8 rotor diameters and for higher thrust coefficients, which is in line with the results obtained in this work. Nonetheless, these studies have been conducted with very narrow setups, such as fixed turbine thrust coefficients and constant distances between turbines. Therefore, it is difficult to conclude which are the parameters that contribute the most for the differences between the models.

Albeit the differences between the two wake loss models, one might say that turbine mobility will, in the worst case scenario, generate the same energy as a wind farm composed of fixed turbines. The results obtained with the FarmFlow model appear to indicate that floating mobility generate benefits if the turbine layout is coordinately optimized, whereas with the Jensen model all the optimized layouts perform better than the standard layout. Furthermore, according to both models the highest energy improvements were observed when the wind farm layout was optimized using movable wind turbines.

The relative differences in the results were originated from the fact that the Jensen model was used in the optimization process and the FarmFlow was only employed to validate the efficiency of the final layouts. These results demonstrate the importance of developing fast-accurate models which may be applied for the optimization of future large OWFs. The impact of the energy efficiency on the project levelized cost of energy (LCOE) is discussed next.

6.6.3 Impact on the Levelized Cost of Energy

The LCOE is the project lifetime cost per unit of power generated and may be calculated as [22, 23]:

$$LCOE = \frac{1}{AEP} \left(\frac{CAPEX}{a} + OPEX \right) \tag{6.4}$$

where CAPEX is the capital expenditure, OPEX is the operational expenditure, a is the annuity factor $a = (1 - (1 + r)^{-n}) \, r^{-1}$, r is the interest rate and n is the wind farm exploitation time.

Table 6.2: LCOE variation for the different scenarios.

Scenario	1	2	3	4	5	6
LCOE [%]	0	-4.17	0.37	1.51	-3.37	-5.19

Assuming the annuity factor as a weight factor ω_1 and the OPEX as a percentage of the CAPEX, ω_2:

$$LCOE = \frac{1}{AEP} (\omega_1 \cdot CAPEX + \omega_2 \cdot CAPEX) \tag{6.5}$$

Summing the two weighing factors the LCOE becomes:

$$LCOE = \frac{CAPEX}{AEP} \cdot \omega \tag{6.6}$$

Assuming an interest rate of 7%, a wind project exploration time of 20 years and the OPEX costs to be 2% of the CAPEX [22, 23], a weighting factor of $\omega = 0.114$ is obtained. Table 6.2 shows the variation of the LCOE when considering an initial LCOE value of 90 €/MWh for the initial standard layout, constant CAPEX for the different scenarios and a weighing factor of $\omega = 0.114$. The wind farm layout of Scenario 6, which has the highest efficiency, presents a variation of -5.19% leading to a LCOE of 85.33 €/MWh. This results in a CAPEX saving of € 35 million.

6.7 Conclusions

This work presented the first optimization framework for designing OWFs composed of floating and movable turbines. It demonstrated that the energy gain is further increased through a simultaneous optimization of two factors: firstly, the anchoring locations of the wind turbines – which lead to non-standard grid-based layouts - and, secondly, the turbines locations within the mooring lines for each individual wind direction. The results of the wind farm efficiencies showed relative differences between the Jensen model, used in the optimization process, and FarmFlow, which was applied to validate the efficiency of the final layouts. These results demonstrate the importance of developing accurate wake models which are also fast enough to be applied during the optimization process of future large OWFs. Finally, up to 4.4% higher wind farm efficiencies were observed when larger maneuver areas were assigned to the turbines, which may be traduced to a 5% reduction of the LCOE and a capital gain of € 35 million. The results obtained in this work corroborate that turbine and wind farm developers should cooperate to optimize future OWFs. As future work, the optimization framework can be extended to assess the energy gain for different wind farm sizes and different turbines.

References

[1] European Wind Energy Association (EWEA), "The european offshore wind industry - key trends and statistics," Tech. Rep., 2012.

[2] EWEA, "Deep water - the next step for offshore wind energy," Tech. Rep., 2013.

[3] LORC. [Last accessed 1st March 2015]. [Online]. Available: www.lorc.dk/offshore-wind-farms-map/list

[4] 4C Offshore. [Last accessed 23rd March 2015]. [Online]. Available: www.4coffshore.com/windfarms

[5] The Wind Power. (2014) [Last accessed 1st March 2015]. [Online]. Available: www.thewindpower.net/windfarms_offshore_en.php

[6] Renewables Map. [Last accessed 1st March 2015]. [Online]. Available: www.renewables-map.co.uk/windfarm.asp

[7] M. Bilgili, A. Yasar, and E. Simsek, "Offshore wind power development in europe and its comparison with onshore counterpart," *Renew. and Sustainable Energy Reviews*, vol. 15, no. 2, pp. 905–15, 2011.

[8] Main(e) International Consulting LLC, "Floating offshore wind foundations: Industry consortia and projects in the united states, europe and japan - an overview," Maine, USA, Tech. Rep., May 2013.

[9] IDEOL. (2014) [Last accessed 22th August 2014]. [Online]. Available: http://www.ideol-offshore.com

[10] T. Sorensen, M. L. Thogersen, and P. Nielsen, "Adapting and calibration of existing wake models to meet the conditions inside offshore wind farms," EMD International A/S, Aalborg, Denmark, Tech. Rep., 2008.

[11] O. Rahbari *et al.*, "Towards realistic designs of wind farm layouts - application of a novel placement selector approach," *Energy Conversion and Management*, vol. 81, no. 0, pp. 242–254, 2014.

[12] S. Rodrigues, P. Bauer, and J. Pierik, "Modular approach for the optimal wind turbine micro siting problem through cma-es algorithm," in *Proceeding of the fifteenth annual conference companion on Genetic and evolutionary computation conference companion*, ser. GECCO '13 Companion. New York, NY, USA: ACM, 2013, pp. 1561–1568.

[13] M. Wagner *et al.*, "Optimizing the layout of 1000 wind turbines," in *European Wind Energy Association Annual Event*. Brussels, Belgium: European Wind Energy Association, 2011, pp. 1–10.

[14] B. Perez, R. Minguez, and R. Guanche, "Offshore wind farm layout optimization using mathematical programming techniques," *Renewable Energy*, vol. 53, no. 0, pp. 389–399, 2013.

[15] J. Serrano-Gonzalez *et al.*, "Overall design optimization of wind farms," *Renew. Energy*, vol. 36, no. 7, pp. 1973–1982, 2011.

[16] S. Grady, M. Hussaini, and M. Abdullah, "Placement of wind turbines using genetic algorithms," *Renewable Energy*, vol. 30, no. 2, pp. 259–270, 2005.

[17] Y. Eroglu, and S. U. Seckiner, "Design of wind farm layout using ant colony algorithm," *Renew. Energy*, vol. 44, no. 0, pp. 53–62, 2012.

[18] M. Veigas, and G. Iglesias, "Potentials of a hybrid offshore farm for the island of Fuerteventura," *Energy Conversion and Management*, vol. 86, no. 0, pp. 300–308, 2014.

[19] S. Chowdhury *et al.*, "Unrestricted wind farm layout optimization (UWFLO): Investigating key factors influencing the maximum power generation," *Renew. Energy*, vol. 38, no. 1, pp. 16–30, 2012.

[20] S. Rajper, and I. J. Amin, "Optimization of wind turbine micrositing: A comparative study," *Renew. and Sustainable Energy Reviews*, vol. 16, no. 8, pp. 5485–5492, 2012.

[21] G. Mosetti, C. Poloni, and B. Diviacco, "Optimization of wind turbine positioning in large windfarms by means of a genetic algorithm," *Journal of Wind Engineering and Industrial Aerodynamics*, vol. 51, no. 1, pp. 105–116, Jan 1994.

[22] M. A. Lackner, and C. N. Elkinton, "An analytical framework for offshore wind farm layout optimization," *Wind Engineering*, vol. 31, pp. 17–31, Jan. 2007.

[23] C. N. Elkinton, J. F. Manwell, and J. G. McGowan, "Offshore wind farm layout optimization (OWFLO) project: an introduction," in *In Proceedings of the European Offshore Wind Conference & Exhibition*, Copenhagen, Denmark, Oct. 2005.

[24] S. Rodrigues *et al.*, "Trends of offshore wind projects," *Renewable and Sustainable Energy Reviews*, vol. 49, pp. 1114–1135, Sept. 2015.

[25] European Wind Energy Association (EWEA), "Wind in our sails - the coming of europe's offshore wind energy industry," Tech. Rep., 2011.

[26] Renewable Energy World. (2013) [Last accessed 24th August 2014]. [Online]. Available: http://www.renewableenergyworld.com/rea/news/article/2011/05/a-buoyant-future-for-floating-wind-turbines

[27] Main(e) International Consulting LLC. (2013) Japan's floating offshore wind projects: An overview. [Last accessed 24th August 2014]. Maine, USA.

[28] Blue H. (2013) [Last accessed 17th October 2013]. [Online]. Available: http://www.bluehgroup.com/

[29] A. Tesauro, P.-E. Rethore, and G. Larsen, "State of the art of wind farm optimization," in *Proceedings of European Wind Energy Conference & Exhibition*, Copenhagen, Denmark, April 2012.

[30] C. N. Elkinton, J. F. Manwell, and J. G. McGowan, "Algorithms for Offshore Wind Farm Layout Optimization," *Wind Engineering*, vol. 32, pp. 67–84, 2008.

[31] C. Igel, N. Hansen, and S. Roth, "Covariance matrix adaptation for multi-objective optimization," *Evolutionary Computation*, vol. 15, no. 1, pp. 1–28, 2007.

[32] N. Hansen. (2009) Reference to cma-es applications. Last accessed in 26th August 2014. [Online]. Available: https://www.lri.fr/~hansen/cmaapplications.pdf

[33] GHWindFarmer. [Last accessed 20th April 2014]. [Online]. Available: http://www.gl-garradhassan.com/en/software/GHWindFarmer.php

[34] WindPRO. [Last accessed 20th April 2014]. [Online]. Available: www.emd.dk/WindPRO

[35] S. Rodrigues, P. Bauer, and J. Pierik, "A clustering approach for the wind turbine micro siting problem through genetic algorithm," in *39th Annual Conference IECON*, 2013.

[36] S. J. Andersen *et al.*, "Comparison of Engineering Wake Models with CFD Simulations," *Journal of Physics: Conference Series*, vol. 524, p. 012161, 2014.

[37] M. Gaumond *et al.*, "Evaluation of the wind direction uncertainty and its impact on wake modeling at the Horns Rev offshore wind farm," *Wind Energy*, vol. 17, no. 8, pp. 1169–1178, 2014.

[38] R. J. Barthelmie *et al.*, "Comparison of Wake Model Simulations with Offshore Wind Turbine Wake Profiles Measured by Sodar," *Journal of Atmospheric and Oceanic Technology*, vol. 23, no. 7, pp. 888–901, 2006.

[39] B. Sanderse, "Aerodynamics of wind turbine wakes - literature review," Energy Research Centre of the Netherlands (ECN), Petten, The Netherlands, Tech. Rep., 2009.

[40] J. Annoni *et al.*, "Evaluating wake models for wind farm control," in *Proceedings of the American Control Conference*, 2014, pp. 2517–2523.

[41] A. Crespo, J. Hernandez, and S. Frandsen, "Survey of modelling methods for wind turbine wakes and wind farms," *Wind Energy*, vol. 2, no. 1, pp. 1–24, 1999.

[42] L. Vermeer, J. Sorensen, and A. Crespo, "Wind turbine wake aerodynamics," *Progress in Aerospace Sciences*, vol. 39, pp. 467–510, 2003.

[43] N. Jensen, "A note on wind generator interaction," Riso National Laboratory, Roskilde, Denmark, Tech. Rep. Riso-M-2411, 1983.

[44] F. F. Ainslie, "Calculating the flowfield in the wake of wind turbines," *Journal of Wind Engineering and Industrial Aerodynamics*, vol. 27, no. 1, pp. 213–224, 1988.

[45] S. Frandsen *et al.*, "Analytical modelling of wind speed deficit in large offshore wind farms," *Wind Energy*, vol. 9, no. 1–2, pp. 39–53, 2006.

[46] M. C. Brower, and N. M. Robinson, "The openwind deep-array wake model - development and validation," Tech. Rep., 2012.

[47] L. G. C., "A simple stationary semi-analytical wake model," Riso National Laboratory, Roskilde, Tech. Rep. Riso-R-1713(EN), 2009.

[48] "Dynamic wake meandering modeling," Riso National Laboratory, Roskilde, Tech. Rep. Riso-R-1607(EN), 2007.

[49] R. Mikkelsen, "Actuator disc methods applied to wind turbines," Ph.D. dissertation, Technical University of Denmark, 2003.

[50] P. Torres, J.-W. van Wingerden, and M. Verhaegen, "Modeling of the flow in wind farms for total power optimization," in *International Conference on Control and Automation (ICCA)*, 2011, pp. 963–968.

[51] M. J. Churchfield *et al.*, "A large-eddy simulation of wind-plant aerodynamics," *AIAA paper*, no. 2012-0537, 2012.

[52] E. Bot, "Farmflow - improved near wake modelling and validation against four full scale wind farms," Energy Research Centre of the Netherlands, Tech. Rep., 2012.

[53] S. Ott, J. Berg, and M. Nielsen, "Linearised cfd models for wakes," Riso National Laboratory, Tech. Rep., 2011.

[54] J. F. Herbert-Acero *et al.*, "A review of methodological approaches for the design and optimization of wind farms," *Energies*, vol. 7, no. 11, pp. 6930–7016, 2014.

[55] I. Katic, J. Hojstrup, and N. Jensen, "A simple model for cluster efficiency," in *EWEC'86. Proceedings. Vol. 1*, 1986, pp. 407–410.

[56] Y. Chen *et al.*, "Wind farm layout optimization using genetic algorithm with different hub height wind turbines," *Energy Conversion and Management*, vol. 70, no. 0, pp. 56–65, 2013.

[57] L. Chen, and E. MacDonald, "A system-level cost-of-energy wind farm layout optimization with landowner modeling," *Energy Conversion and Management*, vol. 77, no. 0, pp. 484–494, 2014.

[58] J. S. Gonzalez *et al.*, "A review and recent developments in the optimal wind-turbine micro-siting problem," *Renew. and Sustainable Energy Reviews*, vol. 30, no. 0, pp. 133–144, 2014.

[59] A. Behnood *et al.*, "Optimal output power of not properly designed wind farms, considering wake effects," *International Journal of Electrical Power & Energy Systems*, vol. 63, no. 0, pp. 44–50, 2014.

[60] Y. Eroglu, and S. U. Seckiner, "Wind farm layout optimization using particle filtering approach," *Renew. Energy*, vol. 58, no. 0, pp. 95–107, 2013.

[61] S. Turner *et al.*, "A new mathematical programming approach to optimize wind farm layouts," *Renew. Energy*, vol. 63, no. 0, pp. 674–680, 2014.

[62] A. Crespo *et al.*, "Experimental validation of the UPM computer code to calculate wind turbine wakes and comparison with other models," *Journal of Wind Engineering and Industrial Aerodynamics*, vol. 27, no. 1-3, pp. 77–88, 1988.

[63] E. Berge *et al.*, "Modelling of offshore wind resources. Comparison of a mesoscale model and measurements from FINO 1 and North Sea oil rigs," in *European Wind Energy Conference and Exhibition (EWEC)* , 2009.

[64] N. Hansen, and S. Kern, "Evaluating the cma evolution strategy on multimodal test functions," in *Parallel Problem Solving from Nature (PPSN VIII)*, vol. 3242.   Springer, 2004, pp. 282–291.

CHAPTER **7**

Conclusions and Recommendations

In this chapter, the conclusions for the key questions posed in the Introduction will be presented. Thereafter, the main conclusions of the thesis will be given, followed by recommendations for future research and the offshore wind industry.

What are the trends of the main characteristics of offshore wind farms?

Chapter 2 presented the current situation of the main market players of the European offshore wind industry as well as the trends of the key characteristics of the commissioned and under construction European offshore wind farms (OWFs), namely: commissioning country, installed capacity, energy production, number of turbines, water depth, project area, distance to shore, transmission technology and investment cost.

The analysis showed that the initial OWFs mostly served as proof of concept and were located in shallow waters close to shore, were composed of only a few wind turbines and with low investment costs. In contrast, recent OWFs have, on average, a higher number of turbines, are located further away from shore and located in deeper waters. Although the average investment cost per project rises with higher distances to shore and water depths (due to foundations, grid connection and installation), it is believed that the trend of building OWFs further offshore will continue.

The transmission technology of choice has also been evolving throughout the years. Initially, the OWFs were connected to shore via medium-voltage ac (MVac) cables. When the distances to shore alongside with the installed capacities increased, wind farm developers turned to high-voltage ac (HVac) technology. Recently, also high-voltage dc (HVdc) technology was employed in the field as a way of transporting the energy generated offshore to the onshore electrical networks.

227

What are the industrial trends of offshore wind farm components?

The research performed on the industrial trends of the main wind farm components showed that the wind turbine manufacturers are heading towards turbines with larger rotors and higher rated powers. They are also equipping these turbines mainly with permanent-magnet synchronous generators or asynchronous generators with both solutions being used together with full-rated back-to-back voltage source converters. Regarding the support structure, monopile is by far the most common solution. Furthermore, even though there are other support structures, such as jackets, suction buckets and tripods, it is believed that the monopile will continue to be the preferred choice in the coming years, whereas floating solutions are envisioned to dominate the deep waters market.

Recent OWFs make use of highly complex collection systems. Cables with different cross sections are used to minimize the total collection system length. Furthermore, branching systems are employed with the same goal. Although all collection systems of large OWFs have used a 33 kV collection voltage, the usage of 66 kV systems is envisioned in the near future.

The transmission technology demonstrated a strong correlation with the distance to shore and capacity of the project. The use of offshore substations has started due to the need to minimize transmission losses. The analysis showed that recent large OWFs make use of two internal substations to minimize the total length of the collection system. For both HVac and HVdc technologies the transmission voltages have increased in the past years with the aim of further increasing the transmission efficiency. Although HVdc currently accounts for 25% of the total installed capacity, it is still unclear which technology will predominate in the market in the future.

Which is the best multi-objective optimization algorithm for the design of offshore wind farm layouts and their electrical infrastructure?

This is a key question which had to be answered to ensure that the trade-offs obtained with the algorithm were, in fact, optimized. In Chapter 3, the Multi-Objective Wind Farm Layout Optimization Problem (MOWFLOP) was investigated. The performance of the Nondominated Sorting Genetic Algorithm II (NSGA-II), which is one of the most well-known multi-objective optimization algorithms, was compared to the Multi-Objective Gene-pool Optimal Mixing Evolutionary Algorithm (MOGOMEA). Additionally, a slightly altered variant of each algorithm was considered.

The case study showed that the MOGOMEA variant that used a linkage tree learned offline provided, in general, better wind farm layouts. The main characteristics that differentiate the MOGOMEA form the NSGA-II are as following:

- use of specific solutions to guide optimization towards individual goals;

- assuming a continuity of the solution space via clustering of solutions;

- use of problem-dependent knowledge into the optimization algorithm.

The best results were obtained when the offline MOGOMEA was equipped with the resampling constraint-handling technique. The results also showed that the algorithms provided better wind farm layouts when the areas were discretized with a multi-step approach, in which wind farm layouts were consecutively designed using more refined grids.

Which modeling techniques are required?

Evolutionary multi-objective algorithms are highly versatile as virtually any wind-farm model may be used since only the model's output is necessary to guide optimization. However, these advantages come at a cost. One of their main weaknesses is that no algorithm can efficiently solve all problems, hence there is a need to bias the search, exploiting problem features that are of importance in the type of problems being considered. Furthermore, depending on the inherent difficulty of the problem being solved, evolutionary multi-objective optimization strategies require several thousand of function evaluations to reach convergence.

One of the main conclusions is that the models are required to be computationally light to avoid overwhelming optimization runs. On the other hand, the models should be able to present relative differences between similar OWF layouts. In this way, the models cannot be over-simplified, and also very importantly, they should capture all the main sources of losses.

Chapter 4 presented power losses models for ac and dc cables, modular multilevel converters and transformers. The results show that the proposed models were able to capture the main sources of power losses while considering environmental factors, such as type of soil surrounding the cables and ambient temperature. The assumptions made for the models are reasonable if one considers that they will be used in the assessment of the efficiency of large OWFs during a long period. Finally, these results were achieved with low computational requirements.

Which are the important variables and objectives in the optimization process?

Chapter 5 showed that the turbine-related parameters play one of the most important roles in the optimization of an OWF. The number, location and model of turbines are very important variables that have to be optimized. Due to the high number of wind turbines, the collection system proved to be an important design aspect of recent OWFs. The location, type and number of offshore substations is also a highly relevant design aspect. The type of substation is directly related to the transmission technology being used, whereas the location and quantity of substations are highly relevant to the collection system design.

Different layouts demonstrated to be the best alternative when distinct economic indicators, e.g. levelized cost of energy (LCOE) and net present value (NPV), were applied. The optimization framework was able to design wind farm layouts with different characteristics. For example, one OWF presented a NPV 71% higher when compared to a standard layout that was manually designed. Another layout composed of only 18 turbines had a LCOE 7% lower compared to the same standard layout. Furthermore, it was also shown that choosing different economic parameters, e.g. price of energy and interest rate, also influences the outcome of the optimization

even while using the same economic indicator. A small wind farm obtained the highest NPV when a 12% interest rate was used, whereas a very large project maximized the same indicator when the lifetime was extended by five years.

In Chapter 6, it was demonstrated that the use of movable floating wind turbines may lead higher annual energy production (AEP) through a simultaneous optimization of the anchoring locations of the wind turbines – which lead to non-standard grid-based layouts - and the turbines locations within the mooring lines for each wind direction. A wind farm with an increased efficiency of 4.4% higher was obtained when larger maneuver areas were assigned to the turbines, which may be traduced to a 5% reduction of the LPC and a capital gain of 35 M€.

Why is (multi-objective) optimization needed?

In Chapter 5 it is concluded that a multi-objective approach brings advantages over its single-objective counterpart. Although multi-objective optimization is generally slower and computationally more demanding, it requires only one optimization routine since the optimization and decision phases are decoupled. A multi-objective approach presents designers with optimized trade-offs between different project objectives, such as AEP, capital expenditure and operational expenditure, by simultaneously optimizing them. With this extra degree of freedom, designers may have a clearer understanding of the possibilities and associated trade-offs and be better equipped to identify wind farm layouts and respective electrical infrastructures that meet their desires. In the proposed framework, no *a priori* economic assumptions or weighted combination of the goals are required since the wind farm designer only acts after the optimization phase.

7.1 Final conclusions

The multi-objective optimization framework presented in this thesis represents a mindset change to a well-established market in which the different entities have their working procedures already defined and proved. The work presented here aims at demonstrating to the offshore players that a design philosophy based on multi-objective optimization may bring different advantages to the industry. In particular, the designers will have a clearer picture of the design possibilities at hand and will be more able to choose the wind farm layout and respective electrical infrastructure that they prefer. Furthermore, it implicitly implies that bringing different entities to work together, e.g. manufacturers, designs and installation companies, may create value and reduce costs, bringing a sustainable future closer to reality.

7.2 Recommendations for future research

3. Multi-Objective Optimization of Wind Farm Layouts

For future work it would be interesting to assess the influence of smaller grid steps and wind farms with larger areas. It would also be interesting to test instances of the multi-objective wind farm layout optimization problem with more than two optimization goals. Other population-sizing-free schemes could be proposed and tested in future work. Furthermore, the multi-step approach demonstrated to provide good results and hence, an in-depth study into the competences and true scalability of this approach should be carried out in future work. If wind farm developers show interest in tackling the siting of the wind turbines via a real-coded approach, one could research what is the best way to tackle this problem with a mixed-integer approach. Nonetheless, this would raise many new challenging, but not less interesting, questions for future research.

4. Steady-state loss models for Optimization Purposes

As future work, it could be interesting to extend the MMC model to the full-bridge sub-modules. The model could be tested for different switches to realize how much their characteristics impact the overall efficiency of the converter. Additionally, it would be interesting to research the relation between the number of submodules and the effective switching frequency, which plays a major role in the overall efficiency of the converter.

5. Multi-Objective Optimization Framework for Offshore Wind Farms

Including a sensitivity analysis in the optimization procedure as well as a robustness test for the wind farm layouts, e.g. dependency with the wind direction variation and perturbation could be a potential path for future research. External and future wake effects, caused respectively by existing and future neighboring OWFs, should also be considered during the design of wind farm layouts due to the closer distances between projects.

It would also be very interesting to run the optimization framework with detailed and accurate input values which only wind farm developers have access to, such as detailed seabed information and cost data. More detailed operational cost models and investigating component failure are also interesting research paths.

6. Wake Losses Optimization of Offshore Wind Farms with Movable Floating Wind Turbines

The AEPs obtained showed relative differences between the Jensen model, used in the optimization process, and FarmFlow, which was applied to validate the efficiency of the final layouts. These results demonstrate the importance of developing accurate wake models which are also fast enough to be applied during the optimization process of future large OWFs.

7.2.1 Recommendations for offshore wind farm developers

The use of multi-objective optimization algorithms should become standard practice in the offshore wind industry. This thesis demonstrates that these algorithms bring several advantages during the design phase of a project which ultimately lead to a lower cost of energy. Additionally, wind farm developers should validate and compare the results obtained with the simplified/fast models used in the optimization phase with their own models.

The results of this thesis show that bringing different entities, e.g. manufacturers, designs and installation companies, to work together can create value and reduce costs. Although this may be considered a risk since companies usually do not collaborate due to the fear of knowledge leakage, a higher collaboration may bring cost savings to all the players and bring the cost of offshore wind to more attractive values.

List of Publications

Conference Proceedings

- R. Teixeira Pinto, S. Rodrigues, P. Bauer, and J. Pierik, "Comparison of direct voltage control methods of multi-terminal dc (mtdc) networks through modular dynamic models," in Proceedings of the 14th European Conference on Power Electronics and Applications (EPE), 2011.

- S. Rodrigues, P. Bauer, and J. Pierik, "Comparison of offshore power transmission technologies: A multi-objective optimization approach," in 15th International Power Electronics and Motion Control Conference (EPE/PEMC), 2012.

- S. Rodrigues, R. Teixeira Pinto, P. Bauer, and J. Pierik, "Optimization of social welfare and transmission losses in offshore mtdc networks through multi-objective genetic algorithm," in Power Electronics and Motion Control Conference (IPEMC), 2012 7th International, 2012, pp. 1287-1294.

- S. Rodrigues, R. Pinto, P. Bauer, E. Wiggelinkhuizen, and J. Pierik, "Optimal power flow of vsc-based multi-terminal dc networks using genetic algorithm optimization," in Energy Conversion Congress and Exposition (ECCE), 2012.

- R. Teixeira Pinto, S. Rodrigues, P. Bauer, and J. Pierik, "Optimal control tuning of grid connected voltage source converters using a multi-objective genetic algorithm," in Proceedings of the Power Conversion Intelligent Motion (PCIM Europe), Nuremberg, Germany, 14-16 May 2013, pp. 1-8.

- S. Rodrigues, R. Teixeira Pinto, P. Bauer, and J. Pierik, "Multi-objective optimization of a pmsg control system through small-signal analysis," in ECCE Asia Downunder (ECCE Asia), 2013 IEEE, 2013, pp. 1189-1195.

- R. Teixeira Pinto, S. Rodrigues, P. Bauer, and J. Pierik, "Operation and control of a multi-terminal dc network," in ECCE Asia Downunder (ECCE Asia), 2013 IEEE, 2013, pp. 474-480.

- S. Rodrigues, P. Bauer, and J. Pierik, "Modular approach for the optimal wind turbine micro siting problem through cma-es algorithm," in Proceedings of the fifteenth annual conference companion on Genetic and evolutionary computation conference companion, GECCO13 Companion. New York, NY, USA: ACM, 2013, pp. 1561-1568.

- S. Rodrigues, P. Bauer, and J. Pierik, "A clustering approach for the wind turbine micro siting problem through genetic algorithm," in 39th Annual Conference IECON, 2013.

- R. Teixeira Pinto, S. Rodrigues, P. Bauer, and J. Pierik, "Grid code compliance of vsc-hvdc in offshore multi-terminal dc networks," in 39th Annual Conference IECON, 2013.

- S. Rodrigues, P. A.N. Bosman, and P. Bauer, "Collection network cable routing and wake losses optimization in offshore wind farms," in Proceedings of the XIII Symposium of Specialists in Electric Operational and Expansion Planning, Brazil, 2014.

- S. Rodrigues, P. Bauer and P. A.N. Bosman, "A Novel Population-based Multi-Objective CMA-ES and the Impact of Different Constraint Handling Techniques," in Proceedings of the sixteenth annual conference companion on Genetic and evolutionary computation conference, GECCO14. New York, NY, USA: ACM, 2014.

- E. Kontos, S. Rodrigues, R. Teixeira Pinto and P. Bauer, "Optimizing Reactive power provided by an offshore transmission system," in Energy Conversion Congress and Exposition (ECCE), 2014.

- A. Papadopoulos, S. Rodrigues, E. Kontos, T. Todorcevic and P. Bauer, "A Fast Steady-State Loss Model of a Modular Multilevel Converter for Optimization Purposes," in IEEE ECCE ASIA, 2015.

- S. Rodrigues, T. Brys, R. Teixeira Pinto, A. Nowé and P. Bauer, "Online Distributed Voltage Control of an Offshore MTdc Network using Reinforcement Learning," in IEEE CEC, 2015.

- A. Papadopoulos, S. Rodrigues, T. Todorcevic, R. Teixeira Pinto and P. Bauer, "Collection and Transmission Losses of Offshore Wind Farms for Optimization Purposes," IEEE ECCE USA, 2015.

- R. Teixeira Pinto, S. Rodrigues, E. Kontos and P. Bauer, "Optimal Power Flow in MTDC Networks for Large Offshore Wind Power Plants: Validation of the Distributed Voltage Control," in 41st Annual Conference IECON, 2015.

Journal Publications

- S. Rodrigues, R. Teixeira Pinto, P. Bauer and J. Pierik, "Optimal power flow control of vsc-based multi-terminal dc network for offshore wind integration in the north sea," IEEE Transactions on Emerging and Selected Topics in Power Electronics, 2013.

- R. Teixeira Pinto, S. Rodrigues, E. Wiggelinkhuizen, R. Scherrer, P. Bauer, and J. Pierik, "Operation and power flow control of multi-terminal dc networks for grid integration of offshore wind farms using genetic algorithms," Energies, vol. 6, no. 1, pp. 1-26, 2012.

- R. Teixeira Pinto, S. Rodrigues, P. Bauer, and J. Pierik, "Description and comparison of dc voltage control strategies for offshore mtdc networks: Steady-state and fault analysis," European Power Electronics Journal, vol. 22, no. 4, pp. 13-21, 2013.

- R. Teixeira Pinto, P. Bauer, S. Rodrigues, E. Wiggelinkhuizen, J. Pierik, and B. Ferreira, "A novel distributed direct-voltage control strategy for grid integration of offshore wind energy systems through mtdc network," IEEE Transactions on Industrial Electronics, vol. 60, no. 6, pp. 2429-2441, 2013.

- E. Kontos and R. Teixeira Pinto, S. Rodrigues and P. Bauer, "Impact of HVdc Transmission System Topology on Multi-terminal DC Network Faults," IEEE Transactions on Power Delivery, 2014.

- S. Rodrigues, R. Teixeira Pinto, M. Soleimanzadeh, P. A.N. Bosman and P. Bauer, "Wake Losses Optimization of Offshore Wind Farms with Moveable Floating Wind Turbines," Elsevier Energy Conversion and Management, vol. 89, no. 0, pp. 933-941, 2015.

- S. Rodrigues, C. Restrepo, E. Kontos, R. Teixeira Pinto and P. Bauer,"Trends of Offshore Wind Projects," Elsevier Renewable and Sustainable Energy Reviews, vol. 49, pp. 1114-1135, Sep. 2015.

- S. Rodrigues, A. Papadopoulos, E. Kontos, T. Todorcevic and P. Bauer, "Steady-State Loss Model of Half-Bridge Modular Multilevel Converters," in IEEE Transactions on Industry Applications, 2016.

- S. Rodrigues, C. Restrepo, G. Katsouris, R. Teixeira Pinto, M. Soleimanzadeh, P. Bosman and P. Bauer, "A Multi-Objective Optimization Framework for Offshore Wind Farm Layouts and Electric Infrastructures,", Energies, vol. 9(3), March, 2016.

- S. Rodrigues, P. Bauer , P. A.N. Bosman, 'Multi-Objective Optimization of Wind Farm Layouts – Complexity, Constraint Handling and Scalability," *2nd review round at* Elsevier Renewable & Sustainable Energy Reviews.

Acknowledgements

. Acknowledgements

being always helpful no matter what and for letting me use the server. I would also like to thank Andrew for revising and correcting the introduction and conclusions of this thesis. Niels, Olivier, Gerard and Pieter also have to be mentioned here. Good times guys!

An enormous thank to all my friends from Portugal. Good friendships last independently of the distance that separate us and it is really good to feel at home during my shorts travels to Portugal.

A person that became very important in my life during the last stretch of the PhD journey was Marije. She has always been there for me and has helped immensely. Thank you very much for being so caring, lovely, funny, supportive and most importantly, for being with me.

Finally, I would like to thank my parents and sister. They have supported me during my entire life and worked hard to give me a chance to pursue my goals. To them a special thank you.

Biography

Sílvio Rodrigues was born in Lisbon, Portugal, on April 15th 1988. In 2006 he joined the Instituto Superior Tecnico, in Lisbon, Portugal, for a bachelor degree in Electrotechnical Engineering and Computer Science. In 2011 he received his MSc. in the Energy Department at the same institution. Since October 2011 until December 2015 he worked as a PhD student on the Flow research project at the DC systems, Energy conversion and Storage group of the Delft University of Technology. His research interests include the modeling and optimization of offshore wind farms and multi-objective optimization algorithms.